STUDY OF TOPOLOGICAL FORMATION OF LANTHANIDE LUMINESCENT SUPRAMOLECULAR EDIFICES

HUI TING HIN

PhD

The Hong Kong Polytechnic University

2023

The Hong Kong Polytechnic University

Department of Applied Biology And Chemical Technology

Study of Topological Formation of Lanthanide Luminescent Supramolecular Edifices

Hui Ting Hin

A thesis submitted in partial fulfilment of the requirements for the degree of Doctor of Philosophy

Aug 2022

CERTIFICATE OF ORIGINALITY

I hereby declare that this thesis is my own work and that, to the best of my knowledge and belief, it reproduces no material previously published or written, nor material that has been accepted for the award of any other degree or diploma, except where due acknowledgement has been made in the text.

_____ (Signed)

_____Hui Ting Hin____ (Name of student)

Abstract

Lanthanide supramolecular self-assembly is an emerging technological advancement not only in fundamental science but also with wide range of applications such as drug-delivery system, medical imaging and batteries. The unique photophysical properties and coordination chemistry provide researchers a great opportunity to devise new supramolecular system. The control in topological formation in supramolecular edifices has become particularly crucial in developing biomedical and daily-life application. This thesis, therefore, aims at studying the correlation between the ligand structure and their supramolecular self-assembling behaviors. To introduce the area of supramolecular chemistry, ***chapter 1*** encompasses general chemistry in lanthanide and the development in lanthanide supramolecular chemistry.

Chapter two focuses on reviewing various pyridine-dicarboxamide (pcam) with different offsetting and spacing properties and their correlation to their ultimate supramolecular structure upon complexation to lanthanide. The offsetting angle and distance are found to be one of deciding parameter in ultimate topologies while the first lanthanide chiral supramolecular cubes are reported. Additionally, the solvent-induced self-assembling and transformation is also included.

Supramolecular self-assembly is known to be a collective result from various weak non-covalent interaction. The thermodynamic stability from lanthanide-ligand coordination bonds have played an important role to maintain the entropically disfavored ordered supramolecular architectures. The functionalization of luminescence and stable 1,2-di- Hydroxypyridinones (HOPO) ligands are, therefore,

included in ***Chapter 3***. This chapter encompasses the detailed synthetic work on functionalizing HOPO units and basic photophysical properties. Meanwhile, the investigation on incorporating the HOPO building blocks to ultimate assembly is also included.

In the view of intrinsic instability and ineffectiveness in lanthanide sensitization of pcam chromophores, ***chapter 4*** investigate the synthesis in new class of chiral hydroxyquinoline (HQ) based chromophores while the detailed synthetic attempts are included. With the new class of chromophores, the effect of chelating strength towards final supramolecular self-assembling can be studied.

Acknowledgement

First and foremost, I would like to express my sincere gratitude to my chief supervisor Prof. Ga-Lai Law for offering me life-changing opportunity to conduct the research under her supervision. She is passionate and determined to be a great scientist. She is also the one who always pursue the highest standard in research and educate us the same way. Although my performance was far from satisfactory in most of the time, she is still patiently guide me through my PhD study. Through these few years of study, we might have different considerations and, sometimes, conflicts but this would not stop me from sending my heartfelt appreciation of your guidance, help and patience. Also, I would like to thank my co-supervisor Prof. Wing-Tak Wong who provided me resources to run the projects.

I would like to take this chance to thank my mentor Dr. Wai-Sum Lo. I would not be able to finish my PhD study without the guidance from you. Since I am still FYP students in the group, you have shared your wisdom not only regarding the research but also personal levels. You helped a lot in guiding me through my personal anger, depression and frustration.

I would also thank my second mentor Dr. Ho-Yin Wong and I cannot mention in words how much I did own him for this long journey. His guidance and patience are not only limited to research but also as a friend and comrade. I would never forget what we have been through during those days, and I sincerely hope we could meet again in one day.

Lastly, I would like to send my appreciation to past and current group member from Prof Wong's and Prof. Law, particularly Dr. C. T. Yeung, Dr. K. H. Yim, Dr. L. X. Dai, Dr. W. Y. Xu, Dr. X. L. Zhou, Leo, Pei, Diasy, Hugo, Honam, Eunice, Carlos, Marcus, James and Spencer.

Table of content

List of Abbreviation

ACN	Acetonitrile
A. U.	Arbitrary Unit
CHCl3	Chloroform
COSY	Correlated Spectroscopy
DCM	Dichloromethane
DMSO	Diethyl sulphoxide
DMF	Dimethylformamide
EA	Ethyl acetate
EtOH	Ethanol
ESI	Electrospray ionization
HOPO	Hydroxypyridinones
HQ	hydroxyquinoline
HR	High Resolution
MeOH	Methanol
MS	Mass spectroscopy
NMR	Nuclear Magnetic Resonances
pcam	pcam)
THF	Tetrahydrofuran
UV/Vis	Ultravoilet/Visible

Chapter 1: Introduction to supramolecular chemistry of lanthanide complexes

1.1. Introduction to General Lanthanide Chemistry

1.1.1. Introduction

Lanthanides are series of chemical elements with the atomic numbers of 57 – 71 in period table, from lanthanum through lutetium. These elements are named as lanthanides since they share similar chemical properties with lanthanum. Although lanthanum is not always classified as a lanthanide due to lacking in 4f-orbital electron, they are often included in discussions of the lanthanide chemistry.[1-3] In general, lanthanides have electronic configuration that follow the Aufbau rule ranging from [Xe] $4f^{n+1}$ $6s^2$ except lanthanum, cerium, gadolinium and lutetium due to non-filled, half-filled or fully filled 4f or 5d subshells. Lanthanides predominantly exists in a form of trivalent ions with the electronic configuration of [Xe] $4f^n$ where n = 0 – 14 that empower them unique physical and chemical properties. Lanthanide chemistry was introduced in different well-written book chapters and reviews.[3-7]

Elements	Symbol	Z	Ground State Electronic Configuration	
			Ln	Ln^{3+}
Lanthanum	La	57	[Xe]$5d^1$ $6s^2$	[Xe]
Cerium	Ce	58	[Xe]$4f^1$ $5d^1$ $6s^2$	[Xe] $4f^1$
Praseodymium	Pr	59	[Xe]$4f^3$ $6s^2$	[Xe] $4f^2$
Neodymium	Nd	60	[Xe]$4f^4$ $6s^2$	[Xe] $4f^3$
Promethium	Pm	61	[Xe]$4f^5$ $6s^2$	[Xe] $4f^4$
Samarium	Sm	62	[Xe]$4f^6$ $6s^2$	[Xe] $4f^5$

Europium	Eu	63	$[Xe]4f^7\,6s^2$	$[Xe]\,4f^6$
Gadolinium	Gd	64	$[Xe]4f^7\,5d^16s^2$	$[Xe]\,4f^7$
Terbium	Tb	65	$[Xe]4f^96s^2$	$[Xe]\,4f^8$
Dysprosium	Dy	66	$[Xe]4f^{10}6s^2$	$[Xe]\,4f^9$
Holmium	Ho	67	$[Xe]4f^{11}\,6s^2$	$[Xe]\,4f^{10}$
Erbium	Er	68	$[Xe]4f^{12}\,6s^2$	$[Xe]\,4f^{11}$
Thulium	Tm	69	$[Xe]4f^{13}\,6s^2$	$[Xe]\,4f^{12}$
Ytterbium	Yb	70	$[Xe]4f^{14}\,6s^2$	$[Xe]\,4f^{13}$
Lutetium	Lu	71	$[Xe]4f^{14}\,5d^16s^2$	$[Xe]\,4f^{14}$

Table 1-1: Ground state electronic configurations of lanthanides

1.1.2. Electronic Properties of Trivalent Lanthanide Ions

As mentioned in last section, the ground state electronic configuration of trivalent lanthanide ions is $[Xe]4f^n$ (n = 0 – 14, La to Lu). The $5s^25p^6$ electron subshells in Xenon core with larger radial expansion are shielded by 4f orbitals which attributes the increase in effective nuclear charge with atomic number. In addition to fully filled Xenon core, each of the n electrons in Ln^{III} ions occupies one of the seven 4f (ℓ = 3) wavefunctions and associated with a spin of ±1/2. Taking both angular momentum and spin quantum number in consideration, there are numbers of ways to fill n electrons in 4f orbitals which the multiplicity is given by the following formula.

$$\frac{(4l+2)!}{n!(4l+2-n)!} = \frac{14!}{n!(14-n)!} \quad \text{if } \ell = 3 \text{ (4f orbital)}$$

Based on Russell-Saunders coupling scheme, these ways of associating n electrons can be distinguished with different microstates $[(m_\ell, m_s)_1, (m_\ell, m_s)_2, \ldots (m_\ell, m_s)_n]$. A set of microstates are collectively grouped in accordance to its M_L and M_S where M_L and M_S is the sum of magnetic quantum number (m_ℓ) and spin projection quantum number (m_s) respectively.[1] Additionally, M_L and M_S also correspond to the projections of one

value of L and S which are specified with a spectroscopic term i.e. $^{(2S+1)}L_J$ where S specifies the total spin angular momentum, L refers to the total orbital angular momentum (S, P, D, F, G, …) and J is the total angular momentum. Since there are numerous combinations in electron associations, the calculation processes for entire all possible spectroscopic term are too tedious except for the ground state term symbol.

To evaluate the ground state term symbol, Hund's rule is applied that the term with the largest spin multiplicity and the largest orbital multiplicity is the lowest in energy. Taking Eu^{III} as example, the largest spin multiplicity is 3 ($m_s = 1/2 \times 6$, M_S = +3, +2, +1, 0, -1, -2, -3, S = 3) while the largest orbital multiplicity is 3 (with M_S = +3, M_L = +3, +2, +1, 0, -1, -2, -3). Therefore, the ground term of Eu(III) is ^7F_J with the overall multiplicity of (2S+1)(2L+1) = 49 while the total angular quantum number are given by L+S, L+S−1, …, |L−S| i.e. 6, 5, 4, 3, 2, 1 and 0. Based on the third rule of Hund's rule, the state with lowest J will be the lowest in energy if the subshell is less than half-filled and the state with highest J on the contrary. The ground state energy level for Eu^{III} is thus $^7F_0$ and the following table summarize ground state term symbol for different trivalent lanthanide.

Ln^{III}	Multiplicity	S	L	J_{max}	J_{min}	Ground term
La^{III} ($4f^0$)	1	0	0	0	0	$^1S_0$
Ce^{III} ($4f^1$)	14	1/2	3	7/2	5/2	$^2F_{5/2}$
Pr^{III} ($4f^2$)	91	1	5	6	4	$^3H_4$
Nd^{III} ($4f^3$)	363	3/2	6	15/2	9/2	$^4I_{9/2}$
Pm^{III} ($4f^4$)	1,001	2	6	8	4	$^5I_4$
Sm^{III} ($4f^5$)	2,002	5/2	5	15/2	5/2	$^6H_{5/2}$
Eu^{III} ($4f^6$)	3,003	3	3	6	0	$^7F_0$
Gd^{III} ($4f^7$)	3,432	7/2	0	7/2	7/2	$^8S_{7/2}$
Tb^{III} ($4f^8$)	3,002	3	3	6	0	$^7F_6$
Dy^{III} ($4f^9$)	2,002	5/2	5	15/2	5/2	$^6H_{15/2}$
Ho^{III} ($4f^{10}$)	1,001	2	6	8	4	$^5I_8$
Er^{III} ($4f^{11}$)	364	3/2	6	15/2	9/2	$^4I_{15/2}$
Tm^{III} ($4f^{12}$)	91	1	5	6	4	$^3H_6$
Yb^{III} ($4f^{13}$)	14	1/2	3	7/2	5/2	$^2F_{7/2}$
Lu^{III} ($4f^{14}$)	1	0	0	0	0	$^1S_0$

Table 1-2: Electronic properties and Ground term of Ln^{III} free ions[4]

1.1.3. Optical Properties of Trivalent Lanthanide Ions

1.1.3.1. Absorption

Due to intraconfigurational $4f^N - 4f^N$ transition (*f-f* transition hereafter), the absorption spectra of the lanthanides show sharp absorption bands in UV and Visible light regions in which the spectra are reported by Prandtl and Scheiner in 1934.[8] The sharp absorption bands are attributed to intraconfigurational *f-f* transition which are parity-forbidden according to Laporte's parity selection rules as the initial and final states share same parity. However, it is relaxed when lanthanide ions are situated in the influence of a ligand field, non-centrosymmetric interaction allow the mixing of electronic state with opposite parity into 4f wavefunctions by crystal-field effect. For

this reason, the transitions become partially allowed and weak absorptions (i.e. molar extinction coefficient < 10 L $mol^{-1}cm^{-1}$) are still observable.

1.1.3.2. Emission

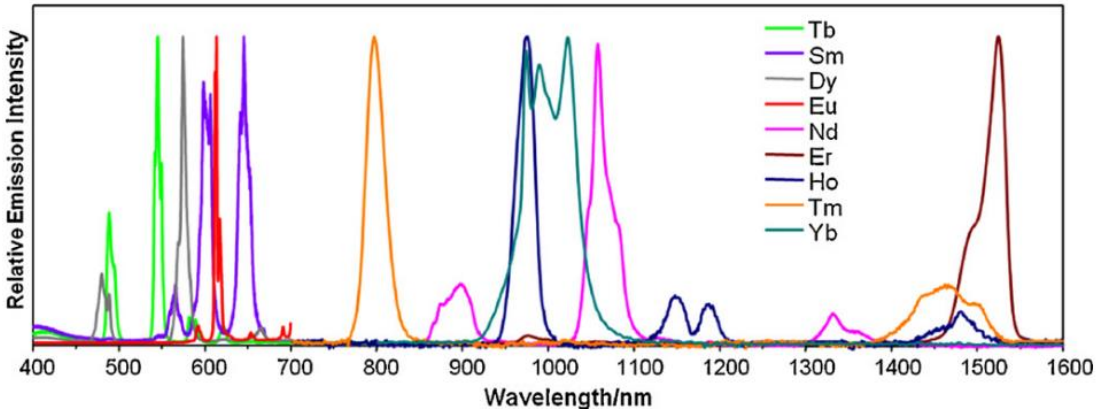

Figure 1-1: Normalized emission spectra of luminescent lanthanide complexes in solution[9]

The trivalent lanthanide ions exhibit unique spectral profile (except La^{III} and Lu^{III}) which cover wide range of spectrum with sharp and narrow bands (UV: Gd^{III}; Visible: Pr^{III}, Sm^{III}, Eu^{III}, Tb^{III}, Dy^{III}; NIR: Nd^{III}, Er^{III}, Yb^{III}). The characteristic sharp emission lines are attributed from well-shield 4f orbitals by Xenon core. The shielding results in weak contribution of 4f orbital in coordination and thus the electron transition involving 4f orbital have less-pronounced effects on nuclear attractions. Since the intranuclear distance in ground state and excited state are similar, the small Stokes shift is resulted.

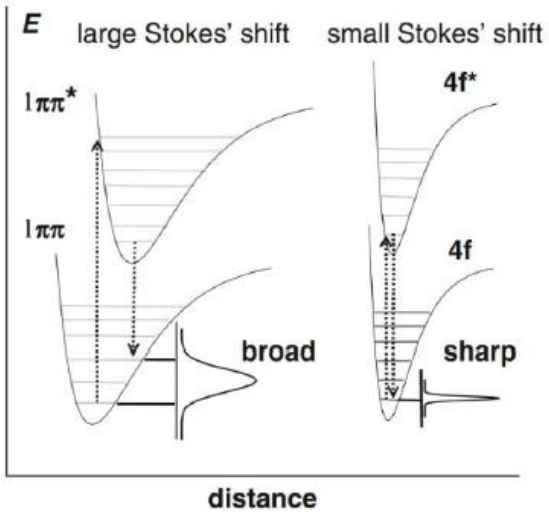

Figure 1-2: illustration of Stokes' Shift for Organic compound (left) and lanthanide ions[1]

In general, the lanthanide lumine-scence is realized by the odd-parity electric dipole (ED), even-parity magnetic dipole (MD) or electric quadrupole (EQ) transitions while the nature of parity can be easily indicated with inversion symmetry. As similar to absorption, both the electric dipole operation and f orbital share same symmetry and thus ED transitions are parity forbidden. When Ln^{III} are situated in ligand field, the mixing of higher configurations would result in mixing of f-orbitals with some d-orbital characters and thus the Laporte-forbidden transitions become partially allowed.[10-12] It is called induced (or forced) electric dipole transition when the oscillator strength of an induced ED transition is around 10^{-4} times of a fully allowed ED transition.

In contrast, MD transition is of even-parity since the rotatory direction is conversed under inversion while zero net dipole moment in EQ mechanisms also results in even-parity. Both MD and EQ transitions are parity-allowed but their intensity is weaker than induced ED (oscillator strength is approximately 10^{-6} and 10^{-10} times of a fully allowed ED transition).[10] In fact, there is no convincing evidence for electric quadrupole transition in lanthanide spectra since they are too weak to be observed. Taking other quantum number in consideration, mathematics of time-dependent perturbation theory is simplified by Judd and Ofelt and the selection rules are shown below.[13,14]

Mechanism	Parity	ΔS	ΔL	ΔJ^a
ED	Odd	0	≤ 6 (2, 4, 6 if J or J' = 0)	≤ 6 (2, 4, 6 if J or J' = 0)
MD	Even	0	0	0, ±1
EQ	Even	0	0, ±1, ±2	0, ±1, ±2

[a] J = 0 to J' = 0 transition are always forbidden

Table 1-3: Selection rules for intra-configurational *f-f* transition

Additionally, some induced ED transitions are hyper-sensitive to minute change in the ligand field environment and sometimes called pseudo-quadrupolar transition as they obey the selection rule for EQ transition.[16] Although the detailed explanations are not given here, a list of experimentally identified hypersensitive transition is presented in **table 1-4**.

Ln	Transition	$\tilde{\nu}$/cm^{-1}	λ/nm
Pr	$^3H_4 \rightarrow {}^3F_2$	5,200	1,920
Nd	$^4I_{9/2} \rightarrow {}^4G_{5/2}$	17,300	578
	$^4I_{9/2} \rightarrow {}^2H_{9/2}, {}^4F_{5/2}$	12,400	806
	$^4I_{9/2} \rightarrow {}^4G_{7/2}, {}^3K_{13/2}$	19,200	521
Sm	$^6H_{5/2} \rightarrow {}^4F_{1/2}, {}^4F_{3/2}$	6,400	1,560
Eu	$^7F_0 \rightarrow {}^5D_2$	21,500	465
	$^7F_1 \rightarrow {}^5D_1$	18,700	535
	$^7F_2 \rightarrow {}^5D_0$	16,300	613
Gd	$^8S_{7/2} \rightarrow {}^6P_{5/2}, {}^6P_{7/2}$	32,500	308
Tb	—[a]	—	—
Dy	$^6H_{15/2} \rightarrow {}^6F_{11/2}$	7,700	1,300
	$^6H_{15/2} \rightarrow {}^4G_{11/2}, {}^4I_{15/2}$	23,400	427
Ho	$^5I_8 \rightarrow {}^3H_6$	27,700	361
	$^5I_8 \rightarrow {}^5G_6$	22,100	452
Er	$^4I_{15/2} \rightarrow {}^4G_{11/2}$	26,400	379
	$^4I_{15/2} \rightarrow {}^2H_{11/2}$	19,200	521
Tm	$^3H_6 \rightarrow {}^1G_4$	21,300	469
	$^3H_6 \rightarrow {}^3H_4$	12,700	787
	$^3H_6 \rightarrow {}^3F_4$	5,900	1,695

[a] None identified positively, but the $^5D_4 \rightarrow {}^7F_5$ transition shows sometimes ligand-induced pseudo-hypersensitivity

Table 1-4: Experimental observed hypersensitive transition for Ln^{III} ions[5,15]

1.1.3.3. Antenna Effect

Despite the unique emission spectral profile of Ln^{III} ions, the direct excitation of Ln^{III} is not ideal due to poor light absorbing ability (i.e., ε < 10 L mol^{-1}cm^{-1}). Chromophores are, therefore, introduced at proximal distance to harvest light as an antenna and the excited energy can be transferred towards Ln^{III}. In general, three different mechanisms

have been summarized for intra-molecular energy transition in Ln^{III} complexes as depicted in **figure 1-3**.

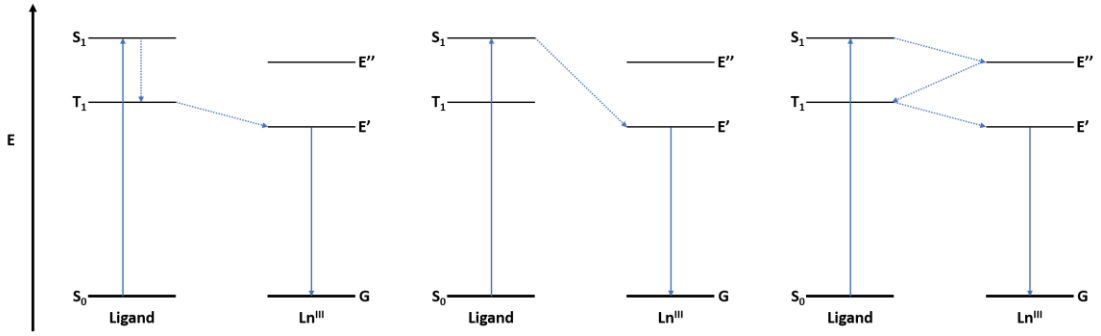

Figure 1-3: A simplified Jablonski diagram depicting the sensitization process. Solid arrows: radiative process; Dotted arrows: non-radiative process; ^{1}S: first singlet excited state; ^{3}T: lowest excited triplet site; A: absorption; F: fluorescence, L: luminescence; NR: non-radiative deactivation; ISC: intersystem crossing; RISC: reserve intersystem crossing; ET: energy transfer; BET: back energy transfer.

In the case of T_1-to-Ln sensitization pathway, ligands are excited to singlet excited state followed by intersystem crossing and energy transfer to Ln^{III} centers for emission. Another pathway refers to direct sensitization from singlet excited state without going through T_1 state. The complex pathway relies on subsequent energy transfer between ligand and lanthanide which ultimately relaxes down to ground emitting level for luminescence. The latter two pathways are beyond the scope of this thesis while the sensitization hereafter will refer to T_1-to-Ln pathway as following simplified Jablonski diagram depicted.

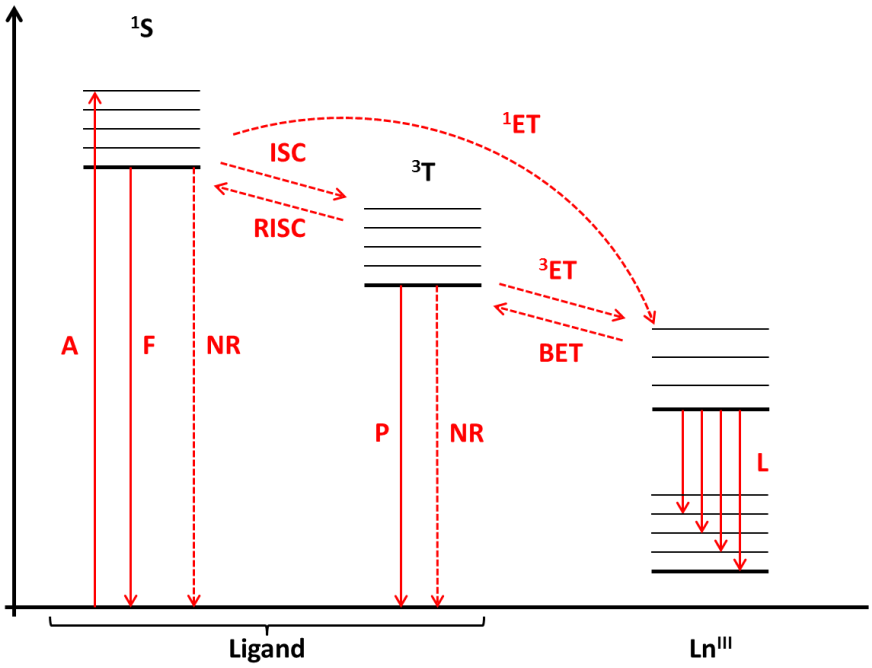

Figure 1-4: A simplified Jablonski diagram depicting the sensitization process. Solid arrows: radiative process; Dotted arrows: non-radiative process; ^{1}S: first singlet excited state; ^{3}T: lowest excited triplet site; A: absorption; F: fluorescence, L: luminescence; NR: non-radiative deactivation; ISC: intersystem crossing; RISC: reserve intersystem crossing; ET: energy transfer; BET: back energy transfer.

In sensitization process, the excitation of chromophore is achieved from the ground state to the excited singlet S_n by absorption of photons. The excited chromophore can possibly undergo fluorescence, thermal relaxation or intersystem crossing (IS) from S_n to the triplet state T_1. Although such S_n-T_1 transition is spin-forbidden, it can be relaxed by spin-orbit coupling by heavy atom effect i.e., Ln^{III}. At this stage, there are three possible energy transfer pathways including reverse intersystem crossing to S_n, phosphorescence and energy transfer to the lanthanide excited states. As stated in Latva's empirical rule, the energy transfer would be favored if the energy gap between T_1 and accepting lanthanide excited state is within the range of 2500 – 4000 cm^{-1}.[1,17]

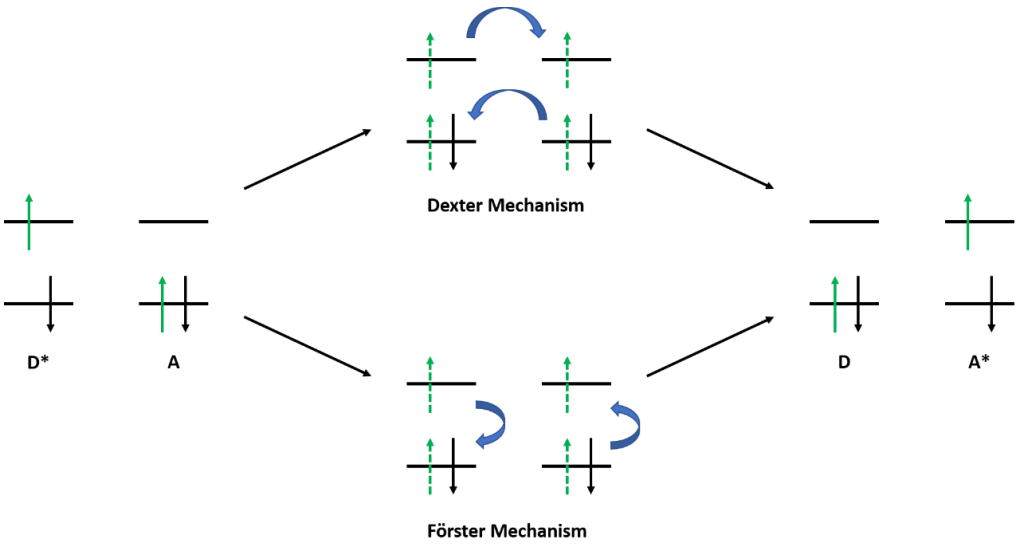

Figure 1-5: The illustrated diagram of Förster and Dexter mechanism mechanisms

In general, the energy transfer between chromophores and Ln^{III} can be achieved by either Dexter or Förster mechanism.[18-23] The double-electron exchange mechanism where an excited electron is transferred from one molecule to second molecule via electron exchange is termed Dexter mechanism. As a result, this mechanism requires good orbital overlapping between chromophore (donor) and Ln^{III} (acceptor) and thus the physical contact at proximal distance is required with the dependence of $e^{(-2r/L)}$. Another mechanism, namely Förster mechanism, are based on "through space" interaction which does not require orbital overlap but the overlap of emission spectrum of donor and the absorption spectrum of acceptor. This process is achieved by the dipole-dipole coupling between chromophore and Ln^{III} where the rate of transfer proportional to r^{-6}.

1.1.3.4. Quantum Yield Measurement

As mentioned previously, the sensitization processes are often involved in lanthanide complexes and thus the calculation of fluorescence quantum yield differs from conventional organic probes. In general, the ordinary fluorescence quantum yields are obtained with equation 1.1 in which the entities responsible for absorbing and emitting photon are essentially identical. However, ligands antennas are often incorporated in lanthanide system such that the quantum yield of lanthanide complexes is given by equation 1.2.

$$\Phi = \frac{\text{number of photons emitted}}{\text{number of photons absorbed}} \quad \text{------ (equation 1.1)}$$

$$Q_L^{Ln} = \eta_{sens} Q_{Ln}^{Ln} \quad \text{------ (equation 1.2)}$$

whereby Q_L^{Ln} and Q_{Ln}^{Ln} are defined as quantum yield from indirect and direct excitation (overall and intrinsic) respectively, while η_{sens} represents the efficiency of energy transfer from ligands to metal ions. The sensitization efficiency depends on two parameters including efficiency of intersystem crossing process and chromophore-to-lanthanide energy transfer. It could be measured experimentally by obtaining both the overall and intrinsic quantum yield or estimated with lifetimes as shown in **equation 1.3**.[3,24,25]

$$\eta_{sens} = \eta_{ISC} \cdot \eta_{et} = \frac{Q_L^{Ln}}{Q_{Ln}^{Ln}} = Q_L^{Ln}\left(\frac{\tau^{rad}}{\tau^{obs}}\right) \quad \text{------ (equation 1.3)}$$

$$\frac{1}{\tau_{rad}} = A_{MD} \times n^3 \times \left(\frac{I_{tot}}{I_{MD}}\right) \quad \text{------ (equation 1.4)}$$

The simplified representation of sensitization efficiency is the rate of radiative relaxation over the rate of overall relaxation.[1,11] Without considering the mathematical derivation, this can be related to observed lifetime and radiative lifetime. The observed

lifetime is typically obtained from measurement while the latter one is calculated through equation 1.4 where A_{MD} is Einstein Coefficient for the MD transition, n is the refractive index and I_{tot} and I_{MD} are the integrated intensity for entire emission profile and MD-transition-leading emission respectively.

As mentioned previously, the quantum yield of lanthanide complexes describes the probability that the excited chromophores are relaxed through energy transfer to lanthanide centers and subsequent lanthanide f-f emission. The quantum yields can be measured by either absolute and relative methods while the former one requires the integrating spheres and latter one compared the result with known standard. The integrating sphere is designed with materials of close to 100% reflectance (barium sulphate or Teflon), thus the emitted light can be fully collected by the detector in both isotropic and anisotropic manner.[26,27]

$$\Phi_X = \Phi_{ST}\left(\frac{m_x}{m_{ST}}\right)\left(\frac{n_x^2}{n_{ST}^2}\right) \text{ ------ } \textbf{(equation 1.5)}$$

The relative methods are generally more common and convenient way to determine the quantum yields while the relationship between the quantum yield of sample and the standard could be calculated by **equation 1.5**. The ideal standard should share same (more overlapped) excitation and emission range with sample to minimize the difference in sensitivity of the spectrophotometer in different spectral range. Meanwhile, it is important to keep all condition including excitation and emission slit the same in all experiments while the absorbance should be kept under 0.1 to avoid the inner-filter effect. In order to validate the result, the cross-checking among

different standards can be performed while the following table lists the literature value and emission range of common standards used in quantum yield measurements.

Standard	Solvent	Literature QY	Emission Range
Quinine sulphate	0.1 M H_2SO_4	0.546	400-600
$Cs_3[Tb(dpa)_3]$	aerated water	0.22	480-670
$Cs_3[Eu(dpa)_3]$	aerated water	0.24	580-690
$[Yb(tta)_3(H_2O)_3]$	Toluene	0.0035	950-1080
$[Ru(bpy)_3]Cl_2$	aerated water	0.028	550-800
	de-aerated water	0.043	550-800

Table 1-5: Common Quantum Yield Standards used in relative quantum yield measurement[28-31]

1.2. Supramolecular Chemistry in Lanthanide Complexes

1.2.1. General Coordination Chemistry in Lanthanide

La	Ce	Pr	Nd	Pm	Sm	Eu	Gd	Tb	Dy	Ho	Er	Tm	Yb	Lu
57	58	59	60	61	62	63	64	65	66	67	68	69	70	71
$4f^0$	$4f^1$	$4f^2$	$4f^3$	$4f^4$	$4f^5$	$4f^6$	$4f^7$	$4f^8$	$4f^9$	$4f^{10}$	$4f^{11}$	$4f^{12}$	$4f^{13}$	$4f^{14}$
103.2	101.0	99.0	98.3	97.0	95.8	94.7	93.8	92.3	91.2	90.1	89.0	88.0	86.8	86.1

Figure 1-6: Ionic radii of Ln^{III} in pm[5]

Along the lanthanide series, the increase in effective nuclear charge (as the atomic number increases) results in a decrease in ionic radii of Ln^{III} which is often termed lanthanide contraction. This high charge density makes Ln^{III} as a highly electropositive Lewis acid. As a hard acid accepter, Ln^{III} interacts preferentially with hard donor (in the order of O > N > S) in non-directional fashion.[32] Hence, the reported coordination number is ranged from 6 to 12 where coordination geometry with CN = 8 or 9 are preferable as a result of steric effects and lanthanide contraction.

Upon ligand complexation, the coordination process mainly contributed from 5d and 6s orbitals due to their large radical expansion while inner 4f electrons are generally considered to be shielded from the coordination environments. Thus, in trivalent lanthanide system, the highly shielded f-orbital electrons have minute participations in bonding and thus the bonding are predominantly ionic in nature. Compared to transition metals, relatively small stabilization energy (~4.18 kJ mol^{-1}) is obtained from ESR spectra and further validate the small contribution in coordinations[33]

1.2.2. Development in Supramolecular Chemistry

1.2.2.1. The Concept of Supramolecular Chemistry

Supramolecular chemistry is the field in chemistry regarding chemical system consisted of a discrete number of molecules which are held together by collection of various weak intermolecular interactions. In contrary to conventional covalent bonding predominated system, supramolecular chemistry emphasizes on weaker and reversible non-covalent interactions such as hydrogen bonding, metal coordination, van der Waals forces, π-π interactions and various hydrophobic interaction.[34-36] In fact, the concept of supramolecular chemistry was originally initiated with small molecules to mimic the naturally existed biological molecules such as enzyme with tiny and specific binding sites.

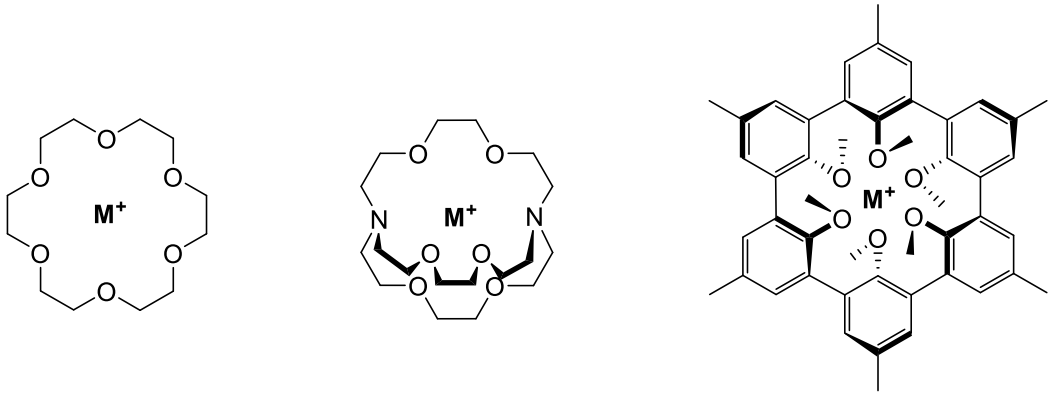

Figure 1-7: Chemical Structure of (left) crown ether (mid) cryptands and (right) spherand hosts

As a pioneering researcher in the field, Pedersan first published the work on synthesizing polyether units which is now named as crown ether.[37] These tiny compounds exhibit excellent binding affinity to alkali metals in which the coordination showed significant differences towards conventional transition metal coordination complexes. With this foundation, the concept was further explored with two pioneering chemists in which bicyclic ether cryptands and host molecules spherands were reported by Lehn and Cram respectively.[38,39] In 1987, these three pioneering chemists were rewarded Nobel Prize in Chemistry for their development of supramolecules with structure-specific interactions of high selectivity to recognize the importance of supramolecular chemistry.

1.2.2.2. Development in Supramolecular Coordination Complexes

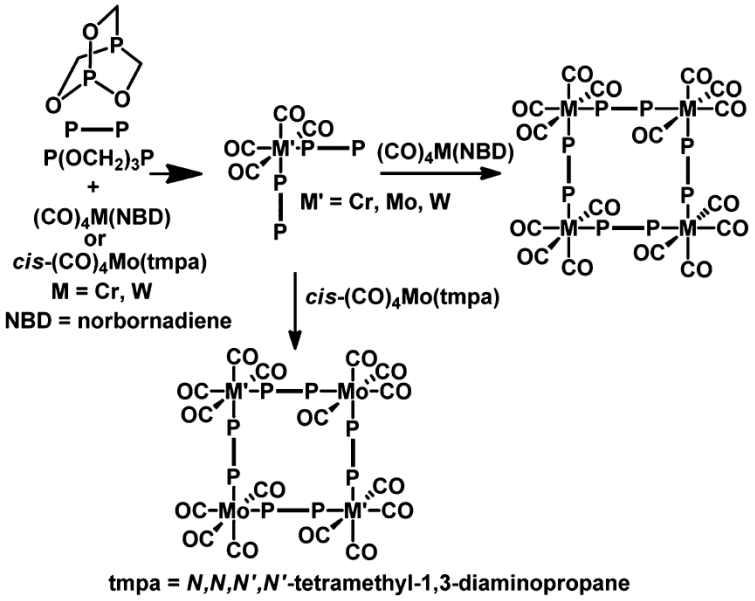

Figure 1-8: The First example of supramolecular coordination complexes (SCCs)[40,41]

In general, supramolecular coordination complexes are discrete architectures typically obtained from mixing metal and organic ligand precursor to afford supramolecular coordination complexes (SCCs). These characteristics compounds utilized metal-ligand coordination bond to synthesize thermodynamically favored complexes.[40] Through mixing diphosphine bridging ligand and transition metal carbonyl precursors, the first example on SCCs was reported to synthesize twenty-member tetranuclear supramolecular square in 1983 by Verkade and co-workers as depicted above.[41]

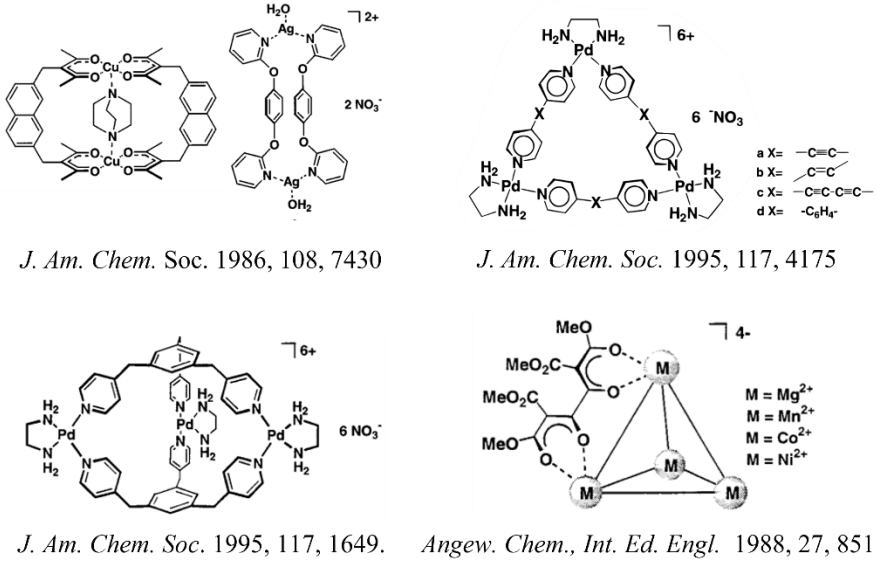

Figure 1-9: Selected early example of supramolecular coordination complexes (SCCs).[42-46]

Soon after, different example of 2D polygon and 3D polyhedral are subsequently reported as shown in **Figure 1-9**.[42-46] With these elegant examples, the field of supramolecular chemistry was rapidly expanded. Prof. Stang and Prof Fujita then reported controlling strategy to systematically construct supramolecular squares.[47,48] In **Figure 1-10**, Prof. Fujita utilized palladium metal precursor with square planar coordination geometry to construct the transition metal square complexes. With this metal precursor, two corners are chelated to diamine while another two are directed to labile nitrates by mixing dipyridine with angularity of 180°, square complexes are resulted. Using similar approaches, Stang utilized hindered phosphine as coordination cap to afford similar structure.[42]

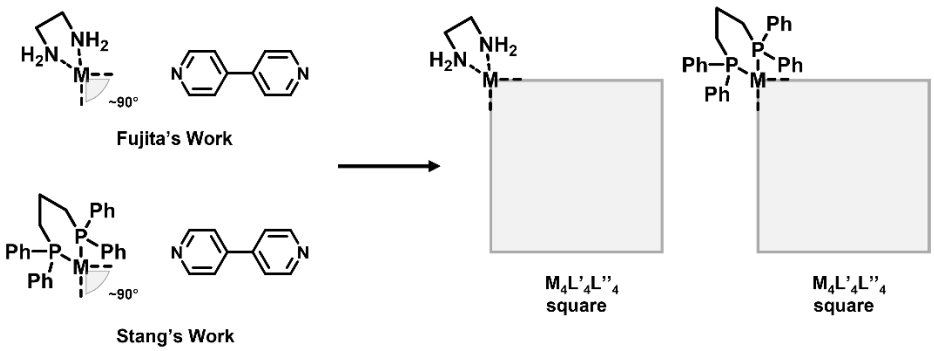

Figure 1-10: graphical illustration on rational design of supramolecular squares[47,48]

With the concept of angularity, Stang and co-workers subsequently proposed "directional bonding" approaches to force the metal coordination in certain direction and developed molecular libraries of 2-fold symmetric subunits.[42,49-54] The subunits are constructed based on two transition metals with square planar coordination geometry. With the incorporation of labile chelator and coordination caps, the directional coordination can be achieved with wide range of angularity ranging from 0 to 180°.

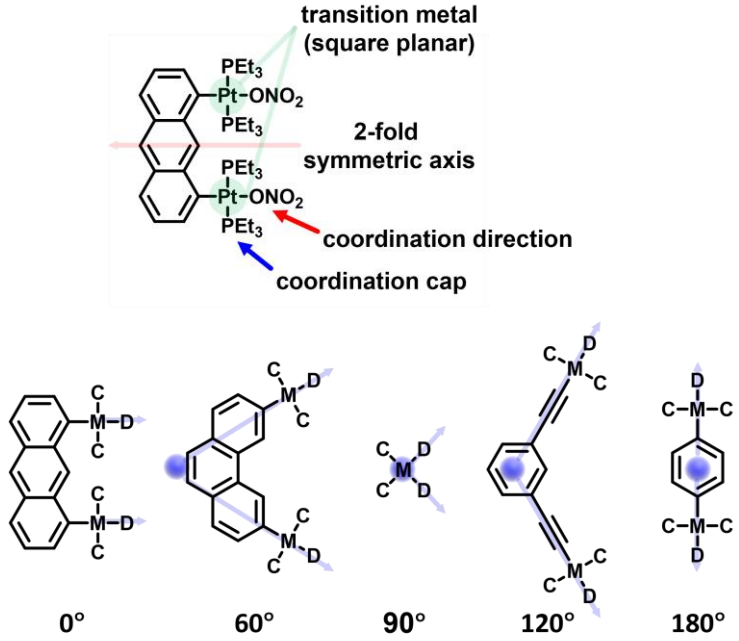

Figure 1-11: The molecular library of 2-fold symmetric subunits.[42,49-54]

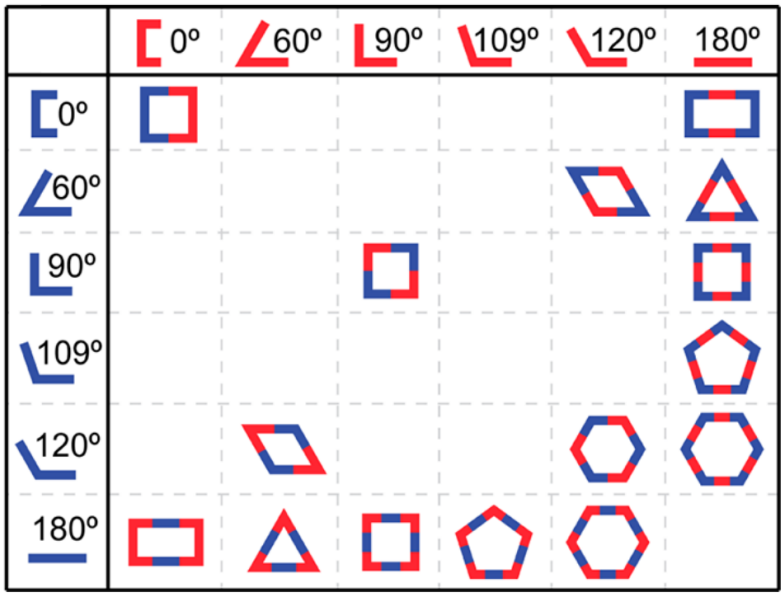

Figure 1-12: The predicted two-dimensional structure from ditopic units[42]

By strategic combination of these ditopic units, different two-dimensional polygons can be systematically constructed. For example, two ditopic subunits with angle of 120° is likely to result hexagon assembly. To expand the scope from two dimensional to three-dimensional system, Stang and co-workers simply increase the connectivity to introduce the driving force of third dimension while the prediction of these three-dimensional polygon are listed in **figure 1-13**.

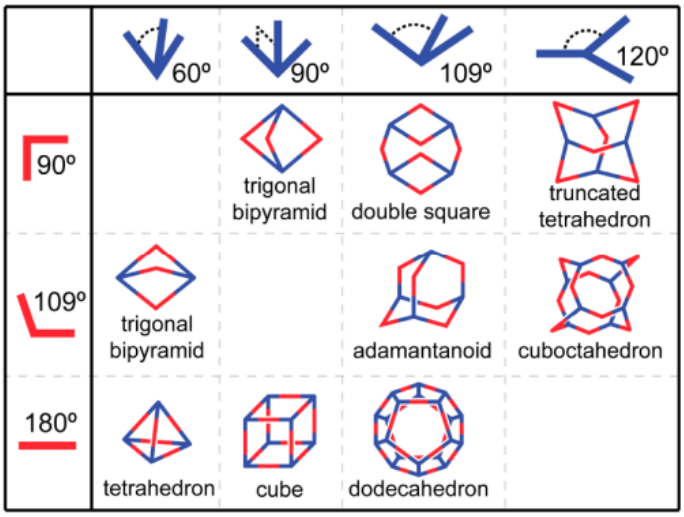

Figure 1-13: The predicted three-dimensional structure from ditopic and tritopic units[42]

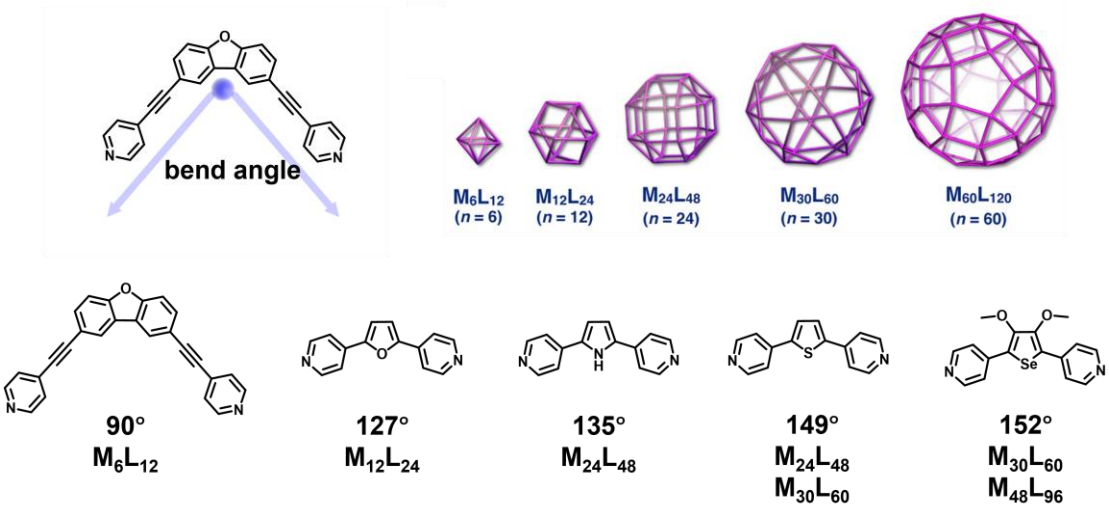

Figure 1-14: Selected examples of SCCs construction using bend angle approaches

Using different strategy, Fujita mainly focused on bend angle modulation to construct higher order M_nL_{2n} transition metal spheres. By mixing metal and ligands with different angularity, different molecular spheres are constructed as depicted in **figure 1-14**. With this foundation, Fujita and co-workers revealed that a clear threshold on bend angle for the formation of different topologies.[55-58] For example, with the bend angle experimental threshold between 131° to 134° showed the transition from $M_{12}L_{24}$ structure to $M_{24}L_{48}$ topologies.

In addition to two mentioned approaches focusing on angularity and directionality, symmetry-interaction approaches are another strategy to construct different supramolecular assemblies.[51] Taking regular transition metal complexes with octahedral geometry as example, each bidentate chelation defines the coordination vector while the summation of coordination vector locate the chelating plane and C_3 rotational axis. The approaching angle is defined as the angle between C_3 rotational axis and the vector that is orthogonal to coordination vector but parallel to two-fold rotational axis of ligands. By varying approaching angle from regular octahedral with

approaching angle of 0° to 35.3°, tetrahedron is likely resulted. Raymond and co-workers utilized this symmetry-interaction approach to successfully construct triple helicate, mesocate and tetrahedron structure.[51]

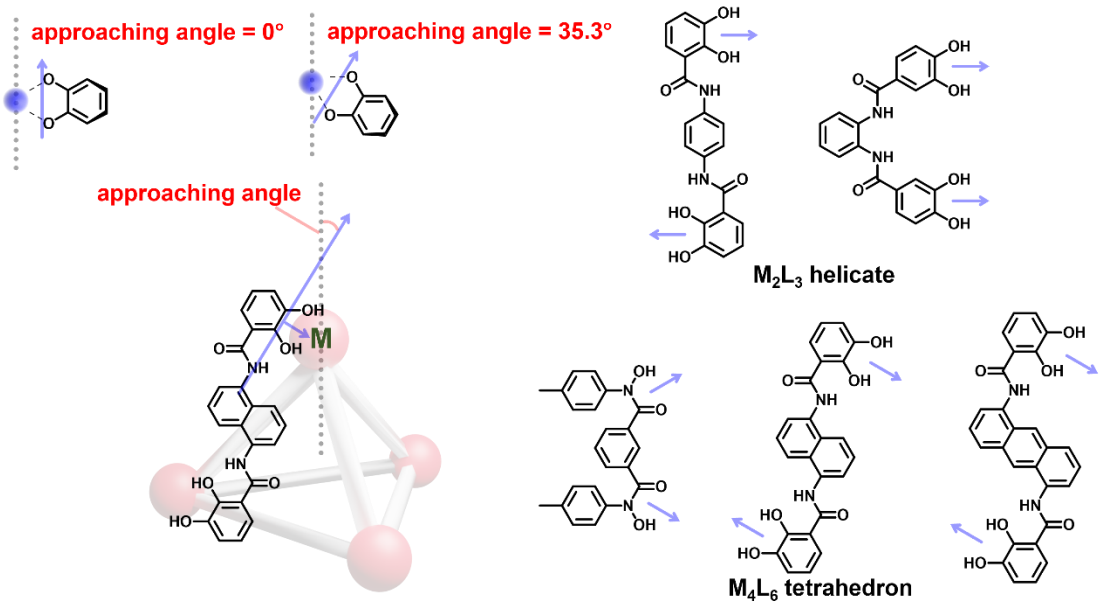

Figure 1-15: Selected examples of SCCs construction using symmetry-interaction approaches.

1.3. Developing Lanthanide luminescence Supramolecular edifices

The trivalent lanthanide coordination systems have attracted much attention with their versatile photophysical properties arising from distinctive 4f-4f transitions. They generally demonstrated line-like and long-lived emission profile which cover wide range of spectrum with excellent tunability. With the introduction of proper chromophore, Ln^{III}-centred luminescence can be effectively sensitized to address intrinsic low-absorption obstacle. Meanwhile, in term of coordination geometry, the Ln^{III} complexes heavily depends on ionic radii and steric factors with flexible coordination numbers and diverse geometries. Despite these characteristic properties,

employing Ln^{III} as luminescent coordination assembly have faced great challenge in enhancing luminescence efficiency and controlling coordination morphology.

1.3.1. Enhancing luminescence efficiency

As already mentioned, the photoluminescence of Ln^{III} complexes is intrinsically forbidden due to the 4f-4f transitions. In contrast with transition metal complexes, the sensitized photoluminescence involves the intersystem crossing and energy transfer to Ln^{III} centres which are basically both spin- and parity-forbidden. Fortunately, the spin-orbit coupling and heavy atom effect relax the spin rule while the mixing of opposite parity upon 4f-5d mixing also partially allows ED transitions.[14, 59] According to equation 1.3, enhancement of luminescence efficiency can be achieved by promoting intersystem crossing, energy transfer and 4f-4f transition with the suppression of non-radiative quenching.

1.3.1.1. Promotion of inter-system crossing and energy transfer to Ln^{III} centers

In lanthanide system, effective energy transfer is usually achieved by excitation of $\pi - \pi^*$ bands of organic chromophores with large absorption coefficients followed by the intersystem crossing and energy transfer to Ln^{III} ions. As already described, these energy transfer processes are generally explained by the Forster and Dexter mechanisms while the energy gap between triplet state of ligands and excited state of Ln^{III} are crucial in photosensitization process.[18-23] According to Latva's empirical rule[17], the energy transfer would be favored if the energy gap between T_1 and accepting lanthanide excited state is within the range of 2500 – 4000 cm^{-1} while the energy back transfers are likely to be observed if it is smaller than 2500 cm^{-1}.[17]

Engineering the triplet state is, therefore, primary approach to promote luminescence efficiency. In general, the introduction of conjugation system will result in dramatic difference in triplet state while electron-withdrawing or donating moieties are responsible for minute changes. Although the ligand design is often based on energy gap modelling, it is also noteworthy that the sensitization process is exceedingly complex with numerous parameters that ligand with similar energy level might result in dramatic change in optical properties.

1.3.1.2. Promotion of 4f-4f transitions

In addition to engineering triple state, promoting 4f-4f transition is another strategy to achieve brighter luminescence. It is evident that the radiative rate constant of f-f transitions is heavily dependent on the geometrical symmetry of Ln^{III} centers in which the transition probabilities have been promoted by introducing asymmetrical geometry.[60] As mentioned previously, the parity selection rule is relaxed via the mixing of non-centrosymmetric characters in ED transitions. It is generally agreed that the ED transition probabilities are enhanced when the coordination lowers the symmetry around the lanthanide and thus alter the radiative f-f transitions. Numerous studies have been conducted to enhance such f-f transitions through manipulating the coordination symmetry such as lowering the symmetry from eight-coordinated square anti-prismatic (D_{4d}) to a dodecahedral (D_{2d}).[60-63] In addition, the decrease in symmetry surrounding Ln^{III} center also results in enhanced luminescence even with same ligands.[64] The phenomena come along with faster radiative f-f transition rate (or shorter lifetime) and thus compete better with non-radiative quenching.

1.3.1.3. Suppression of vibrational quenching

Since Ln^{III} emission is easily de-activated through multiple non-radiative process, suppression of non-radiative quenching is crucial to achieve bright luminescence. Among those non-radiative process, vibrational relaxation is especially effective and thus major concern in enhancing luminescence.[65] The vibration quenching likely to occur when the energy gaps between emissive and ground states of Ln ions couple with the oscillator of chemical bonding ($\nu > 1$). Therefore, chemical bonding with high vibrational frequency i.e., O–H (3600 cm^{-1}), N–H (3300 cm^{-1}) and C–H (2900 cm^{-1}) are common quenchers which result in rapid non-radiative quenching. On the contrary, weaker oscillator such as C=O (1650 cm^{-1}), P=O (1120 cm^{-1}) and O–D (2200 cm^{-1}) can suppress vibration de-activation. Based on this concept, numerous studies have been conducted through replacing oscillator in ligands i.e. deuterated ligands from Hasegawa et. al.[66] and fluorinated ligands from Pikramenous et. al.[67] It is believed that the vibrational quenching can be minimized with a design of rigid metal-ion environment and low-energy vibration in order to protect Ln^{III} ions from solvent interaction.

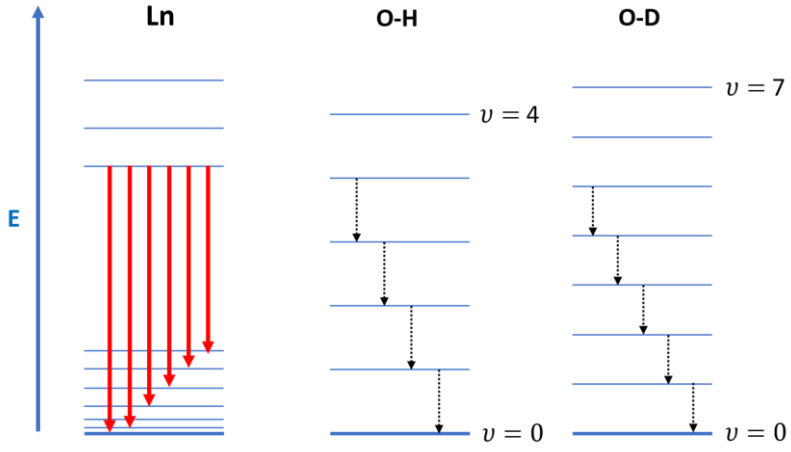

Figure 1-16: Graphical illustration of ΔE between the excited states of Ln^{III} and the next lower state with harmonics of O-H and O-D oscillators

1.3.2. Topological control in lanthanide supramolecular self-assembly

In the development of lanthanide supramolecular chemistry, the first lanthanide helicate was reported by Piguet in 1992.[68] Extensive studies were conducted to investigate different homometallic and heterometallic helical system.[69-71] Sixteen years after, lanthanide-based SCCs was first expanded to 3D polyhedral system in which first lanthanide tetrahedron was reported by Hamacek and co-workers while it took another nine years to realize first edge-directed cubic system.[72-74] More recently, various architectures ranged from two-dimensional polygon, three-dimensional polyhedra and complex helicates have been reported and summarized in few review articles.[75-82]

Although the design principle of transition metal complexes has already been widely studied, the topological formation of lanthanide self-assembly is still in the infancy stage. The coordination chemistry among lanthanide systems significantly differs from well-studied transition metal supramolecular complexes due to their variable angle, coordination number and flexible stereochemical preferences. However, a concrete and comprehensive rational topological controlling scheme has not yet been developed.

1.4. Scope of Thesis

Considering the previously mentioned challenges, this thesis examines the topological control of lanthanide luminescent supramolecular edifices with the investigation on symmetry manipulation and building block synthesis. ***Chapter 2*** is a study of lanthanide self-assembling behaviors through ditopic ligands with different symmetry. In ***chapter 3***, it devises the functionalization of luminescent 1,2-HOPO building block and its

investigation on supramolecular assembling process. ***Chapter 4*** focused on the development of new chiral hydroxyquinoline-based anionic chelator.

1.5. Reference

1. Bünzli, J.-C. G.; Eliseeva, S. V., Basics of Lanthanide Photophysics. In *Lanthanide Luminescence: Photophysical, Analytical and Biological Aspects*, Hänninen, P.; Härmä, H., Eds. **2011**; pp 1-45.

2. Greenwood, N. N.; Earnshaw, A., The Lanthanide Elements (Z = 58–71). In *Chemistry of the Elements*, 2th ed.; Butterworth-Heinemann.: Great Britain **1997**; pp 1227-1249.

3. Eyring, L., Gschneidner, K. A., & Lander, G. H. *Handbook on the physics and chemistry of rare earths*; Elsevier**, 2002**

4. Hänninen, P.; Härmä, H.; Ala-Kleme, T., *Lanthanide luminescence : photophysical, analytical and biological aspects*. Springer: Berlin ; New York, **2011.**

5. Cotton, S. A., *Lanthanide and actinide chemistry*. Wiley: Chichester, England ; Hoboken, NJ, **2006**

6. Eliseeva, S. V.; Bunzli, J. C., Lanthanide luminescence for functional materials and bio-sciences. *Chem Soc Rev* **2010,** *39* (1), 189-227.

7. Huang, C. H.; Bian, Z. Q., Introduction. In *Rare Earth Coordination Chemistry: Fundamentals and Applications*, Huang, C. H., Ed. John Wiley & Sons (Asia) Pte Ltd: Singapore, **2010**; pp 1-39.

8. Evans, C. H., *Biochemistry of the lanthanides*. Plenum Press: New York, 1**990**

9. Uh, H.; Petoud, S. p., Novel antennae for the sensitization of near infrared luminescent lanthanide cations. *Comptes Rendus Chimie* **2010,** *13*, 668-680.

10. Tanner, P. A., Some misconceptions concerning the electronic spectra of tri-positive europium and cerium. *Chem. Soc. Rev.* **2013,** *42* (12), 5090-5101.

11. Tanner, P. A.; Duan, C. K., Luminescent lanthanide complexes Selection rules and design. *Coordin Chem Rev* **2010,** *254* (23-24), 3026-3029.

12. Tanner, P. A. D., C. K., Luminescent lanthanide complexes: Selection rules and design. *Coord. Chem. Rev.* **2010,** *254* (23-24), 3026-3029.

13. Judd, B. R., Optical Absorption Intensities of Rare-Earth Ions. *Phys. Rev.* **1962,** *127*, 750-761.

14. Ofelt, G. S., Intensities of Crystal Spectra of Rare-Earth Ions. *J. Chem. Phys.* **1962,** *37*, 511-520.

15. Binnemans, K., Interpretation of europium(III) spectra. *Coordin Chem Rev* **2015,** *295*, 1-45.

16. Jørgense, C. K. J., B. R., Hypersensitive pseudoquadrupole transitions in lanthanides. *Mol. Phys.* **1964,** *8* (3), 281-290.

17. Latva, M. T., H.; Mukkala, V. M.; Matachescu, C.; Rodríguez-Ubis, J. C.; Kankarea, J., Correlation between the lowest triplet state energy level of the ligand and lanthanide(III) luminescence quantum yield. *J. Lumin.* **1997,** *75* (2), 149-169.

18. Kleinerman, M., Energy Migration in Lanthanide Chelates. *J. Chem. Phys.* **1969,** *51*, 2370-2381.

19. Lamture, J. B. Z., Z. H.; Kumar, A. S.; Wensel, T. G., Luminescence Properties of Terbium(III) Complexes with 4-Substituted Dipicolinic Acid Analogs. *Inorg. Chem.* **1995,** *34* (4), 864-869.

20. Nah, M. K.; Cho, H. G.; Kwon, H. J.; Kim, Y. J.; Park, C.; Kim, H. K.; Kang, J. G., Photophysical properties of near-infrared-emitting Ln(III) complexes with 1-(9-Anthryl)-4,4,4-trifluoro-1,3-butandione (Ln = Nd and Er). *J Phys Chem A* **2006,** *110* (35), 10371-4.

21. Thorne, J. R. G. R., J. M.; Denning, R. G.; Watkins. S. E.; Etchells, M.; Green, M.; Christou, V., Excited State Dynamics of Organo-Lanthanide Electroluminescent Phosphors: The Properties of Tb(tb-pmp)3 and Gd(tb-pmp)3. *J. Phys. Chem. A* **2002,** *106* (16), 4014-4021.

22. Ha-Thi, M. H.; Delaire, J. A.; Michelet, V.; Leray, I., Sensitized emission of luminescent lanthanide complexes based on a phosphane oxide derivative. *J Phys Chem A* **2010,** *114* (9), 3264-9.

23. Rudzinski, C. M. E., D. S.; Hartmann, W. K.; Nocera, D. G., Mechanism for the Sensitized Luminescence of a Lanthanide Ion Macrocycle Appended to a Cyclodextrin. *J. Phys. Chem. A.* **1998,** *102*, 7442-7446.

24. Rilliams, A. T. R. W., S. A.; Miller, J. N. , Relative fluorescence quantum yields using a computer-controlled luminescence spectrometer. *Analyst* **1983,** *108*, 1067-1071.

25. Werts, M. H. V. J., R. T. F.; Verhoeven, J. W. , The emission spectrum and the radiative lifetime of Eu3+ in luminescent lanthanide complexes. *Phys. Chem. Chem. Phys.* **2002,** *4*, 1542-1548.

26. De Mello, J. C. W., F. H.; Friend, R. H, An improved experimental determination of external photoluminescence quantum efficiency. *Adv. Mater.* **1997,** *9*, 230-232.

27. Porres, L.; Holland, A.; Palsson, L. O.; Monkman, A. P.; Kemp, C.; Beeby, A., Absolute measurements of photoluminescence quantum yields of solutions using an integrating sphere. *J Fluoresc* **2006,** *16* (2), 267-72.

28. Zucchi, G. S., R.; Bünzli, J.-C. G., A p-tert-butylcalix[4]arene functionalised at its lower rim with ether-amide pendant arms acts as an inorganic–organic receptor: structural and photophysical properties of its lanthanide complexes. *Dalton Trans.* **2001,** (21).

29. Katsumi, K., Synthesis, Luminescence Quantum Yields, and Lifetimes of Trischelated Ruthenium(II) Mixed-ligand Complexes Including 3,3′-Dimethyl-2,2′-bipyridyl. *Bull. Chem. Soc. Jpn.* **1982,** *55* (9), 2697-2705.

30. Chauvin, A.-S. G., F.; Imbert, D.; Bünzli, J.-C. G., Europium and Terbium tris(Dipicolinates) as Secondary Standards for Quantum Yield Determination. *Spectroscopy*

Lett. **2004,** *40*, 517-532.

31. Meshkova, S. B. T., Z. M.; Bolshoy, D. V.; Beltyukova, S. V.; Tsvirko, M. P.; ; Venchikov, V. Y., Quantum Efficiency of the Luminescence of Ytterbium(III) ß-Diketonates. *Acta Phys. Pol. A* **1999,** *95*, 983-990.

32. Richardson, F. S., Terbium(Iii) and Europium(Iii) Ions as Luminescent Probes and Stains for Biomolecular Systems. *Chemical Reviews* **1982,** *82* (5), 541-552.

33. Jørgensen, C. K., Partly filled shells constituting anti-bonding orbitals with higher ionization energy than their bonding counterparts. In *Rare Earths*, 1975; pp 49-51.

34. Chakrabarty, R.; Mukherjee, P. S.; Stang, P. J., Supramolecular coordination: self-assembly of finite two- and three-dimensional ensembles. *Chem Rev* **2011,** *111* (11), 6810-918.

35. Cook, T. R.; Stang, P. J., Recent Developments in the Preparation and Chemistry of Metallacycles and Metallacages via Coordination. *Chem Rev* **2015,** *115* (15), 7001-45.

36. Young, N. J.; Hay, B. P., Structural design principles for self-assembled coordination polygons and polyhedra. *Chem Commun (Camb)* **2013,** *49* (14), 1354-79.

37. Pedersen, C. J., Cyclic polyethers and their complexes with metal salts. *J. Am. Chem. Soc.* **1967,** *89* (26), 7017-7036.

38. Lehn, J. M., Cryptates: inclusion complexes of macropolycyclic receptor molecules. *Pure & Appl. Chem.* **1978,** *50*, 871-892.

39. Cram, D. J. C. J. M., Host-Guest Chemistry: Complexes between organic compounds simulate the substrate selectivity of enzymes. *Science* **1974,** *183* (4127), 803-809.

40. Cook, T. R.; Zheng, Y. R.; Stang, P. J., Metal-organic frameworks and self-assembled supramolecular coordination complexes: comparing and contrasting the design, synthesis, and functionality of metal-organic materials. *Chem Rev* **2013,** *113* (1), 734-77.

41. Stricklen, P.; Verkade, J., Novel homo and heterometallic coordination macrocycles. *J.*

Am. Chem. Soc. **1983,** *105* (8), 2494-2495.

42. Leininger, S.; Olenyuk, B.; Stang, P. J., Self-assembly of discrete cyclic nanostructures mediated by transition metals. *Chem Rev* **2000,** *100* (3), 853-908.

43. Maverick, A. W., Buckingham, S. C., Yao, Q., Bradbury, J. R., & Stanley, G. G. Intramolecular coordination of bidentate Lewis bases to a cofacial binuclear copper (II) complex. *Journal of the American Chemical Society* **1986** *108*(23), 7430-7431.

44. Fujita, M., Ibukuro, F., Yamaguchi, K., & Ogura, K. A molecular lock. *Journal of the American Chemical Society* **1995** *117*(14), 4175-4176.

45. Fujita, M., Nagao, S., & Ogura, K. Guest-Induced Organization of a Three-Dimensional Palladium (II) Cagelike Complex. A Prototype for" Induced-Fit" Molecular Recognition. *Journal of the American Chemical Society* **1995**, *117*(5), 1649-1650.

46. Saalfrank, R. W., Stark, A., Peters, K., & von Schnering, H. G. The first “adamantoid” alkaline earth metal chelate complex: synthesis, structure, and reactivity. *Angewandte Chemie International Edition in English* **1988**, *27*(6), 851-853.

47. Fujita, M., Yazaki, J., & Ogura, K. Preparation of a macrocyclic polynuclear complex,[(en) Pd (4, 4'-bpy)] 4 (NO3) 8 (en= ethylenediamine, bpy= bipyridine), which recognizes an organic molecule in aqueous media. *Journal of the American Chemical Society* **1990,** *112*(14), 5645-5647.

48. Stang, P. J., & Cao, D. H. Transition metal based cationic molecular boxes. Self-assembly of macrocyclic platinum (II) and palladium (II) tetranuclear complexes. *Journal of the American Chemical Society* **1994**, *116*(11), 4981-4982.

49. Northrop, B. H.; Yang, H. B.; Stang, P. J., Coordination-driven self-assembly of functionalized supramolecular metallacycles. *Chem Commun (Camb)* **2008,** (45), 5896-908.

50 Li, S. S.; Northrop, B. H.; Yuan, Q. H.; Wan, L. J.; Stang, P. J., Surface confined

metallosupramolecular architectures: formation and scanning tunneling microscopy characterization. *Acc Chem Res* **2009,** *42* (2), 249-59.

51. Caulder, D. L.; Raymond, K. N., Supermolecules by Design. *Acc. Chem. Res.* **1999,** *32* (11), 975-982.

52. Fujita, M.; Tominaga, M.; Hori, A.; Therrien, B., Coordination assemblies from a Pd(II)-cornered square complex. *Acc Chem Res* **2005,** *38* (4), 369-78.

53. Gianneschi, N. C.; Masar, M. S., 3rd; Mirkin, C. A., Development of a coordination chemistry-based approach for functional supramolecular structures. *Acc Chem Res* **2005,** *38* (11), 825-37.

54. Oliveri, C. G.; Ulmann, P. A.; Wiester, M. J.; Mirkin, C. A., Heteroligated supramolecular coordination complexes formed via the halide-induced ligand rearrangement reaction. *Acc Chem Res* **2008,** *41* (12), 1618-29.

55. Suzuki, K., Tominaga, M., Kawano, M., & Fujita, M. Self-assembly of an M 6 L 12 coordination cube. *Chemical Communications* **2009**, 13, 1638-1640.

56. Sun, Q. F., Iwasa, J., Ogawa, D., Ishido, Y., Sato, S., Ozeki, T., ... & Fujita, M. Self-assembled M24L48 polyhedra and their sharp structural switch upon subtle ligand variation. *Science* **2010**, *328*(5982), 1144-1147.

57. Harris, K., Fujita, D., & Fujita, M. Giant hollow M n L 2n spherical complexes: structure, functionalisation and applications. *Chemical Communications* **2013,** *49*(60), 6703-6712.

58. Fujita, D., Ueda, Y., Sato, S., Mizuno, N., Kumasaka, T., & Fujita, M. Self-assembly of tetravalent Goldberg polyhedra from 144 small components. *Nature*, **2016**, *540*(7634), 563-566.

59. Judd, B. R., Optical Absorption Intensities of Rare-Earth Ions. *Phys. Rev* **1962,** *127*, 750-761.

60. Harada, T.; Nakano, Y.; Fujiki, M.; Naito, M.; Kawai, T.; Hasegawa, Y., Circularly

polarized luminescence of Eu(III) complexes with point- and axis-chiral ligands dependent on coordination structures. *Inorg Chem* **2009,** *48* (23), 11242-50.

61. Harada, T.; Tsumatori, H.; Nishiyama, K.; Yuasa, J.; Hasegawa, Y.; Kawai, T., Nona-coordinated chiral Eu(III) complexes with stereoselective ligand-ligand noncovalent interactions for enhanced circularly polarized luminescence. *Inorg Chem* **2012,** *51* (12), 6476-85.

62. Miyata, K.; Nakagawa, T.; Kawakami, R.; Kita, Y.; Sugimoto, K.; Nakashima, T.; Harada, T.; Kawai, T.; Hasegawa, Y., Remarkable luminescence properties of lanthanide complexes with asymmetric dodecahedron structures. *Chemistry* **2011,** *17* (2), 521-8.

63. Miyata, K. H., Y.; Kuramochi, Y.; Nakagawa, T.; Yokoo, T.; Kawai, T., Characteristic Structures and Photophysical Properties of Nine-Coordinate Europium(III) Complexes with Tandem-Connected Tridentate Phosphane Oxide Ligands. *Eur. J. Inorg. Chem.* **2009,** *2009* (32), 4777-4785.

64. Shavaleev, N. M. E., S. V.; Scopelliti, R.; Bünzli, J. G., Influence of Symmetry on the Luminescence and Radiative Lifetime of Nine-Coordinate Europium Complexes *Inorg Chem* **2015,** *54*, 9166-9173.

65. Bunzli, J. C.; Piguet, C., Taking advantage of luminescent lanthanide ions. *Chem Soc Rev* **2005,** *34* (12), 1048-77.

66. Hasegawa, Y.; Ohkubo, T.; Sogabe, K.; Kawamura, Y.; Wada, Y.; Nakashima, N.; Yanagida, S., Luminescence of Novel Neodymium Sulfonylaminate Complexes in Organic Media. *Angew Chem Int Ed Engl* **2000,** *39* (2), 357-360.

67. Glover, P. B.; Bassett, A. P.; Nockemann, P.; Kariuki, B. M.; Van Deun, R.; Pikramenou, Z., Fully fluorinated imidodiphosphinate shells for visible- and NIR-emitting lanthanides: hitherto unexpected effects of sensitizer fluorination on lanthanide emission properties.

Chemistry **2007,** *13* (22), 6308-20.

68. Piguet, C.; Williams, A. F.; Bernardinelli, G., The First Self-Assembled Dinuclear Triple-Helical Lanthanide Complex: Synthesis and Structure. *Angew Chem Int Ed Engl* **1992,** *31* (12), 1622-1624.

69. Leonard, J. P.; Jensen, P.; McCabe, T.; O'Brien, J. E.; Peacock, R. D.; Kruger, P. E.; Gunnlaugsson, T., Self-assembly of chiral luminescent lanthanide coordination bundles. *J Am Chem Soc* **2007,** *129* (36), 10986-7.

70. Bocquet, B.; Bernardinelli, G.; Ouali, N.; Floquet, S.; Renaud, F.; Hopfgartner, G.; Piguet, C., The first self-assembled trimetallic lanthanide helicate: different coordination sites in symmetrical molecular architectures. *Chem Commun (Camb)* **2002,** (9), 930-1.

71. Andre, N.; Scopelliti, R.; Hopfgartner, G.; Piguet, C.; Bunzli, J. C., Discriminating between lanthanide ions: self-assembly of heterodimetallic triple-stranded helicates. *Chem Commun (Camb)* **2002,** (3), 214-5.

72. Hamacek, J.; Bernardinelli, G.; Filinchuk, Y., Tetrahedral Assembly with Lanthanides: Toward Discrete Polynuclear Complexes. *Eur. J. Inorg. Chem.* **2008,** (22), 3419-3422.

73 Li, X. Z.; Zhou, L. P.; Yan, L. L.; Yuan, D. Q.; Lin, C. S.; Sun, Q. F., Evolution of Luminescent Supramolecular Lanthanide M2nL3n Complexes from Helicates and Tetrahedra to Cubes. *J Am Chem Soc* **2017,** *139* (24), 8237-8244.

74. Zhao, L.; Qu, S.; He, C.; Zhang, R.; Duan, C., Face-driven octanuclear cerium(IV) luminescence polyhedra: synthesis and luminescent sensing natural saccharides. *Chem Commun (Camb)* **2011,** *47* (33), 9387-9.

75. Yim, K. H.; Yeung, C. T.; Wong, H. Y.; Law, G. L., Structural variation of self-assembled lanthanide supramolecular complexes induced by reaction conditions. *Inorg. Chem. Front.* **2021,** *8* (12), 2952-2964.

76. Wong, H. Y.; Lo, W. S.; Yim, K. H.; Law, G. L., Chirality and Chiroptics of Lanthanide Molecular and Supramolecular Assemblies. *Chem* **2019,** *5* (12), 3058-3095.

77. Barry, D. E.; Caffrey, D. F.; Gunnlaugsson, T., Lanthanide-directed synthesis of luminescent self-assembly supramolecular structures and mechanically bonded systems from acyclic coordinating organic ligands. *Chem Soc Rev* **2016,** *45* (11), 3244-74.

78. Li, X. Z.; Tian, C. B.; Sun, Q. F., Coordination-Directed Self-Assembly of Functional Polynuclear Lanthanide Supramolecular Architectures. *Chem Rev* **2022,** *122* (6), 6374-6458.

79. Lessmann, J. J.; Horrocks, W. D., Jr., Supramolecular coordination chemistry in aqueous solution: lanthanide ion-induced triple helix formation. *Inorg Chem* **2000,** *39* (15), 3114-24.

80. Stomeo, F.; Lincheneau, C.; Leonard, J. P.; O'Brien, J. E.; Peacock, R. D.; McCoy, C. P.; Gunnlaugsson, T., Metal-directed synthesis of enantiomerially pure dimetallic lanthanide luminescent triple-stranded helicates. *J Am Chem Soc* **2009,** *131* (28), 9636-7.

81. Lincheneau, C.; Peacock, R. D.; Gunnlaugsson, T., Europium directed synthesis of enantiomerically pure dimetallic luminescent "squeezed" triple-stranded helicates; solution studies. *Chem Asian J* **2010,** *5* (3), 500-4.

82. Kotova, O.; Comby, S.; Pandurangan, K.; Stomeo, F.; O'Brien, J. E.; Feeney, M.; Peacock, R. D.; McCoy, C. P.; Gunnlaugsson, T., The effect of the linker size in C2-symmetrical chiral ligands on the self-assembly formation of luminescent triple-stranded di-metallic Eu(iii) helicates in solution. *Dalton Trans* **2018,** *47* (35), 12308-12317.

Chapter 2: Topological Formation of Supramolecular Assembly from Ditopic Ligands

2.1. Introduction

2.1.1. Background

With the unique properties and potential application in lanthanide system, high order polynuclear lanthanide supramolecular assembly have attracted raising attention over the past decades.[1-6] With the effort of pioneering researcher, the construction of different complex supramolecular edifices including two-dimensional polygon, three-dimensional platonic solids[1,2,8,9] and complex helicates[10,11] have been realized. These sophisticated examples have initiated the investigation on the relationship between ligand and ultimate topology while various scholar have proposed different terminologies such as ligand symmetry, offsetting properties, metal size and templating effects.[1,4,5,12]

Supramolecular self-assembly are known to be a collective result from various weak non-covalent interactions while the metal-to-ligand interaction obviously contributes as major driving force in such complex architectures in providing both thermodynamic stability and predetermined coordination preferences.[13, 14] With examples of transitional metal supramolecular assemblies, Raymond and co-workers have postulated the symmetry-directed approaches to construct the formation of metal-organic supramolecular assemblies via manipulation on offsetting properties between the chelating units and metal centers.[14,15]

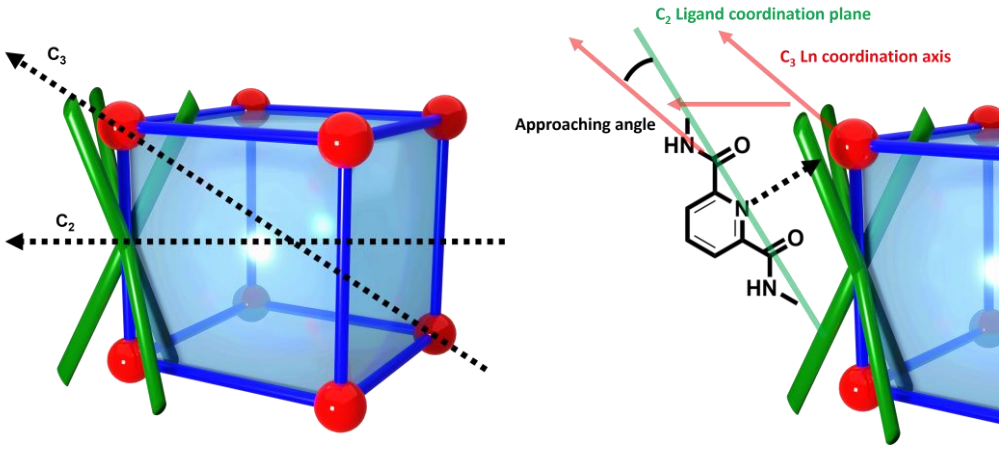

Figure 2-1: Illustration on geometrical consideration in regular O_h cubic structure

Taking regular edge-directed cubic cages as demonstration, the cubic assembly adopts regular O_h cubic symmetry while it must contain four C_3 rotational axis spanning vertices of the cubic assembly and six C_2 rotational axis across the center of each ligand edge. Meanwhile, the symmetry and approaching angle in pre-engineered ligand have provided coordination orientation and stoichiometric preferences to guide the final topology of metal-organic cluster These rationales have governed the foundation in developing strategic formation of higher-order supramolecular edifices in which higher-order structure generally require more symmetrical requirements.

As a pioneering work in polynuclear lanthanide supramolecular system, Piguet and Bünzli have contributed a leading role in developing lanthanide helical system.[16-19] With a series of C_2-symmetric benzimidazole-pyridine based chelating units and flexible V-shaped spacer, first dinuclear triple-helical lanthanide self-assembly $\mathbf{Eu_2(R_1)_3}$ was reported in 1992.[16] Through selected metal-to-ligand stoichiometry, europium(III) ions was coordinated with six N atoms from benzimidazole unit and another three N atoms from pyridine moiety to afford stable pseudo tricapped trigonal prism geometry. With the support of ESI-MS and absorption spectroscopy, it is postulated that the

construction of triple-stranded helicates is originated from a stepwise self-assembling process through LnL_2, Ln_2L_2 to Ln_2L_3 while the high concentration and stoichiometry of ligand promote the formation of thermodynamically stable $\mathbf{Eu_2(S_1)_3}$ triple-stranded helical structure.[20, 21]

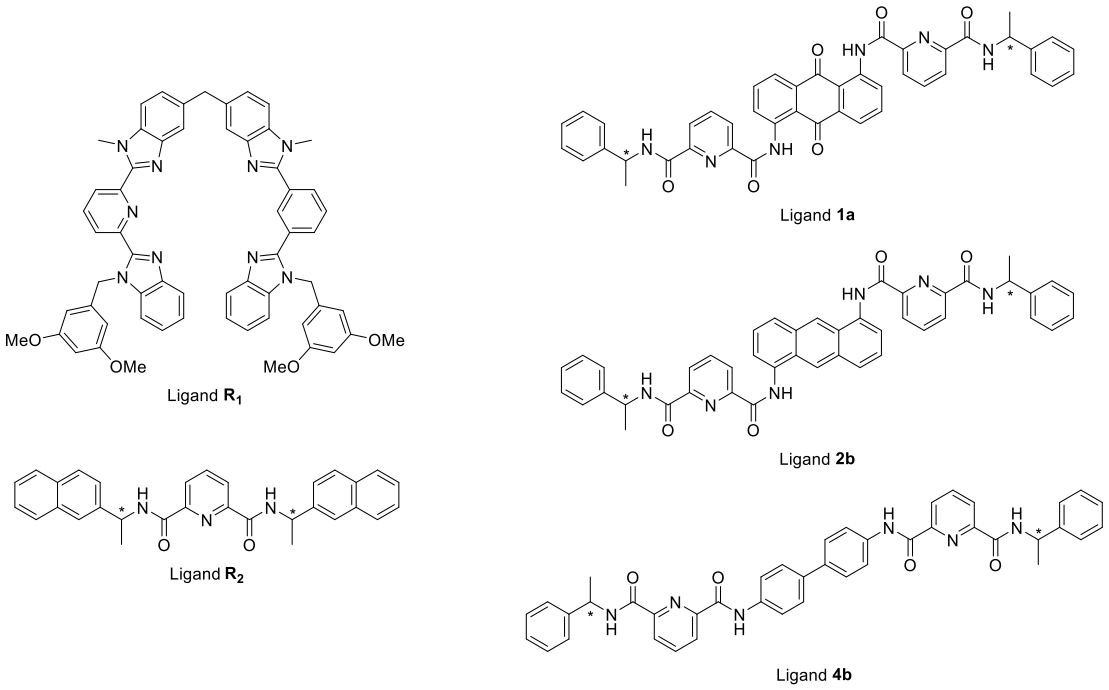

Figure 2-2: selected example of ditopic ligand

In addition to these benzimidazole-pyridine based ligand, 2,6-pyridnedicarboxamide (pcam) are another common chelating unit for lanthanide coordination which allow incorporation of chiral moiety.[5, 22-24] The first X-ray structure $\mathbf{Eu_2(L_{4b})_2}$ was reported by Law sevens year after the preceding example in chiral pcam-based helicate $\mathbf{Eu_2(R_2)_3}$.[25] With the combination of chiral pcam-based chelating with rigid non-twisting spacer, diastereoselective and non-diastereoselective supramolecular formation behaviors of bimetallic triple-stranded helicate were realized through extending the point chirality from lanthanide coordination sphere.

Not soon after, two groundbreaking examples on lanthanide supramolecular tetrahedral and cubic structures were reported independently. Law and Sun utilized the offsetting properties of different rigid ligand $\mathbf{L_{1a}}$ and $\mathbf{L_{2b}}$ to realize the formation of thermodynamically stable supramolecular edifices.[1, 2] Both findings have acknowledged the important of offsetting properties of ligands and their correlation with the ultimate topologies of metal assembly. In Sun's work, it is claimed that the offsetting distance dictated the final outcomes of the lanthanide assembly, ranging from Ln_2L_3 helicates and Ln_4L_6 tetrahedron to Ln_8L_{12} cubes. Meanwhile, the author also emphasized on the formation of helicate/tetrahedron mixture from "borderline case" ligands.

More recently, Law reported helicate-tetrahedron transformation with similar type of pcam-based ligands. Through systematic variation of spacing distance, ligand spacing with one to three phenyl rings have been reported. Helicate-to-tetrahedron evolution is achieved by simply shortening the spacing distance without varying offsetting distance. With the sufficiently short linker, thermodynamically disfavored tetrahedron can be resulted by concentration effects through crystallizations. In the investigation, the dependence on ionic radii towards pcam-based ligands are also observed that lanthanide with smaller ionic radii is better accommodated and affording more stable structure. These finding established the new era of lanthanide supramolecular chemistry and more sophisticated lanthanide polygon and polyhedra have been reported recently.[5, 8]

With these elegant examples of different topological edifices, it consolidates the ideas on employing symmetry-interaction approaches in transition metal supramolecular chemistry to lanthanide system. It is a clear indication that the offsetting properties and flexibility of ligands have played a critical role in constructing the polynuclear lanthanide complexes. In general, an ideal spacer should provide sufficient rigidity to govern the offsetting properties to guide the formation of entropically disfavored topologies. At the same time, moderate flexibility provides higher thermodynamically stability and empower the twisting behavior of ligands. However, the correlation between the offsetting properties and rigidity in ditopic ligand and ultimate topologies have not yet been comprehensively studied in lanthanide system. Considering this problem, this chapter aims to investigate the interrelation between supramolecular self-assembling behaviors and different offsetting properties and symmetry.

2.1.2. Scope of study

In this chapter, a series of pcam-based ligands were compared for their offsetting properties, spacing distance and rigidity as depicted in figure **2-3**. To investigate the lanthanide contraction, different metal ions were also employed ranged from early lanthanide to late lanthanide (La, Sm, Eu, Gd, Lu) and synthesized complexes were studied with mass and NMR spectroscopy while the crystallographic and photophysical properties were also investigated whenever possible. In addition, The phenomenon of helicate-to-polyhedra transformation of synthesized complexes were also studied.

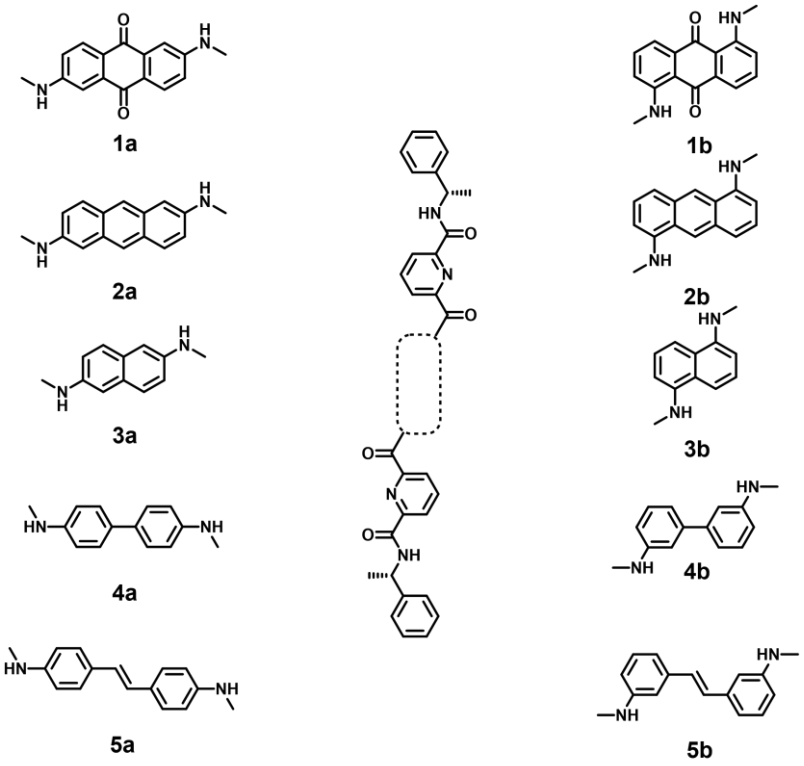

Figure 2-3: Summary of compound in *Chapter 2*

2.2. Result & Discussion

2.2.1. Design Rationale

Based on preceding literature, each structural similar spacing units are further derived into two different offsetting angles. For instance, anthracene-2,6-diamine (1a) and anthracene-1,5-diamine (1b) are categorized into same anthracene-based linker while pcam-chelating unit were retained for detailed comparison. To correlate the spacing unit and ultimate topologies, these spacing units are generally categorized into three groups which include (1) opposing pseudo-C_2, (2) offsetting pseudo-C_{2v} symmetric and (3) non-offsetting pseudo-C_{2h} symmetric, symmetric spacing units as depicted in **Figure 2-4.** Due to the unique structure of spacer 4b, two simulated structures will be resulted based on the orientation of amine periphery group.

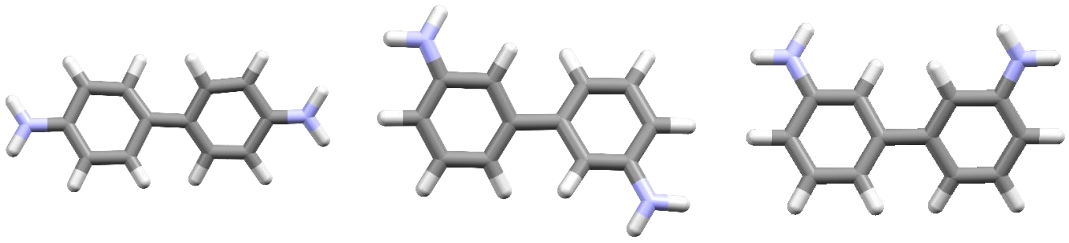

4a (opp-C_2) 4b-1 (C_{2v}) 4b-2 (C_{2h})

Figure 2-4: illustration of three different group of spacing units

2.2.2. Synthesis & Characterization

2.2.2.1. Synthesis of Ligand

According to reported procedure, the chiral peripheral arm (S)-1-phenylethylamine is first coupled with dipicolinic acid. Upon standard HATU amide coupling, the resulting dipicolinic chelating units are coupled with corresponding spacer **1a-4a**, **1b-2b** to prepare corresponding ligands. The spacer 2a, 2b, 3-4a are prepared by reduction or palladium-catalysed amination while spacer 5b was synthesized with 5-steps Wittig reaction. The synthesized intermediates and ligands are characterized with ^{1}H NMR, ^{13}C NMR and ESI-HRMS whenever possible and detailed characterization are provided in section 2.4.

2.2.2.2. Synthesis of Complexes

The complexations are performed in pure acetonitrile or mixture of acetonitrile/ methanol (4:1) with lanthanide triflate (La, Sm, Eu, Gd, Lu) at reflux temperature under the concentration of 2.5 mM unless specified otherwise. Upon overnight reaction, the resulting solution was concentrated with compressed air followed by precipitation with diethyl ether. The obtained precipitates are washed with diethyl ether to afford

pure complexes. All the complexes are characterized with ^{1}H NMR, ^{1}H-^{1}H COSY NMR, ^{13}C NMR ESI-MS, elemental analysis whenever possible.

2.2.2.3. Characterization of Complexes

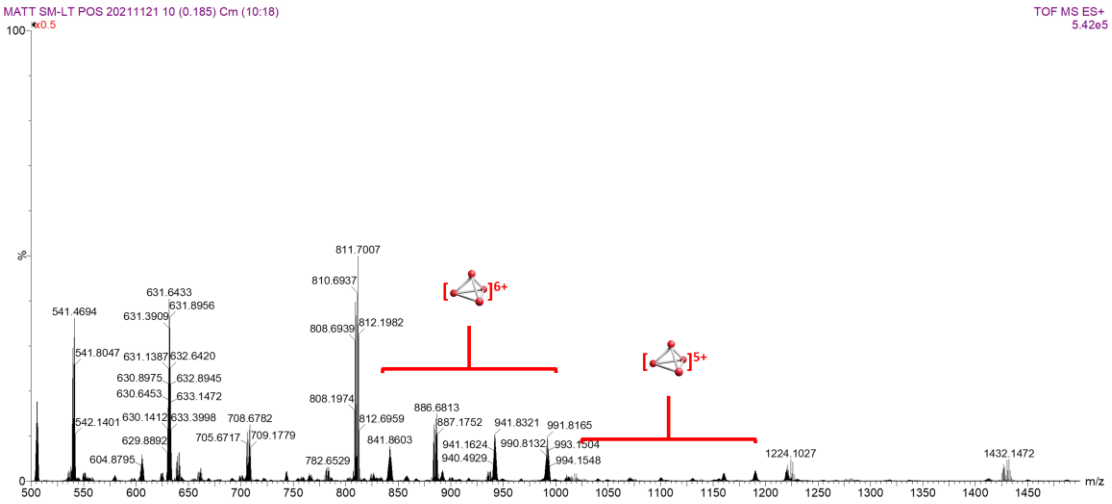

Spectrum S2-1: ESI-HRMS spectrum of **SmL_{1a}**

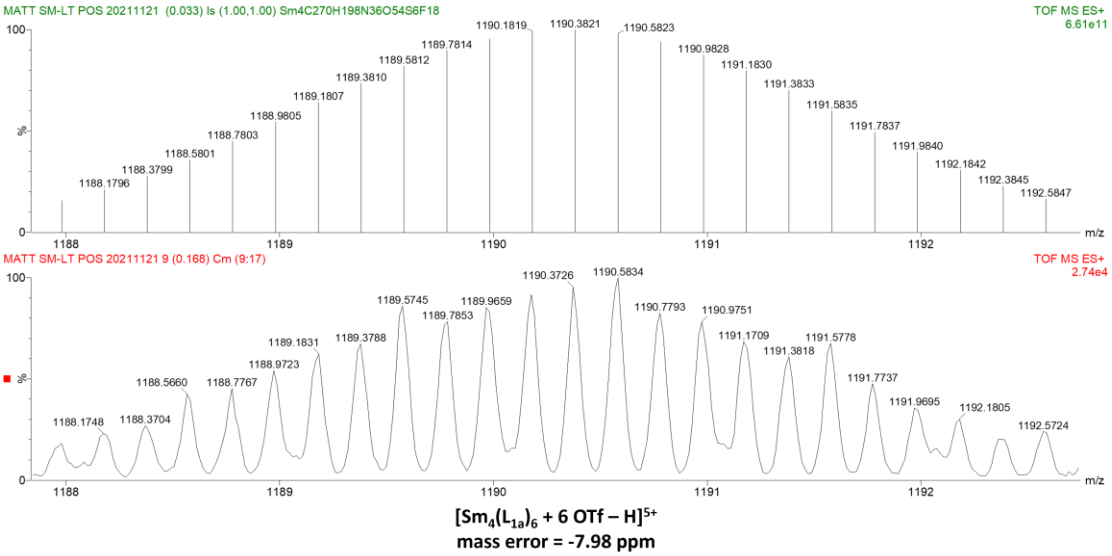

Spectrum S2-2: isotopic distribution of selective ion species in **SmL_{1a}**

Complex LnL_{1a}. To characterize the complexes, NMR spectroscopy was performed to confirm formation of single species in both ligand system. However, NMR

spectroscopic data is not conclusive which is likely attributed from C=O rich environments which allow extra hydrogen bonding formation and interaction to metal sphere. As anticipated with the previous publication, complexation of L_{1a} afford tetrahedral cages in which characteristic ion peak $[Ln_4(L_{1a})_6 + x\ OTf - y\ H]^{n+}$ (Ln = Sm, Eu and Lu, n = 4 & 5, x & y is variable) as depicted in spectrum **S2-1** and **S2-2** while other characterization data are summarized in appendix section.

Complex LnL_{1b}. To characterize the complexes, NMR spectroscopy was performed while non-conclusive data is obtained due to C=O rich environment and intramolecular hydrogen bonding. Therefore, the characterization of complexes LnL1b mainly replies on HRMS spectrum. As shown in S2-3 and S2-4, the complexes are likely to be in helicates form in which the characteristic ion peaks are denoted as depicted while the other characterization data for europium and lutetium are attached in appendix section.

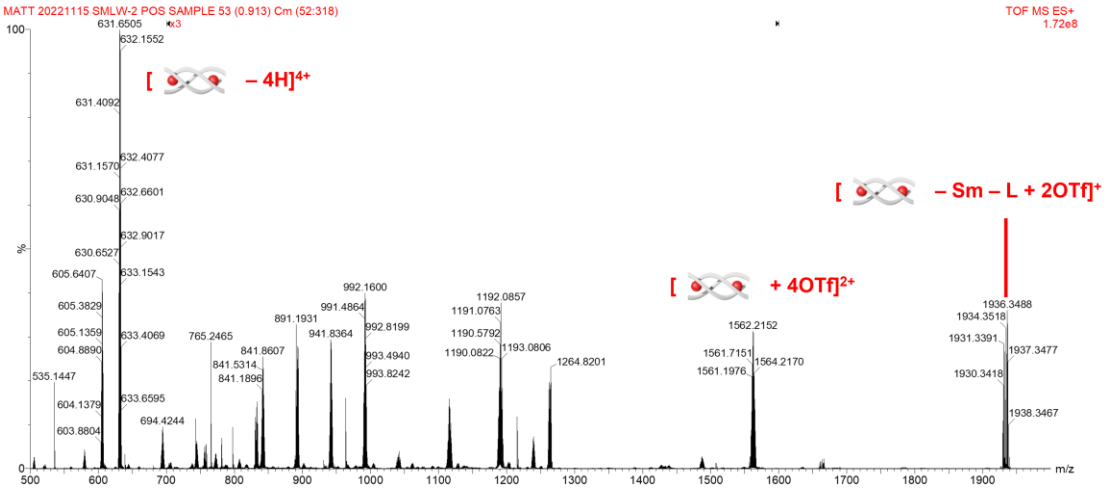

Spectrum S2-3: ESI-HRMS spectrum of **SmL_{1b}**

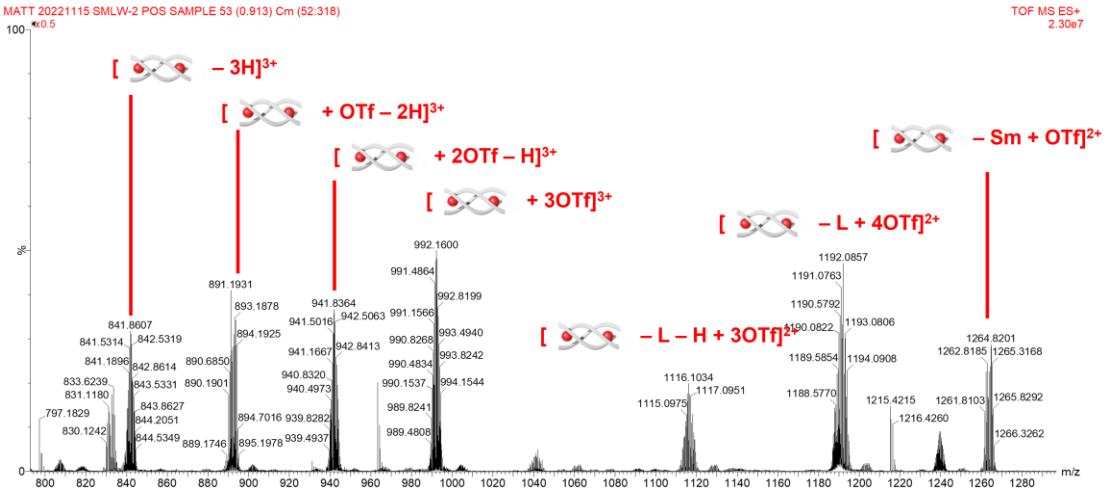

Spectrum S2-4: expanded ESI-HRMS spectrum of **SmL_{1b}**

Compared to other complexes of pcam ligands, the spectrum shows a significant amount of dissembling species including $[LnL1b - Sm]^{m+}$ and $[LnL1b - L]^{m+}$ species which indicates the instability of resulting complexes while it is likely attributed from the intermolecular hydrogen bonding.

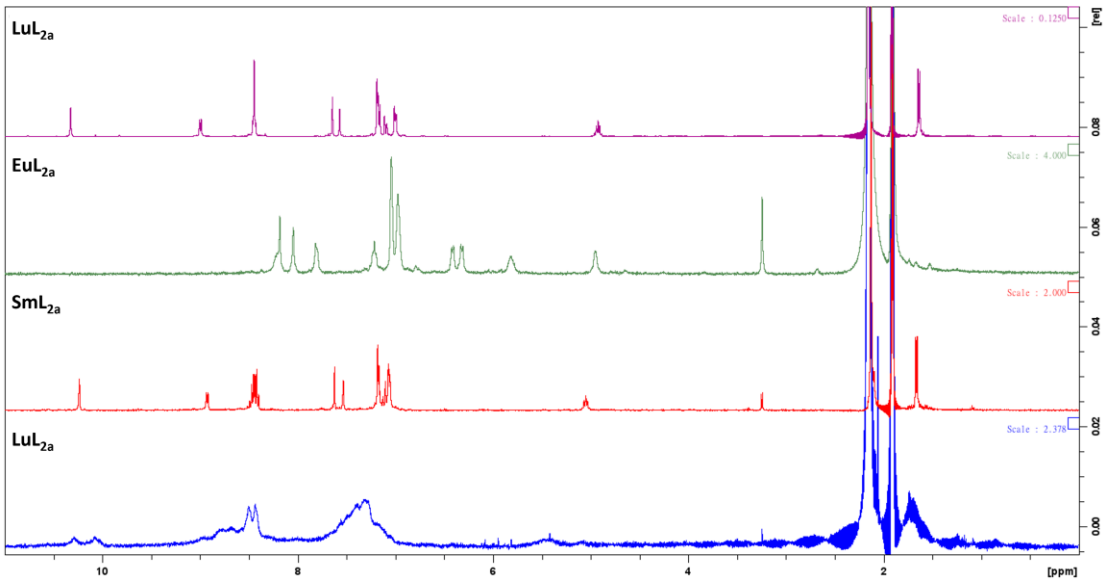

Spectrum S2-5: Stacked ^{1}H NMR spectrum of Complex LnL_{2a}

Complex LnL_{2a}. With the NMR spectroscopy, it is evident that only single species of supramolecular structures are resulted from the complexation of Sm^{III}, Eu^{III} and Lu^{III}

metal while unknown species are formed for **LaL_{2a}** as shown in spectrum **S2-5**. In general, **SmL_{2a}** and **LuL_{2a}** has demonstrated similar pattern while paramagnetic shift was observed in EuL_{2a}. With the aid of ^{1}H-^{1}H COSY NMR spectrum (**S2-7**), the proton N**H**$_i$ can be assigned at approx. 5 ppm as it demonstrates correlation between the chiral C**H**$_j$. meanwhile, other protons on pcam chelating unit i.e. **H**$_{e-h}$ are also influenced by the paramagnetic field of europium and resulting in upfielding shift. Through similar manner, the proton assignment of other **LnL_{2a}** complexes were also conducted and included in **S2-61** to **S2-67**.

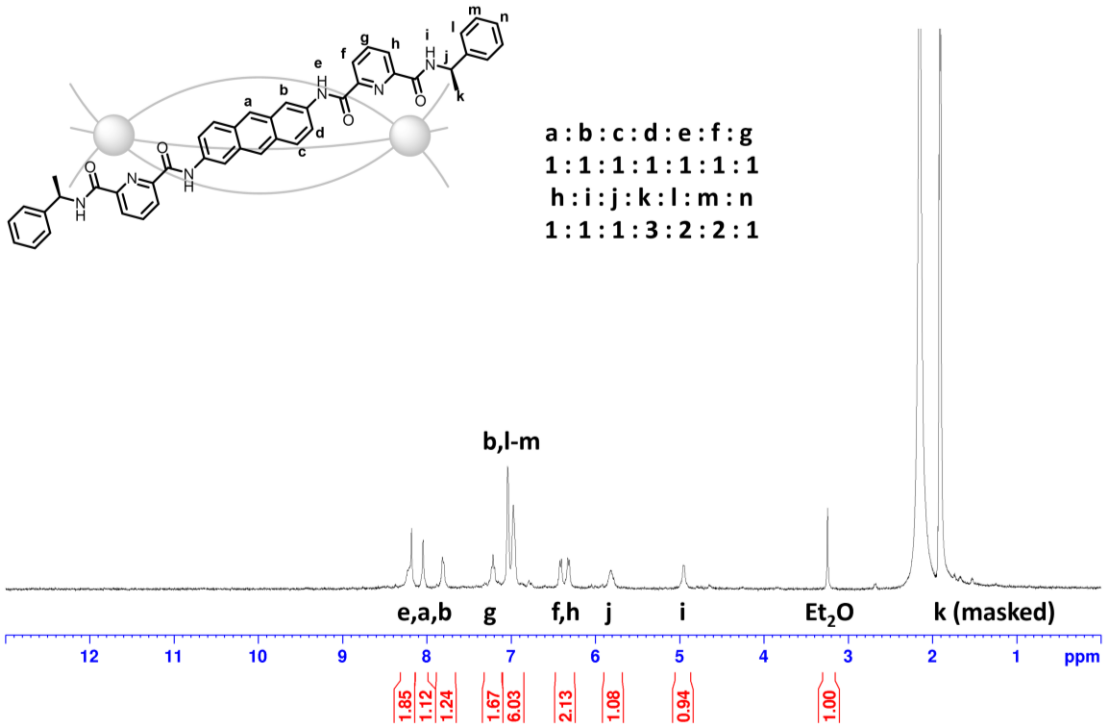

Spectrum S2-6: ^{1}H NMR spectrum of **EuL_{2a}**

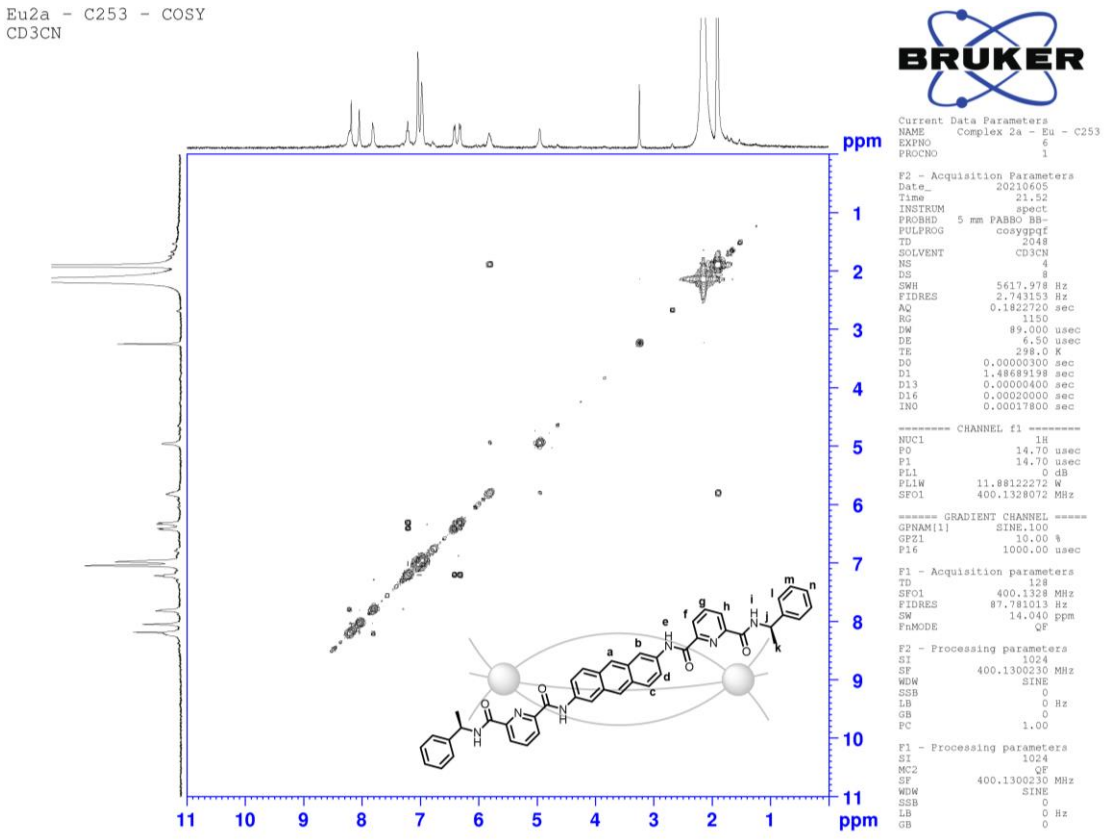

Spectrum S2-7: ^{1}H-^{1}H COSY NMR spectrum of **EuL$_{2a}$**

With the confirmation of single species, ESI-HRMS have identified the helical conformation with $[Ln_2(L_{2a})_3 + x\ OTf - yH]^{n+}$ species (Ln = Sm, Eu, Gd and Lu, n = 3-5, x & y = variable) while no other species were identified from the obtained complexes. As complex **LaL$_{2a}$** show no conclusive information in both MS and NMR analysis, unstable coordination complexes are likely formed.

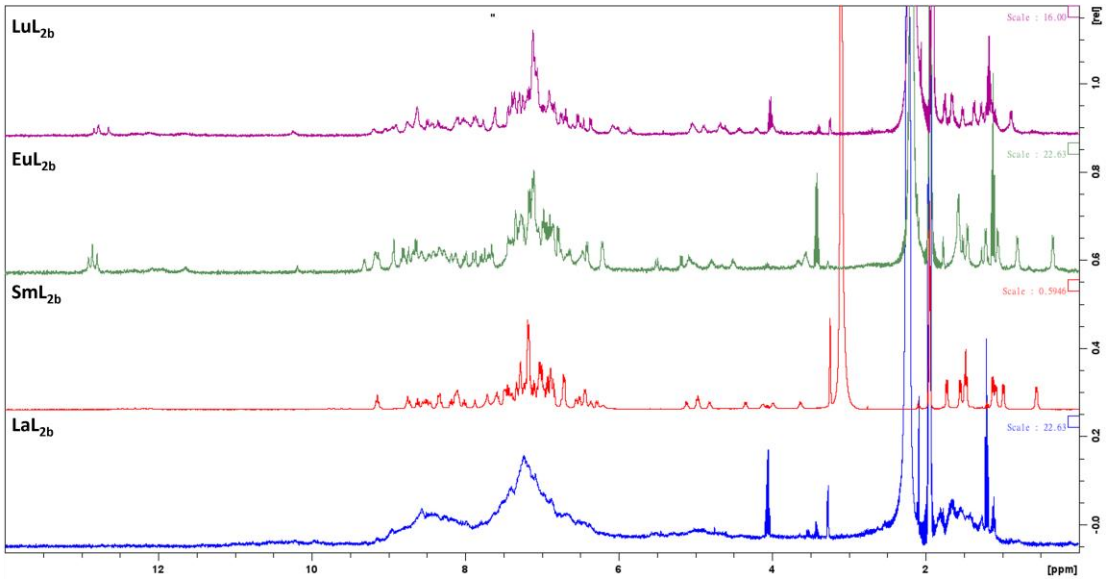

Spectrum S2-8: Stacked ^{1}H NMR spectrum of Complex **LnL$_{2b}$**

Complex LnL$_{2b}$. In analogy to complex **LnL$_{2a}$**, spectrum **S2-8** showed the uniform pattern in ^{1}H NMR spectrum from samarium to lutetium in our complexation system. The complex pattern in NMR possibly infers the existence of higher order asymmetric structure. The detailed proton assignment on aromatic regions is not feasible due to overlapped signal while only **SmL$_{2b}$** demonstrates clear isolation within individual signal in aliphatic regions. The combination of ^{1}H NMR and ^{1}H-^{1}H COSY NMR reveals that there are seven different set of non-identical proton environment (denoted as square and circle with different colors) in a ratio of approx. 1 : 3 with twenty-four -C**H**CH$_3$ and seventy-two -CHC**H$_3$** protons.

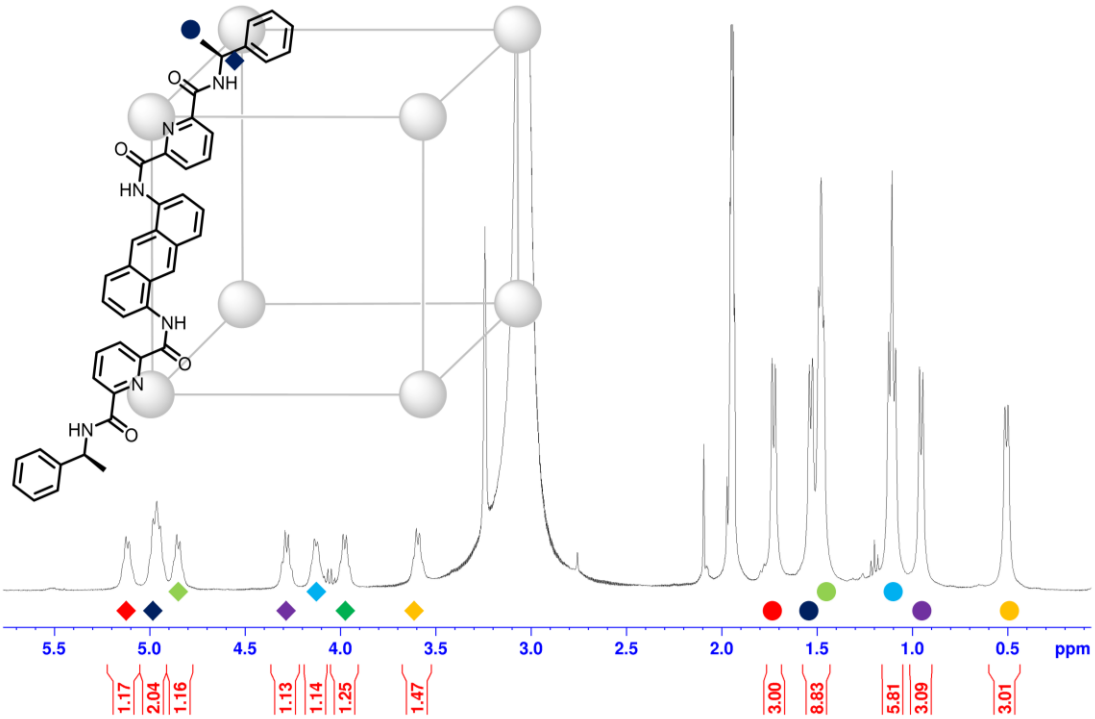

Spectrum S2-9: ^{1}H NMR spectrum of **SmL$_{2b}$**

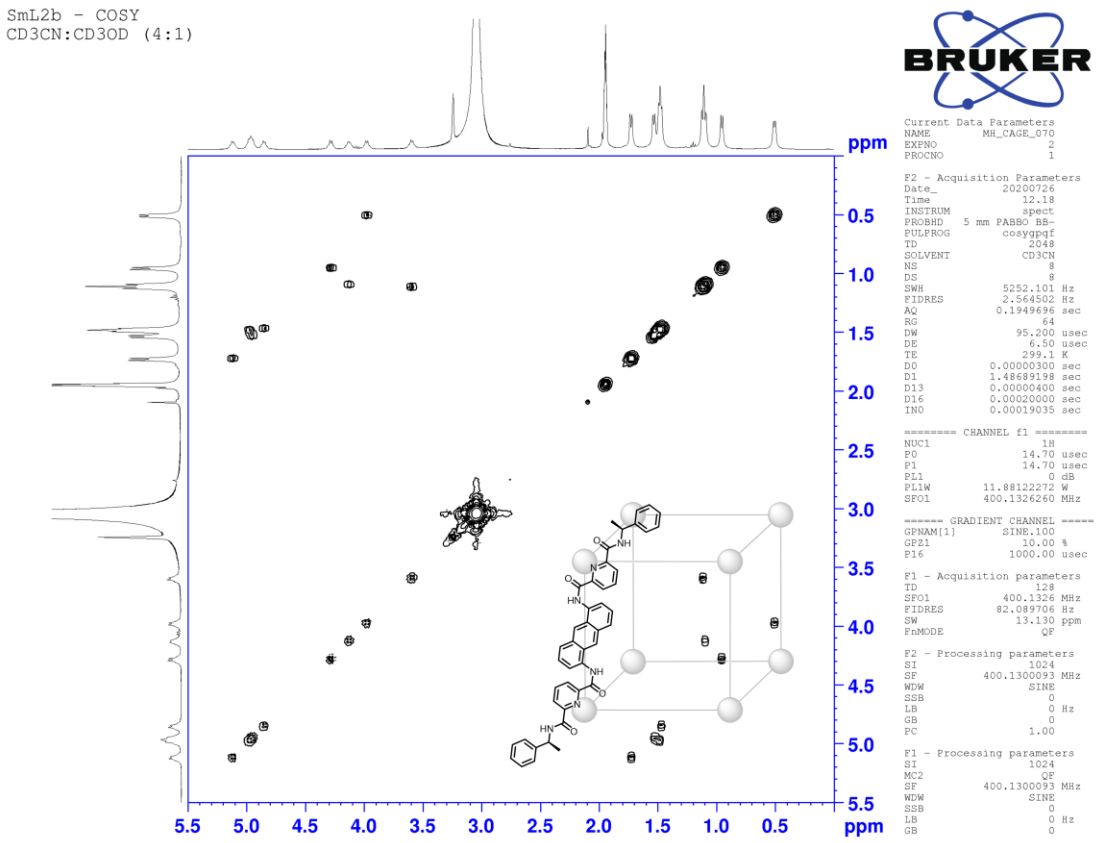

Spectrum S2-10: ^{1}H-^{1}H COSY NMR spectrum of **SmL$_{2b}$**

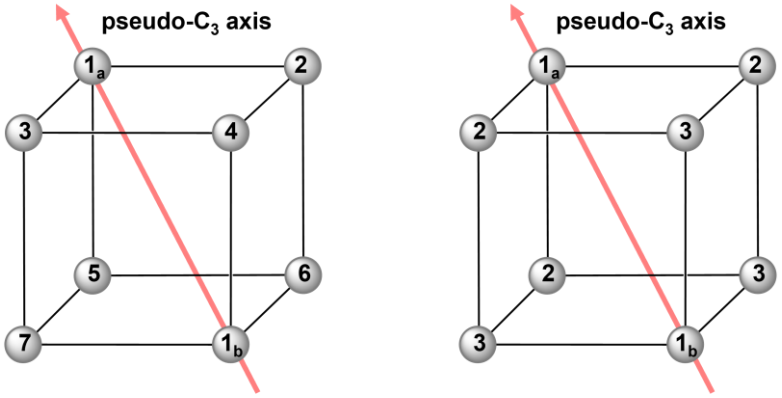

Figure 2-5: illustration of two different metal environments in cubic structure

Based on seven different proton environments, two inference can be concluded including (1) eight different metal environments while two of them are of similar (2) four different metal environment while two of them are of similar. In former case, the slight difference in metal 1a and 1b leads to other six different proton environments with *pseudo*-C_3 rotational symmetry spanning along two similar metals. For latter case, there will be four different metal environments while metal 1a and metal 1b are of similar. Due to ditopic nature of ligand, ligand connecting metal 1a and 2 will have two different proton environments locating on 1a and 2 separately and thus eight different proton environments in total are resulted. As metal 1a and 1b are similar, underlying protons on ditopic ligand connecting metal **1a**-2 and metal 3-**1b** are most likely identical and ultimately resulted in seven different proton environments.

Although detailed assignments in **EuL$_{2b}$** and **LuL$_{2b}$** are not feasible, the identical patterns are side evidence on the formation of same topology. In addition to NMR spectroscopy, ESI-HRMS spectrum revealed the existence of $[Ln_8(L_{2b})_{12} + xOTf - yH]^{n+}$ (Ln = Sm, Eu, Gd & Lu, n = 4 – 8, x & y = variable) without other species (**S2-72** to **S2-84**). Among the synthesized complexes, the first chiral lanthanide cubes **SmL$_{2b}$** is successfully crystallized in the co-solvent of methanol and acetonitrile while x-ray crystal structure agrees with other previous inference that four different metal environments are interpreted while two of them are of similar environment.

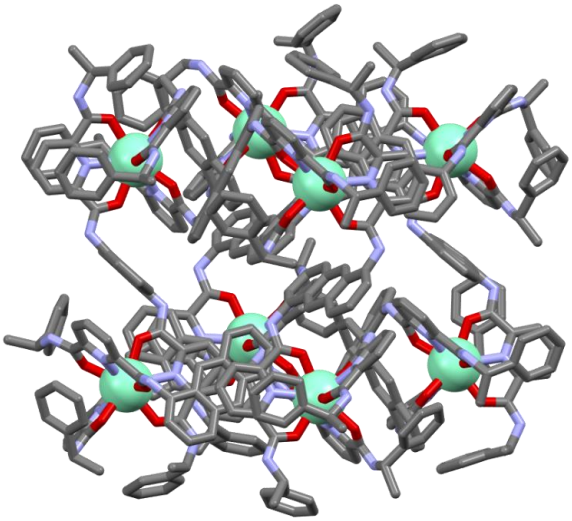

Figure 2-6: crystal structure of $Sm_8(L_{2b})_{12}$

Complex LnL$_{3a}$ Based on NMR spectroscopy, only single set of protons is identified in **LnL$_{3a}$** (Ln = Sm, Eu, Lu). In analogy to **LnL$_{2a}$**, **LnL$_{3a}$** (Ln = Sm, Eu, Lu) have shown similar pattern while up-fielding signal are observed in paramagnetic europium coordination. With the aid of ^{1}H-^{1}H COSY NMR spectrum, similar proton assignments are performed as previous illustration while the detailed assignment are included in S to **S2-85** to **S2-92**.

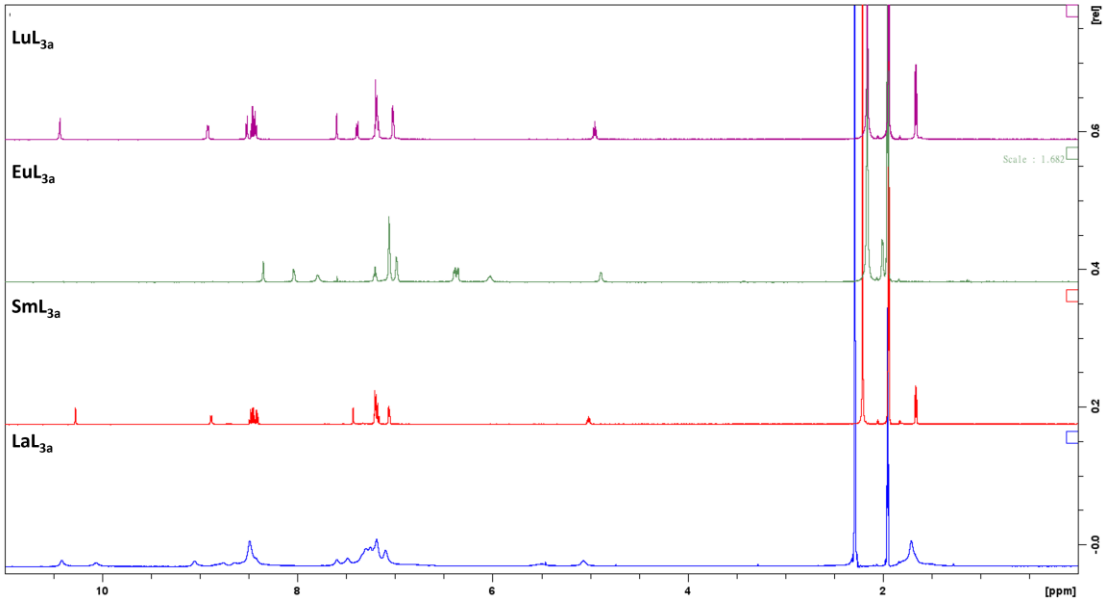

Spectrum S2-11: stacked ^{1}H NMR spectrum of **LnL$_{3a}$**

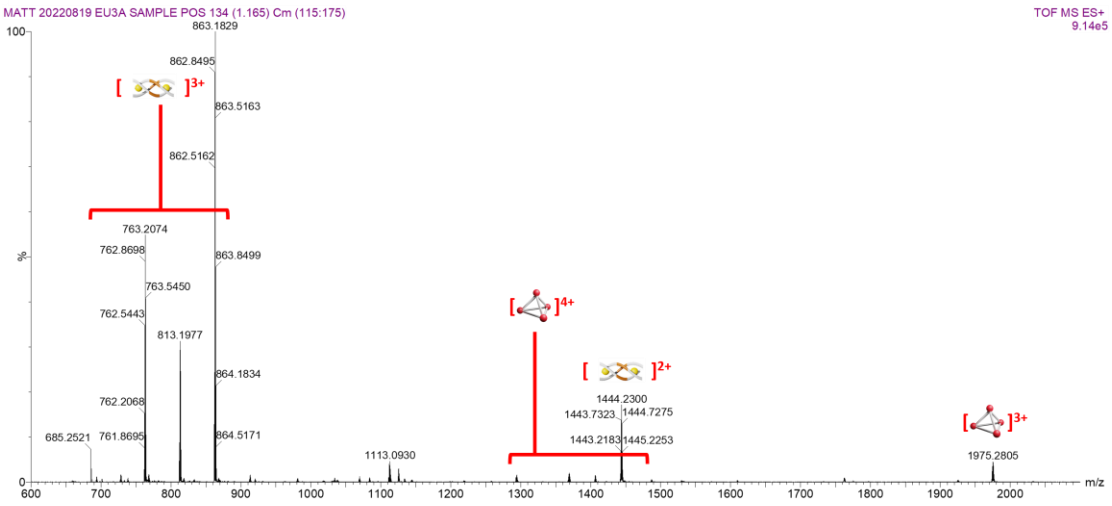

Spectrum S2-12: ESI-HRMS spectrum of **EuL$_{3a}$**

As depicted in spectrum **S2-12**, the ESI-HRMS spectrum was initially assigned with sole helical arrangement from the major signal. Upon detailed analysis on high-mass regions (**S2-13** and **S2-14**), it indicated that tetrahedron species are identified while the signal at m/z = 1,444.23 region are actually signal overlapping of both helicates and tetrahedral species as proved by the isotopic simulation.

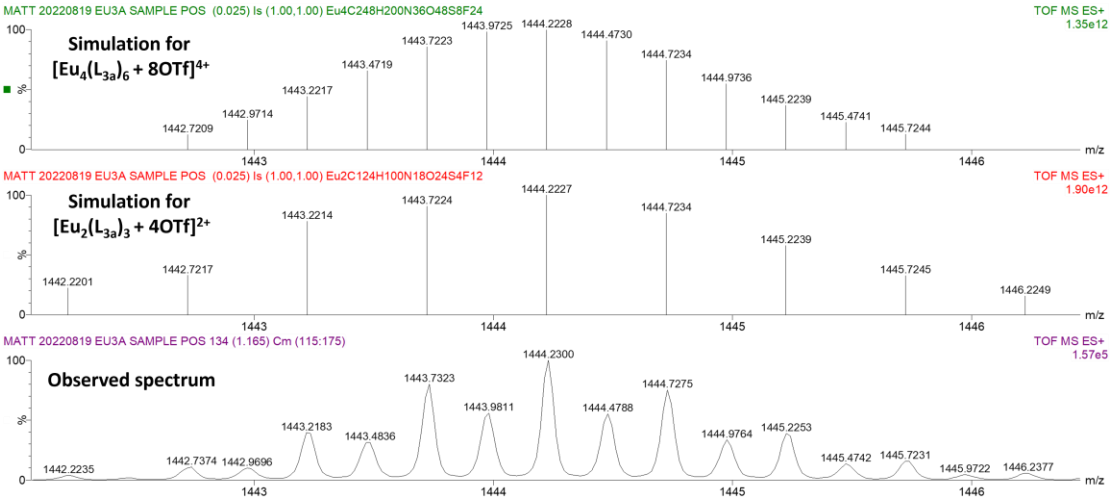

Spectrum S2-13: isotopic distribution of selective ion species in **EuL_{3a}** (m/z = 1444.23)

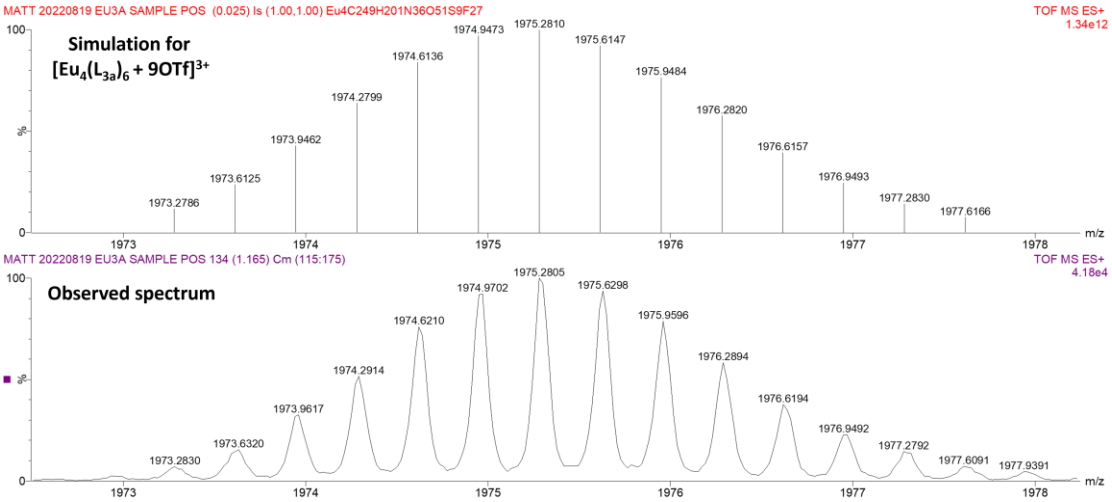

mass error: 0.25 ppm

Spectrum S2-14: isotopic distribution of selective ion species in **EuL_{3a}** (m/z = 1975.28)

Meanwhile, the mass signal at 1,975.28 region further reveals the formation of the tetrahedral species. This phenomenon is not only observed in europium complexes but also in Sm and Lu complexes (spectrum **S2-93** and **S2-94**). With these observations, there are two possibilities including (1) m/z signal of helicates is fragmented from tetrahedral species and (2) m/z signal of tetrahedral is 1+1 adducts from constituent helical structure. In facts, it is uncommon that case (2) will occur while all three lanthanide complexes must have same coincidence on adducts

formation. Together with single predominated species identification in NMR analysis, the complexation of ligand $\mathbf{L_{3a}}$ most likely resulted in homochiral tetrahedral species with some minute dissociated helicates.

Complex $\mathbf{LnL_{4b}}$ The NMR spectroscopy revealed the formation of single species for all synthesized complexes including lanthanum, samarium, europium and lutetium. As expected from previous result, proton in $\mathbf{Eu_2(L_{4b})_3}$ have experienced the paramagnetic field. The detailed assignments are not performed as ^{1}H-^{1}H COSY experiment is not completed while the individual ^{1}H NMR spectrums are reported (**S2-95** to **S2-98**). The ESI-HRMS spectrum revealed the helical conformation with the characteristic ions peak $[Ln_2(L_{4b})_3 + xOTf - yH]^{n+}$ (Ln = La, Sm, Eu, Lu, n = 2-4, x & y = variable).

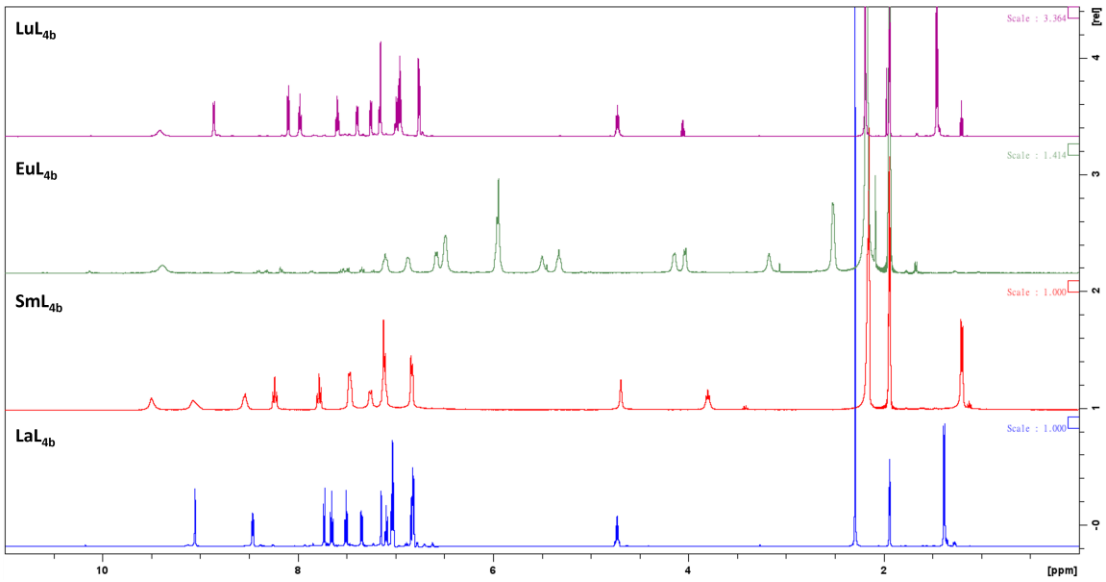

Spectrum S2-15: stacked ^{1}H NMR spectrum of $\mathbf{LnL_{4b}}$

Ligand $\mathbf{L_{5b}}$ In contrast to other ligand systems, synthesis of ligand L_{5b} have experienced significant difficulties that the amide coupling of spacers 5b and pcam chelator cannot properly afford final ligands even with different coupling reagents such

as PyBOP and thionyl chloride activation. From the synthesis, only minute amounts of ligands are formed with large amount of impurity which hinder the purification and subsequent complexation study.

2.2.3. Transformation Among Different Topologies

2.2.3.1. Solvent dependent helicate-to-tetrahedron evolution of LnL_{2a}

With the prediction of similar offsetting properties, $\mathbf{L_{2a}}$ are expected to accommodate tetrahedral topology as $\mathbf{L_{1a}}$ does. As discussed previously, direct complexation of $\mathbf{L_{2a}}$ result in helical structure. Upon standing the complex solution in d-acetonitrile in NMR tube, non-bright complexes $\mathbf{EuL_{2a}}$ was found to be luminescent after two weeks of standing. Based on this observation, a series of time-dependent study was then conducted to investigate the transformation progress.

Time dependent NMR Study. As an initial study, 2 mg of isolated complexes of $\mathbf{EuL_{2a}}$ with approximate concentration of 0.5 mM were dissolved in 0.5 mL molecular sieved dried d-acetonitrile and the transformation progress is monitored by NMR spectroscopy.

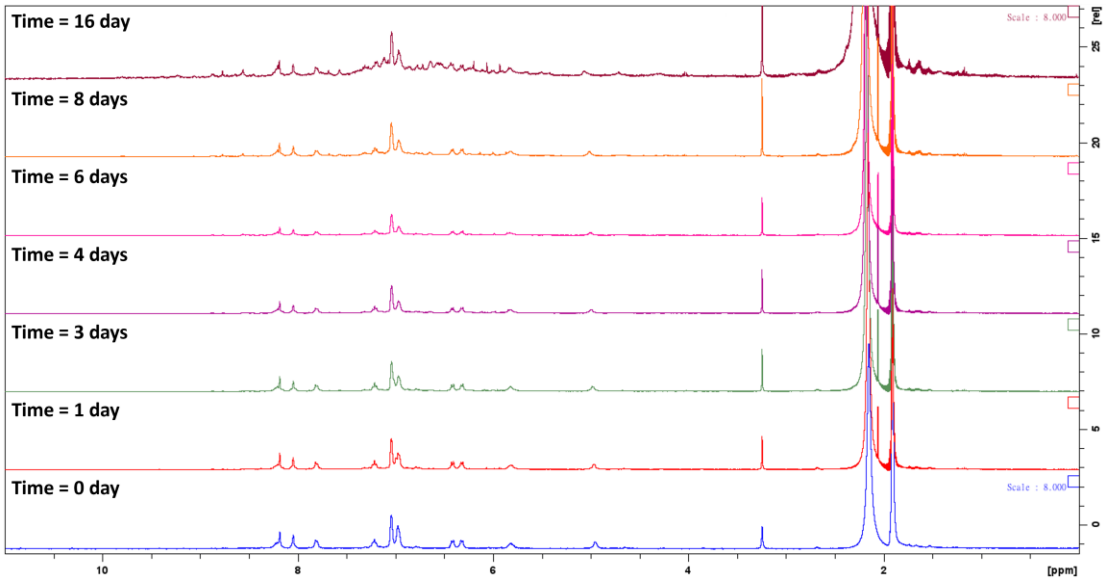

Spectrum S2-16: Initial Time dependent study on transformation of **EuL_{2a}** (0.5 mM)

The spectrum **S2-16** show slow transformation from pure helicate to high-order structure in 16 days while the species cannot be identified at that moment. To promote the transformation and expand the investigation, other studies are conducted in higher concentration of 5 mM using isolated helicate **$Eu_2(L_{2a})_3$** and **$Sm_2(L_{2a})_3$** with same conditions.

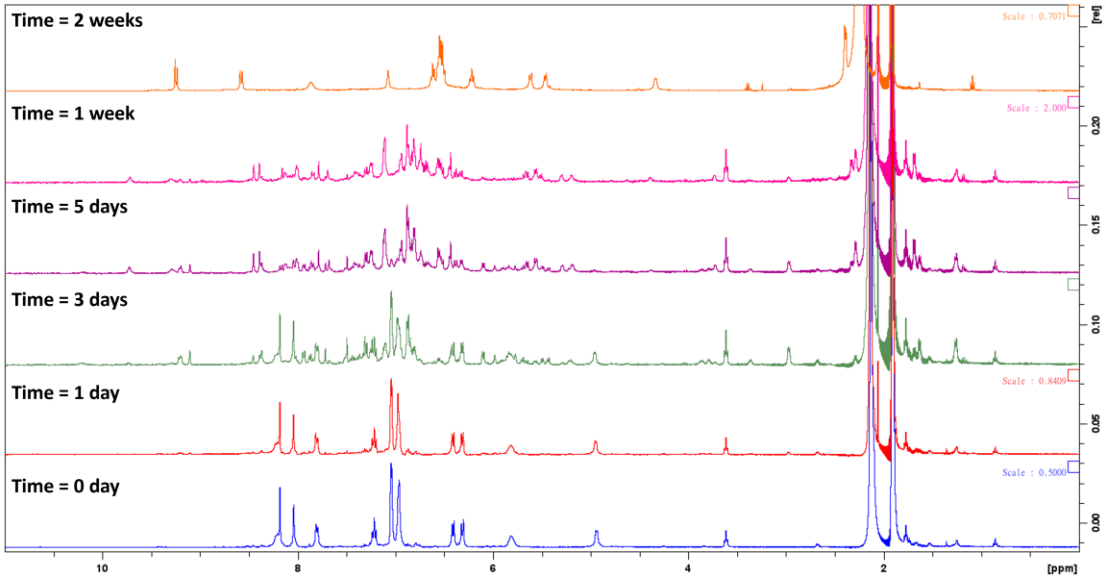

Spectrum S2-17: Time dependent study on transformation of **$Eu_2(L_{2a})_3$** (5 mM)

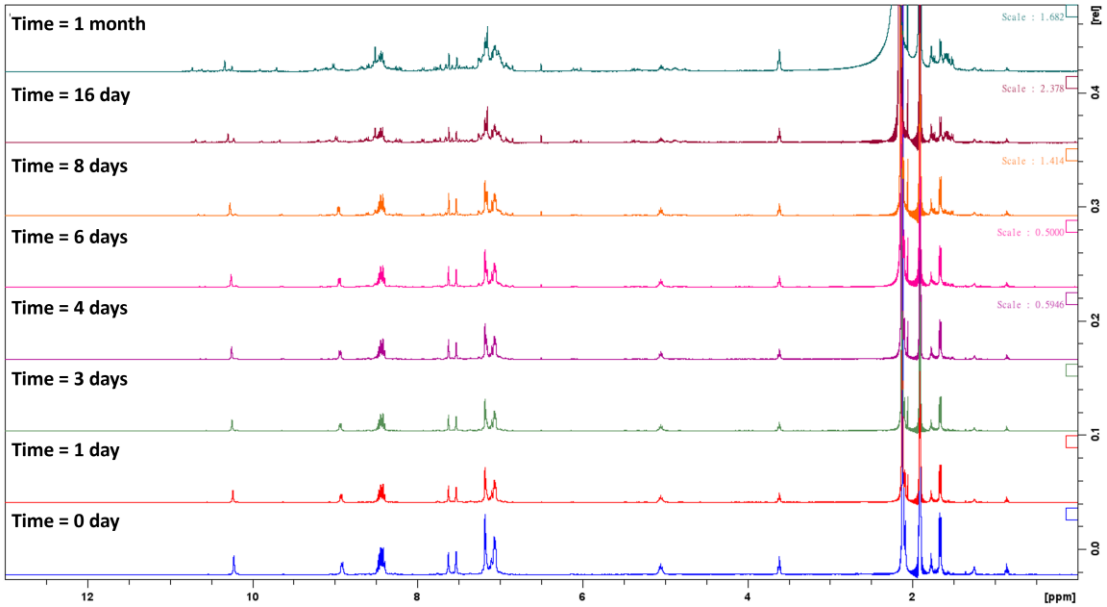

Spectrum S2-18: Time dependent study on transformation of $\mathbf{Sm_2(L_{2a})_3}$ (5 mM)

As indicated in the spectrum **S2-16**, europium helicates started to convert from day 3 and slowly converged to new intermediate species without any helicate structure in day 5. The further transformation was completed with the duration of 2 weeks by standing the solution in room temperature. However, the transformation in samarium is much slower compared to europium in which a mixture of species was identified after 1 month. Based on the NMR spectroscopy study, there are no observable difference from t = 16 days and t = 1 month. The transformation in $\mathbf{SmL_{2a}}$ is believed to stay in the mixture of helicate and unknown species upon standing.

Solvent dependence study To investigate the formation of tetrahedron species, the direct complexation of Ligand L_{2a} with anhydrous acetonitrile was performed. However, no desired tetrahedron species were observed even prolonged heating was employed. Different strategy was therefore employed that the isolated complexes were dissolved in different solvent in which the result is tabulated in the table **2-1**.

Solvent	DCM	$CHCl_3$	$CDCl_3$	THF	EA	Dioxane	CH_3CN	CD_3CN
Emission under UV	✘	✘	✘	✘	✘	✘	✘	✓

Table 2-1: solvent screening on $Eu_2(L_{2a})_3$ transformation

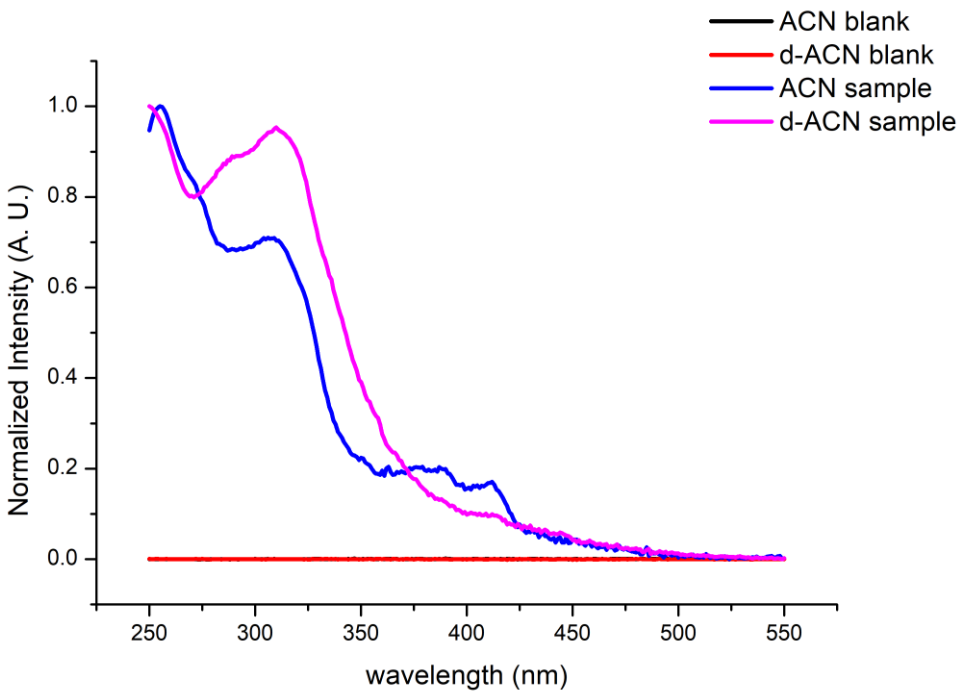

Spectrum S2-19: UV spectrum of CH_3CN and CD_3CN sample

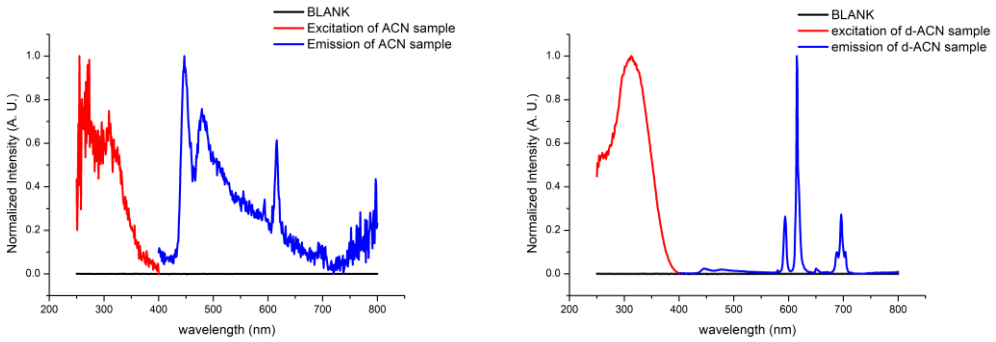

Spectrum S2-20: Excitation & Emission spectrum of CH_3CN and CD_3CN sample

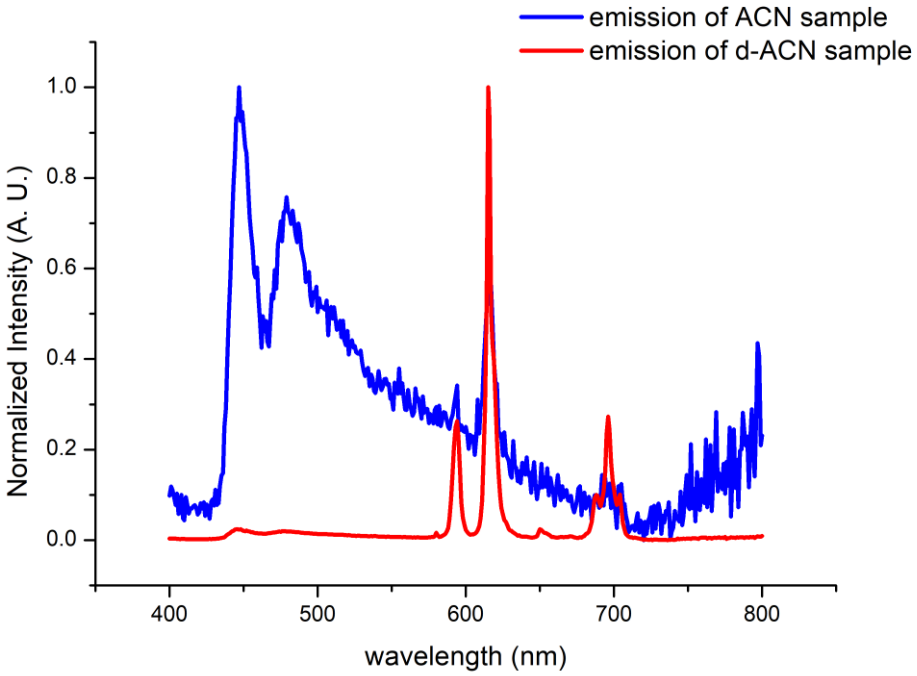

Spectrum S2-21: stacked emission spectrum of CH_3CN and CD_3CN sample

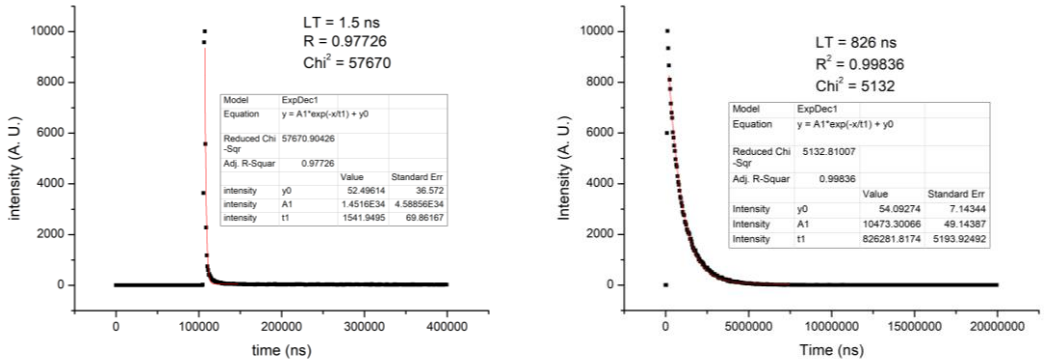

Spectrum S2-22: LT spectrum of CH_3CN (left) and CD_3CN (right) sample

The resulting solution of CD_3CN and CH_3CN are then further investigated with photophysical means in terms of emission and lifetimes. From the above photophysical data, it is cleared that new species were formed in CD_3CN with significant deviation in photophysical properties. The sample in CH_3CN show no europium emission signal while sample in CD_3CN does. The lifetime measurement further confirmed the results as species with longer lifetime was only observed in CD_3CN sample. Although the

result can also be attributed from different phonon between C-D and C-H oscillator, these photophysical data still provide indirect evidence on the formation of new luminescence species with longer lifetime.

Characterization of transformed species. To characterize the transformed specie, the transformed solution was directly analyzed with ESI-HRMS while the spectrum of pure helicate **EuL_{2a}** was also included for comparison.

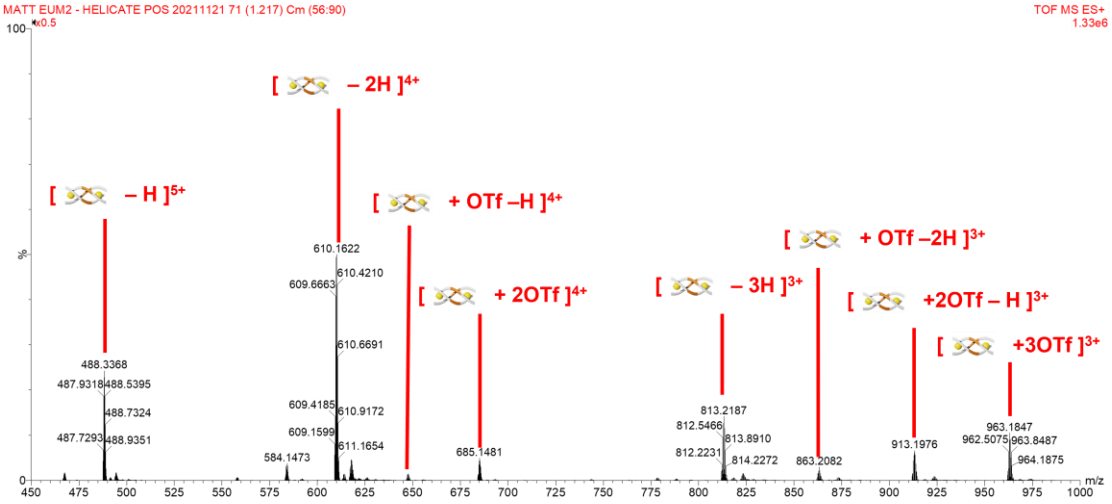

Spectrum S2-23: ESI-HRMS spectrum of **EuL_{2a}** before transformation

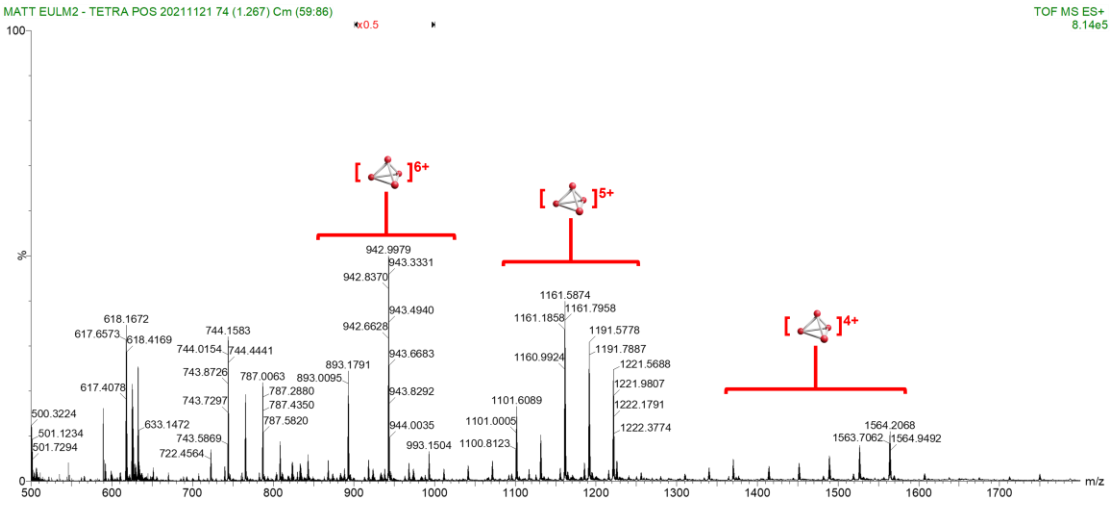

Spectrum S2-24: ESI-HRMS spectrum of **EuL_{2a}** upon transformation

As indicated in above spectrum, ESI-HRMS spectrum of transformed species agrees with NMR spectroscopic data that no original helicate are observed. The characteristic ions peaks $[Eu_4L_6]^{n+}$ (n = 4 – 6) provide solid evidence that tetrahedron species were formed. However, the detailed assignment of the ions fragment revealed some interesting findings that the tetrahedral species $[Eu_4(L_{2a})_6$ + 30 Da$]^{n+}$ were mainly observed instead of anticipated $[Eu_4(L_{2a})_6]^{n+}$ ions signal as depicted in **S2-25**.

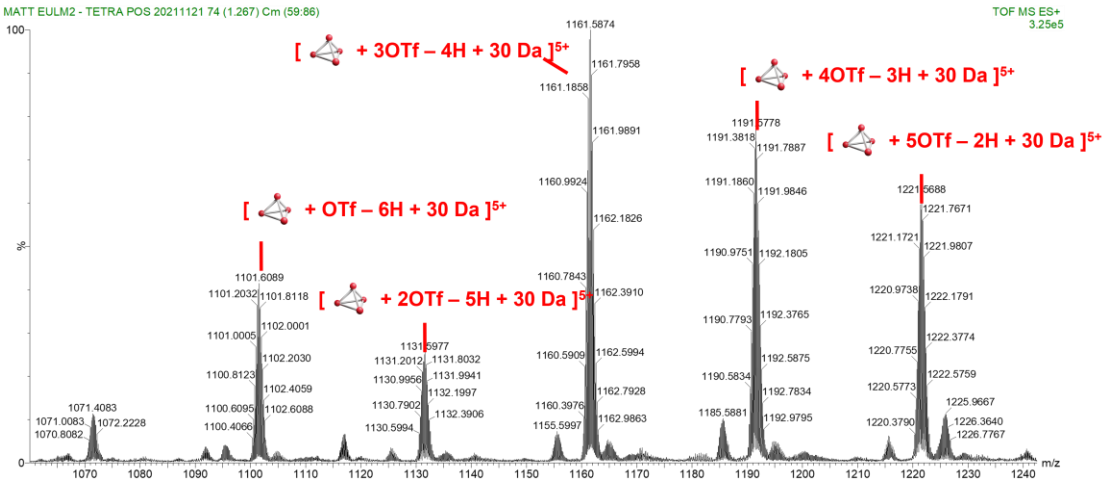

Spectrum S2-25: ESI-HRMS spectrum with assignment on $[Ln_4(L_{2a})_6$+30Da$]^{n+}$ species

Upon detailed assignment on additional 30 Da fragment, it is postulated that auto-oxidation and tetrahedral transformation are simultaneously occurred and resulting in +30 Da species. Interestingly, the oxidized species are also another system that this chapter have investigated. From spectrum **S2-26**, the unknown species with 30 Da artifacts were identified as **$[Eu_4(L_{1a})_6]^{n+}$** species with mass error of 3.87 ppm. Meanwhile, the NMR spectrum of transformed species agrees with the inference that it show identical signal shift with reported complexes **$Eu_4(L_{1a})_6$.** Although the detailed mechanism of auto-oxidation is still under investigation, it is strongly evident that the oxidation and transformation occurred in a parallel manner and resulting in a helicate-to-tetrahedron transformation from **$Eu_2(L_{2a})_3$** to **$Eu_4(L_{1a})_6$**.

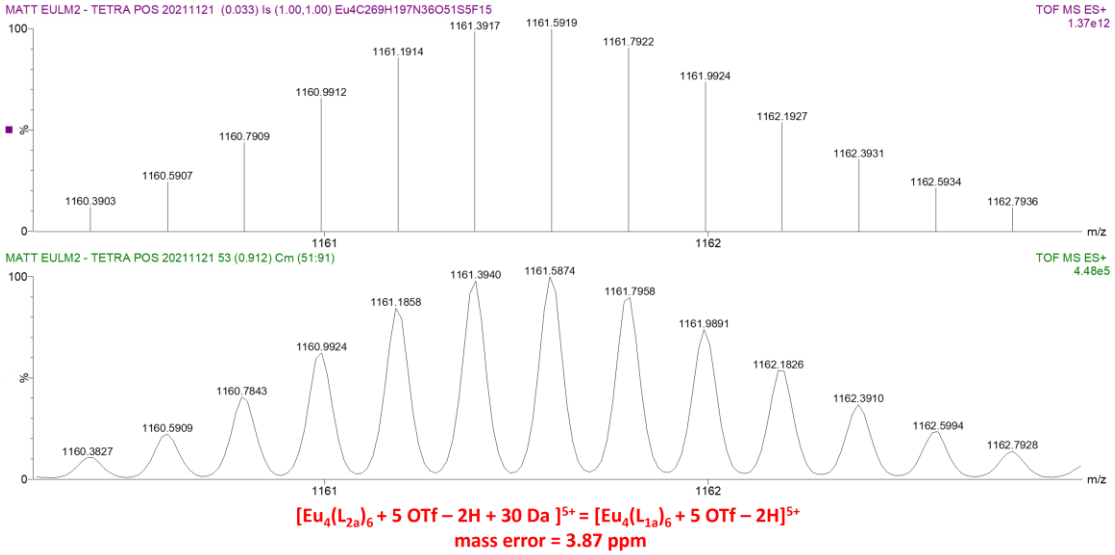

Spectrum S2-26: isotopic distribution of $[Eu_4(L_{1a})_6 + 5\ OTf - 2H]^{5+}$

The similar investigations are also performed in obtained mixture of **$Sm_2(L_{2a})_3$** and newly formed species. The result generally agrees with the findings in NMR study that a mixture of helicate and tetrahedron species were resulted with the helicate conformation as major species. Surprisingly, auto-oxidation behaviors are not observed in SmL_{2a} system that only mixture of **$Sm_2(L_{2a})_3$** and **$Sm_4(L_{2a})_6$** are identified as shown in **S2-27** to **S2-29**.

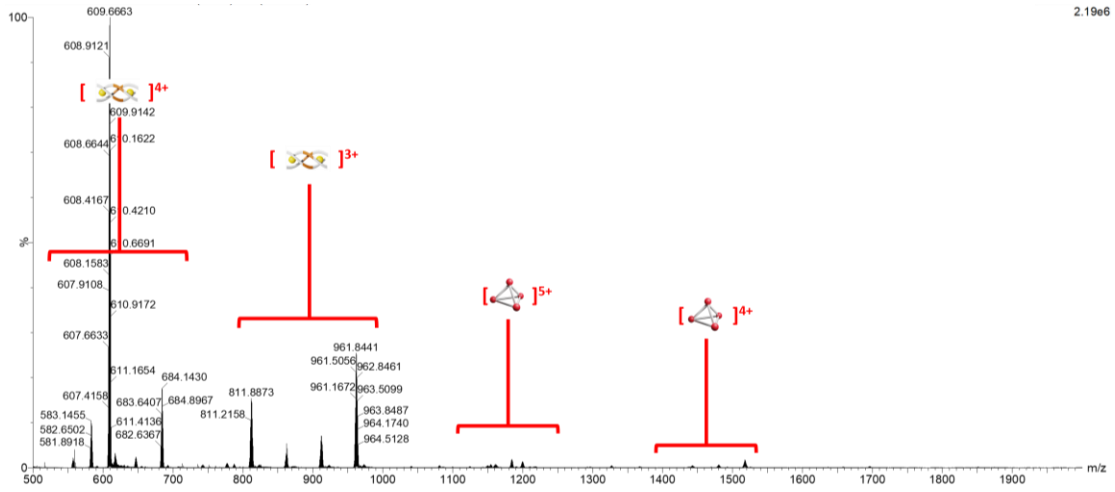

Spectrum S2-27: ESI-HRMS spectrum of **SmL_{2a}** upon one month transformation

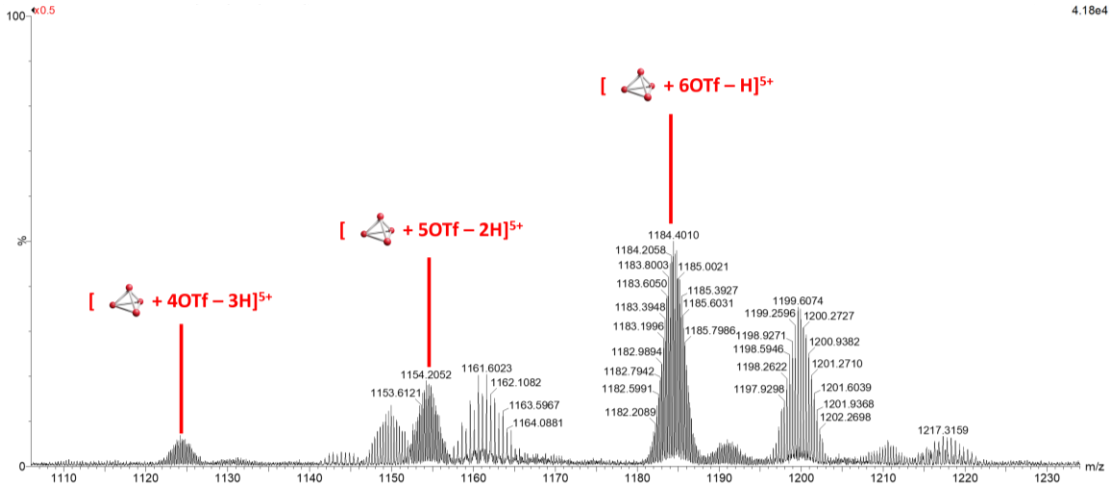

Spectrum S2-28: Expanded ESI-HRMS spectrum of **$[Sm_4(L_{2a})_6]^{5+}$** species

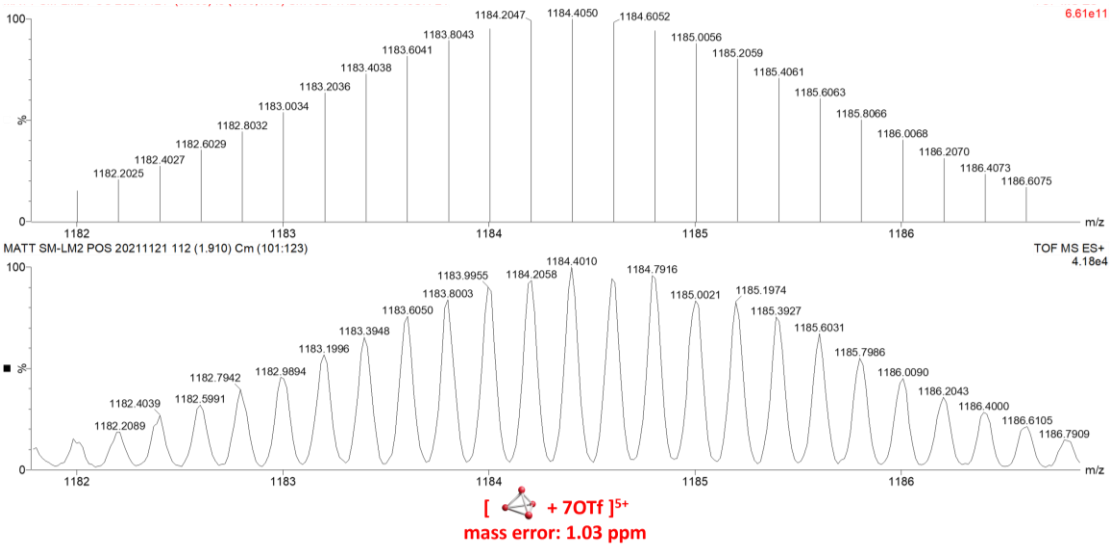

Spectrum S2-29: isotopic distribution of $[Sm_4(L_{2a})_6 + 7OTf]^{5+}$ species

To further understand the auto-oxidation processes, some control experiments are conducted by standing the solution of 2 mg of $Eu_2(L_{2a})_3$ and $Sm_2(L_{2a})_3$ in 1 mL d-acetonitrile in three different conditions in 60°C water bath: (1) under air, (2) under nitrogen and (3) under dark and nitrogen while the solvent is pre-dried with activated molecular sieves.

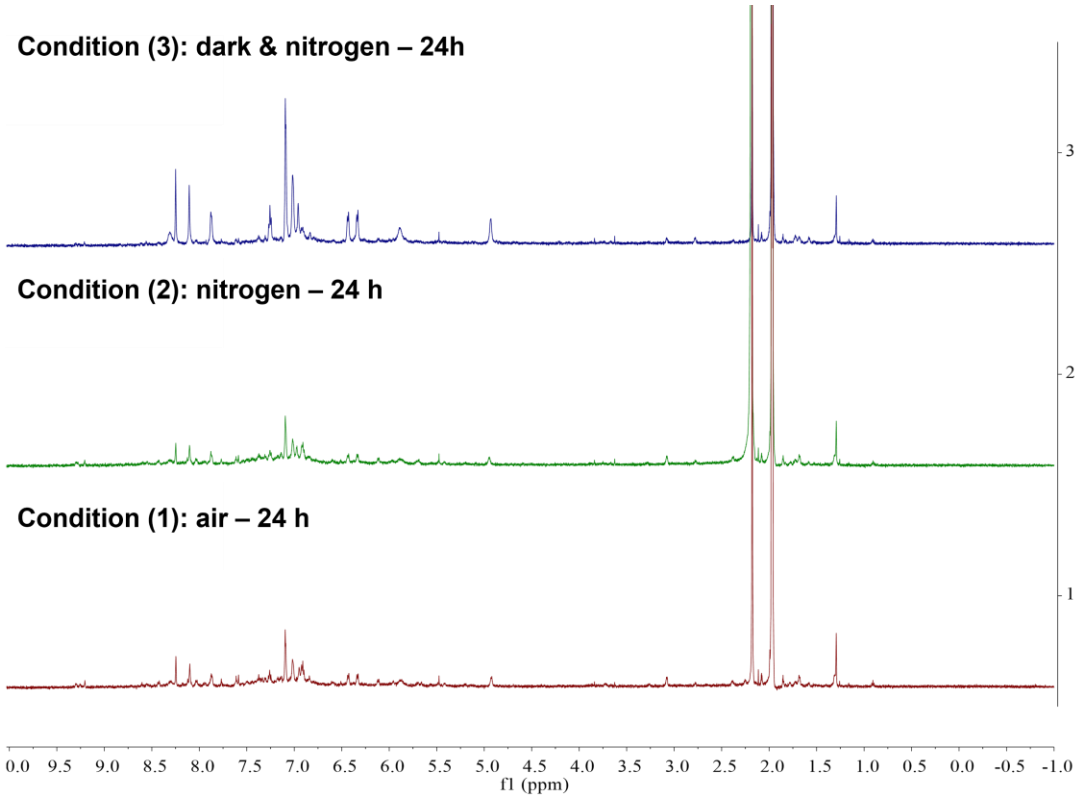

Spectrum S2-30: controlled experiment for $Eu_2(L_{2a})_3$ (24h)

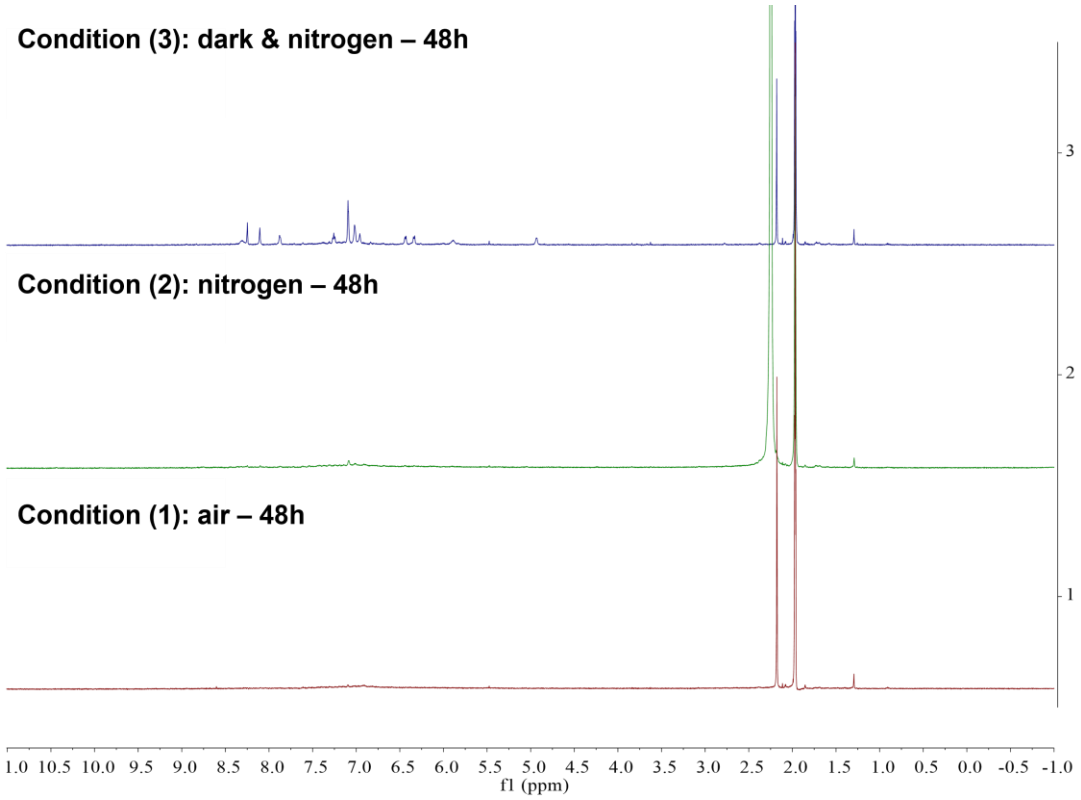

Spectrum S2-31: controlled experiment for $Eu_2(L_{2a})_3$ (48h)

As shown in figure **S2-30** and **S2-31**, the sample in condition (1) and (2) started the conversion on day 1 and the NMR signal is greatly suppressed upon 48 h which is attributed from the transformation to intermediates species. Additionally, the sample in condition (3) stays intact as original helicates without observable changes. On the contrary, no observable changes in NMR spectrum for sample of $Sm_2(L_{2a})_3$ under all three conditions after 48h. This simple control experiments revealed that the europium is likely to be determining factor for such transformation while light sources are possibly required for the transformation.

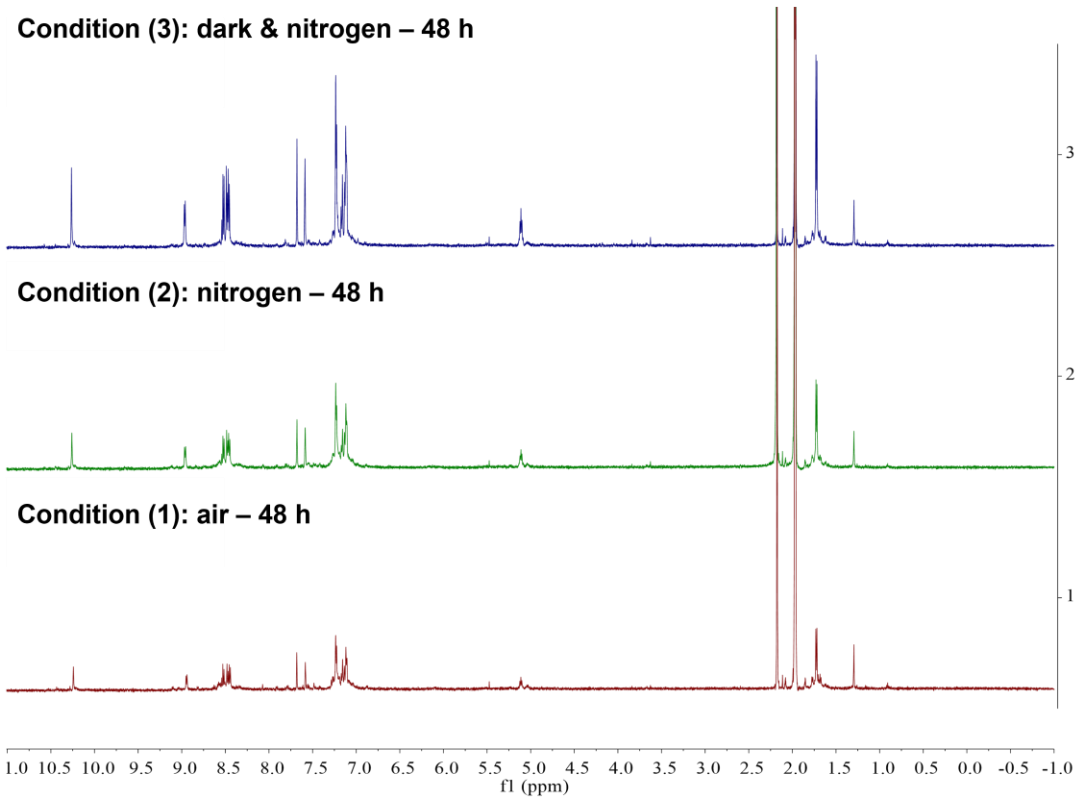

Spectrum S2-32: controlled experiment for $Sm_2(L_{2a})_3$ (48h)

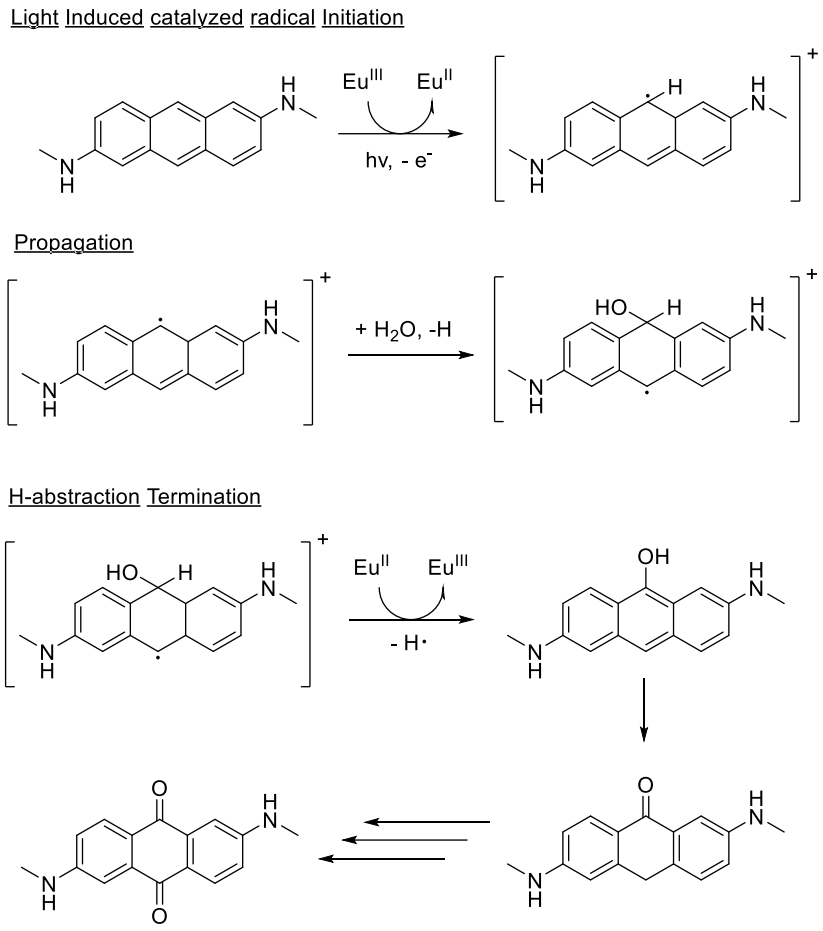

Figure 2-7: proposed mechanism for auto-oxidation of anthracene units

Considering such parameters, it is inferred that the auto-oxidation process in $Eu_2(L_{2a})_3$ is possibly metal-catalyzed radical induced oxidation. As hypothesized mechanism, anthracene is first activated by absorbing light to form an excited species in initial step. The excited species lead to the formation of a radical cations (anthracene+) which can react with water molecules in the system to from anthracene-$OH^{\cdot+}$ radical cation followed by the H-abstraction to afford anthracene-OH. Upon enol-keto tautomerization, first stage oxidation is accomplished while the subsequent oxidation gives anthraquinone while the detailed mechanism is under investigation.

2.2.3.2. Solvent dependent helicate-to-cube evolution of LnL_{2b}

Based on the reported literature, it is known that **$Eu_2(L_{2b})_3$** would undergo helicate-to-cube transformation under concentration effect. Sun reported that the synthesis of $Ln_8(L_{2b})_{12}$ (Ln = La, Eu & Nd) is achieved by either crystallization by slow diffusion of antisolvent to **$Ln_2(L_{2b})_3$** solution or high concentration complexation in CD_3NO_2.

To further investigate transformation process, different methodologies are employed in which the complexation of **L_{2b}** with corresponding lanthanide (La, Sm, Eu, Gd and Lu) was performed in two different type of solvent system including (1) pure acetonitrile and (2) mixture of acetonitrile:methanol (4:1) at 70 °C. The results indicated that pure acetonitrile would solely afford the pure helicate regardless of concentration and temperature in which spectrum **S2-31** revealed no sign of conversion even with prolonged heating at 70°C.

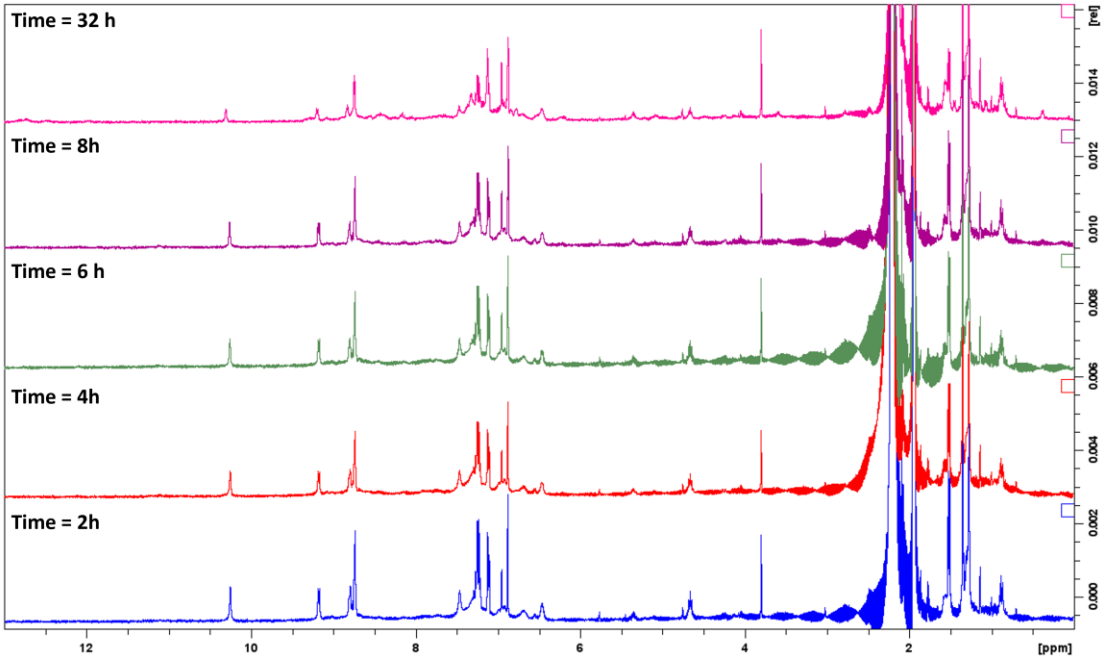

Spectrum S2-33: time-dependent study in complexation of **SmL_{2b}** in CD_3CN at 70°C

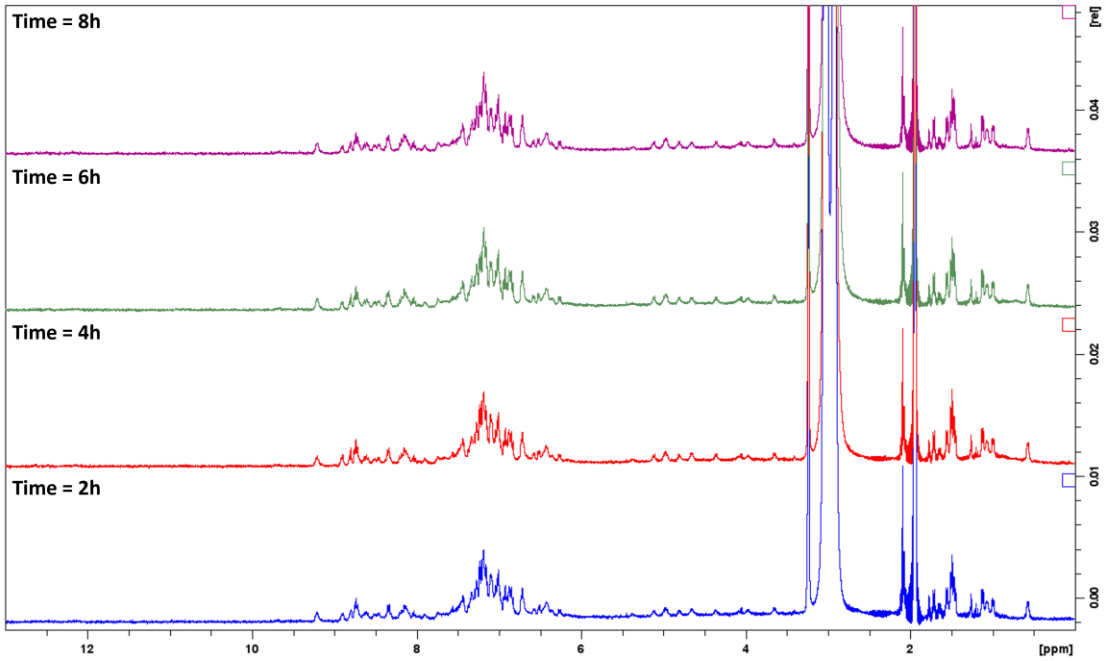

Spectrum S2-34: time-dependent study in complexation of **SmL_{2b}** in the mixture of CD_3CN:CD_3OD (4:1) at 70°C

Under the same concentration and temperature, the addition of methanol induces the rapid formation of cubic structure with the detailed HRMS, NMR characterization and crystallographic data in section 2.2.2.3. The same phenomena are also observed in other lanthanide system including europium, gadolinium and lutetium. However, in our study, complexation with lanthanum does not exhibit similar behaviors which is probably attributed from labile coordination in the presence of protic methanolic environments.

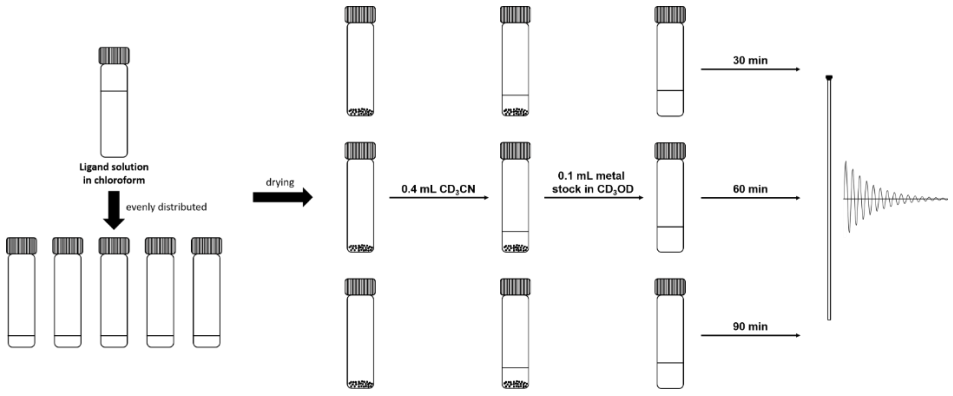

Figure 2-8: The experimental set-up for time-depending study of **SmL_{2b}** transformation

To understand the formation process of cubic structure, time-dependent NMR study are conducted at RT and elevated temperature with low concentration of ligands (1 mM). Figure 7 shows the experimental set-up with collection of individual data point to minimize the mankind artifacts during transferal of solvent within each treatment.

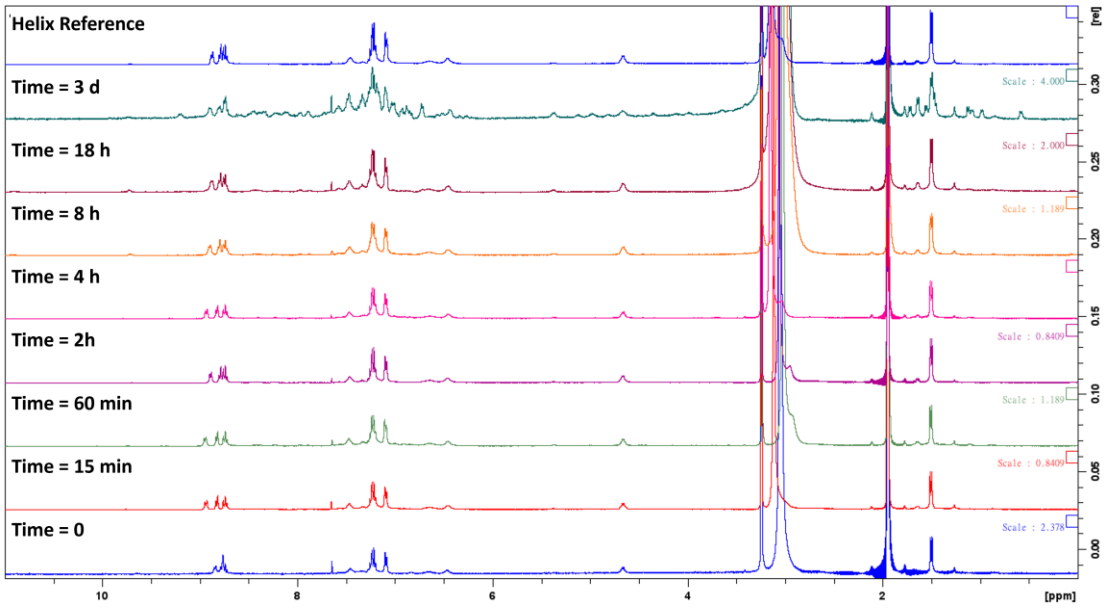

Spectrum S2-35: time-dependent study in complexation of **SmL_{2b}** in the mixture of CD_3CN:CD_3OD (4:1) at RT (1mM)

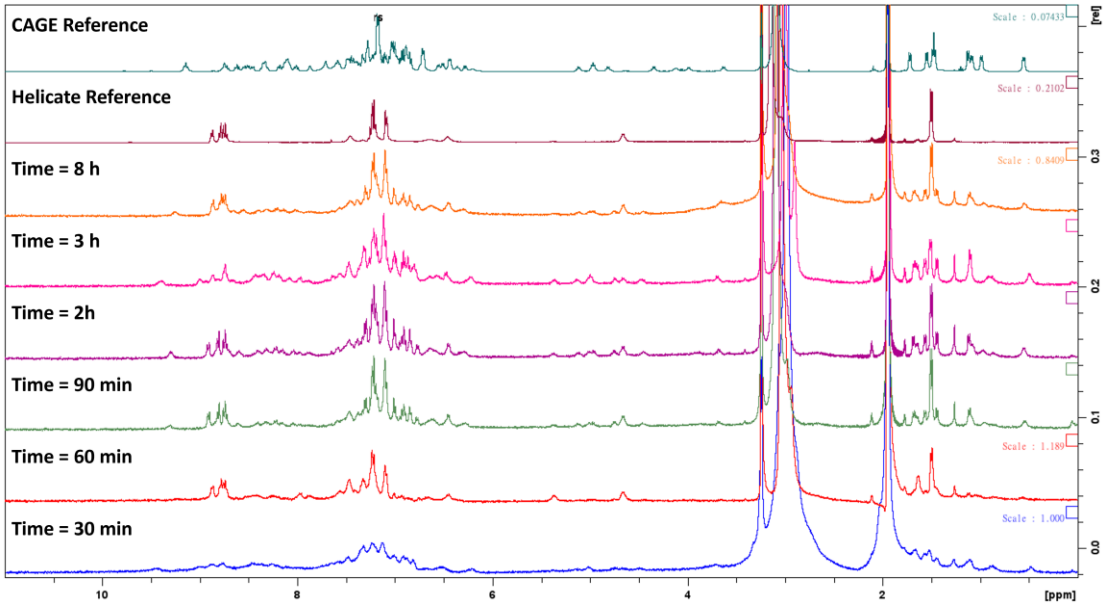

Spectrum S2-36: time-dependent study in complexation of **SmL_{2b}** in the mixture of CD_3CN:CD_3OD (4:1) at 70°C (1mM)

Spectrum **S2-35** and **S2-36** indicates that the formation of cubic structure is either achieved from the evolution from pure helicate to cubic structure or direct complexation in the presence of methanolic environments. although a clear cubic formation is resulted in both situations, it is important to note that slightly deviated patterns are observed between helicate transformed and direct complexation products which is possibly attributed from different stereochemical or spatial arrangement in afforded cubic structure.

2.2.4. Correlation Between Offsetting Properties & Ultimate Topology

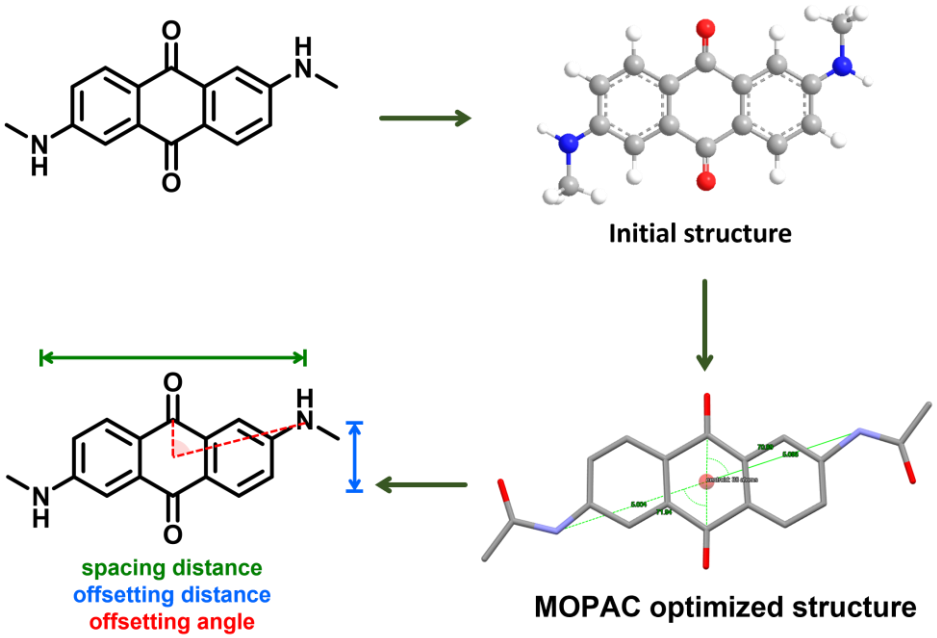

Figure 2-9 graphical illustration of computational analysis of spacing units

Spacing unit[a]	Point Group	Offsetting angle	Offsetting distance	Spacing distance	Interpreted topology
1a	C_{2h}	71.4 (0.5)	3.22	9.57	Tetrahedron
1b	C_2	43.6 (0.2)	5.49	5.24	Helicates
2a	C_{2h}	71.1 (0.7)	3.22	9.43	Helciates or tetrahedron

2b	C_{2h}	41.9 (0.2)	5.42	4.86	Helicates or cubes
3a	C_{2h}	71.2 (1.9)	2.53	7.42	Tetrahedron
3b	C_2	20.7 (1.8)	5.77	2.18	Tetrahedron
4a	C_{2h}	3.9 (1.5)	Nil	9.90	Helicates
4b[b]	C_{2v}	41.3 (2)	Nil	6.61	Helicates
	C_{2h}	38.7 (3)	6.58	5.26	Helicates

[a] The data is obtained by semi-empirical MOPAC software.

[b] Two simulation results can be obtained based on orientation on amide arm

Table 2-2: summary on selected parameter based on simulated spacer units.

To correlate the offsetting properties and final topology, table **2-2** summarized simulated offsetting properties and spacing distance of eight bridging units without consideration of chelating arm while the simulation details are provided in appendix. In general, spacer unit **3** and **4** generally agree with the prediction that they result in corresponding supramolecular assembly. However, the experimental results of spacer unit **1b** and **2a** deviated from the predication. With reference to table, spacing unit **1b** and **2a** exhibit similarities in all three parameters including offsetting angle, offsetting distance as well as spacing distance. It is anticipated to accommodate the formation of tetrahedral structure and experimental revealed that $\mathbf{LnL_{1a}}$ affords pure tetrahedron while $\mathbf{LnL_{2a}}$ results in mixture of helical and tetrahedral products.

It is expected that spacing unit with such close parameters should afford similar supramolecular self-assembling behaviors while the difference should be accounted from the extra steric bulkiness on C=**O** moiety and electrostatic properties in anthraquinone. The crowded anthraquinone spacer in helical environment possibly disfavor the formation of helicate. Meanwhile, the electron rich anthraquinone

apparently provide extra stability by *π-π* stacking interactions which govern the formation of tetrahedral structure.

With similar terminology, it is expected that ligand $\mathbf{L_{1b}}$ and $\mathbf{L_{2b}}$ should afford similar self-assembling arrangements. However, complexation of ligand $\mathbf{L_{1b}}$ results in pure helicates while that of ligand $\mathbf{L_{2b}}$ afford either helicate or cubic structures. The findings are possibly attributed from unstable helicate species of ligand L_{1b}. Based on the HRMS spectrum, a significant amount of dissembling species is identified compared to other synthesized complexes. It is inferred that the intramolecular hydrogen bonding destabilizes the structure and further hinder the formation of higher order species.

With the similarity in offsetting angle and distance in spacing unit **1a** and **3a**, they should share similar self-assembling behaviors. From our interpretation, homochiral tetrahedron are predominantly resulted from both ligand $\mathbf{L_{1a}}$ and $\mathbf{L_{3a}}$. As there are significant difference between the simulated properties in **3a** and **3b**, it is unlikely that the tetrahedral structure is inherited from naphthalene linkage while it is believed that the tetrahedron preference is originated from deviation of idealized helicate forming offsetting angle. Compared to other spacer, spacer **4b** has very idealized offsetting properties for helicate formation while the results agree that only pure helicates are identified.

2.3. Conclusion & Future Work

In this chapter, eight ditopic pcam-based ligands with different offsetting and spacing properties are compared with their supramolecular self-assembling behaviors. Based on the findings, it reveals that the spacer with similar offsetting angle and offsetting distance have the possibility to result similar self-assembling topology. Meanwhile, solvent-dependence complexations are observed in ligand 2a and 2b in our investigation in which introducing different solvent system significantly affect the result of self-assembling process especially in labile chelating system. Yet, the comprehensive relationship between the symmetry and ultimate topology is not fully understood due to high lability of pcam-based ligand and limited examples. This chapter also revealed the significance on hydrogen bonding in ultimate topologies. As future works, more examples with more detailed complexation with different solvent system is suggested. Meanwhile, the methyl linkage can be employed to suppress the intramolecular hydrogen bonding so as increase the solubility of the ligand system.

2.4. Experimental Section

2.4.1. General Considerations

All chemical used for synthesis were obtained from commercial suppliers and used without further purification. All moisture-sensitive reactions were conducted under a nitrogen atmosphere in oven-dried glassware. Anhydrous solvents were freshly distilled or dried over 4A molecular sieves unless otherwise specified. 1D and 2D NMR spectra were conducted on a Bruker AVANCE-III 400 MHz and 600MHz FT-NMR. The elemental analysis was performed using an Elementar Vario Micro Cube elemental analyzer. High Resolution-ESI mass spectrum were obtained from Agilent 6540 Liquid Chromatography - Electrospray Ionization Quadrupole-Time-of-Flight Mass Spectrometer or Waters Synapt G2-Si Ion Mobility Quadrupole MS and the chemical shifts were determined with tetramethylsilane (TMS) or solvents in parts per million (ppm).

2.4.2. Synthesis of ligand

anthracene-2,6-diamine (2a)

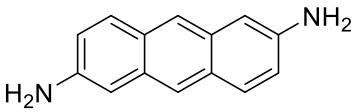

To the slurry mixture of 2,6-diaminoanthracene-9,10-dione (3.02 g, 12.6 mmol, 1 equiv.) in EtOH/NaOH solution (100 mL, EtOH: 2.5 M NaOH = 1:1 v/v), activated zinc powder (5.14 g, 76.5 mmol, 6 equiv.) was added by portion with the duration of 30 minutes. The reaction mixture was then brought to reflux temperature and reacted for 24h. The reaction mixture was filtered and washed with hot water until no colored residues were come off. The collected dull yellow crude was dried and rinsed with minimal acetone to obtain powdery solids.

The powdery solids were subjected to Soxhlet extraction for 3 days with 200 mL acetone and another Soxhlet extraction was performed for another 2 days with 200 mL solvent mixture (acetone: methanol = 1:1). The resulting solids were transferred to centrifuge tube and the resulting solids were washed with acetone (5X, 50 mL) to afford compound 1a (95% purity) (0.6267, 24%). ^{1}H NMR (400 MHz, DMSO-d_6) δ 7.81 (s, 2H), 7.63 (d, J = 8.9 Hz, 2H), 6.92 (dd, J = 8.9, 2.2 Hz, 2H), 6.79 (d, J = 2.2 Hz, 2H), 5.21 (s, 4H). ^{13}C NMR (101 MHz, DMSO-d_6) δ 144.52, 131.12, 128.43, 127.71, 121.82, 120.93, 104.22.

anthracene-1,5-diamine (2b)

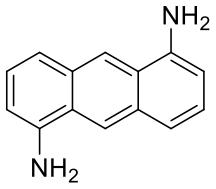

To the suspension of 1-5-diaminoantracene-9,10-dione (0.6 mmol, 1 equiv.) in 20 mL isopropyl alcohol, sodium borohydride (33 equiv.) was added with caution under nitrogen atmosphere. The reaction mixture was then brought to reflux temperature for further reaction. After 24h, the reaction mixture was cooled and filtered to obtain dark oil. The dark oil was then re-dissolved in dichloromethane and washed with water (3X), brine (2X) and dried over anhydrous sodium sulphate to afford dark crude. The crude oil was then loaded to column chromatography (silica gel, hexane to DCM, R_f = 0.3 in DCM) to yield brown solid (47%). ^{1}H NMR (400 MHz, Chloroform-*d*) δ 8.35 (s, 2H), 7.51 (d, *J* = 8.5 Hz, 2H), 7.33 – 7.17 (m, 4H), 6.75 (dd, *J* = 7.1, 1.0 Hz, 2H), 4.30 (s, 4H).^{13}C NMR (101 MHz, DMSO-d_6) δ 144.63, 131.75, 126.25, 123.40, 120.95, 116.38, 105.17.

naphthalene-2,6-diamine (3a)

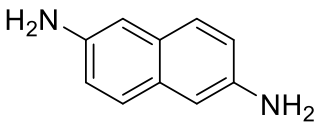

To the suspension of 2,6-dibromonaphthalene (1.4299 g, 5 mmol, 1 equiv.), and P(t-Bu)$_3$ (0.1 M, 0.5 mL, 0.5 mmol, 10 mol%) in 15 mL of anhydrous toluene was purged with nitrogen for 30 mins. The mixture was then added Pd_2dba_3 (114 mg, 125 µmol, 2.5 mol%) and LiHMDS (1.3 M, 9.62 mL, 12.5 mmol, 2.5 equiv.) under nitrogen and reacted in pre-heated oil baths at 80°C. Upon 24 h reaction, 3N HCl (1 mL) was added to the reaction mixture and further reacted for 3h. The resulting solution was filtered and washed with EA/H_2O. The organic solvent was removed in rotatory evaporator followed by the dilution of EA/H_2O. The aqeous layer was then extracted trice with ethyl acetate. The organic fraction was then dried over anhydrous sodium sulphate and followed by solvent removal with rotatory evporator. The crude was then loaded in column chromatography (silica gel, elution with DCM to EA/DCM) and collected fractions are acidified with acetic acid. Upon removal of solvent, titled compound was obtained by precipitaed with MeOH/Et_2O. ^{1}H NMR (400 MHz, DMSO-d_6) δ 7.23 (d, J = 8.6 Hz, 2H), 6.75 (dd, J = 8.7, 2.2 Hz, 2H), 6.66 (d, J = 2.2 Hz, 2H), 4.81 (s, 4H).

[1,1'-biphenyl]-3,3'-diamine (4a)

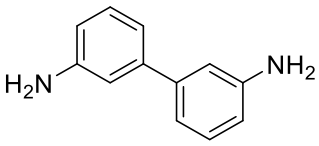

To the suspension of 3,3'-dibromo-1,1'-biphenyl (614 mg, 2 mmol, 1 equiv.) and P(t-Bu)$_3$ (0.1 M, 0.8 mL, 80 µmol, 4 mol%) in 5 mL of anhydrous toluene was purged with nitrogen for 30 mins. The mixture was then added Pd_2dba_3 (18.3 mg, 20 µmol, 1 mol%) and LiHMDS (1.3 M, 3.38 mL, 2.2 equiv.) under nitrogen and the mixture was heated in pre-heated oil baths at 80°C. Upon 24 h reaction, 3N

HCl (1 mL) was added to the reaction mixture and further reacted for 3h. The resulting solution was filtered and washed with MeOH/H_2O. The organic solvent was removed in rotatory evaporator followed by the dilution of DCM/H_2O. The aqeous layer was then extracted trice with dichloromethane. The organic fraction was then dried over anhydrous sodium sulphate and followed by solvent removal with rotatory evporator. The crude was then loaded in column chromatography (silica gel, elution with DCM to EA/DCM) to afford titled compound. ^{1}H NMR (400 MHz, Chloroform-d) δ 7.27 (t, J = 7.8 Hz, 1H), 7.03 (d, J = 7.6 Hz, 1H), 6.91 (s, 1H), 6.71 (d, J = 7.8 Hz, 1H), 3.67 (s, 2H). ^{13}C NMR (101 MHz, Chloroform-d) δ 146.77, 142.64, 129.63, 117.64, 114.20, 113.97.

(E)-3,3'-(ethene-1,2-diyl) dianiline (5b)

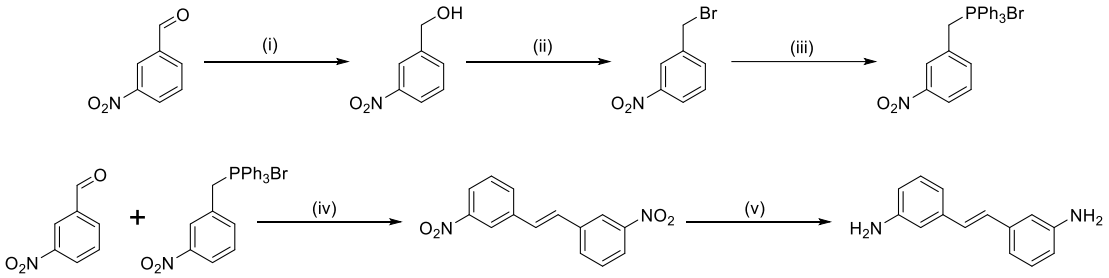

To the solution of 3-nitrobenzaldehyde (2.0034 g, 13 mmol, 1 equiv.) in 100 mL absolute ethanol, sodium borohydride (0.612 g, 16 mmol, 1.22 equiv.) was added at room temperature. Upon overnight stirring, the reaction mixture was quenched by H2O and the organic solvent was removed. The aqueous layer was then extracted with dichloromethane (3X), dried over anhydrous sodium sulphate, filtered, and concentrated in vacuo. to afford pure pale-yellow oil. (1.64 g, 82%). ^{1}H NMR (400 MHz, Methanol-d_4) δ 8.21 (s, 1H), 8.09 (d, J = 8.2 Hz, 1H), 7.71 (d, J = 7.6 Hz, 1H), 7.55 (t,

J = 7.9 Hz, 1H), 4.71 (s, 2H). ^{13}C NMR (101 MHz, Methanol-d_4) δ 148.35, 144.08, 132.41, 129.13, 121.58, 120.83, 62.54.

To the solution of (3-nitrophenyl) methanol (5.7026 g, 36.08 mmol, 1 equiv.) in anhydrous dichloromethane (100 mL), phosphorus tribromide (3.54 mL, 10.7 mmol, 1 equiv.) in anhydrous dichloromethane (20 mL) was added at ice temperature in dropwise manner. The reaction mixture was slowly warmed to room temperature and stirred overnight. Upon completion of reaction, the reaction mixture was diluted with H2O and dichloromethane. The organic extracts were washed with H_2O (2X) and brine (3X), dried over anhydrous sodium sulphate, filtered, and concentrated in vacuo. to afford white powder. (6.3863 g, 80%). ^{1}H NMR (400 MHz, Chloroform-d) δ 8.26 (t, J = 2.1 Hz, 1H), 8.22 – 8.12 (m, 1H), 7.73 (dt, J = 7.7, 1.4 Hz, 1H), 7.54 (t, J = 7.9 Hz, 1H), 4.54 (s, 2H). ^{13}C NMR (101 MHz, Chloroform-*d*) δ 139.75, 134.99, 129.89, 123.93, 123.32, 31.08.

A mixture of 3-nitrobenzyl bromide (6.3869 g, 29 mmol, 1 equiv.), and triphenylphosphine (7.81. g, 29 mmol, 1 equiv.) in toluene (100 mL) was refluxed overnight with vigorous stirring. The reaction was cooled to room temperature and the white solid obtained was filtered, washed with diethyl ether, and dried. The titled products were obtained as pale beige powder (12.8032 g, 92%) ^{1}H NMR (400 MHz, DMSO-d_6) δ 8.15 (d, J = 4.1 Hz, 1H), 7.91 (ddt, J = 8.9, 5.3, 1.7 Hz, 3H), 7.80 – 7.64 (m, 13H), 7.56 (t, J = 8.0 Hz, 1H), 7.46 (d, J = 9.0 Hz, 1H), 5.34 (d, J = 15.9 Hz, 2H).

To a mixture of triphenyl-3-nitrophenylphosphonium bromide (7.17 g, 15 mmol, 1 equiv.) and 3-nitrobenzaldehyde (2.25 g, 1 mmol, 1 equiv.) in anhydrous THF (70 mL) was added dropwise a solution of potassium tert-butoxide (5.04 g, 45 mmol, 3 equiv.) in anhydrous tert-butanol (100 mL) over a period of 1.5 h at 0℃. The resulting reaction was stirred at 0℃ for 2 h, and then allowed to stir at room temperature overnight before quenching with 1N HCl. The solid was then collected by filtration and judged to be pure with NMR spectroscopy. 1H NMR (400 MHz, DMSO-d_6) δ 8.10 (ddd, J = 8.0, 2.7, 1.3 Hz, 1H), 8.04 (t, J = 2.0 Hz, 1H), 7.66 – 7.58 (m, 1H), 7.56 (t, J = 7.9 Hz, 1H), 6.93 (s, 1H).

To (E)-1,2-bis(3-nitrophenyl) ethene (2.6 g, 9.6 mmol, 1 equiv.) in 50 mL absolute ethanol, anhydrous tin (II) chloride (10 g) was added. The resulting suspension was heated to reflux temperature for overnight reaction. Upon completion of reaction, the solvent was removed under reduced pressure and the crude was diluted with ethyl acetate and trace methanol. The yellow solution was then filtered with silica pad (5 cm, eluted from EA (discarded) to 30% MeOH/EA) to afford yellow solid. The yellow solid was then suspended in water and solids were removed while the resulting filtrate was dried under reduced pressure to afford titled compound. ^{1}H NMR (600 MHz, DMSO-d_6) δ 6.86 (t, J = 7.7 Hz, 1H), 6.48 (s, 1H), 6.43 – 6.38 (m, 2H), 6.36 (s, 1H).

Ligand L_{1a}-L_{4a}, L_{2a-2b}

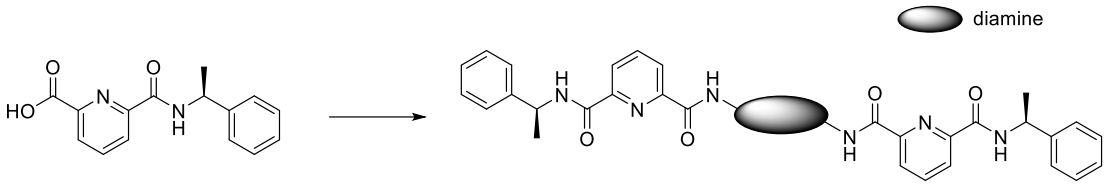

General Procedure. To the solution of chelator (2.2 equiv.) in 25 mL of anhydrous DMF was added HATU (3 equiv.). The resulting mixture was stirred at room temperature for 30 mins before adding diamine spacer (1.15 mmol, 1 equiv.). Upon stirring for another 30 minutes, DIPEA 6 equiv.) was added and the reaction mixture was stirred for 3 days before partition with DCM/H_2O. The organic solvent was removed under reduced pressure and the crude was redissolved in ethyl acetate and washed with H_2O (5X); brine (3X) followed by dried over anhydrous magnesium sulphate to afford crude products. The crude oil was then purified by column chromatography or precipitation.

Ligand L_{1a}. 1H NMR (400 MHz, DMSO-d_6) δ 11.39 (s, 2H), 9.72 (d, J = 8.8 Hz, 2H), 8.72 (s, 2H), 8.37 (dd, J = 7.5, 1.4 Hz, 2H), 8.32 (dd, J = 7.8, 1.5 Hz, 2H), 8.25 (t, J = 7.6 Hz, 2H), 8.02 (dd, J = 8.7, 1.2 Hz, 2H), 7.78 (d, J = 7.1 Hz, 2H), 7.58 (dd, J = 8.6, 7.1 Hz, 2H), 7.43 (d, J = 7.4 Hz, 4H), 7.30 (dd, J = 8.5, 6.8 Hz, 4H), 7.24 – 7.15 (m, 2H), 5.43 – 5.28 (m, 2H), 1.59 (d, J = 7.0 Hz, 6H). ^{13}C NMR (101 MHz, DMSO-d_6) δ 163.28, 163.15, 149.71, 149.28, 144.64, 140.21, 133.46, 132.16, 128.79, 128.24, 127.76, 127.22, 126.61, 125.91, 125.69, 125.53, 123.86, 123.10, 48.42, 22.31.

Ligand L_{1b} ^{1}H NMR (600 MHz, $CDCl_3$) δ 14.34 (s, 2H), 9.37 (dt, *J* = 9.3, 2.0 Hz, 4H), 8.49 (ddd, *J* = 26.0, 7.7, 1.1 Hz, 4H), 8.15 (t, *J* = 7.7 Hz, 2H), 7.73 – 7.54 (m, 8H), 7.37 (t, *J* = 7.7 Hz, 4H), 7.31 – 7.23 (m, 4H), 5.74 – 5.56 (m, 2H), 1.82 (d, *J* = 7.0 Hz, 6H).

^{13}C NMR (151 MHz, $CDCl_3$) δ 186.86, 163.31, 162.71, 149.12, 148.32, 143.50, 141.16, 139.45, 136.20, 134.98, 128.66, 127.22, 126.13, 126.09, 125.87, 125.23, 123.28, 118.02, 48.41, 22.55.

Ligand L_{2a} ^{1}H NMR (400 MHz, DMSO-d_6) δ 11.13 (s, 2H), 9.69 (d, *J* = 8.5 Hz, 2H), 8.70 (d, *J* = 2.0 Hz, 2H), 8.58 (s, 2H), 8.42 (dd, *J* = 6.8, 2.1 Hz, 2H), 8.35 – 8.24 (m, 4H), 8.19 (d, *J* = 9.2 Hz, 1H), 7.88 (dd, *J* = 9.1, 2.0 Hz, 2H), 7.55 – 7.47 (m, 4H), 7.44 – 7.34 (m, 4H), 7.32 – 7.21 (m, 2H), 5.34 (p, *J* = 7.2 Hz, 2H), 1.68 (d, *J* = 7.0 Hz, 6H). ^{13}C NMR (101 MHz, DMSO-d_6) δ 163.13, 162.52, 149.65, 149.16, 144.64, 140.29, 135.16, 131.38, 129.95, 129.09, 128.86, 127.30, 126.65, 125.97, 125.44, 123.13, 117.48, 48.67, 22.31.

Ligand L_{2b}. ^{1}H NMR (400 MHz, DMSO-d_6) δ 11.32 (s, 2H), 9.66 (d, J = 8.4 Hz, 2H), 8.67 (d, J = 2.3 Hz, 2H), 8.44 – 8.20 (m, 12H), 7.95 (d, J = 8.5 Hz, 2H), 7.56 – 7.45 (m, 4H), 7.38 (t, J = 7.6 Hz, 4H), 7.35 – 7.22 (m, 4H), 6.93 (dd, J = 8.6, 2.4 Hz, 2H), 6.72 (s, 4H), 5.33 (p, J = 7.2 Hz, 2H), 1.67 (d, J = 6.9 Hz, 6H). ^{13}C NMR (101 MHz, DMSO-d_6) δ 163.28, 163.15, 149.71, 149.28, 144.64, 140.21, 133.46, 132.16, 128.79, 128.24, 127.76, 127.22, 126.61, 125.91, 125.69, 125.53, 123.86, 123.10, 48.42, 22.31.

Ligand L_{3a} ^{1}H NMR (600 MHz, DMSO-d_6) δ 11.08 (s, 1H), 9.66 (d, *J* = 8.5 Hz, 1H), 8.52 (d, *J* = 1.9 Hz, 1H), 8.40 (d, *J* = 7.3 Hz, 1H), 8.31 – 8.22 (m, 2H), 8.04 (d, *J* = 8.8 Hz, 1H), 7.87 (d, *J* = 8.8 Hz, 1H), 7.49 (d, *J* = 7.7 Hz, 2H), 7.38 (t, *J* = 7.6 Hz, 2H), 7.26 (t, *J* = 7.3 Hz, 1H), 5.34 (p, *J* = 7.3 Hz, 1H), 1.67 (d, *J* = 7.0 Hz, 3H).

Ligand L_{4b}. ^{1}H NMR (400 MHz, Chloroform-d) δ 9.92 (s, 2H), 8.85 (d, J = 8.3 Hz, 2H), 8.25 (dd, J = 18.8, 7.7 Hz, 4H), 7.90 (t, J = 7.8 Hz, 2H), 7.44 – 7.28 (m, 8H), 7.24 – 7.10 (m, 7H), 7.06 (d, J = 7.7 Hz, 2H), 5.29 (t, J = 7.4 Hz, 2H), 1.47 (d, J = 6.9 Hz, 6H). ^{13}C NMR (101 MHz, Chloroform-d) δ 163.07, 162.11, 149.00, 148.53, 143.14, 141.08, 138.89, 137.13, 129.14, 128.56, 127.32, 126.26, 125.48, 124.99, 123.91, 120.15, 49.02, 21.44.

2.4.3. Computation simulations

The simulation of ligand was performed in using semi-empirical calculation software MOPAC v22.0.4 using KEYWORD: PM7 PRECISE CHARGE=0 EF LET AUX XYZ BONDS GNORM=0.0100 CHARGE=0 while the initial guess is pre-simplified through Chem3D. The detailed calculations are summarized on appendix section.

2.5. Reference

1. Li, X. Z.; Zhou, L. P.; Yan, L. L.; Yuan, D. Q.; Lin, C. S.; Sun, Q. F., Evolution of Luminescent Supramolecular Lanthanide M2nL3n Complexes from Helicates and Tetrahedra to Cubes. *J Am Chem Soc* **2017,** *139* (24), 8237-8244.

2. Yeung, C. T.; Yim, K. H.; Wong, H. Y.; Pal, R.; Lo, W. S.; Yan, S. C.; Yee-Man Wong, M.; Yufit, D.; Smiles, D. E.; McCormick, L. J.; Teat, S. J.; Shuh, D. K.; Wong, W. T.; Law, G. L., Chiral transcription in self-assembled tetrahedral Eu4L6 chiral cages displaying sizable circularly polarized luminescence. *Nat Commun* **2017,** *8* (1), 1128.

3. Wong, H. Y.; Lo, W. S.; Yim, K. H.; Law, G. L., Chirality and Chiroptics of Lanthanide Molecular and Supramolecular Assemblies. *Chem* **2019,** *5* (12), 3058-3095.

4. Yim, K. H.; Yeung, C. T.; Wong, H. Y.; Law, G. L., Structural variation of self-assembled lanthanide supramolecular complexes induced by reaction conditions. *Inorg. Chem. Front.* **2021,** *8* (12), 2952-2964.

5. Li, X. Z.; Tian, C. B.; Sun, Q. F., Coordination-Directed Self-Assembly of Functional Polynuclear Lanthanide Supramolecular Architectures. *Chem Rev* **2022,** *122* (6), 6374-6458.

6. Barry, D. E.; Caffrey, D. F.; Gunnlaugsson, T., Lanthanide-directed synthesis of luminescent self-assembly supramolecular structures and mechanically bonded systems from acyclic coordinating organic ligands. *Chem Soc Rev* **2016,** *45* (11), 3244-74.

7. Feng, X. S.; Li, X. Z.; Hu, S. J.; Yan, D. N.; Zhou, L. P.; Sun, Q. F., Base- and Metal-Dependent Self-Assembly of Lathanide-Organic Coordination Polymers or Macrocycles with Tetradentate Acylhydrazone-based Ditopic Ligands. *Chem Asian J* **2021,** *16* (11), 1392-1397.

8. Wang, Z.; He, L.; Liu, B.; Zhou, L. P.; Cai, L. X.; Hu, S. J.; Li, X. Z.; Li, Z.; Chen, T.; Li, X.; Sun, Q. F., Coordination-Assembled Water-Soluble Anionic Lanthanide Organic Polyhedra for Luminescent Labeling and Magnetic Resonance Imaging. *J Am Chem Soc* **2020,**

142 (38), 16409-16419.

9. Tang, X.; Chu, D.; Gong, W.; Cui, Y.; Liu, Y., Metal-Organic Cages with Missing Linker Defects. *Angew Chem Int Ed Engl* **2021,** *60* (16), 9099-9105.

10. Bing, T. Y.; Kawai, T.; Yuasa, J., Ligand-to-Ligand Interactions That Direct Formation of D2-Symmetrical Alternating Circular Helicate. *J Am Chem Soc* **2018,** *140* (10), 3683-3689.

11. Zhu, Q. Y.; Zhou, L. P.; Cai, L. X.; Li, X. Z.; Zhou, J.; Sun, Q. F., Chiral auxiliary and induced chiroptical sensing with 5d/4f lanthanide-organic macrocycles. *Chem Commun (Camb)* **2020,** *56* (19), 2861-2864.

12. Yim, K.-H.; Yeung, C.-T.; Probert, M. R.; Chan, W. T. K.; Mackenzie, L. E.; Pal, R.; Wong, W.-T.; Law, G.-L., Helicate-to-tetrahedron transformation of chiral lanthanide supramolecular complexes induced by ionic radii effect and linker length. *Communications Chemistry* **2021,** (116).

13. Cook, T. R.; Zheng, Y. R.; Stang, P. J., Metal-organic frameworks and self-assembled supramolecular coordination complexes: comparing and contrasting the design, synthesis, and functionality of metal-organic materials. *Chem Rev* **2013,** *113* (1), 734-77.

14. Caulder, D. L.; Raymond, K. N., Supermolecules by Design. *Acc. Chem. Res.* **1999,** *32* (11), 975-982.

15. Caulder, D. L.; Raymond, K. N., The rational design of high symmetry coordination clusters. *J. Chem. Soc., Dalton Trans.* **1999,** (8), 1185-1200.

16. Piguet, C.; Williams, A. F.; Bernardinelli, G., The First Self-Assembled Dinuclear Triple-Helical Lanthanide Complex: Synthesis and Structure. *Angew Chem Int Ed Engl* **1992,** *31* (12), 1622-1624.

17. Lessmann, J. J.; Horrocks, W. D., Jr., Supramolecular coordination chemistry in aqueous solution: lanthanide ion-induced triple helix formation. *Inorg Chem* **2000,** *39* (15), 3114-24.

18. Andre, N.; Scopelliti, R.; Hopfgartner, G.; Piguet, C.; Bunzli, J. C., Discriminating between lanthanide ions: self-assembly of heterodimetallic triple-stranded helicates. *Chem Commun (Camb)* **2002,** (3), 214-5.

19. Bocquet, B.; Bernardinelli, G.; Ouali, N.; Floquet, S.; Renaud, F.; Hopfgartner, G.; Piguet, C., The first self-assembled trimetallic lanthanide helicate: different coordination sites in symmetrical molecular architectures. *Chem Commun (Camb)* **2002,** (9), 930-1.

20. Hamacek, J.; Blanc, S.; Elhabiri, M.; Leize, E.; Van Dorsselaer, A.; Piguet, C.; Albrecht-Gary, A. M., Self-assembly mechanism of a bimetallic europium triple-stranded helicate. *Journal of the American Chemical Society* **2003,** *125* (6), 1541-1550.

21. Piguet, C.; Bunzli, J. C. G.; Bernardinelli, G.; Hopfgartner, G.; Williams, A. F., Self-Assembly and Photophysical Properties of Lanthanide Dinuclear Triple-Helical Complexes. *Journal of the American Chemical Society* **1993,** *115* (18), 8197-8206.

22. Brayshaw, P. A.; Bunzli, J. C. G.; Froidevaux, P.; Harrowfield, J. M.; Kim, Y.; Sobolev, A. N., Synthetic, Structural, and Spectroscopic Studies on Solids Containing Tris(Dipicolinato) Rare-Earth Anions and Transition or Main-Group Metal-Cations. *Inorganic Chemistry* **1995,** *34* (8), 2068-2076.

23. Leonard, J. P.; Jensen, P.; McCabe, T.; O'Brien, J. E.; Peacock, R. D.; Kruger, P. E.; Gunnlaugsson, T., Self-assembly of chiral luminescent lanthanide coordination bundles. *J Am Chem Soc* **2007,** *129* (36), 10986-7.

24. A.Kitchen, J., Lanthanide-based self-assemblies of 2,6-pyridyldicarboxamide ligands: Recent advances and applications as next-generation luminescent and magnetic materials. *Coordin Chem Rev* **2017,** *340*, 232-246.

25. Yeung, C. T.; Chan, W. T.; Yan, S. C.; Yu, K. L.; Yim, K. H.; Wong, W. T.; Law, G. L., Lanthanide supramolecular helical diastereoselective breaking induced by point chirality:

mixture or P-helix, M-helix. *Chem Commun (Camb)* **2015,** *51* (3), 592-5.

Chapter 3: Functionalization of stable luminescence 1,2-HOPO-based building blocks

3.1. Introduction

3.1.1. Background

In the previous chapter, the supramolecular self-assembly of ditopic tridentate ligands were studied while a series of spacer unit with different offsetting properties and symmetry have been investigated. However, the lack of the stability in chelating units obstructs the diverse exploration of higher-order architectures in which the prospect from spacer modification is hindered from the intrinsic volatility of metal coordination in pyridine-2,6-dicarboxamide (pcam) moiety. It is not surprised that strong Ln-L interaction are favored to safeguard the thermodynamic and kinetic stability of final assembly.[1,2] With natural self-assembling processes as example, metal coordination underlies the construction of many biological molecular assemblies such as daily example in chlorophyll and hemoglobin.[3,4]

The core investigation of this chapter is, therefore, devising a stable luminescence building blocks which provide sufficient stability and considerable photophysical properties. For that purpose, numerous study have been conducted to prepare inert ligand scaffold such as cryptand, podand or macrocyclic system.[3-7] Among the devised chelator, 1,2-hydroxypyridionate (1,2-HOPO) are known to be one of the most balanced sensitizer for europium which stayed intact in aqueous environments.[7-15] As

reported by Raymond, the coordination of di-1,2-HOPO system results in extremely stable structure even in different temperature and pH environment.[7, 8, 11, 12, 16]

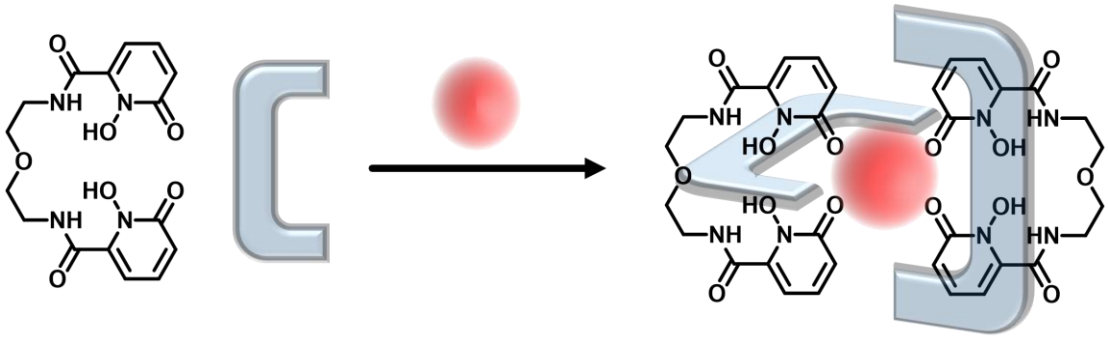

Figure 3-1: graphic illustration of LnL_2 lock-like coordination

As depicted in the figure, oxygen-rich and anionic 1,2-HOPO ligands complex as stable ML_2 lock structure with the oxyphilic and electropositive characteristic of lanthanide ions.[7, 17] This macrocyclic-like system provides sufficient stability without extensive pre-organization in bicyclic or other macrocyclic structure such as cryptand and DOTA.

As mentioned in the introduction chapter, Prof. Stang and Prof. Fujita adopt the concept of angularity and directionality in their transition metal supramolecular self-assembling complexes. In general, the concept utilizes the directionality in transition metal originated from d-orbital overlapping that they generally share similar coordination geometry such as square planar, tetrahedral and octahedral with predefined metal-coordination directionality. Through selectively capping, transition metal precursor with certain angularity can be engineered to different ditopic and tritopic units.

When the concept is applied to lanthanide system, it is obvious that lanthanide does not proceed predefined geometry as transition metal. To facilitate the lanthanide coordination in place, macrocyclic like ligands are preferred as chelating scaffold to lock trivalent lanthanide ions. With the functionalized building blocks, the C_2-rigid linker and spacer are also introduced to provide angularity and directionality as well as flexibility for the twisted coordination lock. With the three component or two component design, it is expected to allow the investigation on the supramolecular self-assembling behaviors yielding different two-dimensional polygons through systematic engineering in angularity, directionality and flexibility.

3.1.2. Scope of study

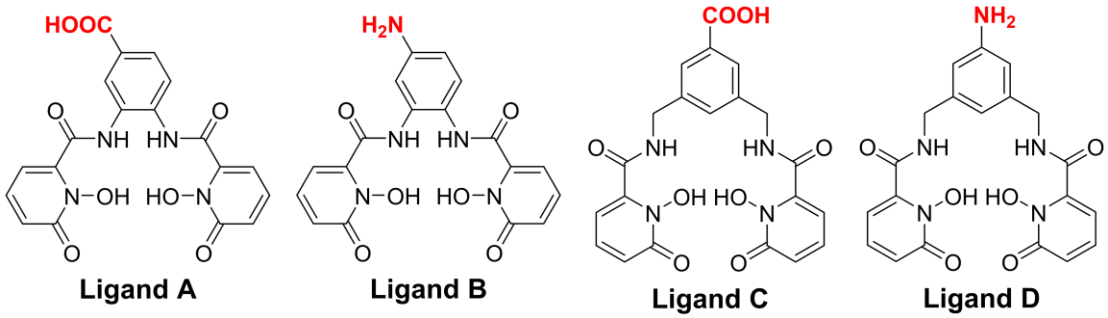

Figure 3-2: Summary in the functionalization of di-1,2-HOPO unit in Chapter three

In *Chapter Three*, there are two parts consisting of (1) functionalization of di-1,2-HOPO building blocks and (2) investigation in supramolecular self-assembly with functionalized di-1,2-HOPO moiety. The functionalized designs are shown in Figure **3-2** which their detailed synthesis, characterization and photophysical properties are shown in the first section. The second section summarize the current investigation on adopting such units in supramolecular self-assembling system.

3.2. Result & Discussion

3.2.1. Synthesis & Characterization

3.2.1.1. Synthesis & Characterization of Ligand

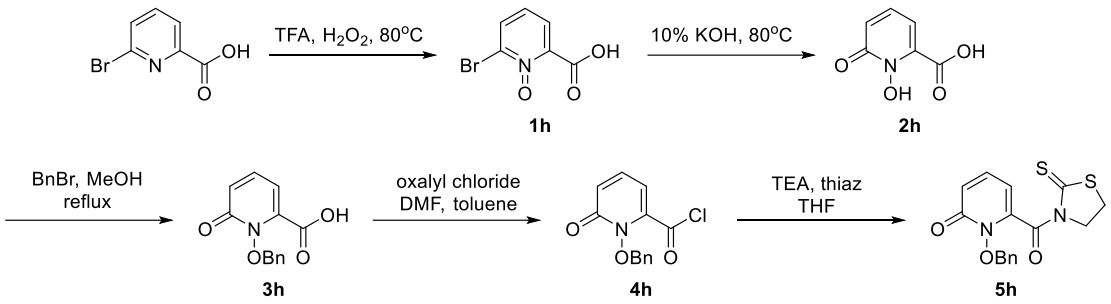

Figure 3-3: synthetic scheme of HOPO compound

Synthesis of 1,2-HOPO-OBn derivative. Based on the reported procedure[15], 2-bromopiconlic acid are first oxidized to afford N-oxide followed by heating in strongly basic hydroxide medium to afford 1,2-HOPO. The subsequent benzyl protection yields 1,2-HOPO-OBn with satisfactory yield and purity. The compound **3h** is then either activated by oxalyl chloride for amide coupling or converted to stable HOPO-thiaz with two-steps procedure. The former acid chloride version is freshly prepared and used directly without further purification while the compound **5h** is stored in the dark and fridge to avoid degradation. All the compound except compound **4h** are isolated and purified while the detailed synthetic procedure and structural characterization are included in experimental section.

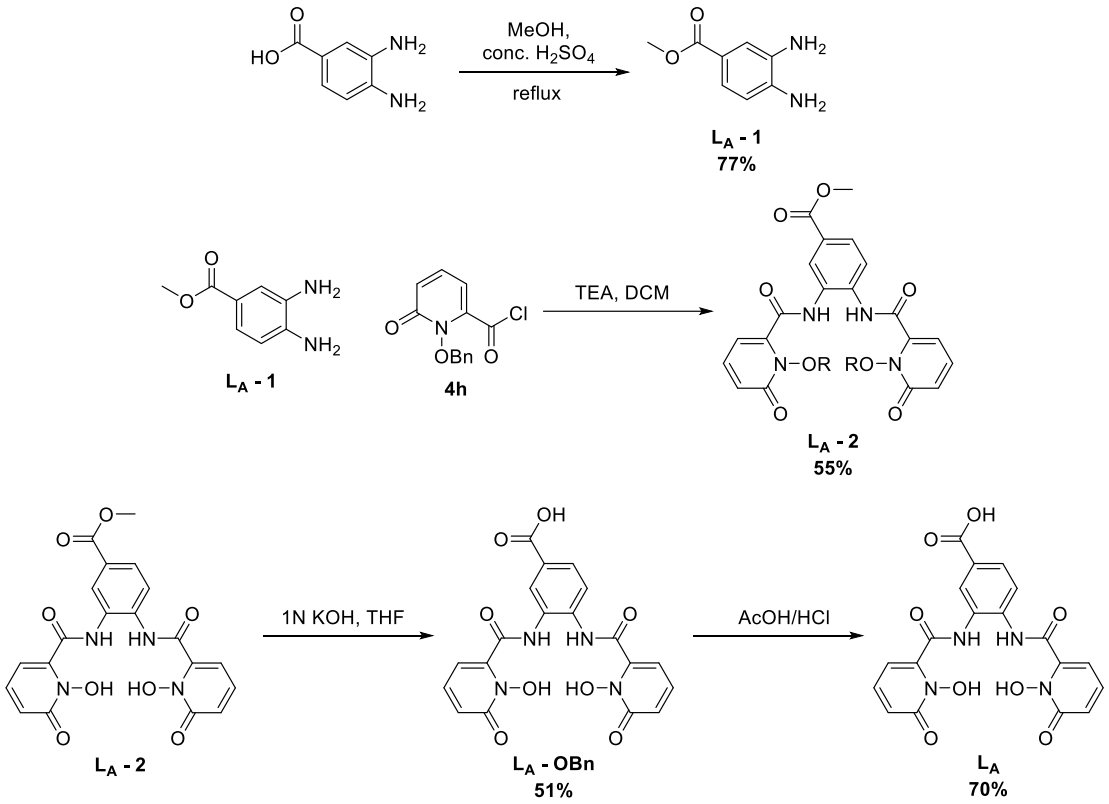

Figure 3-4: Synthetic Scheme of ligand $\mathbf{L_A}$

Synthesis and characterization of ligand $\mathbf{L_A}$. The methyl protection of diaminobenzoic acid is performed in standard Fischer esterification with the catalyst of concentrated H_2SO_4.[18, 19] Upon purification, the compound **$\mathbf{L_A}$-1** are then coupled with compound 4h in dichloromethane to afford compound **$\mathbf{L_A}$-2**. Two subsequent deprotection of methyl group and benzyl group afford ligand **$\mathbf{L_A}$**. In this section, all the listed compounds are isolated and purified with standard column chromatography in silica while the detailed synthetic procedures are provided in experimental section.

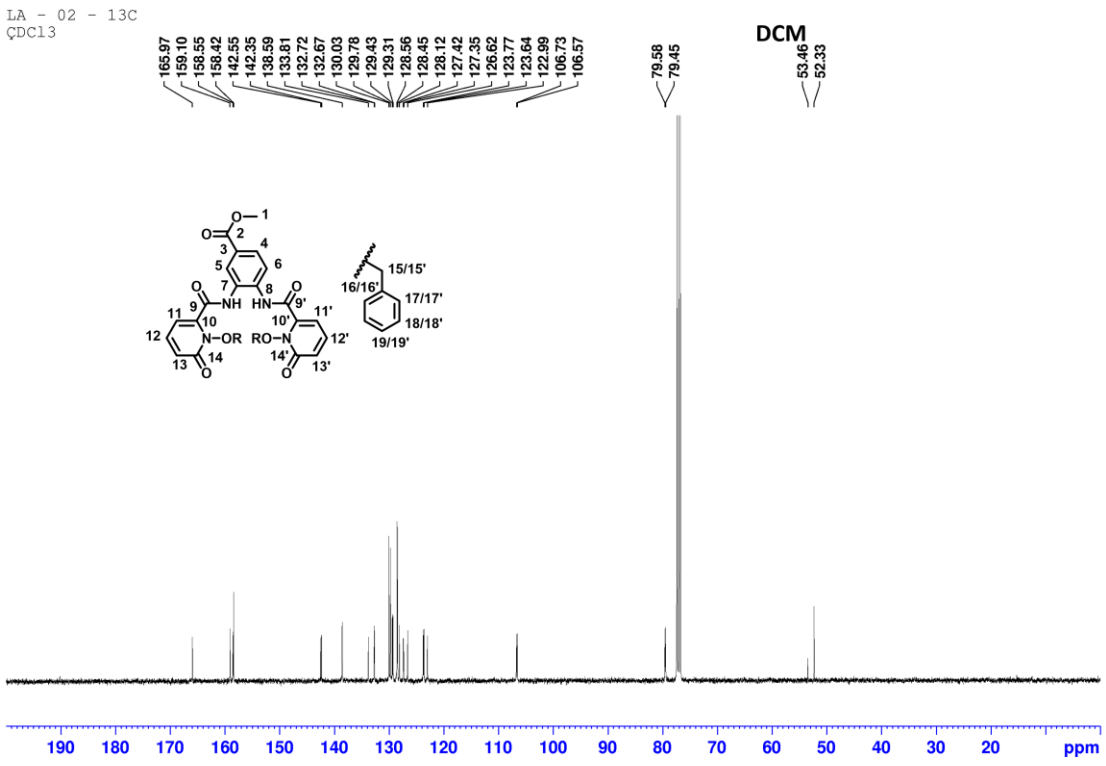

Spectrum S3-1: ^{13}C NMR spectrum of **L_A-2**

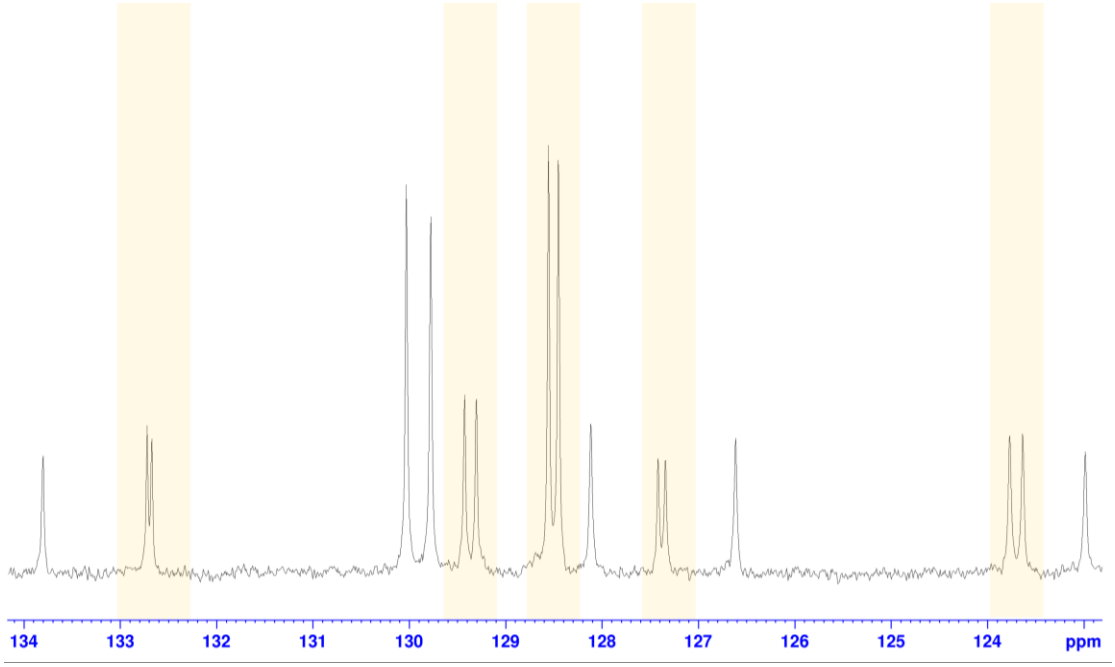

Spectrum S3-2: illustration on spilt-like signal in ^{13}C NMR spectrum of **L_A-2**

Due to the asymmetric nature of intermediate **L_A-2** and **L_A-OBn** and ligand **L_A**, some of the carbon will experience two environments when the asymmetric acid/ester

moiety is in close proximity. With the illustration of the spectrum **S3-1**, there are splitting-like carbon signal (denoted as denoted as 9' to 19'.) while some may occasionally disappear due to resolution of NMR spectroscopy. In contrast to ^{13}C NMR, ^{1}H-NMR is generally not sensitive to such minimal environment change as indicated in spectrum **S3-3**. Without the detailed discussion, the characterization of all intermediates and ligand $\mathbf{L_A}$ are assigned with similar manner and listed in experimental sections.

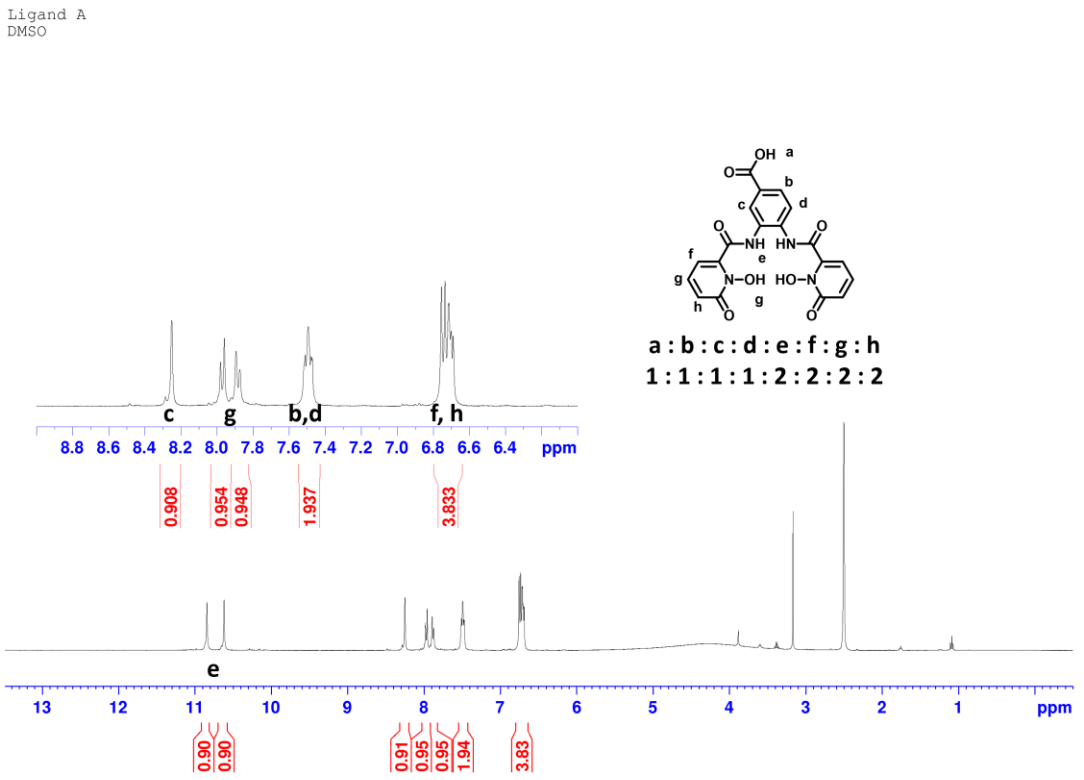

Spectrum S3-3: ^{1}H NMR spectrum of $\mathbf{L_A}$

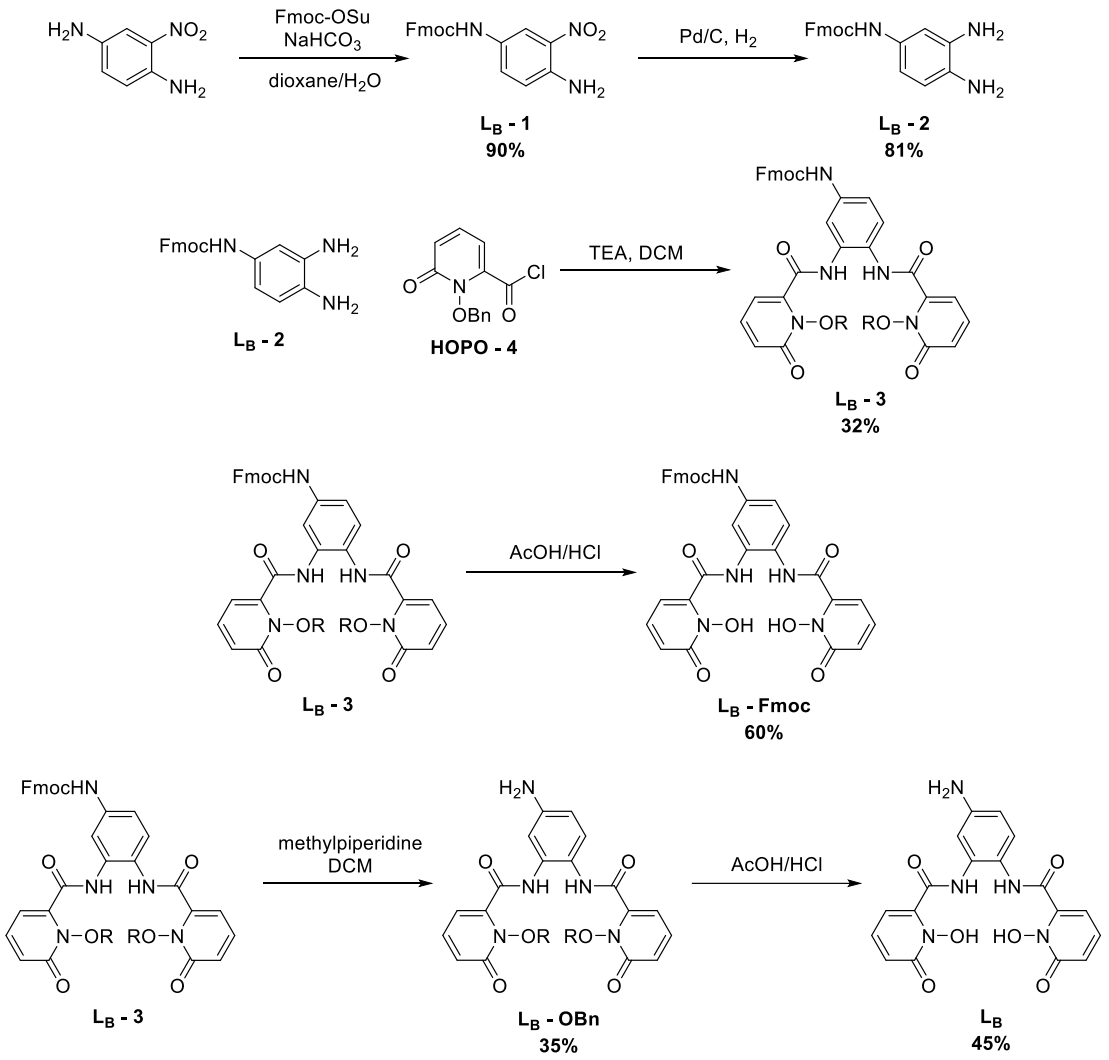

Figure 3-5: Synthetic Scheme of Ligand L_B

Synthesis and Characterization of ligand L_B. To prepare ligand L_B, diamino-nitrobenzene is first protected with Fmoc-OSu in weakly basic biphasic system. The purified bright yellow intermediates **L_B-1** are reduced with hydrogen balloon under Pd/C catalysts to afford compound **L_B-2**. With dropwise addition of compound **4h** to the solution of L_B-2 in freshly distilled dichloromethane and triethylamine, compound **L_B-3** are isolated and purified with column chromatography. To facilitate further investigation, both protection and unprotection version of final ligand **L_B-fmoc** and **L_B** are synthesized while the detailed synthetic procedure is provided in experimental

section. In analogy to ligand **L_A**, asymmetric nature leads to splitting-like carbon signal in compound **L_B-3**, **L_B-OBn** and two final ligands. The detailed proton assignment and carbon count are performed in spectrum **S3-18** to **S3-27**.

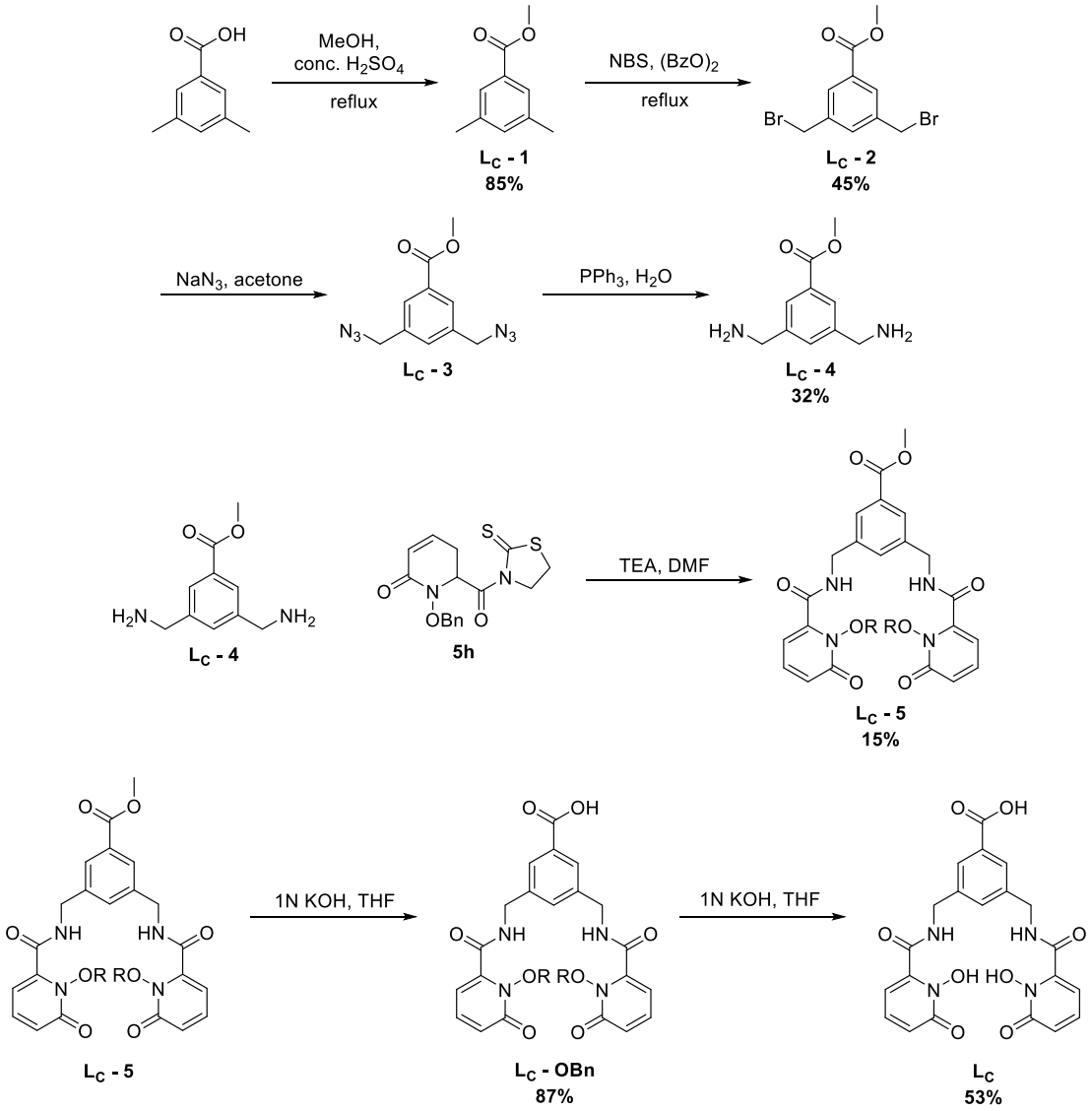

Figure 3-6: Synthetic Scheme of Ligand **L_C**

Synthesis and characterization of ligand L_C. In contrast to previous ligand, the ligand L_C is synthesized with different methodology. Dimethylbenzoic acid is first protected with standard Fischer esterification. The protected intermediates **L_C-1** is brominated using radical substitution in nitrogen-purging system. Upon completion of

reaction, the mixture is then purified and re-crystallized from hot hexane to afford pure intermediates **L_C-2**.[20,21]

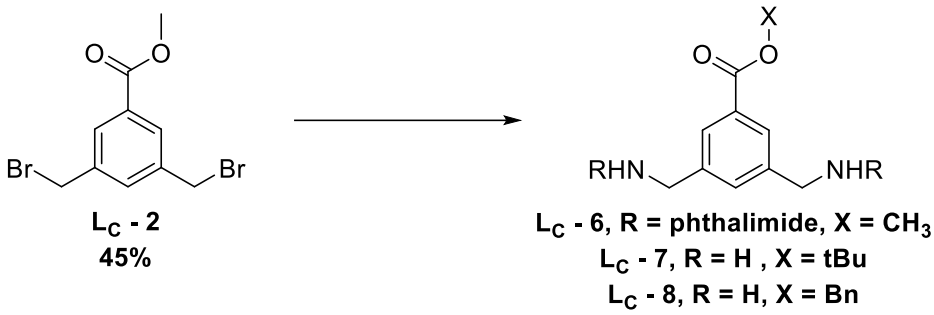

Figure 3-7: Synthesis of compound **L_C-6**, **L_C-7** & **L_C-8**

To avoid the use of sodium azide, the initial protocol makes use of Gabriel synthesis which substitutes bromide with S_N2 nucleophilic substitution to afford compound **L_C-6**. Upon purification, the compound is deprotected with either (i) NaOH, followed by HCl neutralization or (ii) hydrazine hydrate to afford compound **L_C-4**.[22,23]

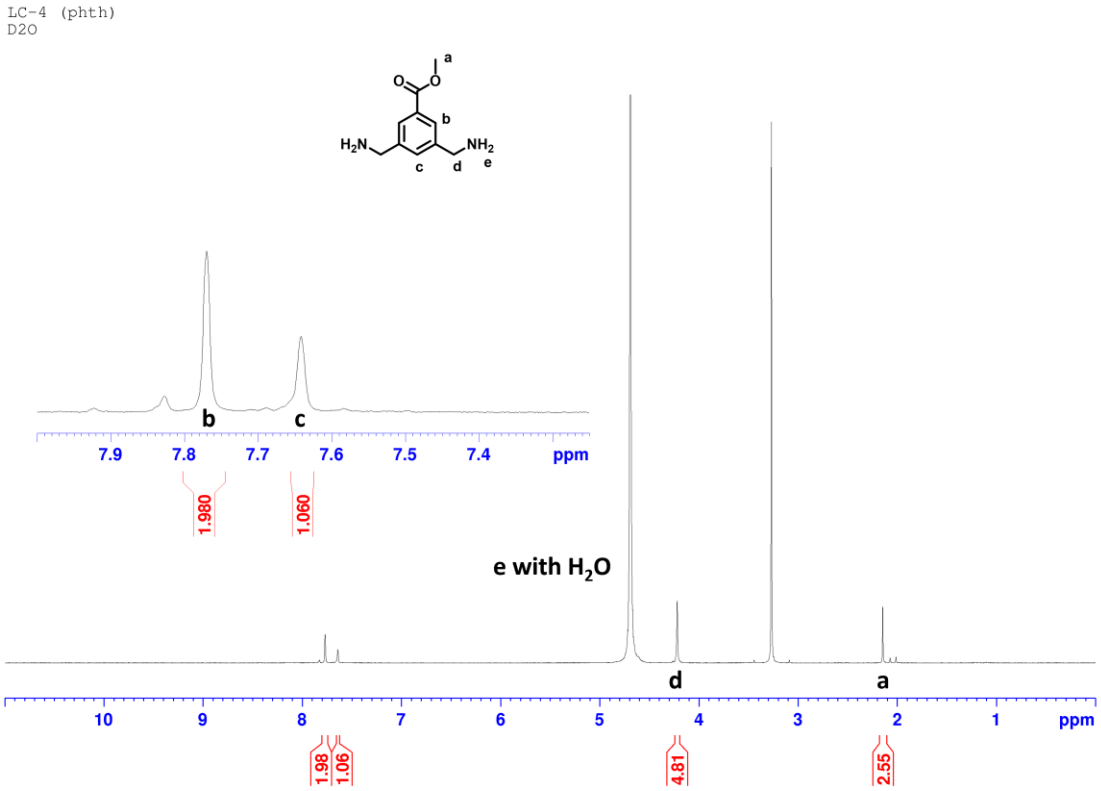

Spectrum 3-4: ^{1}H NMR spectrum of compound **L_C-4** obtained from phthalimide deprotection.

The proton NMR of obtained compound is shown in spectrum **S3-4** which it is evident with mass spectroscopy data that desired intermediates are afforded. However, the subsequent amide coupling failed to afford the desired compound **L_C-5** with different activation and amide coupling reagent such as HATU, thiaz, NHS, EDCI and HOBt. To address the issue, the protecting group is modified to t-butyl group and benzyl group (compound **L_C-7** and **L_C-8**) while no successful trials in amide coupling are obtained.

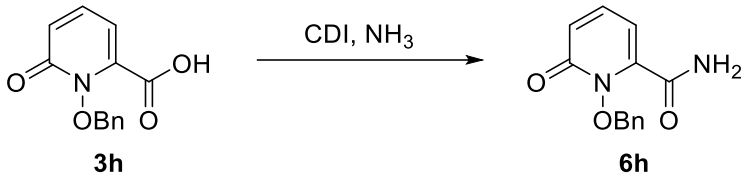

3h **6h**

Figure 3-8: amide conversion of compound **3h**

As an alternative approach, compound 3h is converted to amide **6h** using CDI coupling. Multiple attempts were then employed to couple compound **6h** and compound **L_C-2** using copper or palladium catalyst. However, no desired compounds are identified.

The ultimate scheme using sodium azide followed by reduction amination to yield intermediates **L_C-4**.[24,25] The subsequent amide coupling with compound **5h** is successful using high concentration condition in N, N'-dimethylformamide. It is inferred that the phthalimide salt residues or trace side products from previous step hinder the subsequent amide coupling. Upon purification in column chromatography, the obtained compound undergoes two deprotection to obtain final ligand **L_C**. All the obtained intermediates are isolated and purified except instable compound **L_C-3.** The detailed experimental procedures are listed in section 3.4.2 while the completed characterizations are included in spectrum **S3-28** to **S3-38**.

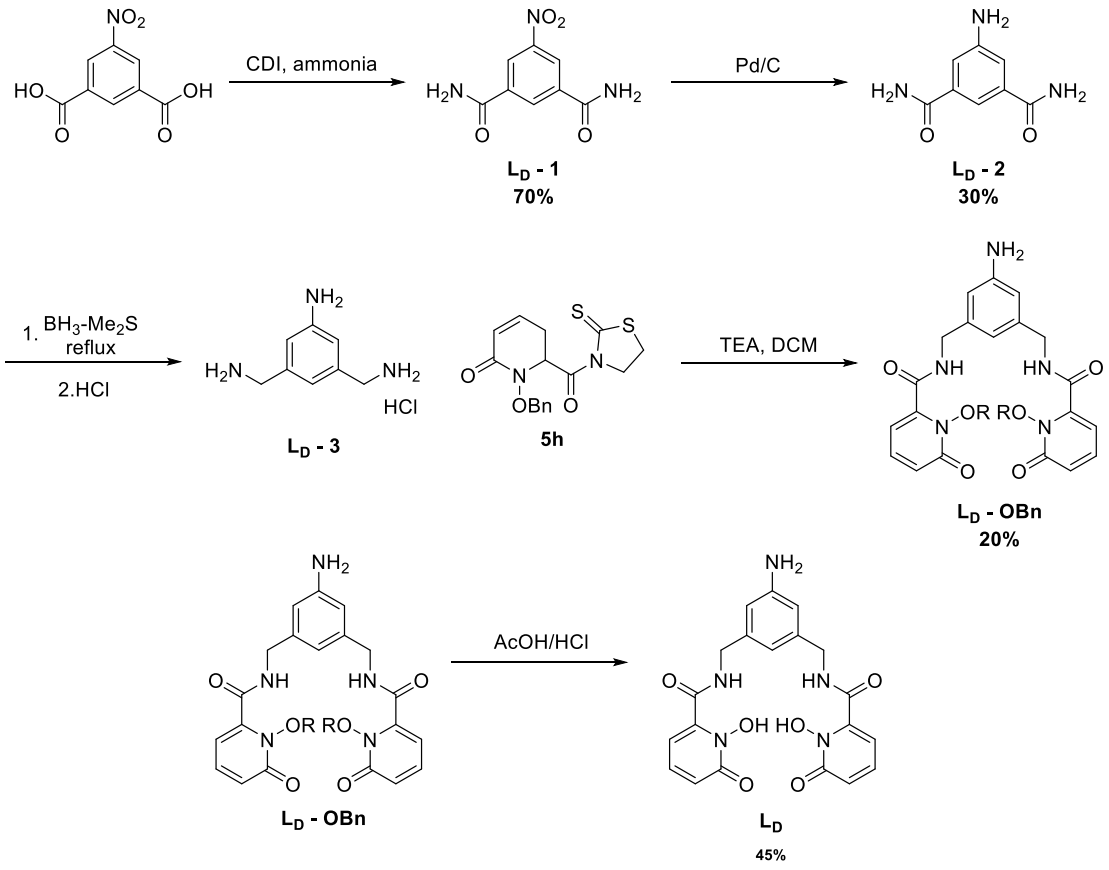

Figure 3-9: Synthetic Scheme of Ligand $\mathbf{L_D}$

Synthesis and Characterization of ligand $\mathbf{L_D}$. The synthesis of ligand $\mathbf{L_D}$ start with amidation of 5-nitroisophthalic acid with CDI coupling followed by reduction with Pd/C as catalyst.[26] The intermediates $\mathbf{L_D}$**-2** is further reduced with borane reagent to afford intermediates $\mathbf{L_D}$**-3**. The obtained crude is then hydrolyzed with 3N HCl and the hydroscopic solids are collected with MeOH/Et_2O precipitation and used without further purification. Upon amide coupling with compound **5h**, the purified compound $\mathbf{L_D}$**-OBn** is then deprotected under glacial acetic acid and concentrated hydrochloric acid to afford final ligand $\mathbf{L_D}$. With the exception of highly hydroscopic intermediate $\mathbf{L_D}$**-3**, all the compounds are isolated and purified while the detailed synthetic procedures and characterization are included in experimental section and appendix respectively.

3.2.1.2. Complexation of Ligand A-D and Structural Characterization of Complexes

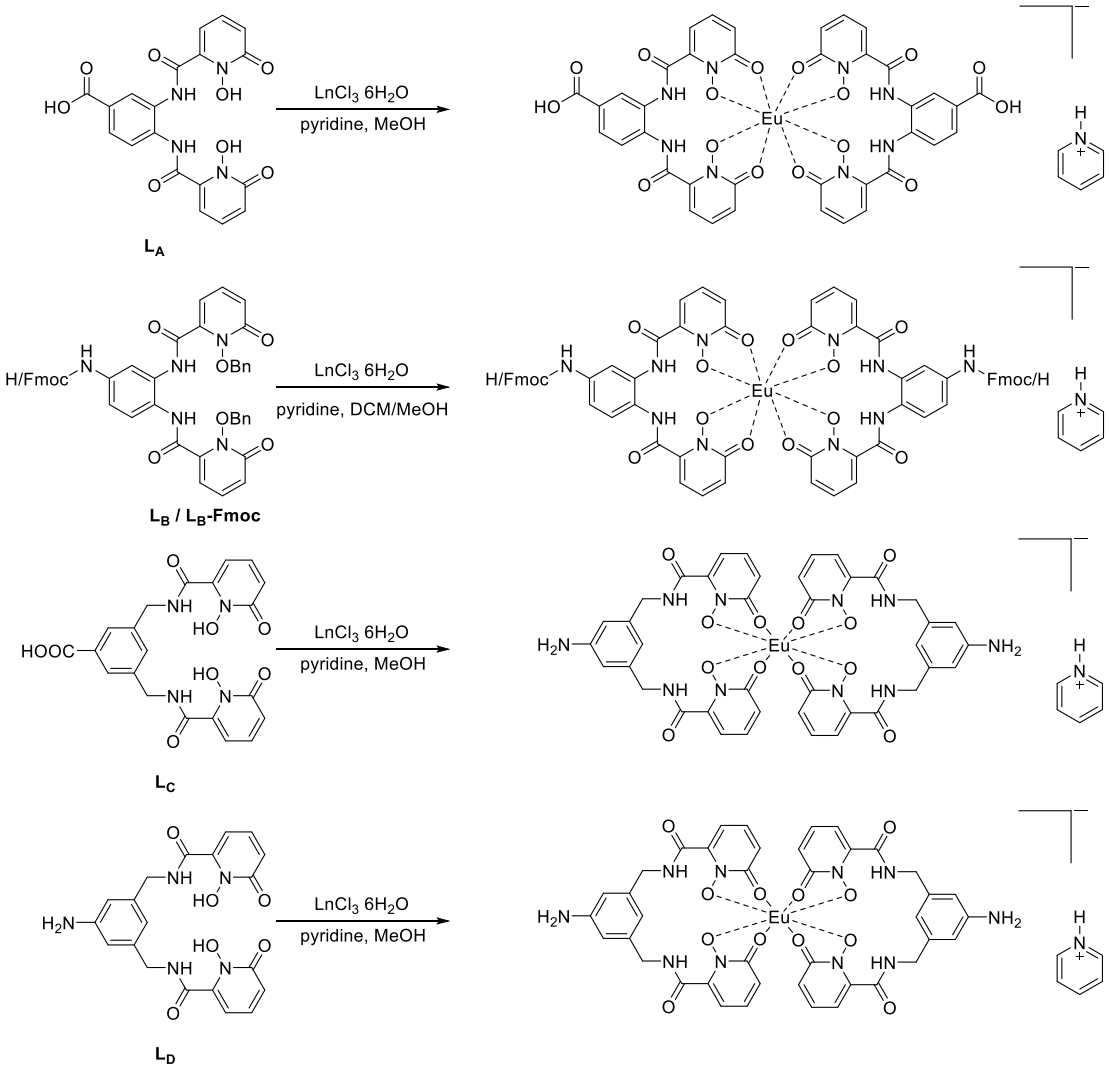

Figure 3-10: Synthetic Scheme of complexes Eu$\mathbf{L_x}$

General Procedure of Complexation To the solution of ligand (2 equiv., 20 mg, 20mL, Chloroform/MeOH, 1:1) is added 2 drops of pyridine. Upon 30 minutes stirring at 50°C, lanthanide(III) chloride hexahydrate (1.025 equiv.) in 1 mL methanol is added. The reaction is stirred overnight at same temperature before solvent removal in vacuo. The crude plate is redissolved with hot methanol followed by precipitation with diethyl ether. The complexes are then collected with centrifuge followed by few washings of

diethyl ether. The obtained complexes are investigated with HRMS, ^{1}H NMR, ^{1}H-^{1}H COSY NMR spectroscopy whenever possible.

Characterization of Complexes Due to the paramagnetic nature of some lanthanide complexes, the characterization with NMR spectroscopy is less informative for coordinated structure. The synthesized complexes are mainly characterized with ESI-HRMS. As illustration, synthesized europium complexes are analyzed as depicted in spectrum **S3-5** to **S3-10** while the full spectrums are included in the appendix section for clarity. From TOF-ESI-HRMS spectrum, it is evident that anticipated ML_2 complexes are resulted while the amino functionalized ligand demonstrated another typical signal of $[MLCl_2]^-$ (**S3-6** & **S3-10**).

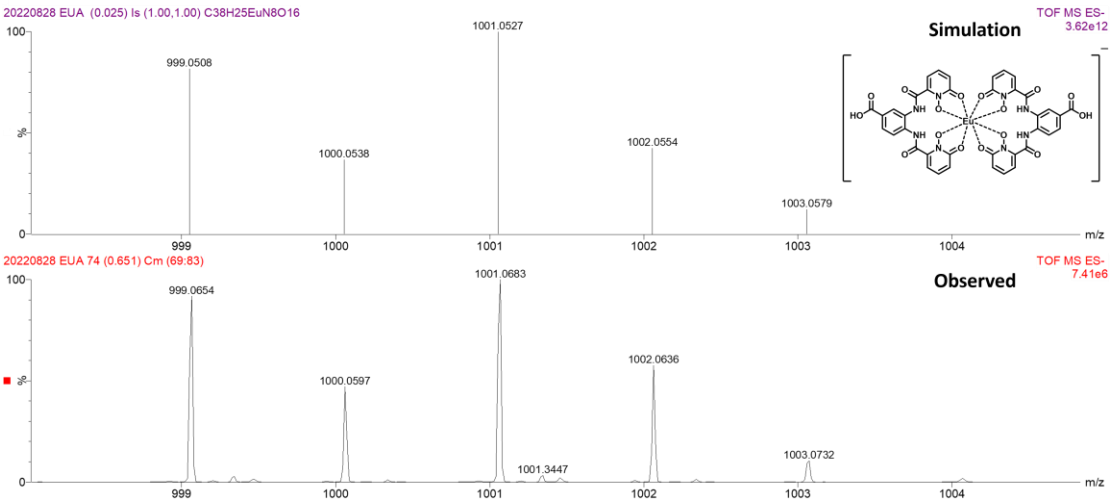

Spectrum S3-5: simulated & observed isotopic distribution of complexes **EuL_A**

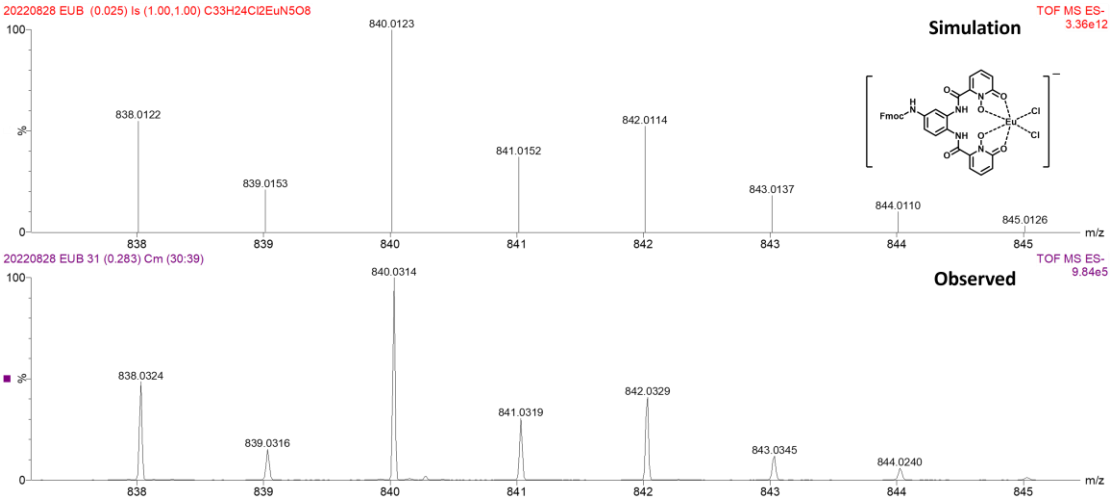

Spectrum S3-6: simulated & observed isotopic distribution of complexes **EuL$_B$-fmoc** (ML species)

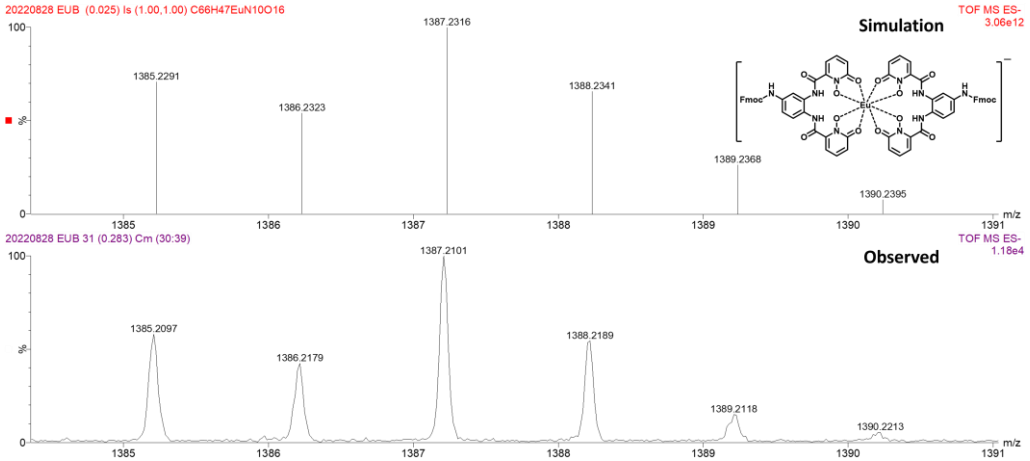

Spectrum S3-7: simulated & observed isotopic distribution of complex **EuL$_B$-fmoc** (ML_2 species)

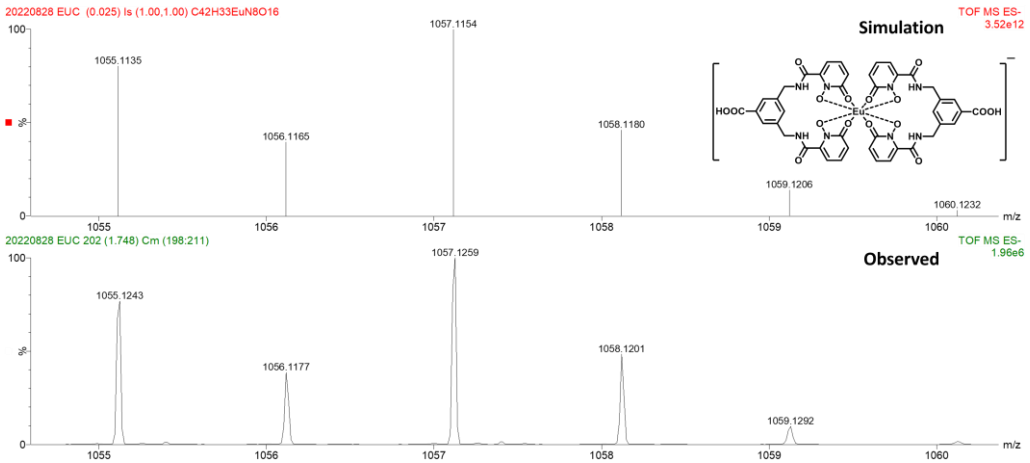

Spectrum S3-8: simulated & observed isotopic distribution of complexes **EuL$_C$**

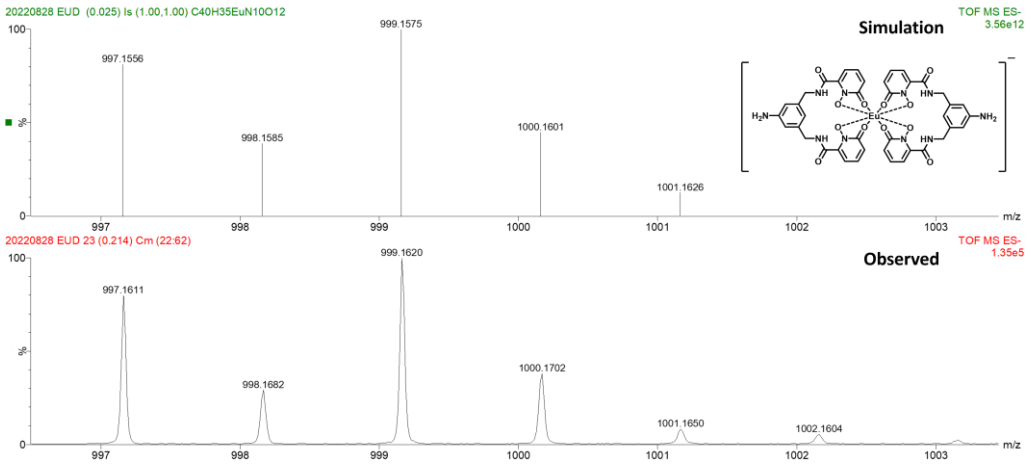

Spectrum S3-9: simulated & observed isotopic distribution of complexes **EuL$_D$** (ML_2 species)

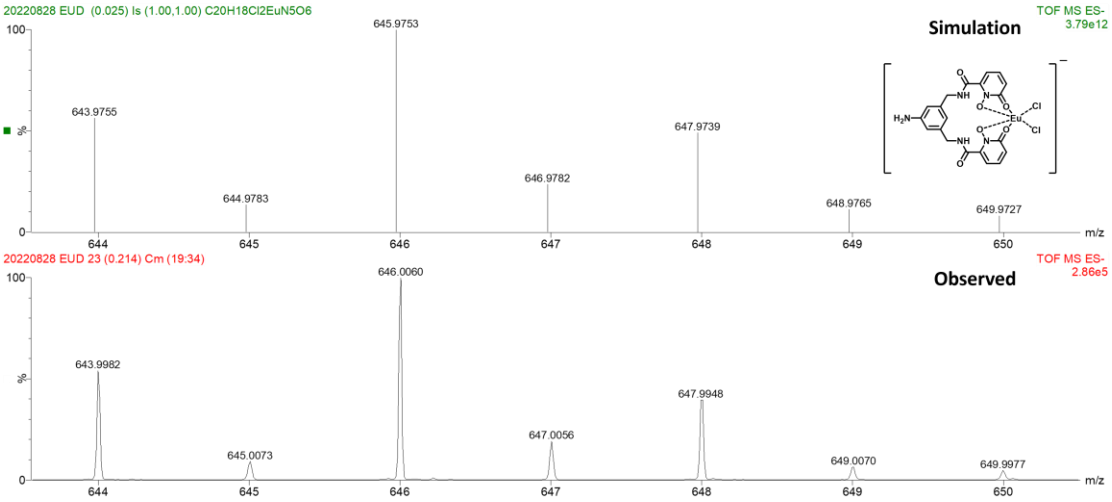

Spectrum S3-10: simulated & observed isotopic distribution of complexes **EuL$_D$** (ML species)

3.2.1.3. Photophysical Measurement

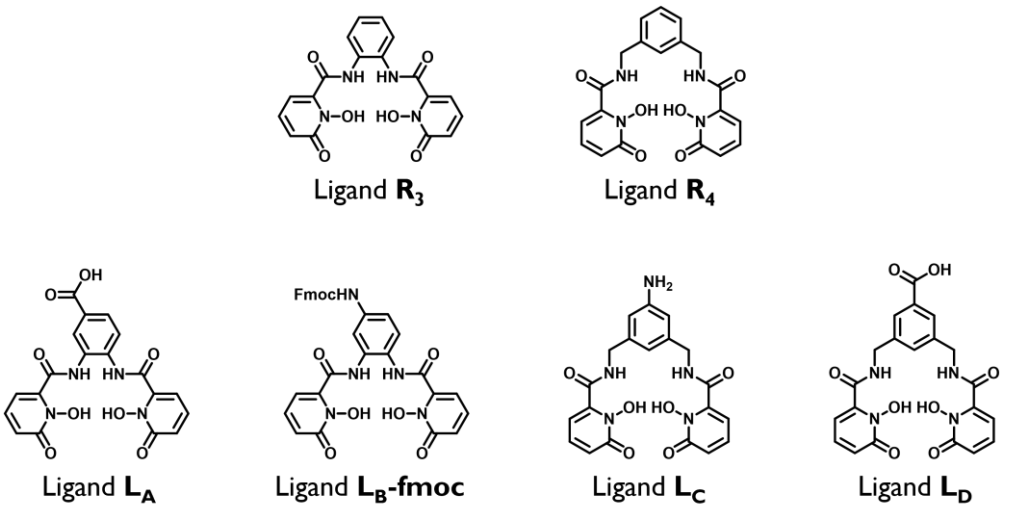

Figure 3-11: summary on reference and synthesized ligands

	λ_{ABS}^{max} (nm)	ε (M-1cm-1)	Φ_{TOT}	Φ_{Eu}	η_{sens}	τ(H_2O) (μs)	τ(D_2O) (μs)
Reference complexes							
$[Eu(R_3)_2]^-$	342	21,020	6.2%	36.5%	17%	536	734
$[Eu(R_4)_2]^-$	333	16,264	22%	43.6%	50%	733	1022
Synthesized complexes[e]							
$[Eu(L_A)_2]^-$	340	29,669 (3,000)[f]	8.5%[a] 2.1%[b]	40.0%	5.3%[d]	494	636
$[Eu(L_B\text{-fmoc})_2]^-$	356	28,861 (2,000)[f]	3.4%[a] 0.7%[b]	37.8%	1.9%[d]	410 118	481 131
$[Eu(L_C)_2]^-$	332	18,844 (500)[f]	5.8%[b]	41.7%	13.9%[d]	729	996
$[Eu(L_D)_2]^{-a}$	332	16,264 (2,000)[f]	16.0%[a] 3.7%[b]	41.2%	9.0%[d]	714 138	987 346

a The measurement is performed in Edinburgh Instruments FLSP920 spectrophotometer

b The measurement is performed in HORIBA Fluoromax-4 Spectrofluorometer

c Calculation is based on the QY obtained from Edinburgh Instruments FLSP920 spectrophotometer

d Calculation is based on the QY obtained from HORIBA Jobin Yvon Fluoromax-4 Spectrofluorometer

e All the measurements are conducted in 5% DMSO/H_2O (duplicate) and 5% DMSO/0.1 M HEPES (1x)

f Standard deviation from the measurements

Table **3-1**: Summary in basic photophysical measurement on complex **EuL_x**

To understand the photophysical properties of synthesized complexes, some basic photophysical measurements are conducted and the results are summarized in table **3-1**. Due to the malfunction of Edinburgh Instruments FLSP920 spectrophotometer, HORIBA Jobin Yvon Fluoromax-4 spectrofluorometer are used for secondary equipment for quantum yield (QY) measurements.

As depicted in the table, same compound exhibits a substantial four-fold difference in QY even quantum yields are obtained in relative to freshly prepared quinine sulphate standard (in 0.1 M H_2SO_4, λ_{ex}= 350 nm, Φ = 0.546[27]). As all measurements from two instruments have been repeated for at least triplicate set with good statistical fit (i.e. R^2 is close to 0.996 - 1) while the obtained spectrum is included in appendix. It is believed that the deviation in fluoromax spectrophotometer is attributed from the inherent instrumentation limitation that hinder the detection of emission.

As shown in Table 3-1, the ligand L_A and L_B are considered to be derivatives of ligand R_3 while ligand Lc and L_D are categorized as derivatives of ligand R_4. In general, the obtained quantum yields from R_3 derivatives are higher than those from R_4 with three to five-fold differences. This agrees with the literature findings that the ligand with five-carbon spacing between chelating units generally possess higher quantum yields. It is believed that the metal-ligand distance take an important role in such enhancement as the energy transfer mechanism are generally distance-dependent. In addition Table **3-1** show 3-fold increases from complexes **EuL_A** to **EuL_C**. At the same time, the introduction of acid moiety likely to promote the quantum yield while that of amino moiety would suppress the emission.

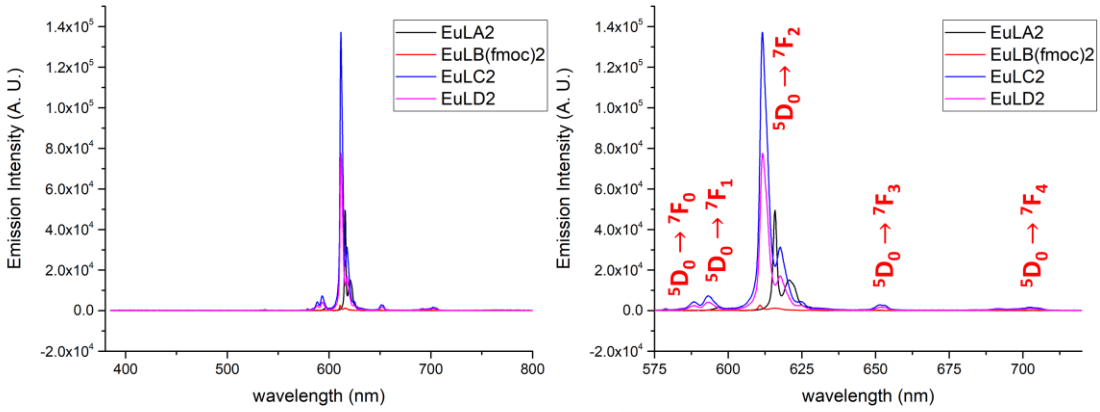

Figure 3-12: Stacked emission spectrum of **EuLx**

In figure 3-12, the emission spectrum of four complexes is stacked without normalization. It is clearly indicated that complexes **EuL$_A$** and **EuL$_B$** have significantly lower emission intensity while complexes C and D shared similar patterns in the hypersensitive transition.

	$[Eu(L_A)_2]^-$		$[Eu(L_B\text{-fmoc})_2]^-$		$[Eu(L_C)_2]^-$	$[Eu(D)_2]$
Parker's Equation	0.2	0.1[a]	0.7[b]	0.1	0.2[a]	4.9[b]
Horrocks' Equation	0.2	0.06[a]	0.6[b]	0.06	0.09[a]	4.5[b]

[a,b] calculated from long-lived species and short-lived species respectively

Table **3-2**: summary on hydration state calculation

For further investigation, the emission lifetime measurements are performed and reveals that ligand **L$_A$** and **L$_C$** with acid moiety generally agree with mono-exponential decay while ligand **L$_B$-fmoc** and **L$_D$** fit better in bi-exponential decay. To identify the unknown species, the hydration number is calculated with both Parker's Equation and Horrocks' Equation.[28,29] From the table, it can be observed that the short-lived species in synthesized **EuL$_B$-fmoc** and **EuL$_D$** complexes have higher hydration state which is

probably coordinated to the aqueous medium. Gathering the information from HRMS, it is likely that the mixture of ML and ML_2 coordination complexes exist in amino-functionalized complexes **EuL_B-fmoc** and **EuL_D** which is likely attributed to coordination with solvent molecules.

3.2.1. Investigation in Supramolecular Self-Assembly

3.2.1. Design Principle

To examine the supramolecular self-assembling behaviors of 1,2-di-HOPO-based building blocks, photoluminescent ligand LC and L_D are employed for further investigation. In general, the design consists of three components containing (1) linker units, (2) spacer units and (3) HOPO- based chelating units. With reference to crystal structure of reference compound,[7] the synthesized chelating units are most likely to be complexed with distorted bicapped trigonal prismatic (C_{2v}) geometry. In such ML_2 systems, the ligands must align in a specific manner to facilitate the coordination.

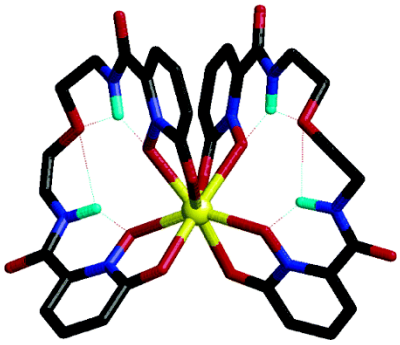

Figure **3-13:** Bicapped trigonal prismatic molecular geometry of reference[7]

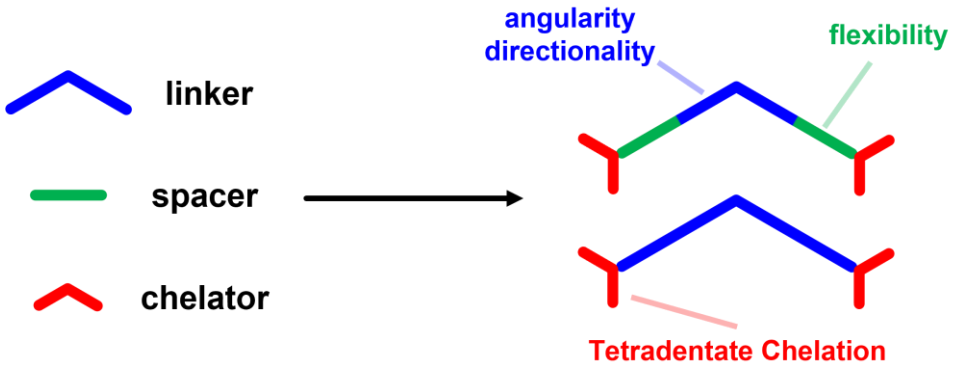

Figure 3-14: Design principle on di-HOPO-based ditopic ligands

Taking advantage of such characteristics, different linker and spacing units can be employed to modify the supramolecular self-assembling preference. For the linker, it should contain sufficient steric bulkiness to avoid twisting and provide a directing angle to guide the coordination. Meanwhile, non-conjugated spacing units are required to promote the energy sensitization and govern the flexibility. With such design, it is anticipated that different topologies can be resulted through varying the different angularity on the ligands as depicted in figure **3-15.**

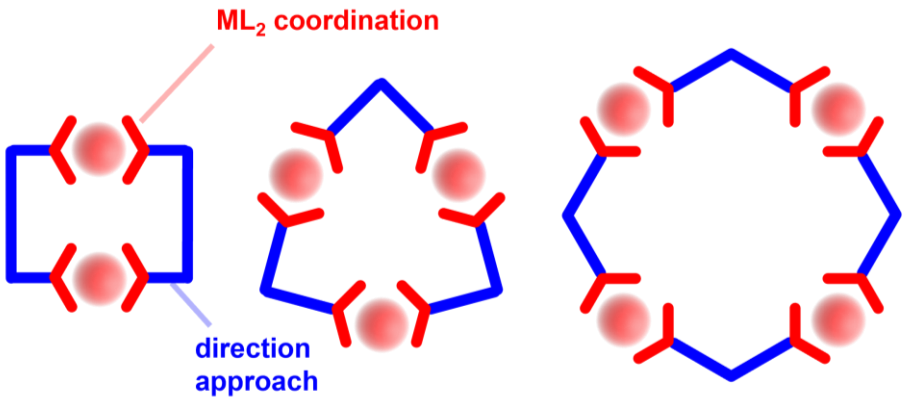

Figure **3-15**: graphic illustration on possible self-assembly

3.2.1. Investigation on ligand L_E

As a primary investigation, pyridine-2,6-dicarboxamide units are employed as linker which provides directing angle towards same sides. To synthesize the compound, dipicolinic acids are first functionalized with aminophenol followed by connecting with four-carbon spacing units as shown in figure **3-17**. With the characterization of ^{1}H, ^{13}C NMR spectroscopy and ESI-HRMS, compound **L_E-OBn** is successfully prepared while the subsequent deprotection is failed upon detailed investigation. As shown in spectrum **S3-15**, protected ligand **L_E-OBn** should contain three amide protons (denoted as proton c, k and m). However, all proton signals from amide are

disappeared with the benzyl protons e upon deprotonation with acidic medium which indicate the dissociation of ligand structure. As most aromatic regions are remained intact from the spectrum. The most likely dissociation is occurred at ether linkage between spacer and linker units. For further investigation, alternative linkage is under investigation while investigations on other two ligand design **L_F** and **L_G** are conducted in parallel.

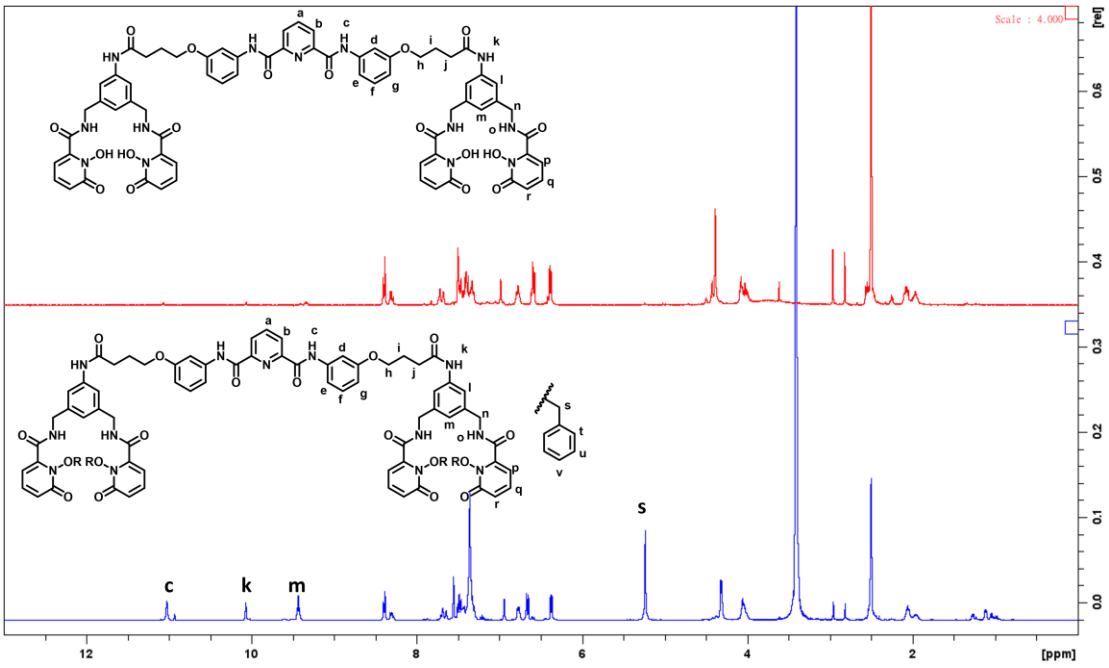

Spectrum S3-15: stacked spectrum in deprotecting **L_E-OBn**

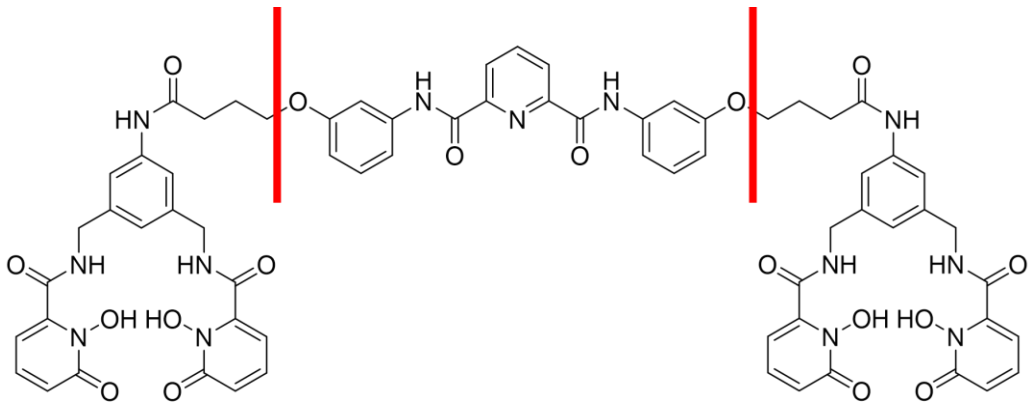

L_E

Figure 3-16: illustration on the dissociation in ligand

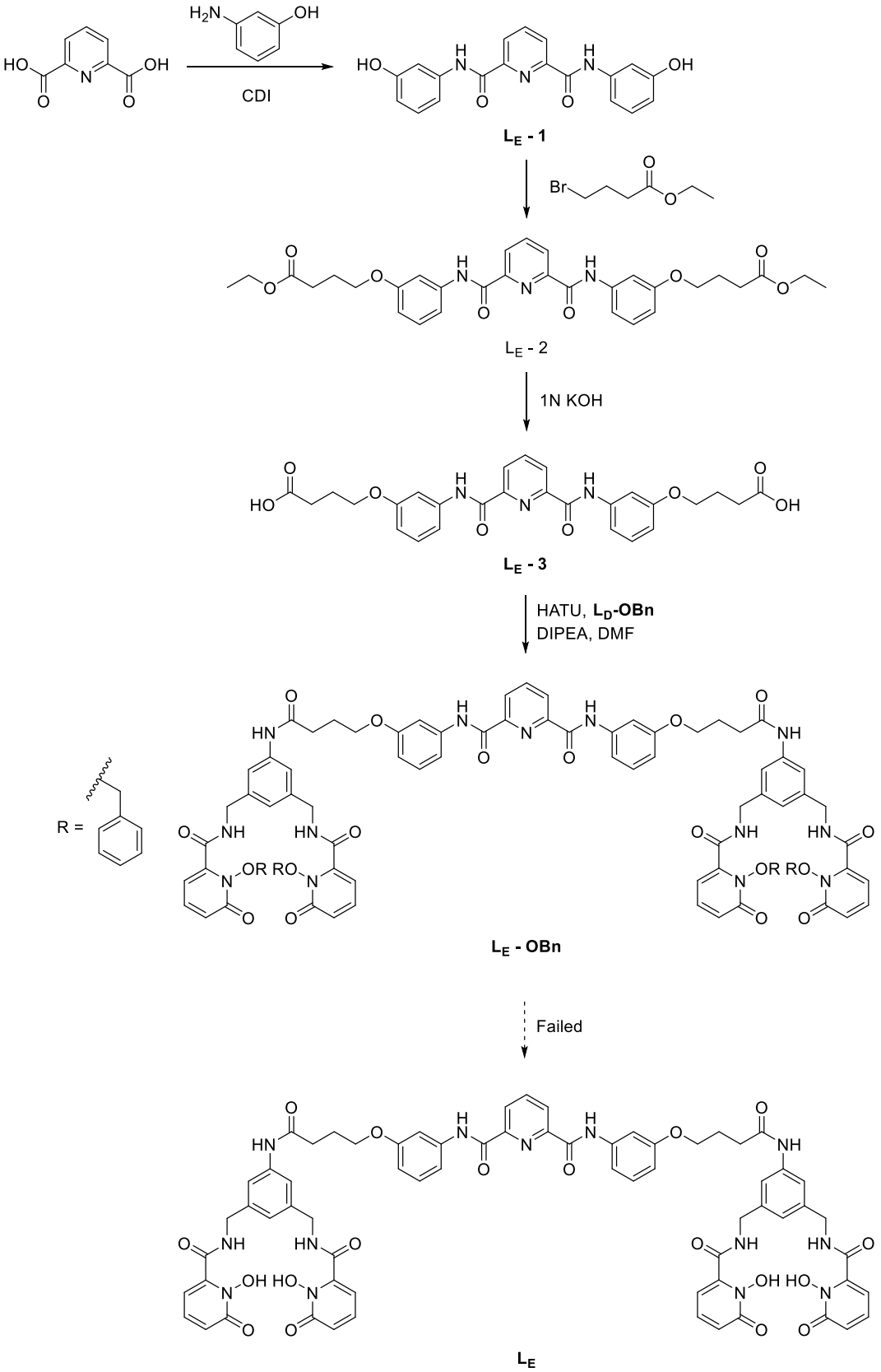

Figure 3-17: synthetic scheme of Ligand L_E

3.2.1. Investigation on ligand L_F & L_G

In addition to primary design, the synthesis of two different ligands based on ligand **L_C** and **L_D** are attempted as shown in following figure.

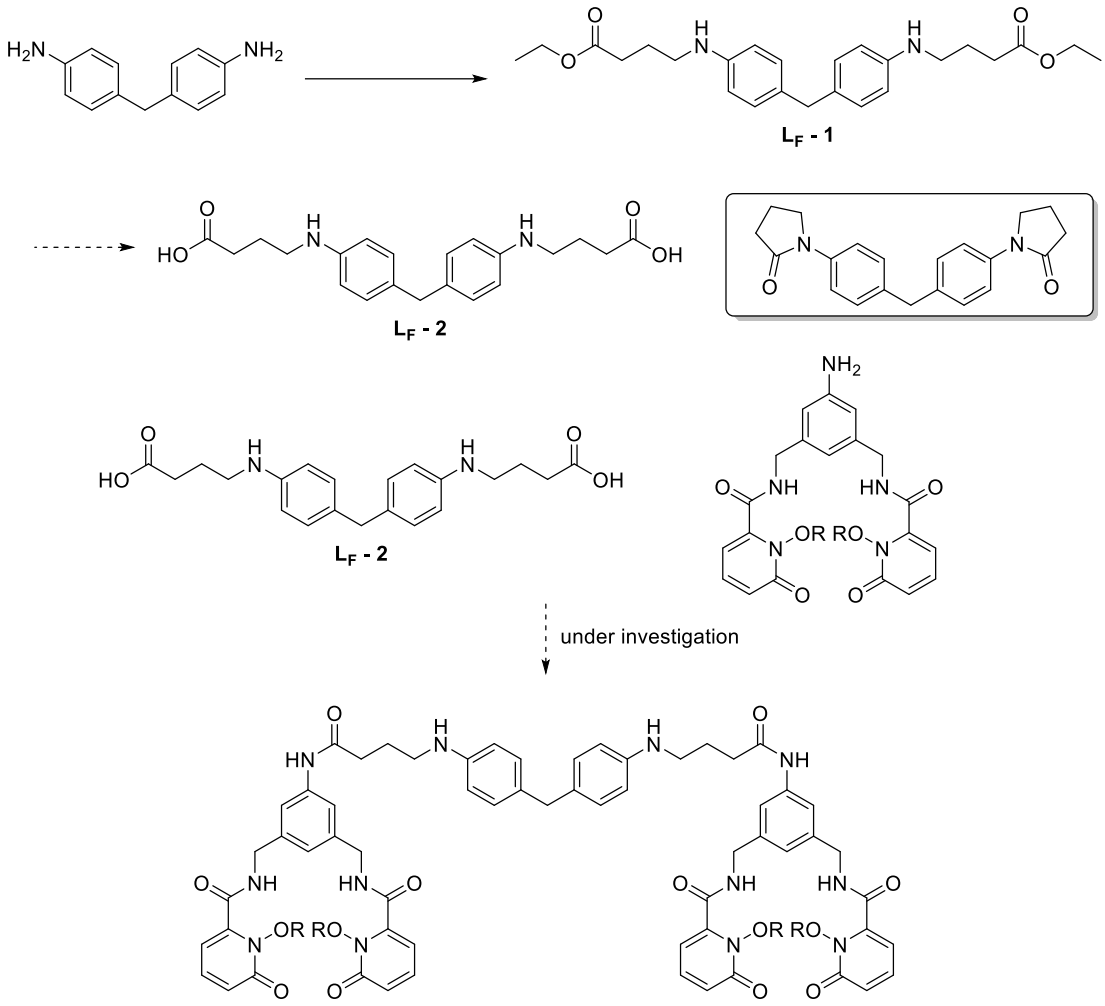

Figure 3-18: Synthetic scheme of ligand **L_F**

To synthesize the intermediate **L_F-1**, the slow addition of ethyl bromobutyrate (1.9 equiv.) with low concentration in dichloromethane to diamine (1 equiv.) is required to suppress the di-alkyl products. Upon completion of reaction, the mixture can be purified with column chromatography while the subsequent deprotection can be attempted in KOH solution. However, the initial attempt of amide coupling with HATU standard coupling is not successful. Upon detailed investigation, it is found that

intramolecular cyclization products are observed which is probably attributed from extra stability of five-member ring closure.

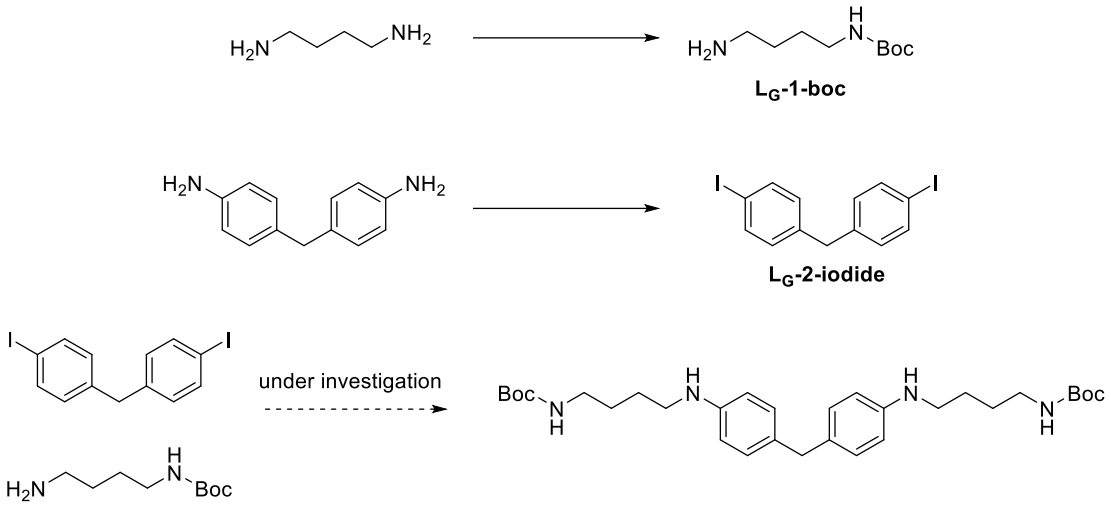

Figure 3-19: Synthetic scheme of ligand $\mathbf{L_G}$

In contrast to ligand $\mathbf{L_F}$, ligand $\mathbf{L_G}$ require an amino end spacing unit while it require two precursor including mono-protected diamine spacer and iodinated linker. Based on the experimental results, only boc group can be successfully synthesized in bulk quantities while the reaction kinetics of fmoc or Cbz are too fast that di-protected products are resulted even in low concentrations and temperature. Meanwhile, the iodination of diamine is realized by one-pot Sandmeyer reaction with $KI/NaNO_2$/p-TsOH system. However, the subsequent Pd-catalyzed coupling is still under investigation.

3.3. Conclusion & Future Work

To conclude, this chapter have successfully functionalized di-1,2-HOPO-based ligand with four different variations while their basic photophysical properties are investigated. The photophysical measurement revealed that functionalization of di-1,2-HOPO would still retain their optical properties while a mixture of ML and ML_2

coordination complexes are observed. With these building blocks, synthesis of three di-HOPO-based ditopic ligands **L_E**, **L_F** & **L_G** is attempted but still under investigation while the successful coupling in **L_E-OBn** demonstrate the possibility to engine high-order ditopic ligands with functionalized building blocks.

3.4. Experimental Section

3.4.1. General Consideration

All chemical used for synthesis were obtained from commercial suppliers and used without further purification. All moisture-sensitive reactions were conducted under a nitrogen atmosphere in oven-dried glassware. Anhydrous solvents were freshly distilled or dried over 4A molecular sieves unless otherwise specified. 1D and 2D NMR spectra were conducted on a Bruker AVANCE-III 400 MHz and 600MHz FT-NMR. The elemental analysis was performed using an Elementar Vario Micro Cube elemental analyzer. High Resolution-ESI mass spectrum were obtained from Agilent 6540 Liquid Chromatography - Electrospray Ionization Quadrupole-Time-of-Flight Mass Spectrometer or Waters Synapt G2-Si Ion Mobility Quadrupole MS and the chemical shifts were determined with tetramethylsilane (TMS) or solvents in parts per million (ppm).

3.4.2. Synthetic Details

Synthesis of HOPO derivatives

Compound 1h 6-bromopicolinic acid (20.5 g, 96 mmol) was dissolved in trifluoroacetic acid (250 mL) at room temperature. The hydrogen peroxide (30%, 50 mL) was added dropwise with caution. The orange solution was heated to 80°C and stirred for 48 h. the orange solution was concentrated to a quarter of original volume

and poured into 1000 mL of water. The product was collected by filtration and washed with water. The powder was heated with ethyl acetate and methanol followed by filtration to remove remaining starting material. The obtained pale pink powder was judged to be pure without further purification. (17.52 g, 81%) ^{1}H NMR (400 MHz, DMSO-d^{6}) δ 8.39 (dd, J = 8.2, 1.9 Hz, 1H), 8.34 (dd, J = 7.9, 2.0 Hz, 1H), 7.80 (t, J = 8.0 Hz, 1H). ^{13}C NMR (101 MHz, DMSO-d_6) δ 160.95, 138.89, 135.15, 133.04, 131.89, 128.25. Melting point: 200.0°C (3 replicates). Elemental analysis (%) calcd for $C_6H_4BrNO_3$: C, 33.06; H, 1.85; N, 6.43. Found: C, 33.01; H, 1.925; N, 6.25.

Compound 2h To a round bottom flask, compound **1h** (17.52 g, 78 mmol) was dissolved in aqueous potassium hydroxide solution (10%, 350 mL, 673 mmol) and stirred for 3 days at 80°C. The cooled solution was then acidified with concentrated hydrochloric acid and the pale-yellow precipitate was collected by filtration. The obtained was judged to be pure without further purification (Yield: 11.52 g, 95%). ^{1}H NMR (400 MHz, DMSO-d_6) δ 7.44 (dd, *J* = 9.0, 7.0 Hz, 1H), 6.71 (dd, *J* = 9.0, 1.7 Hz, 1H), 6.63 (dd, *J* = 7.0, 1.7 Hz, 1H). ^{13}C NMR (101 MHz, DMSO-d_6) δ 160.95, 138.89, 135.15, 133.04, 131.89, 128.25. Melting point: 179.5°C (3 replicates). Elemental analysis (%) calcd for $C_6H_5NO_4$: C, 46.46; H, 3.25; N, 9.03. Found: C, 46.14; H, 3.186; N, 8.9.

Compound 3h To the suspension of compound **2h** (11.52 g, 73 mmol) in MeOH, benzyl bromide (15.37 g, 88 mmol) and potassium carbonate (20.3223 g, 145 mmol) was added. After refluxing for 24 h, the mixture was filtered, and the solvent removed *in vacuo*. The yellow residue was taken up in water and acidified to pH = 2 with 6 N HCl. The white precipitate was collected by filtration and dried under vacuum (Yield:

15.34 g, 85%). ^{1}H NMR (400 MHz, DMSO-d_6) δ 7.49 – 7.33 (m, 6H), 6.67 (dd, J = 9.3, 1.7 Hz, 1H), 6.47 (dd, J = 6.8, 1.7 Hz, 1H), 5.25 (s, 2H).^{13}C NMR (101 MHz, DMSO-d_6) δ 162.31, 158.35, 142.07, 139.41, 134.23, 130.13, 129.54, 128.93, 123.67, 106.05, 78.34. Melting Point: 176℃ (3 replicates). Elemental analysis (%) calcd for $C_{13}H_{11}NO_4$: C, 63.67; H, 4.52; N, 5.71. Found: C, 63.66; H, 4.383; N, 5.53.

Compound 4h In two-neck round bottom flask, compound **3h** (2 g, 8 mmol, 1 equiv.) was vacuumed for an hour and subsequently suspended in 100 mL anhydrous toluene. Oxalyl chloride (1.26 mL, 14 mmol, 1.81 equiv.) and few drops of DMF were sequentially added at room temperature under nitrogen. The reaction was stirred 4 hours to result in yellow reaction mixture. The solvent and excess oxalyl chloride were removed under rotatory evaporator and mixture was further dried under high vacuum to afford a yellow sticky mixture which was then used without further purification.

To the separated round-bottom flask of compound **4h** (8 mmol, 1 equiv.) and 2-mercaptothaizoline (0.95 g, 8 mmol, 1 equiv.), 50 mL of freshly distilled dichloromethane was added under nitrogen. The triethylamine (1.33 mL, 9.6 mmol, 1.2 equiv.) was then then added to 2-mercaptothiazoline. Compound **4h** in DCM was then transferred to dropping funnel through cannula and dropped slowly to diamine with the duration of 30 minutes. The reaction was stirred under room temperature and monitored with TLC and mass spectroscopy. After completion of reaction, the reaction crude was partitioned with DCM and water. The organic layer was washed with HCl (1N, 20 mL, 3X), K_2CO_3 (0.5 N, 20 mL, 3X) and brine (2X) followed by drying under rotatory evaporator to afford yellow oil. The yellow crude was loaded to column chromatography (silica, 5% EA/DCM, R_f = 0.2) to afford pare yellow plate. The crude was then redissolved in ethyl acetate and precipitated with hexane to afford pale yellow powder. ^{1}H NMR (400 MHz, Chloroform-d) δ 7.43 (dd, J = 6.7, 3.0 Hz, 2H),

7.39 – 7.32 (m, 3H), 7.29 – 7.21 (m, 3H with d-chloroform), 6.75 (dd, *J* = 9.2, 1.6 Hz, 1H), 6.14 (dd, *J* = 6.9, 1.7 Hz, 1H), 5.29 (s, 2H), 4.42 (t, *J* = 7.4 Hz, 2H), 3.12 (t, *J* = 7.4 Hz, 2H).

Synthesis of ligand L_A

Compound L_A-1 To the suspension of 3,4-methyl-diaminobenzoic acid (2 g, 12.6 mmol, 1 equiv.) in 60 mL methanol, concentrated sulphuric acid (catalytic amount) was added dropwise under ice cooling. The organic solvent was dried under rotatory evaporator and resulting crude was partitioned in ethyl acetate and saturated sodium bicarbonate solution. Upon three times extraction with ethyl acetate, the organic extracts were washed with sat'd $NaHCO_3$ followed by brine solution and the solvent was removed in vacuo. The resulting mixture was load to column chromatography (silica gel, EA: DCM = 1:1, R_f = 0.8 in ethyl acetate). (1.1859, 55%). LCMS (ESI): calcd. for $C_8H_{10}N_2O_2$ M^+: 293.09; found 293.09. ^{1}H NMR (400 MHz, Chloroform-*d*) δ 7.48 (dd, *J* = 8.1, 1.9 Hz, 1H), 7.43 (d, *J* = 1.9 Hz, 1H), 6.69 (d, *J* = 8.1 Hz, 1H), 3.86 (s, 3H). ^{13}C NMR (101 MHz, CDCl3) δ 167.33 (s), 140.40 (s), 133.11 (s), 123.32 (s), 121.18 (s), 118.40 (s), 114.94 (s), 51.68 (s).

Compound L_A-2 To two necks round bottom flask, compound **3h** (3.0 g, 11.9 mmol, 1 equiv.) was vacuumed for an hour and subsequently suspended in 20 mL anhydrous toluene. Oxalyl chloride (2 mL, 22.8 mmol, 1.9 equiv.) and few drops of DMF were sequentially added at room temperature under nitrogen. The reaction was stirred 2 hours to result in yellow reaction mixture. The solvent and excess oxalyl chloride were removed under rotatory evaporator and mixture was further dried under high vacuum to afford a yellow sticky mixture (compound **4h**) which was then used without further purification.

To the separated round-bottom flask of compound **4h** (5 mmol, 5 equiv.) and methyl-3,4diaminobenzoate (0.1568 g, 1 mmol, 1 equiv.), 25 mL of dry dichloromethane was added under nitrogen. The pyridine (0.18 mL, 2.2 mmol, 2.2 equiv.) was then added to compound **L_A-1**. The compound 4h in dichloromethane was then transferred to dropping funnel through cannula. The compound 4h was dropped slowly to diamine with the duration of 30 minutes under ice cooling. The reaction was stirred under room temperature for 1 day. The reaction crude was extracted with water (20 mL × 3) and organic extracts were dried with anhydrous sodium sulphate, dried in vacuo to afford brown oil. The crude oil was loaded to column chromatography (silica gel, gradient from 5% to 25% MeOH/EtOAc, Rf = 0.6 in 5% MeOH/EtOAc). The oil was taken up in dichloromethane and precipitated in hexane to obtain beige product (Yield: 302.3 mg, 49%). LCMS (ESI): calcd. for $C_{34}H_{28}N_4O_8$: 620.62; found 621.73 [$C_{34}H_{28}N_4O_8$-H^+], 643.47 [$C_{34}H_{28}N_4O_8$-Na^+], 659.27 [$C_{34}H_{28}N_4O_8$-K^+], 1262.93 [$(C_{34}H_{28}N_4O_8)_2$-Na^+]. ^{1}H NMR (400 MHz, DMSO) δ 10.54 (d, *J* = 23.6 Hz, 2H), 8.28 (s, 1H), 7.92 (d, *J* = 7.5 Hz, 2H), 7.64 – 7.26 (m, 12H), 6.74 (d, *J* = 8.7 Hz, 2H), 6.55 (dd, *J* = 19.9, 5.7 Hz, 2H), 5.33 (s, 4H), 3.91 (s, 3H). ^{13}C NMR (101 MHz, $CDCl_3$) δ 165.97 (s), 159.11 (s), 158.49 (d, *J* = 13.1 Hz), 142.56 (s), 142.35 (s), 138.59 (s), 133.81 (s), 132.70 (d, *J* = 4.8 Hz), 130.03 (s), 129.78 (s), 129.37 (d, *J* = 12.4 Hz), 128.51 (d, *J* = 10.4 Hz), 128.12 (s), 127.39 (d, *J* = 7.4 Hz), 126.62 (s), 123.71 (d, *J* = 13.8 Hz), 122.99 (s), 106.65 (d, *J* = 16.3 Hz), 100.00 (s), 79.52 (d, *J* = 12.2 Hz), 77.41-76.77 (m, $CDCl_3$), 53.47 (s, CH_2Cl_2), 52.34 (s).

Compound L_A-OBn To round bottom flask, compound **L_A-2** (0.1968 g, 0.32 mmol) was suspended in the mixture of THF/H2O (40 mL, 1:1). To the mixture, 3.06 mL 1N

KOH aqueous solution (1.44 mL, 1.9mmol, 6 equiv.) was charged under room temperature. With the monitoring of mass spectroscopy, the mixture was reacted for 2 days and resulting mixture was dried under compressed air at room temperature. The yellow crude was taken up with water and acidified with 1N HCl. The beige precipitate was collected with filtration (Yield: 143 mg, 75%). ^{1}H NMR (400 MHz, DMSO-d_6) δ 10.53 (d, J = 21.0 Hz, 2H), 8.29 (d, J = 1.9 Hz, 1H), 7.95 – 7.78 (m, 2H), 7.64 – 7.30 (m, 12H), 6.73 (dt, J = 9.3, 2.2 Hz, 2H), 6.53 (ddd, J = 15.3, 6.8, 1.7 Hz, 2H), 5.32 (d, J = 2.8 Hz, 4H). LCMS (ESI): calcd. for $C_{33}H_{26}N_4O_8$: 606.18; found 607.60 [$C_{33}H_{26}N_4O_8$-H^+], 629.27 [$C_{33}H_{26}N4O_8$-Na^+], 645.27 [$C_{33}H_{26}N_4O_8$-K^+].

Ligand L_A To round bottom flask, compound **L_A-OBn** (143.4 mg, 231 μmol) was dissolved in glacial acetic acid and concentrated hydrochloric acid (1 : 1 v/v, 14 mL). The reaction was stirred under room temperature for 2 days. The solvent was removed *in vacuo* and desired product was taken up in methanol and precipitated in diethyl ether. The centrifuged products were dried under high vacuum to obtain pale yellow products and judged to be pure. (Yield: 83.7 mg, 82%). LCMS (ESI): calcd. for $C_{19}H_{14}N_4O_8$: 426.08; found 427.53 [$C_{19}H_{14}N_4O_8$ -H^+], 852.80 [$(C_{19}H_{14}N_4O_8)_2$-H^+], 874.87 [$(C_{19}H_{14}N_4O_8)_2$-Na^+]. ^{1}H NMR (400 MHz, DMSO-d_6) δ 10.84 (s, 1H), 10.61 (s, 1H), 8.23 (d, J = 1.9 Hz, 1H), 7.95 (d, J = 8.5 Hz, 1H), 7.87 (dd, J = 8.5, 2.1 Hz, 1H), 7.48 (ddd, J = 10.8, 6.5, 2.8 Hz, 2H), 6.80 – 6.54 (m, 4H).

Synthesis of L_B derivatives

Compound L_B-1 To a solution of 2-nitro-1,4-diamine (2.0040 g, 7.74 mmol, 1 equiv.) and sodium bicarbonate (1.4652 g, 17.1 mmol, 2.2 equiv.) in 200 mL water, (9H-

fluoren-9-yl)methyl (2,5-dioxopyrrolidin-1-yl) carbonate (2.9356 g, 8.5 mmol, 1.1 equiv.) in 50 mL dioxane was added slowly under ice cooling. The reaction mixture was stirred overnight to afford orange suspension. The resulting solution was extracted three times with ethyl acetate followed by washing with 0.5 N HCl (20 mL × 3). The orange solution was dried over anhydrous sodium sulphate and rotatory evaporator. The orange oil was taken up in ethyl acetate and precipitated in hexane to afford yellow precipitate (Yield: 2.176 g, 99%) and judged to be pure without further purification. LCMS (ESI): calcd. for $C_{21}H_{19}N_3O_2$: 375.38; found 414.45 [$C_{21}H_{19}N_3O_2$-K^+]. ^{1}H NMR (400 MHz, DMSO-d_6) δ 9.66 (s, 1H), 8.19 (s, 1H), 7.90 (d, J = 7.5 Hz, 2H), 7.74 (d, J = 7.5 Hz, 2H), 7.42 (t, J = 7.4 Hz, 4H), 7.39 – 7.20 (m, 4H), 6.97 (d, J = 9.1 Hz, 1H), 4.47 (d, J = 6.6 Hz, 2H), 4.30 (t, J = 6.6 Hz, 1H). ^{13}C NMR (101 MHz, DMSO) δ 154.03 (s), 144.24 (s), 143.08 (s), 141.28 (s), 129.87 (s), 128.15 (s), 127.59 (s), 125.57 (s), 120.64 (s), 120.07 (s), 66.06 (s), 47.13 (s).

Compound L_B-2 To round bottom flask, compound **L_B-1** (1.0299 g, 2.58 mmol) was vacuumed for 30 minutes and subsequently dissolved in the mixture of EtOAc/MeOH (40/160 mL). To the reaction mixture, 10% Pd/C (141 mg, 0.129 mmol) was added as catalysts. Upon degassed with small vacuum, the reaction was allowed to stir 24 h with hydrogen balloons. The resulting crude was filtered with celite and dried to afford dark orange product. The crude was then suspended in small amount of dichloromethane. LCMS (ESI): calcd. for $C_{21}H_{19}N_3O_2$: 345.40; found 384.08 [$C_{21}H_{19}N_3O_2$-K^+]. The product was then obtained with filtration and used for next step without further purification (Yield: 767.6 mg, 81%). ^{1}H NMR (400 MHz, DMSO-d_6) δ 9.11 (s, 1H), 7.90 (d, J = 7.5 Hz, 2H), 7.74 (d, J = 7.4 Hz, 2H), 7.42 (t, J = 7.4 Hz, 2H), 7.38 – 7.28 (m,

2H), 6.70 (s, 1H), 6.41 (t, *J* = 11.7 Hz, 2H), 4.47 – 4.05 (m, 7H). ^{13}C NMR (101 MHz, DMSO) δ 144.39 (s), 141.22 (s), 135.77 (s), 128.11 (s), 127.56 (s), 125.70 (s), 121.85 (s), 120.55 (d, *J* = 11.0 Hz), 114.95 (s), 65.43 (s), 47.18 (s), 40.61 (s), 40.30 (d, *J* = 20.9 Hz), 39.98 (s), 39.67 (d, *J* = 21.1 Hz), 39.37 (s), 39.36 (s)

Compound L_B-3 The acid chloride **4h** is prepared with similar procedure described previously. To the separated round-bottom flask of compound **4h** (5 mmol, 5 equiv.) and (9H-fluoren-9-yl)methyl (3,4-diaminophenyl)carbamate (0.3560 g, 1 mmol, 1 equiv.), 40 mL of dry dichloromethane was added under nitrogen. The pyridine (0.3 mL, 2.2 mmol) was then added to compound LB-2 . The compound **4h** in dichloromethane was then transferred to dropping funnel through cannula and dropped slowly to diamine with the duration of 30 minutes under ice cooling. The reaction was stirred under room temperature for 2 days. The reaction crude was partitioned with DCM and water. The organic layer was washed with brine followed by drying under rotatory evaporator to afford yellow oil. The dried oil was afforded to column chromatography (silica gel, 5% MeOH/EtOAC to 10% MeOH/EtOAc, gradient elution, R_f = 0.3 in 1% MeOH/EtOAc) to yield yellow oil. The resulting oil was precipitated with dichloromethane and hexane to obtain pale brown powder (Yield: 278.3 mg, 35%). LCMS (ESI): calcd. for $C_{47}H_{37}N_5O_8$: 799.84; found 800.20 [$C_{47}H_{37}N_5O_8$-H^+], 800.47 [$C_{47}H_{37}N_5O_8$-Na^+], 838.47 [$C_{47}H_{37}N_5O_8$-K^+], 1621.07 [$(C_{47}H_{37}N_5O_8)_2$-Na^+], 1637.00 [$(C_{47}H_{37}N_5O_8)_2$-K^+]. ^{1}H NMR (400 MHz, $CDCl_3$) δ 9.10 (s, 1H), 8.88 (s, 1H), 7.82 (d, *J* = 7.5 Hz, 2H), 7.67 (d, *J* = 7.4 Hz, 2H), 7.58 (s, 1H), 7.45 (t, *J* = 7.2 Hz, 4H), 7.37 (t, *J* = 7.3 Hz, 2H), 7.33 – 7.08 (m, 14H), 6.83 (s, 1H), 6.60 (td, *J* = 9.6, 1.4 Hz, 2H), 6.38 – 6.23 (m, 2H), 5.20 (d, *J* = 3.1 Hz, 4H), 4.62 (d, *J* = 6.4 Hz, 2H), 4.32 (t, *J* =

6.4 Hz, 1H). ^{13}C NMR (101 MHz, MeOD) δ 159.52 (s), 159.22 (s), 158.95 (d, *J* = 3.3 Hz), 144.07 (s), 143.33 (d, *J* = 8.6 Hz), 141.34 (s), 139.23 (d, *J* = 3.7 Hz), 133.77 (d, *J* = 12.7 Hz), 130.97 (s), 130.19 (d, *J* = 19.5 Hz), 129.29 (d, *J* = 5.3 Hz), 128.56 (d, *J* = 4.1 Hz), 127.81 (s), 127.20 (s), 126.30 (s), 125.13 (s), 124.37 (s), 123.25 (s), 120.03 (s), 116.61 (s), 115.14 (s), 105.94 (s), 79.10 (s), 66.34 (s).

Ligand L_B-fmoc To round bottom flask, compound **L_B-3** (322 mg, 396 μmol) was dissolved in glacial acetic acid and concentrated hydrochloric acid (1 : 1 v/v, 24 mL). The reaction was stirred under room temperature for 2 days with the monitoring of mass spectroscopy. The solvent was removed *in vacuo* and desired product was taken up in methanol. The diethyl ether was added to precipitate out the yellow powdery product. The product was collected with filtration and washed with diethyl ether (Yield: 170.5 mg, 60%). LCMS (ESI): calcd. for $C_{33}H_{25}N_5O_8$: 619.59; found 620.19 [$C_{33}H_{25}N_5O_8$-H^+]. ^{1}H NMR (400 MHz, DMSO-d_6) δ 10.46 (d, *J* = 43.5 Hz, 2H), 9.93 (s, 1H), 7.92 (d, *J* = 7.5 Hz, 2H), 7.78 (d, *J* = 7.4 Hz, 2H), 7.54 (d, *J* = 8.8 Hz, 1H), 7.42 (ddt, *J* = 29.4, 22.9, 7.2 Hz, 8H), 6.75 – 6.59 (m, 4H), 4.47 (d, *J* = 6.9 Hz, 3H), 4.32 (t, *J* = 6.9 Hz, 2H).

Compound L_B-OBn To the solution of **compound L_B-3** (300 mg, 375 μmol, 1 equiv.) in dichloromethane (10 mL), methylpiperidine (90 μL, 750 μmol , 2 equiv.) was added under nitrogen atmosphere. Upon reacting for 2 days under room temperature, the reaction crude was partitioned by ethyl acetate and H_2O. The aqueous layer was extracted trice with ethyl acetate followed by washing of brine. The organic fraction was then dried over anhydrous sodium sulphate and dried under reduced pressure to

afford brown oil. The brown oil was then loaded with column chromatography (TEA/EA-flushed, DCM to DCM/EA, gradient elution) to afford brown solid (102 mg, 20%). ^{1}H NMR (400 MHz, DMSO-d_6) δ 9.99 (s, 1H), 9.84 (s, 1H), 7.51 – 7.28 (m, 13H), 7.04 (d, *J* = 8.5 Hz, 1H), 6.94 (d, *J* = 2.5 Hz, 1H), 6.63 (ddd, *J* = 9.2, 3.4, 1.7 Hz, 2H), 6.43 (dd, *J* = 8.6, 2.6 Hz, 1H), 6.39 (dd, *J* = 6.8, 1.7 Hz, 1H), 6.31 (dd, *J* = 6.8, 1.7 Hz, 1H), 5.29 (s, 2H), 5.24 (s, 4H). ^{13}C NMR (101 MHz, Chloroform-*d*) δ 158.36, 158.28, 141.96, 141.89, 138.23, 138.17, 132.84, 131.26, 130.37, 130.35, 129.54, 129.47, 128.60, 128.55, 126.69, 124.55, 124.42, 118.79, 112.93, 109.85, 107.36, 107.23.

Compound L_B To round bottom flask with compound **L_B-OBn** (55 mg, 95 μmol), the mixture of glacial acetic acid and concentrated hydrochloric acid (5 mL, 1:1, v/v) was added under room temperature. Upon three days stirring, the reaction crude was co-evaporated with methanol trice under reduced pressure. The crude was then precipitated by MeOH/Et2O followed by washing of DCM/Hexane to afford brown solid (40 mg, 80%). ^{1}H NMR (400 MHz, DMSO-d_6) δ 10.71 (s, 1H), 10.60 (s, 1H), 7.76 (d, *J* = 2.6 Hz, 1H), 7.67 (d, *J* = 8.6 Hz, 1H), 7.44 (ddd, *J* = 8.9, 7.0, 2.0 Hz, 2H), 7.18 (dd, *J* = 8.7, 2.4 Hz, 1H), 6.73 – 6.56 (m, 4H). ^{13}C NMR (101 MHz, DMSO-d_6) δ 159.51, 159.35, 157.86, 157.82, 141.69, 141.47, 137.40, 137.26, 131.67, 127.12, 120.31, 106.21, 105.92.

Synthesis of Ligand L_C

Compound L_C-1 To the solution of 3,5-dimethylbenzoic acid (10.34 g, 65.4 mmol, 1 equiv.) in methanol (50 mL, 1 mol, 18 equiv.), concentrated sulphuric acid (2 mL, 36.7 mmol, 0.5 equiv.) was added with caution. After overnight reaction at reflux temperature, the reaction mixture was cooled down to room temperature and

partially evaporated. The resulting mixture was diluted with water and extracted with dichloromethane (3X), washed with sodium bicarbonate solution. The organic fraction was then washed with sodium bicarbonate solution, dried with anhydrous magnesium sulphate and in vacuo to obtain colorless oil. (6.9145 g, 64%) ^{1}H NMR (400 MHz, Chloroform-*d*) δ 7.77 – 7.55 (m, 2H), 7.15 (s, 1H), 3.88 (s, 3H), 2.33 (s, 6H). ^{13}C NMR (101 MHz, Chloroform-*d*) δ 167.34, 137.93, 134.50, 130.01, 127.28, 51.87, 21.06.

Compound L_C-2 To the suspension of compound **L_C-1** (7.01 g, 42 mmol, 1 equiv.) in 200 mL nitrogen-purged acetonitrile, N-bromosuccinimide (16.01 g, 89 mmol, 2.1 eqiuv.) and benzoyl peroxide (688 mg, 0.05 equiv.) were added. After heating at reflux temperature overnight with nitrogen purging, the reaction mixture was diluted with water and extracted with dichloromethane. The organic layer was homogenized in hot hexane and settled overnight for crystallization to afford white powders. (8.09 g, 60%) ^{1}H NMR (400 MHz, Chloroform-*d*) δ 8.01 (d, *J* = 1.8 Hz, 2H), 7.63 (d, *J* = 1.9 Hz, 1H), 4.51 (s, 4H), 3.95 (s, 3H).

Compound L_C-3 & L_C-4 To the solution of compound **L_C-2** (1 g, 3.1 mmol, 1 equiv.) in acetone (25 mL) was added solution of sodium azide (0.65 g, 10 mmol, 3.2 equiv.) in H_2O (10 mL). The mixture was then heated at 60°C for 4h before quenching with large excess of H_2O. The ethyl acetate is added for phase partition and the mixture was then extracted trice with ethyl acetate. The solvent is then dried over anhydrous sodium sulphate and removed in caution under compressed air to afford compound **L_C-3** which is used without further purification. The obtained intermediates are diluted with 50 mL tetrahydrofuran and added triphenylphosphine (2.94 g, 11.2 mmol, 2.6 equiv.). The resulting mixture was stirred for 6h and added 2 mL H_2O for overnight

reaction. Upon completion of reaction, ethyl acetate was added for partition and the organic fraction are extracted with 2N HCl (20 mL x 5). The obtained acidic extracts are washed with dichloromethane and evaporated. The solid residues are dissolved in boiling methanol, filtered and precipitated with diethyl ether. The product was then obtained by filtration as a mixture of diamine hydrochloride and diamine dihydrochloride salts.

Compound L_C-5 To the solution of **compound L_C-4** (265 mg, 1 mmol, 1 equiv.) in 20 mL anhydrous N,N'-dimethylformamide, triethylamine (0.55 mL, 4 mmol, 4 equiv.) was added under nitrogen atmosphere. Upon 30 minutes stirring, compound **5h** (0.69 g, 2 mmol, 2 equiv.) was added by portion under nitrogen and stirred in the dark for 2 days. Upon completion of reaction, the reaction mixture was partitioned with water and extract trice with dichloromethane. The crude oil was then loaded to column chromatography (silica, EA to 5% MeOH/EA) to afford pale yellow solution. The solution was then uptake by tetrahydrofuran and precipitated in hexane to afford beige solids (98 mg, 15%). ^{1}H NMR (400 MHz, Chloroform-d) δ 7.86 (d, J = 1.7 Hz, 2H), 7.44 (dq, J = 5.7, 3.1 Hz, 2H), 7.39 – 7.26 (m, 11H), 6.76 (s, 2H), 6.67 (dd, J = 9.3, 1.7 Hz, 2H), 6.28 (dd, J = 6.7, 1.7 Hz, 2H), 5.24 (s, 4H), 4.30 (d, J = 6.1 Hz, 4H), 3.98 (s, 3H). ^{13}C NMR (101 MHz, Chloroform-d) δ 166.56, 160.84, 158.34, 142.51, 138.21, 137.87, 133.34, 130.71, 130.54, 129.46, 129.11, 128.63, 127.34, 124.26, 105.32, 78.97, 52.31, 43.00.

Compound L_C-OBn To round bottom flask, compound L_C-OBn (120 mg, 0.19 mmol) was suspended in the mixture of THF/H_2O (40 mL, 1:1). To the mixture, 1N KOH aqueous solution (6 equiv.) was charged under room temperature. With the monitoring of mass spectroscopy, the mixture was reacted for 2 days and resulting

mixture was dried under compressed air at room temperature. The yellow crude was took up with water and acidified with 1N HCl. The aqueous fraction was then extracted by ethyl acetate trice and obtained organic extracts were dried over anhydrous sodium sulphate and evaporated under rotatory evaporator. The solid residues were redissolved in tetrahydrofuran followed by precipitation to afford beige solids (102 mg, 87%). ^{1}H NMR (600 MHz, Chloroform-*d*) δ 7.77 (d, *J* = 1.7 Hz, 2H), 7.44 – 7.18 (m, 15H), 6.72 (dd, *J* = 9.3, 1.7 Hz, 2H), 6.40 (s, 2H), 6.22 (dd, *J* = 6.7, 1.7 Hz, 2H), 5.22 (s, 4H), 4.21 (s, 4H). ^{13}C NMR (151 MHz, Chloroform-*d*) δ 168.90, 160.96, 158.48, 142.34, 138.17, 137.84, 133.37, 130.93, 130.16, 129.60, 129.26, 128.73, 127.61, 124.56, 105.45, 79.08, 42.99.

Ligand L_C To the round-bottom flask with compound **L_C-OBn** (100 mg), concentrated hydrochloric acid and glacial acetic acid was added (10 mL, 1:1). Upon 3 days stirring at room temperature, the solvent was removed *in vacuo.* and few drops of triethylamine was treated. The resulting mixture was dissolved in methanol and precipitated with diethyl ether to afford pale brown solids. (41 mg, 53%). ^{1}H NMR (600 MHz, DMSO-d_6) δ 9.39 (s, 2H), 7.83 (s, 2H), 7.54 (s, 1H), 7.36 (d, *J* = 37.7 Hz, 3H), 6.58 (s, 2H), 6.33 (s, 2H), 4.49 (s, 4H). ^{13}C NMR (151 MHz, DMSO-d_6) δ 167.64, 160.95, 157.98, 142.49, 139.75, 137.72, 131.54, 130.81, 127.30, 119.98, 104.28, 42.56.

Synthesis of Ligand L_D

Compound L_D-1 To the solution of 5-nitroisophthalic acid (6 g, 28 mmol, 1 equiv.) in 250 mL tetrahydrofuran, 1,1'-carbonyldiimidazole (14 g, 85 mmol, 3 equiv.) was added in caution under ice temperature. Upon stirring for 2h, ammonias solution (28%, 50 mL, 315 mmol, 10 equiv.) was added to the slurry mixture. Upon overnight reaction,

the organic solvent was removed under reduced pressure and methanol was added to induce precipitation. The precipitates were collected by filtration and washed by methanol and tetrahydrofuran to afford white powdery products (2.0257 g, 33%).

Compound L_D-2 To the solution of compound **L_D-1** (2.0257 g, 9.5 mmol, 1 equiv.) in methanol (200 mL), 10% Pd/C (200 mg, catalytic amount) was added and mixture was stirred at room temperature under hydrogen balloons. After 2 days reaction, the reaction mixture was filtered, and the residues were washed by water and methanol. The solvent was removed under reduced pressure and precipitated with EA/Hexane to afford white powder (0.88 g, 52%). ^{1}H NMR (400 MHz, DMSO-d_6) δ 7.68 (s, 1H), 7.39 (t, J = 1.6 Hz, 1H), 7.19 (s, 1H), 7.09 (d, J = 1.5 Hz, 1H), 5.33 (s, 1H).

Compound L_D-3 To the suspension of Compound **L_D-2** (0.88 g, 4.86 mmol, 1 equiv.) in anhydrous tetrahydrofuran (10 mL), borane dimethyl sulphide (2 mL, 19.5 mmol, 4 equiv.) was added in caution at reflux temperature under nitrogen atmosphere. The resulting solution was refluxed overnight before addition of hydrochloric acid (1 mL, 6N) for hydrolysis. Upon hydrolysis at reflux temperature for 2 hours, the solvent was removed under reduced pressure. The slurry mixture was uptake by hot methanol and precipitated in diethyl ether as hydrochloride salt. (700 mg, 68%) ^{1}H NMR (400 MHz, Deuterium Oxide) δ 7.91 (t, J = 1.6 Hz, 1H), 7.64 (d, J = 1.6 Hz, 2H), 7.29 (d, J = 1.6 Hz, 2H), 7.25 (d, J = 1.6 Hz, 4H), 4.08 (s, 4H).

Compound L_D-OBn. To the solution of **compound L_{D-3}** (700 mg, 3.7 mmol, 1 equiv.) and potassium carbonate (2.08 g, 15 mmol, 4 equiv.) in freshly 100 mL distilled dichloromethane, triethylamine (1.15 mL, 8.2 mmol, 2.2 equiv.) was added under nitrogen atmosphere. Upon 30 minutes stirring, compound 5h (2.61 g, 7.4 mmol, 2 equiv.) in 100 mL freshly distilled dichloromethane was added under nitrogen and stirred in the dark for 2 days. Upon completion of reaction, the reaction mixture was

partitioned with water and extract trice with dichloromethane. The crude oil was then loaded to column chromatography (silica, EA to 5% MeOH/EA) to afford pale yellow solution. The solution was then uptake by tetrahydrofuran and precipitated in hexane to afford brown solids. (724 mg, 56%). LCMS (ESI): calcd. for $C_{34}H_{31}N_5O_6$: 605.65; found 606.31 [$C_{34}H_{31}N_5O_6$-H^+], 628.22 [$C_{34}H_{31}N_5O_6$-Na^+], 644.20 [$C_{34}H_{31}N_5O_6$-K^+]. ^{1}H NMR (400 MHz, DMSO-d_6) δ 9.28 (t, *J* = 6.0 Hz, 2H), 7.48 (dd, *J* = 9.3, 6.7 Hz, 2H), 7.45 – 7.32 (m, 10H), 6.65 (dd, *J* = 9.2, 1.7 Hz, 2H), 6.43 (d, *J* = 6.5 Hz, 3H), 6.33 (dd, *J* = 6.7, 1.7 Hz, 2H), 5.25 (s, 4H), 4.22 (d, *J* = 5.9 Hz, 4H).^{13}C NMR (101 MHz, DMSO-d_6) δ 160.80, 158.00, 149.17, 144.49, 139.48, 139.39, 134.35, 130.08, 129.45, 128.93, 122.92, 114.55, 112.15, 104.52, 78.79, 43.04.

Ligand L_D to the round-bottom flask with compound **L_D-OBn** (82 mg, 0.1 mmol), concentrated hydrochloric acid and glacial acetic acid was added (10 mL, 1:1). Upon 3 days stirring at room temperature, the solvent was removed *in vacuo.* and few drops of triethylamine was treated. The resulting mixture was dissolved in methanol and precipitated with diethyl ether to afford pale brown solids. (20 mg, 35%). LCMS (ESI): calcd. for $C_{20}H_{19}N_5O_6$: 425.40; found 426.31 [$C_{20}H_{19}N_5O_6$-H^+], 448.11 [$C_{20}H_{19}N_5O_6$-Na^+]. ^{1}H NMR (400 MHz, Methanol-d_4) δ 7.54 (t, *J* = 7.9 Hz, 3H), 7.34 (s, 2H), 6.80 (d, *J* = 8.9 Hz, 2H), 6.73 (d, *J* = 7.0 Hz, 2H), 4.64 (s, 4H).

3.4.3. Photophysical & Lifetime Measurement

General Consideration Unless stated otherwise, photophysical measurements were average of triplicates. UV-Vis absorption spectra were recorded with an HP UV-8453 spectrophotometer while photoluminescence measurements data are obtained with either (1) Edinburgh Instruments FLSP 920 spectrophotometer equipped with a Xe900 continuous xenon lamp (450 W) or (2) HORIBA Fluoromax-4 Spectrofluorometer as stated in previous section.

Quantum yield measurement. The quantum yield was determined relative to freshly prepared quinine sulphate in 0.1 M sulphuric acid (λ_{em} = 350 nm, Φ = 0.547). The spectrophotometric grade solvents used in measurements are purchased from Sigma-Aldrich. The 0.1 M HEPES buffer is freshly obtained by dilution of purchased spectroscopic grade 1 M HEPES and 0.1 M sulphuric acid.

Lifetime Measurement. The luminescence lifetimes of visible emissions were acquired with FLSP 920 spectrophotometer equipped with nanosecond flash-lamp (nF900) and the decay curve was fitted with Origin 8.5.

3.5. Reference

1. Di Bernardo, P., Melchior, A., Tolazzi, M., & Zanonato, P. L. Thermodynamics of lanthanide (III) complexation in non-aqueous solvents. *Coordination Chemistry Reviews* **2012,** 256(1-2), 328-351.

2. Subramani, K.; Khraisat, A.; George, A., Self-assembly of proteins and peptides and their applications in bionanotechnology. *Curr Nanosci* **2008,** *4* (2), 201-207.

3. Zou, R.; Wang, Q.; Wu, J.; Wu, J.; Schmuck, C.; Tian, H., Peptide self-assembly triggered by metal ions. *Chem Soc Rev* **2015,** *44* (15), 5200-19.

4. Salgado, E. N.; Radford, R. J.; Tezcan, F. A., Metal-directed protein self-assembly. *Acc Chem Res* **2010,** *43* (5), 661-72.

5. Yang, H.; Pritzker, M.; Fung, S. Y.; Sheng, Y.; Wang, W.; Chen, P., Anion effect on the nanostructure of a metal ion binding self-assembling peptide. *Langmuir* **2006,** *22* (20), 8553-62.

6. Dublin, S. N.; Conticello, V. P., Design of a selective metal ion switch for self-assembly of peptide-based fibrils. *J Am Chem Soc* **2008,** *130* (1), 49-51.

7. Moore, E. G.; Xu, J. D.; Jocher, C. J.; Werner, E. J.; Raymond, K. N., "Cymothoe sangaris": An extremely stable and highly luminescent 1,2-hydroxypyridinonate chelate of Eu(III). *Journal of the American Chemical Society* **2006,** *128* (33), 10648-10649.

8. Moore, E. G.; Jocher, C. J.; Xu, J. D.; Werner, E. J.; Raymond, K. N., An octadentate luminescent Eu(III) 1,2-HOPO chelate with potent aqueous stability. *Inorganic Chemistry* **2007,** *46* (14), 5468-5470.

9. Seitz, M.; Pluth, M. D.; Raymond, K. N., 1,2-HOIQO - a highly versatile 1,2-HOPO analogue. *Inorganic Chemistry* **2007,** *46* (2), 351-353.

10. Moore, E. G.; Xu, J. D.; Jocher, J.; Castro-Rodriguez, I.; Raymond, K. N., Highly

luminescent lanthanide complexes of 1-hydroxy-2-pyridinones. *Inorganic Chemistry* **2008,** *47* (8), 3105-3118.

11. D'Aleo, A.; Moore, E. G.; Szigethy, G.; Xu, J.; Raymond, K. N., Aryl Bridged 1-Hydroxypyridin-2-one: Effect of the Bridge on the Eu(III) Sensitization 'Process. *Inorganic Chemistry* **2009,** *48* (19), 9316-9324.

12. Moore, E. G.; D'Aleo, A.; Xu, J. D.; Raymond, K. N., Eu-III Complexes of Octadentate 1-Hydroxy-2-pyridinones: Stability and Improved Photophysical Performance. *Aust J Chem* **2009,** *62* (10), 1300-1307.

13. Werner, E. J.; Kozhukh, J.; Botta, M.; Moore, E. G.; Avedano, S.; Aime, S.; Raymond, K. N., 1,2-Hydroxypyridonate/Terephthalamide Complexes of Gadolinium(III): Synthesis, Stability, Relaxivity, and Water Exchange Properties. *Inorganic Chemistry* **2009,** *48* (1), 277-286.

14. Moore, E. G.; Xu, J. D.; Jocher, C. J.; Corneillie, T. M.; Raymond, K. N., Eu(III) Complexes of Functionalized Octadentate 1-Hydroxypyridin-2-ones: Stability, Bioconjugation, and Luminescence Resonance Energy Transfer Studies. *Inorganic Chemistry* **2010,** *49* (21), 9928-9939.

15. D'Aleo, A.; Moore, E. G.; Xu, J.; Daumann, L. J.; Raymond, K. N., Optimization of the Sensitization Process and Stability of Octadentate Eu(III) 1,2-HOPO Complexes. *Inorg Chem* **2015,** *54* (14), 6807-20.

16. Jocher, C. J.; Botta, M.; Avedano, S.; Moore, E. G.; Xu, J. D.; Aime, S.; Raymond, K. N., Optimized relaxivity and stability of [Gd(H(2,2)-1,2-HOPO)(H2O)](-) for use as an MRI contrast agent. *Inorganic Chemistry* **2007,** *46* (12), 4796-4798.

17. Daumann, L. J.; Tatum, D. S.; Andolina, C. M.; Pacold, J. I.; D'Aleo, A.; Law, G. L.; Xu, J.; Raymond, K. N., Effects of Ligand Geometry on the Photophysical Properties of

Photoluminescent Eu(III) and Sm(III) 1-Hydroxypyridin-2-one Complexes in Aqueous Solution. *Inorg Chem* **2016,** *55* (1), 114-24.

18. Lavigueur, C.; Foster, E. J.; Williams, V. E., Self-assembly of discotic mesogens in solution and in liquid crystalline phases: effects of substituent position and hydrogen bonding. *J Am Chem Soc* **2008,** *130* (35), 11791-800.

19. Kamal, A.; Nagaseshadri, B.; Nayak, V. L.; Srinivasulu, V.; Sathish, M.; Kapure, J. S.; Reddy, C. S., Synthesis and biological evaluation of benzimidazole-oxindole conjugates as microtubule-targeting agents. *Bioorganic Chemistry* **2015,** *63*, 72-84.

20. Appiah Kubi, G.; Qian, Z.; Amiar, S.; Sahni, A.; Stahelin, R. V.; Pei, D., Non-Peptidic Cell-Penetrating Motifs for Mitochondrion-Specific Cargo Delivery. *Angew Chem Int Ed Engl* **2018,** *57* (52), 17183-17188.

21. Qian, Z.; Rhodes, C. A.; McCroskey, L. C.; Wen, J.; Appiah-Kubi, G.; Wang, D. J.; Guttridge, D. C.; Pei, D., Enhancing the Cell Permeability and Metabolic Stability of Peptidyl Drugs by Reversible Bicyclization. *Angew Chem Int Ed Engl* **2017,** *56* (6), 1525-1529.

22. Malachowski, M. R.; Davidson, M. G.; Davis, J. D., The Synthesis of Tetrapyrazole Substituted Phenols. *Heterocycles* **1992,** *34* (6), 1227-1230.

23. Gabutti, S.; Knutzen, M.; Neuburger, M.; Schull, G.; Berndt, R.; Mayor, M., A rigid sublimable naphthalenediimide cyclophane as model compound for UHVSTM experiments. *Chem Commun* **2008,** (20), 2370-2372.

24. Martin, V. V.; Lex, L.; Keana, J. F. W., A Safe and Convenient Procedure for the Synthesis of Polyamines Via Azide Intermediates. *Org Prep Proced Int* **1995,** *27* (1), 117-120.

25. Ryu, E. H.; Yan, J.; Zhong, Z.; Zhao, Y., Solvent-induced amphiphilic molecular baskets: Unimolecular reversed micelles with different size, shape, and flexibility. *Journal of Organic Chemistry* **2006,** *71* (19), 7205-7213.

26. Zahid, M.; Rosspeintner, A.; Angulo, G.; Grampp, G.; Jacques, P.; Mansha, A., Synthesis and photophysical properties of 2,6-dicyano-p-phenylenediamine. *J Photoch Photobio A* **2011,** *220* (1), 54-63.

27. Melhuish, W. H., Quantum efficiencies of fluorescence of organic substances: effect of solvent and concentration of the fluorescent solute. *J. Phys. Chem.* **1961,** *65* (2), 229–235.

28. Beeby, A.; Clarkson, I. M.; Dickins, R. S.; Faulkner, S.; Parker, D.; Royle, L.; de Sousa, A. S.; Williams, J. A. G.; Woods, M., Non-radiative deactivation of the excited states of europium, terbium and ytterbium complexes by proximate energy-matched OH, NH and CH oscillators: an improved luminescence method for establishing solution hydration states. *J Chem Soc Perk T 2* **1999,** (3), 493-503.

29. Supkowski, R. M.; Horrocks, W. D., On the determination of the number of water molecules, q, coordinated to europium(III) ions in solution from luminescence decay lifetimes. *Inorg Chim Acta* **2002,** *340*, 44-48.

Chapter 4: Study in the effect of chelating strength towards supramolecular self-assembly

4.1. Introduction

4.1.1. Background

As mentioned in chapter two, the neutral pcam chelator have intrinsic weakness on chelating ability and stability. Hence, the effect of spacer modification might not be fully transferred to the lanthanide environment due to the labile coordination of pcam units. In addition to these weaknesses, the chromophores are also known to be poor lanthanide sensitizer for extended system and possess poor solubility in biological medium.[1-3] To address the issues, 8-hydroxyquinoline-based (8-HQ-based) chromophore are investigated by different research group[4-9] in which NIR emission from its Ln complexes are observed as illustrated in **figure 4-1** and **figure 4-2** while both of them utilize the amide- modified hydroxyquinoline ligands.

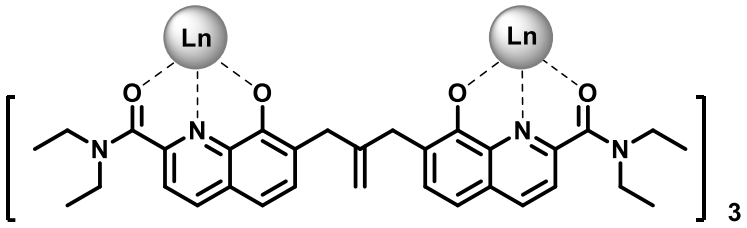

Figure 4-1: Ln helicates based on hydroxyquinoline[6,10]

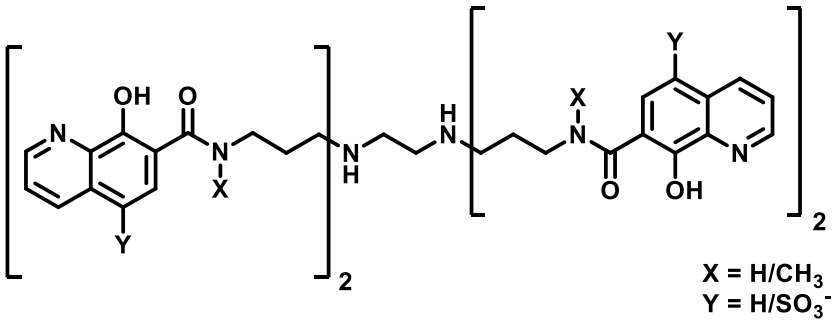

Figure 4-2: hydroxyquinoline-based podand like ligands[4]

In addition to NIR emission, the anionic and oxygen-rich nature of the chromophores facilitate the chelation of lanthanide with the oxophilic hard acid nature while the strong chelation of HQ units exclude water from the coordination environment even in aqueous medium.4

Meanwhile, two novel carboxyl-functionalized HQ-like derivatives 8-hydroxy-1,5-naphthyridine-2-carboxylic acid (R = H) and 7-cyano-8-hydroxy-1,5-naphthyridine-2-carboxylic acid (R = CN) are reported with excellent photoluminescence quantum yield (up to 28% in aqueous medium).[10] more recently, Sun have reported 8-hydroxyquinoline-based bidentate ligands which affords different supramolecular two-dimensional architectures including triangle, square, hexagon and octagon as shown in figure 4-4. [11]

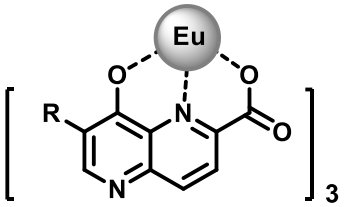

Figure 4-3: 1,5-naphthyridine based complexes

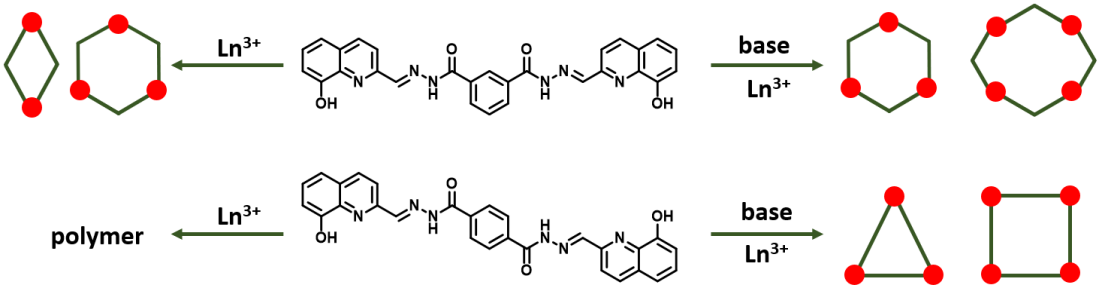

Figure 4-4: Graphical illustration on 8-HQ based ditopic ligands[11]

Unlike ordinary bidentate ligands, the V-shaped bidentate ligand does not simply afford helicate-like structure but also two-dimensional structure. This is probably attributed from higher-than-usual available coordinating sites from the ligand (i.e. 4 coordinates for each side). The high coordination number sufficiently stabilize the lanthanide

complexes in which only two ligands are required for such complexes. Meanwhile, the high stability also provides an opportunity to form relatively steric-bulky 2D topologies. The addition of base deprotonates hydroxyl groups on 8-hydroxyquinoline which further strengthen the coordinating ability as lanthanide prefer anionic chelation to achieve tetranuclear square or octagon.

4.1.2. Scope of study

In light of the characteristic properties in both optical and coordination chemistry from 8-HQ units. This chapter aims at devising new class of chiral chelator based on 8-HQ units which empower the ligands stronger chelation and chiroptical properties. With the functionalization of 8-HQ units, the investigation on the effect of chelating strength toward the ultimate supramolecular self-assembling topologies.

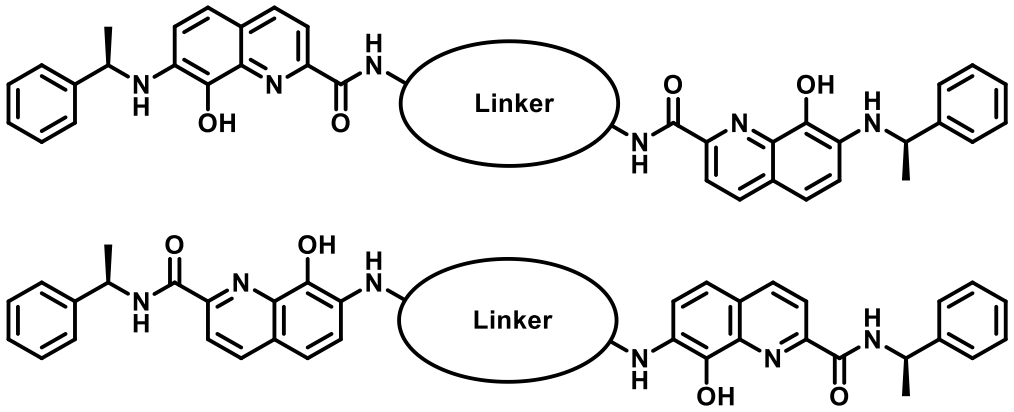

Figure 4-5: Two primary designs in Chapter four

4.2. Result & Discussion

4.2.1. Synthetic Scheme 1

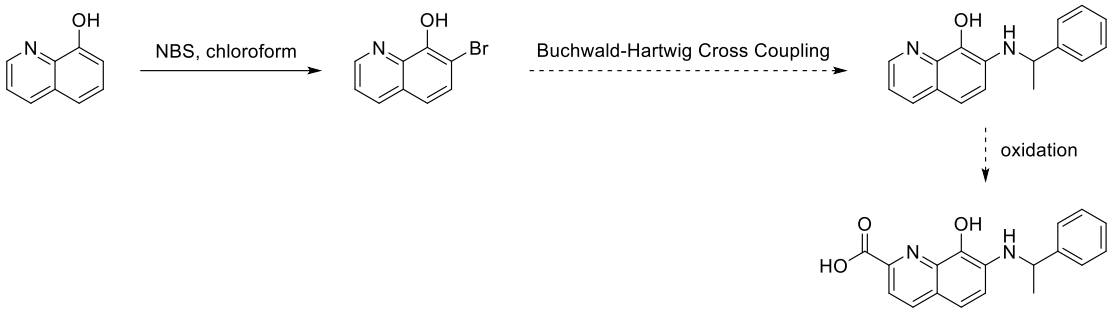

Figure 4-6: synthetic scheme 1a

As an initial attempt, the radical bromination of quinolinol is conducted with reported procedure.[12, 13] In this bromination, quinolinol (1 equiv.) in chloroform was treated with N-bromosuccinimide (0.98 equiv.) as a bromination source. Based on the experimental results, it is found that the high reaction temperature might induce dibrominated product and thus N-bromosuccinimide was added under ice temperature in low concentration and slowly raised to 50 °C to suppress unwanted side products. Upon completion of reaction, the solvent of the reaction crude is first evaporated to obtain a pale brown creamy solid. The solids are suspended in deionized water and the suspensions are collected by filtration.

To introduce the chiral group, different coupling scheme and conditions were attempted to couple the chiral amine on the bromide group. The initial attempts were palladium catalysed Buchwald-Hartwig coupling with different combination of base, phosphine, and solvent. However, no desired products were obtained with these coupling conditions. Therefore, copper-catalyzed coupling is attempted with simple CuI/proline system.

Entry	Reaction Condition
1	$Pd_2(dba)_3$, P(o-tol)$_3$, NaOt-Bu, toluene, 100°C
2[14-16]	$Pd_2(dba)_3$, BINAP, NaOt-Bu, toluene, 100°C
3[17]	$Pd_2(dba)_3$, dppf, NaOt-Bu, toluene, 100°C
4	$Pd_2(dba)_3$, xantphos, NaOt-Bu, toluene, 100°C
5	$Pd_2(dba)_3$, BINAP, LiHMDS, THF, 100°C
6	$Pd_2(dba)_3$, BINAP, Cs_2CO_3, dioxane, 100°C
8	CuI, L-proline, K_2CO_3, 100°C
9	CuI, L-proline, NaOt-Bu, 100°C

Table **4-1**: list of entry with reaction condition performed in synthetic scheme 1a

Unfortunately, no desired products were identified. Based on the structure and literature, the failure is probably attributed from the hydroxyl group next to the coupling site which hinder the formation of catalytic intermediates species. With this hypothesis, a protecting scheme was devised and discussed in next section.

Figure 4-6: benzyl protection scheme of bromoquinolinol

Entry	Reaction condition	Results
1	BnBr, K_2CO_3, methanol, reflux, 2 days	3%
2	BnBr, K_2CO_3, KI, methanol, reflux, 2 days	3%
3	BnBr, K_2CO_3, DMF, reflux, 2 days	5%
4	BnBr, KOH, DMF, reflux, 2 days	5%
5	BnBr, NaH, THF, 0°C to reflux, 2 days	5%
6	**BnBr, NaH, THF, 0°C to reflux, 2 days**	**7%**

Table **4-2**: list of entry with reaction condition performed in benzyl protection

The benzyl protecting group is initially selected due to their tolerance in relatively harsh reaction conditions and ease in deprotection. Different substitution schemes are attempted with different base, solvent, and mole ratio.[18, 19] However, the completion of reaction had never been accomplished even with high equivalent of benzyl bromide and bases, lengthening of reaction duration and elevated temperature. The plausible reason for such failure is attributed from five-member ring formation with deprotonated hydroxyl and quinolinium nitrogen. Additionally, the benzyl group is quite bulky to the crowded environment.

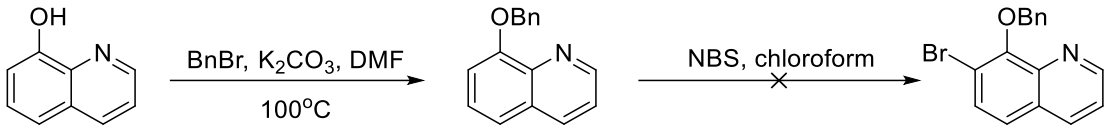

Figure 4-7: synthetic scheme 1b

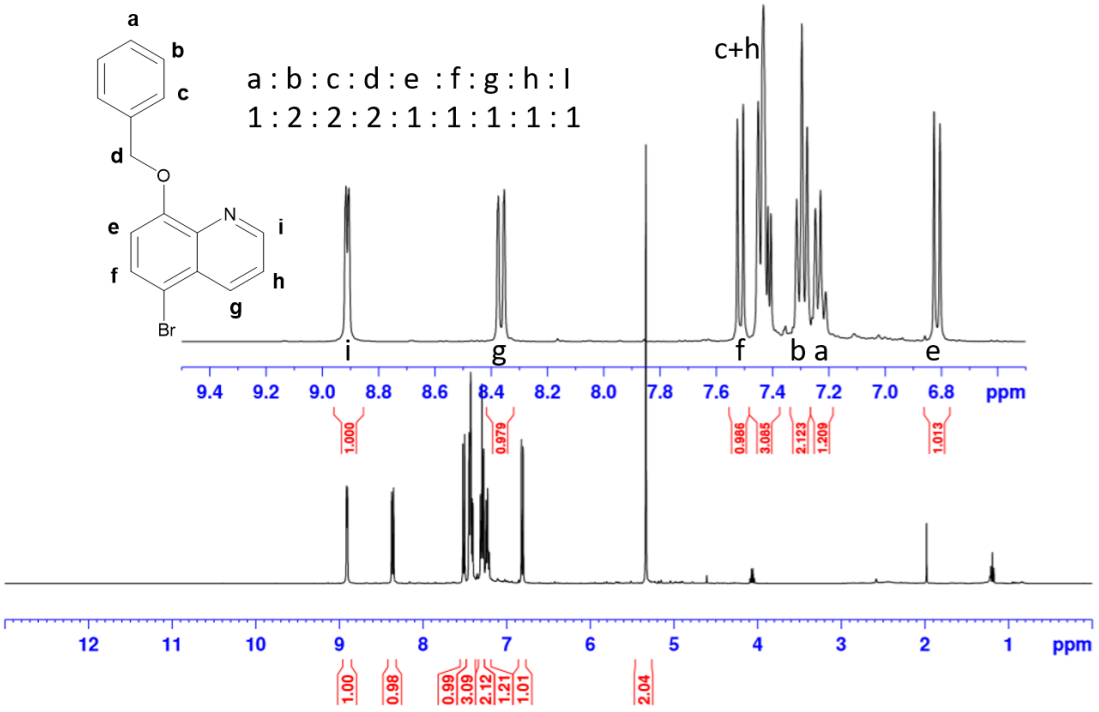

Spectrum S4-1: ^{1}H NMR spectrum of para-brominated product

With the failure in protecting bromoquinolinol, the reaction sequence is modified that the quinolinol is first protected followed by bromination. The protection was first employed prior to bromination in which it successfully affords the benzyl protected intermediates with higher yield. However, the following bromination failed to give ortho-brominated but solely para-brominated product which was probably attributed from the steric effect.

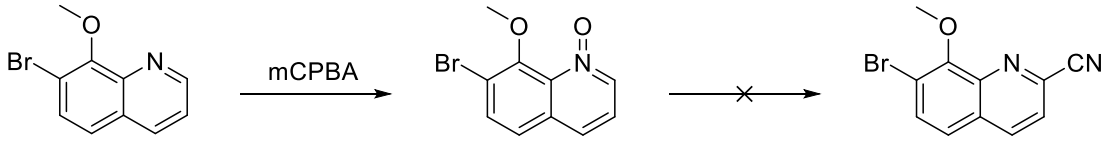

Figure 4-8: synthetic scheme 1c

Upon successful protection of methyl group on bromoquinolinol, the subsequent oxidation was performed using standard oxidation reagents mCPBA to synthesize N-oxide. However, the subsequent cyanation failed to yield the desired cyano-intermediates.

4.2.2. Synthetic Scheme 2

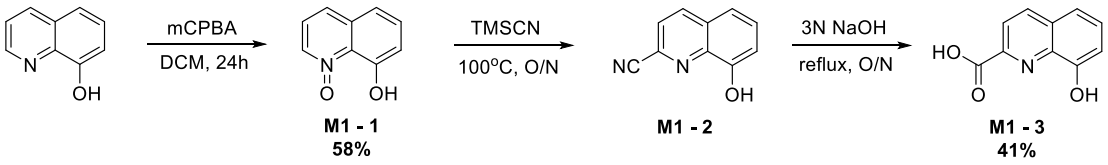

Figure 4-9: Synthetic Scheme 2a

In the view of previous failure, oxidation is conducted prior to the bromination to avoid reduced activity towards sequential oxidation procedures. Based on the modified literature procedure[20, 21], the compound **M1-3** is synthesized. The synthesis started with oxidation of 8-quinolinol to 8-quinolinol N-oxide which are generally obtained from either oxidation with 30% H_2O_2 or mCPBA. The experimental results showed

that oxidation through solid mCPBA oxidants have higher performance with better yield (58% compared to 22%).

Following the literature[20], the cyanation of compound **M1-1** are conducted neat reaction with trimethylsilyl cyanaide (TMSCN) in neat TMSCN at 80°C through auto-catalysis mechanism. The synthesized cyanide intermediates are hydrolyzed directly without further work-up procedures. Upon completion of reaction with the indication of TLC, the reaction mixture was cooled and washed with dichloromethane (3X).

The remaining aqueous extract is acidified with 1N HCl until formation of permanent solid. The solution was then extracted trice with dichloromethane/acetone (95:5 v/v, 3X) and the resulting organic extracts were washed with brine, dried over anhydrous sodium sulphate, solvent removed under reduced pressure to afford yellow plate. The yellow crude was then redissolved in dichloromethane/tetrahydrofuran and precipitated with hexane to afford yellow powder.

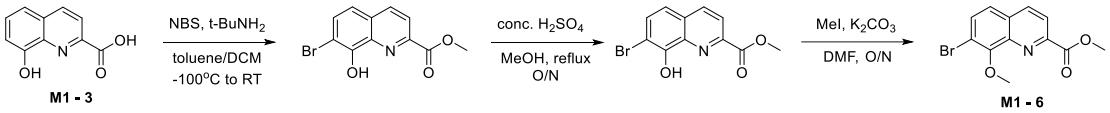

Figure 4-10: Synthetic Scheme 2b

With the compound **M1-3**, it is selectively brominated with N-bromosuccinimide (NBS) according to literature modified literature protocol.[22], the selective bromination of phenol-like compounds was achieved by eliminating hydrogen bromide by precipitating with tert-butylamine in toluene-based reaction medium under -100°C.

Otherwise, para-brominated (X = Br, Y = H) and dibrominated (X = Y = Br) products will be generated and hinder the formation of desired products (X = H, Y = Br)

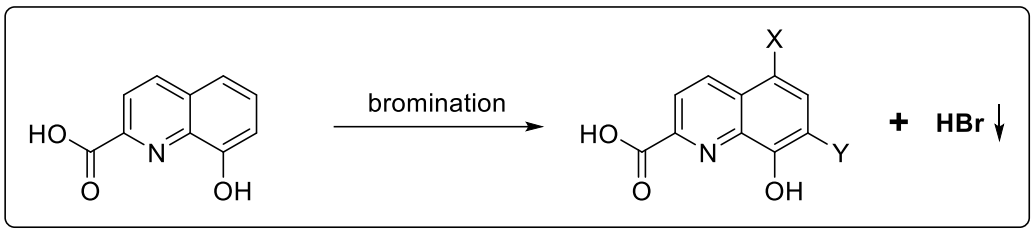

Figure 4-11: selective bromination of quinoline

In the synthetic scheme 2b, compound **M1–3** require great amount of polar protic solvent for dissolution which simultaneously hinder the precipitation t-butyl bromide and temperature control. Meanwhile, highly polar products require 20% methanol/EA for elution to complicate the purification processes. Hence, the reaction scheme 2b has severe dibrominated products up to 50% due to low solubility of the precursor

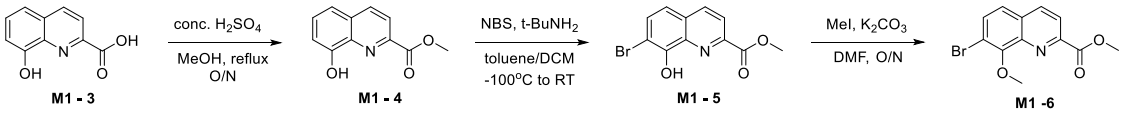

Figure 4-12: Synthetic Scheme 2c

Considering the solubility issue of compound **M1-3,** the new scheme 2c is devised to perform acid protection prior to the bromination. The methyl protection significantly enhances the solubility of precursor resulting in high toluene content in reaction medium and reduction of overall solvent. It is inferred these two factors simultaneously promote the desired bromination while the unwanted bromination on methyl arm via radical substitution was not identified. It is probably attributed from low temperature condition that inactivate and suppress radical formations. Meanwhile, the dibrominated products were significantly suppressed from 50% to less than 10% which further improve the overall efficiency.

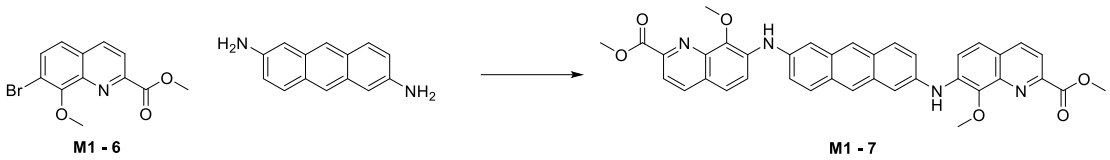

Figure 4-13: Synthetic Scheme 2d

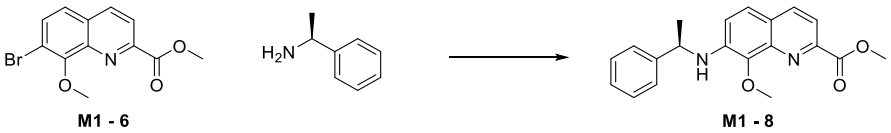

Figure 4-14: Synthetic Scheme 2e

With the protected compound **M1-6**, two synthetic scheme are investigated in parallel manner in which scheme 2d directly couple compound **M1-6** to desired spacer followed by acid group deprotection for chiral amine coupling. As alternative pathway, compound **M1-6** is first coupled with chiral amine to synthesize **M1-8** followed by deprotection to acquire desired compounds. In the initial screening of catalytic system for reaction scheme 2d, six different phosphine was employed, and the result is summarized in following table **4-3**.

Entry	Bromide (equiv.)	Amine (equiv.)	tBuONa (equiv.)	[Pd] (mol %)	Phosphine (mol %)	Condition	Result
A	1.9	1	2	$Pd(OAc)_2$ (6 mol %)	BINAP (6 mol %)	Toluene 100°C	-ve
B	1.9	1	2	$Pd_2(dba)_3$ (3 mol %)	$P(t\text{-}Bu)_3$ (6 mol %)	Toluene 100°C	-ve
C	1.9	1	2	$Pd_2(dba)_3$ (3 mol %)	$P(Cy)_3$ (6 mol %)	Toluene 100°C	-ve
D	1.9	1	2	$Pd_2(dba)_3$ (3 mol %)	$P(o\text{-}tol)_3$ (6 mol %)	Toluene 100°C	-ve
E	1.9	1	2	$Pd_2(dba)_3$ (3 mol %)	PPh_3 (6 mol %)	Toluene 100°C	-ve
F	1.9	1	2	$Pd(OAc)_2$ (5 mol %)	DPEPhos (3 mol %)	Toluene 100°C	-ve

^ The result is interpreted from ^1H NMR and HRMS

Table 4-3: list of entry with reaction condition performed in synthetic scheme 2d

Based on the screen results, the further attempts on scheme 2d are discouraged as no successful trial over wide range of ligand system. For reaction scheme 2e, different coupling schemes were attempted previously while Pd/P(t-Bu)$_3$/NaOt-Bu was found to be effective catalytic system that shows consumption of starting materials. With this previous finding, different palladium-based coupling was attempted to couple the amine to the intermediate bromide. Unfortunately, no positive results were shown yet even less steric hindrance achiral amine was employed as shown table **4-4**. It was inferred that the bromide is not sufficiently active for coupling reaction such that the conversion of bromide to higher activity moiety such as iodide, triflate, mesylate and boronic moiety was investigated.

Entry	Reaction condition	Result
	Chiral amine with bromide	
1	NaOt-Bu, $Pd_2(dba)_3$, dppf, toluene, 80°C	-ve in both MS & ^{1}HNMR
2	NaOt-Bu, $Pd_2(dba)_3$, BINAP, toluene, 80°C	-ve in both MS & ^{1}HNMR
3	NaOt-Bu, $Pd_2(dba)_3$, BINAP, dioxane, 80°C	enhanced solubility
	Achiral amine with bromide	
4	NaOt-Bu, $Pd_2(dba)_3$, BINAP, dioxane, 80°C	-ve in both MS & ^{1}HNMR
5	NaOt-Bu, $Pd_2(dba)_3$, xantphos, dioxane, 80°C	-ve in both MS & ^{1}HNMR
6	NaOt-Bu, $Pd_2(dba)_3$, P(t-Bu)3, dioxane, 80°C	-ve in both MS & ^{1}HNMR
	Achiral amine with iodide	
7	NaOt-Bu, $Pd_2(dba)_3$, BINAP, dioxane, 100°C	**successful**
8	NaOt-Bu, $Pd_2(dba)_3$, P(t-Bu)3, dioxane, 100°C	**successful**

Table 4-4: list of entry with reaction condition performed in synthetic scheme 2e

Due to the synthetic difficulties, the boronic moiety was not feasible while the conversion to triflate and mesylate were still under investigation. Among those, iodide was first synthesized substrate and similar reaction condition were adopted with

ordinary Pd_2dba_3/P(t-Bu)$_3$/NaOt-Bu and Pd_2dba_3/(±)-BINAP/NaOt-Bu. Upon completion of reaction, the reaction crude is analyzed with ^{1}H NMR spectroscopy which show positive sign of reaction and reaction conditions are further optimized with different screening.

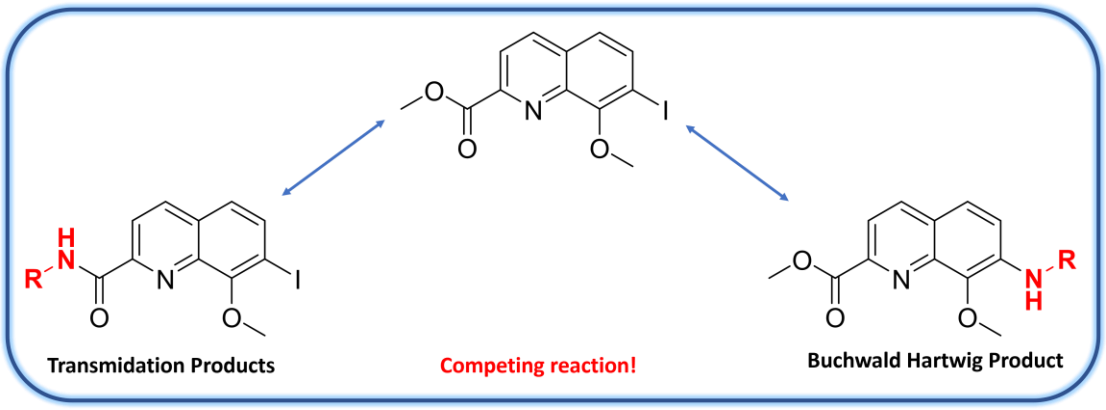

Figure 4-15: competing product between two competing pathways

Upon detailed investigation, it is revealed that the transamidation products were afforded which share similar NMR spectrum with desired Buchwald Hartwig products. To investigate the mechanism of transamidation, several microscale experiments were conducted without palladium or phosphine under room temperature and elevated temperature. It is found that no transamidation reaction occurred without the catalyst of palladium and phosphine ligands.

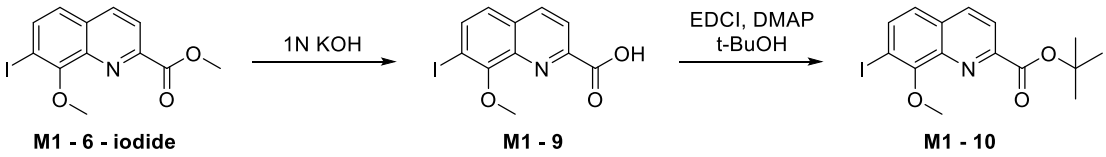

Figure 4-16: Synthetic Scheme 2f

To suppress the transamidation, the steric protecting group was introduced by two subsequent steps. The compound **M1-6** was first deprotected with 1N KOH. With

the monitoring of NMR spectroscopy, the deprotection was completed with 5 equiv. of hydroxide in 2 days. The acid intermediates were isolated and purified under standard work-up procedures followed by EDCI-catalyzed esterification to afford compound **M1-10** (^{1}H and ^{13}C NMR characterized). The obtained intermediates were then subjected to another round of condition screening.

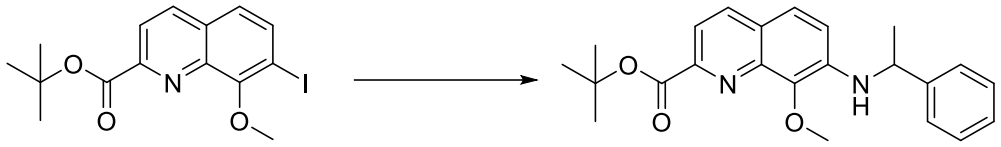

Figure 4-17: Synthetic Scheme 2g

Entry	Pd source (mol %)	Base (equiv.)	Phosphine (mol %)	Amine (equiv.)	Result
1	Pd_2dba_3 (1.5 mol %)	NaOt-Bu (3 equiv.)	SPhos (3 mol%)	(S)-EtPh (2 equiv.)	n.d.
2	$Pd(OAc)_2$ (3 mol %)	$CsCO_3$ (3 equiv.)	SPhos (3 mol%)	(S)-EtPh (2 equiv.)	n.d.
3	Pd_2dba_3 (1.5 mol %)	NaOt-Bu (3 equiv.)	SPhos (3 mol%)	(S)-EtPh (2 equiv.)	n.d.
4	$Pd(OAc)_2$ (3 mol %)	$CsCO_3$ (3 equiv.)	SPhos (3 mol%)	(S)-EtPh (2 equiv.)	n.d.
5	Pd_2dba_3 (1.5 mol %)	NaOt-Bu (3 equiv.)	Xantphos (3 mol%)	(S)-EtPh (2 equiv.)	n.d.
6	Pd_2dba_3 (1.5 mol %)	KOt-Bu (2 equiv.)	Xantphos (3 mol%)	(S)-EtPh (3 equiv.)	n.d.
7	**Pd_2dba_3 (1.5 mol %)**	**KOt-Bu (2 equiv.)**	**BINAP (3 mol%)**	**(S)-EtPh (3 equiv.)**	**12%**
8	$Pd(OAc)_2$ (3 mol%)	KOt-Bu (2 equiv.)	BINAP (3 mol%)	(S)-EtPh (3 equiv.)	6%

9	(H_2O act.) $Pd(OAc)_2$ (3 mol%) (H_2O act.)	KOt-Bu (2 equiv.)	Brettphos (3 mol%)	(S)-EtPh (3 equiv.)	n.d.
10	$Pd(OAc)_2$ (3 mol%) (H_2O act.)	KOt-Bu (2 equiv.)	Xphos (3 mol%)	(S)-EtPh (3 equiv.)	n.d.

Table 4-4: list of entry with reaction condition performed in synthetic scheme 2g

In general, as shown in the following scheme, the t-butyl protection shields the carboxylate moiety which promote the oxidation addition of iodide moiety. The subsequent Pd-amine bond formation were competed with hydride formation which hinder the formation of desired product (reductive amination product).

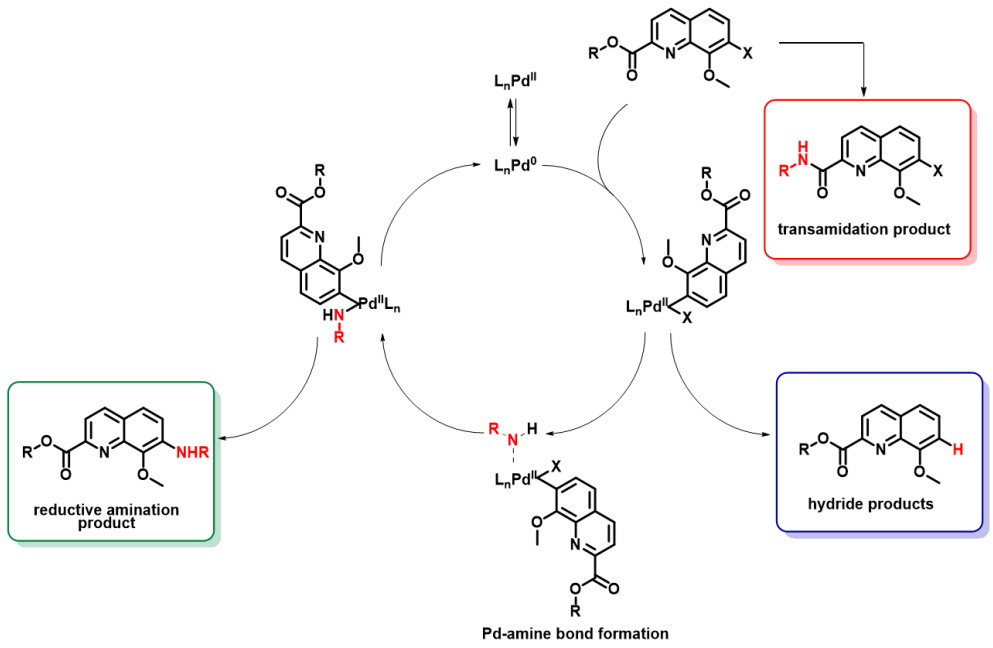

Figure 4-18: simplified catalytic cycle in synthetic scheme 2g

Although products were identified, there are still substantial starting materials and hydride products while the detailed synthetic procedure and characterization is

included in experimental section and appendix respectively. In the further study, different reaction condition must be employed to facilitate Pd-amine bond formation while base equivalent and temperatures will also be another factor to affect the rate of oxidation addition and hydride formation.

4.2.3. Amide coupling study

To investigate the amide coupling conditions, previous precursor is deprotected under KOH to afford compound **M1-12** for condition screening as the obtained amount of chiral precursor is synthetically limited. As depicted in the following table, the amide coupling with different condition and procedures were employed.

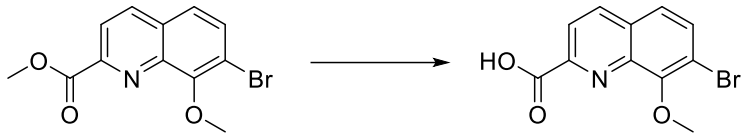

M1 - 6 **M1 - 12**

Figure 4-19: Synthetic Scheme 3a

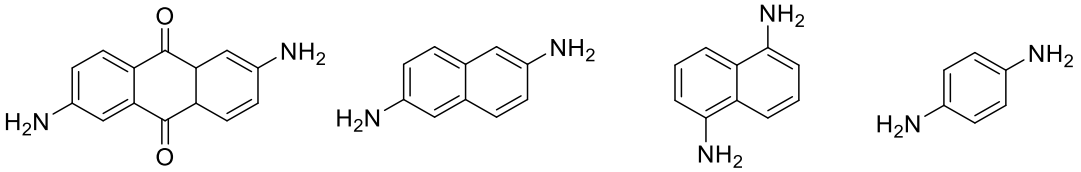

Figure 4-20: list of amine employed for the trials

As an initial trials, standard HATU coupling was employed with room temperature and elevated temperature. However, both show no signs of reaction from NMR spectrum. Using strong activation agent $SOCl_2$, one-pot and two stage attempts were both conducted while no sign of di-coupled products was observed in the NMR spectrum. The sequential HATU coupling is therefore employed in which the acid was coupling to anthraquinone in a stepwise manner. As depicted in the following NMR spectrum,

there are sufficient information that new species were formed during the coupling step. However, due to limited solubility, the detailed characterization of di-coupled products and deprotected products were not feasible.

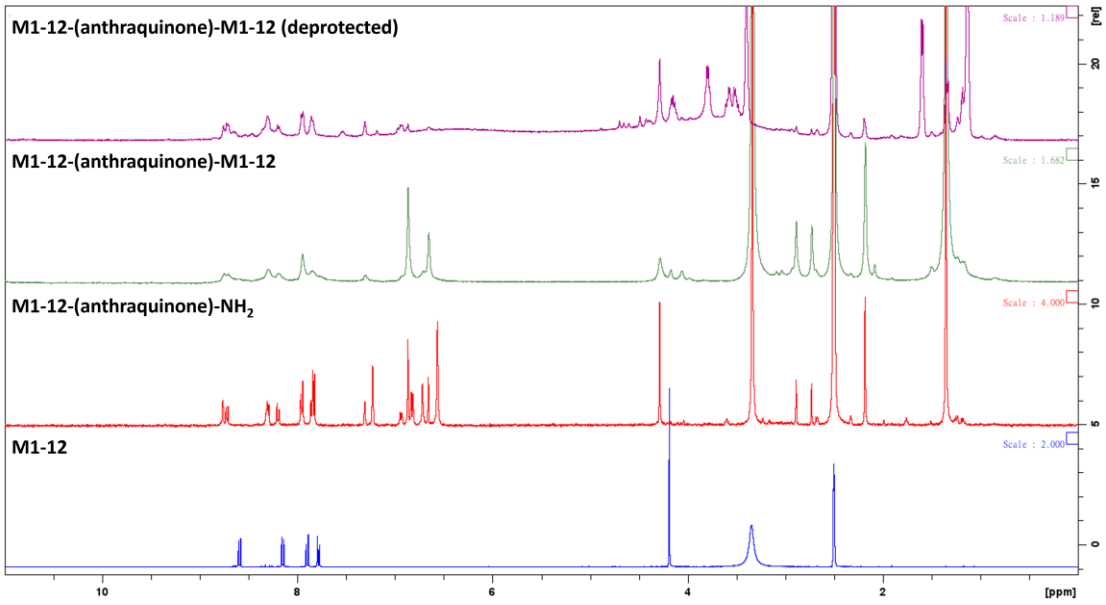

Spectrum S4-2: the stacked ^{1}H NMR spectrum from sequential HATU coupling

As the solubility of the coupling products were limited, stronger coupling agents i.e., PCl_3 was then employed to promote reaction and avoid unreacted intermediates. The stacked NMR spectrum revealed that HATU was more effective coupling procedure compared to PCl_3 as only minute amount of mono-coupled products were identified even excess of acid and PCl_3 was employed.

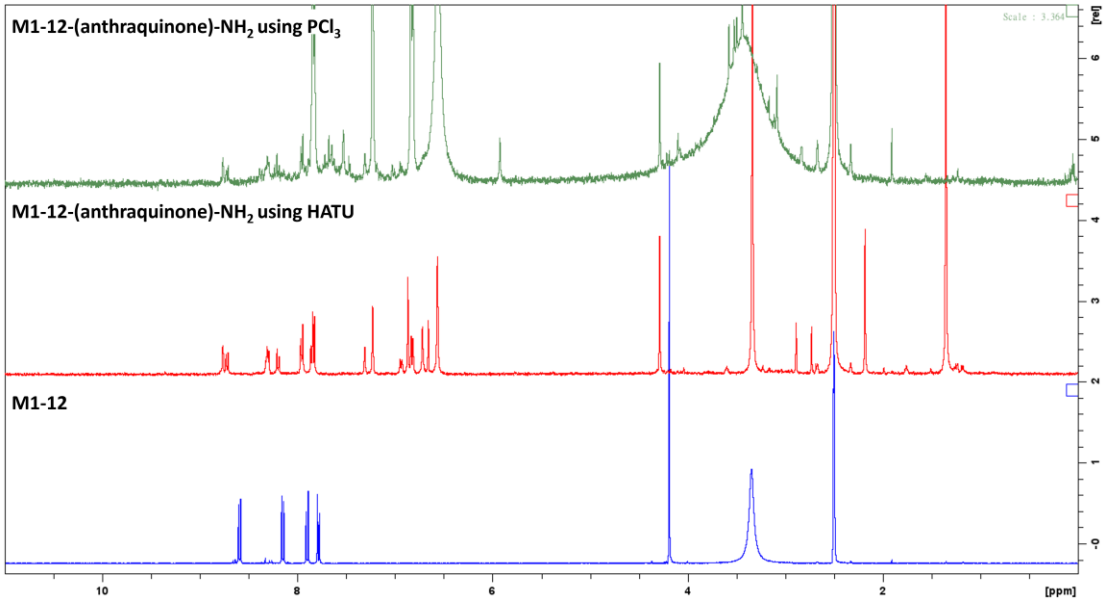

Spectrum S4-3: the stacked ^{1}H NMR spectrum from two different amide coupling

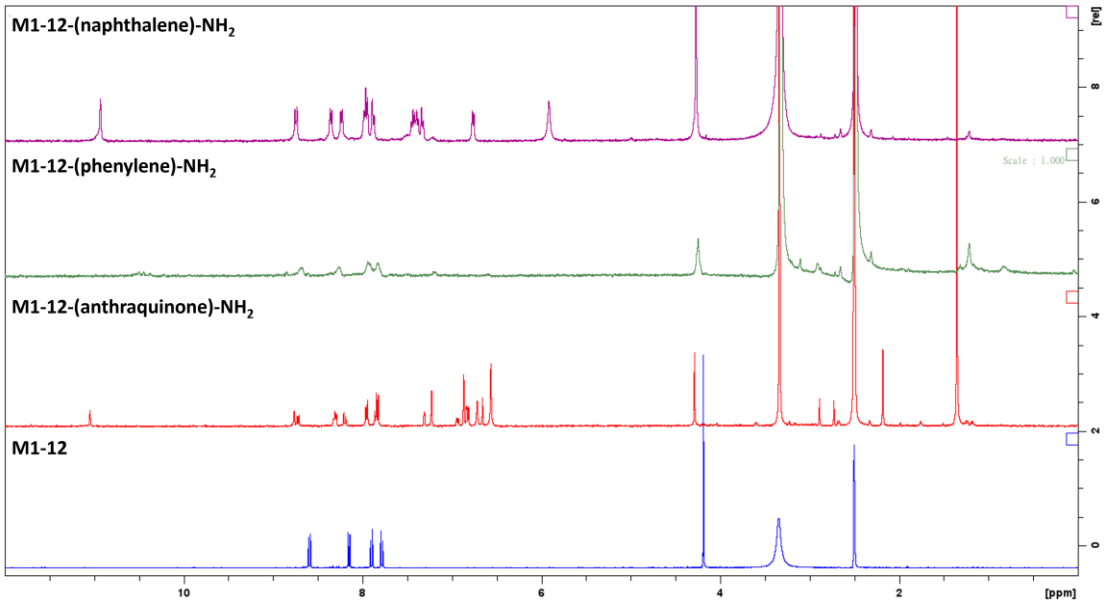

Spectrum S4-4: the stacked ^{1}H NMR spectrum of mono-coupled species with different amines

To investigate the sequential HATU coupling, two less bulky diamine including 2,6-naphthalenediamine and 1,4-phenylenediamine were employed. As depicted in the above spectrum, naphthalene version also successfully affords mono-coupled products while the characterization of phenyl products is not feasible due to limited solubility. In addition, the di-coupled product of naphthalenediamine also suffers from solubility

issues that no NMR signal was obtained. This revealed that the reduction of bulkiness on center linker apparently has adverse effect on the solubility.

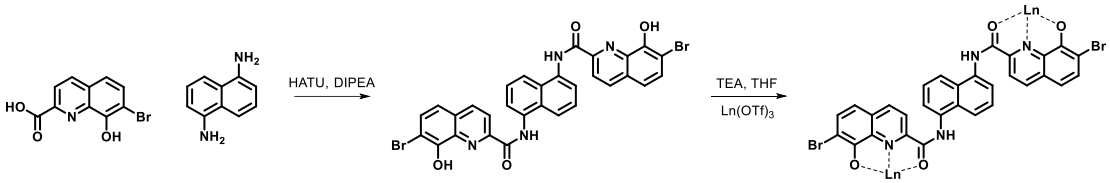

Figure 4-21: Complexation condition of **Compound M1-12 –(1,5-nap)– M1-12**

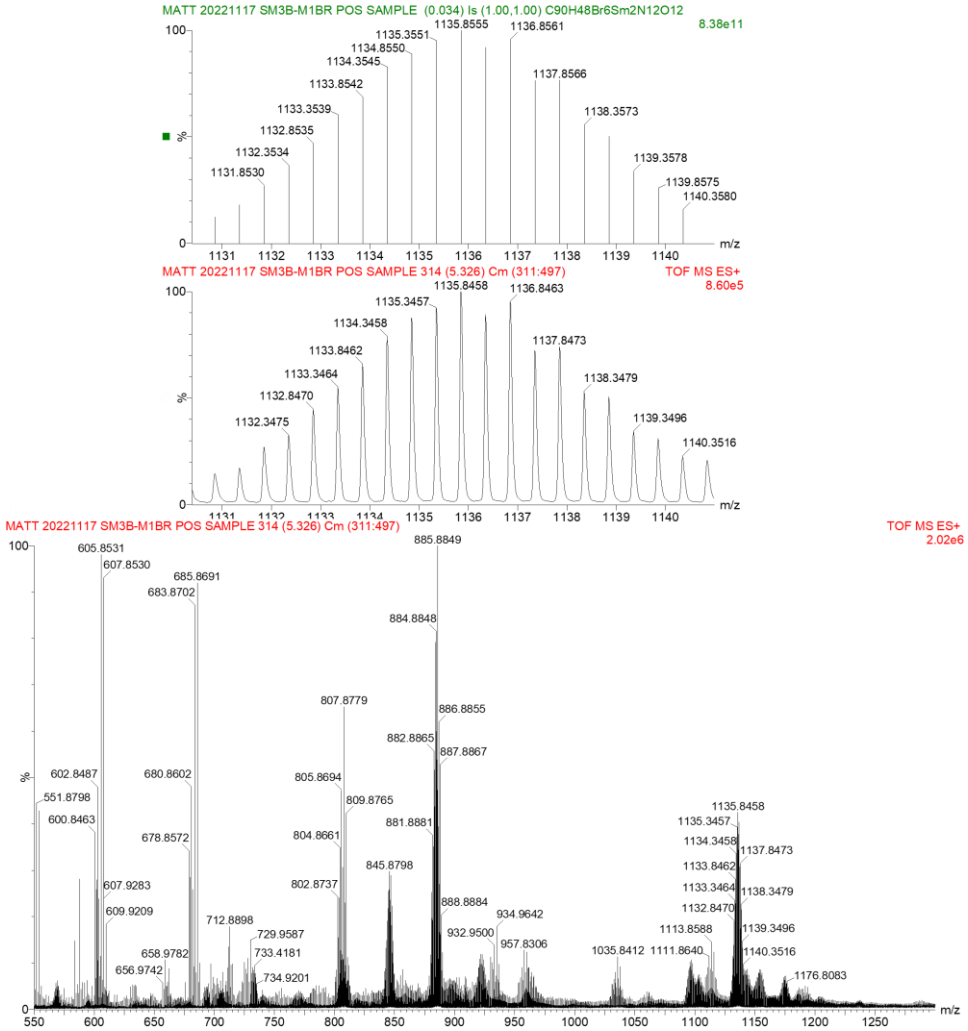

Spectrum S4-5: HRMS spectrum of Sm complexes of **Compound M1-12 –(1,5-nap)– M1-12**

Compared to other series, the amide coupling with 1,5-napthalenediamine using HATU coupling successfully afford the ligand and the subsequent complexation are conducted. Using triethylamine as deprotonating bases, the ligand are complexes with

lanthanide triflates. Upon purification, HRMS analysis show characteristic peak of $[Ln_2(L\text{-}2H)L_2]^{2+}$ for lanthanum, samarium, europium and gadolinium complexes.

4.3. Conclusion & Future Work

To conclude, this chapter investigated different synthetic pathway to functionalize the 8-hydroxyquinoline unit with coupling amine coupling sites. The sequential HATU coupling of the 8-hydroxyquinoline towards different linkers are also developed. Chapter Four have explored different synthetic possibility while it underlies the foundation of ditopic ligand synthesis. However, the complete pathway on synthesizing the 8-hydroxyquinoline-based chiral ditopic ligands are not yet successful due to the synthetic difficulties.

4.4. Experimental Section

4.4.1. General Considerations

All chemical used for synthesis were obtained from commercial suppliers and used without further purification. All moisture-sensitive reactions were conducted under a nitrogen atmosphere in oven-dried glassware. Anhydrous solvents were freshly distilled or dried over 4A molecular sieves unless otherwise specified. 1D and 2D NMR spectra were conducted on a Bruker AVANCE-III 400 MHz and 600MHz FT-NMR. High Resolution-ESI mass spectrum were obtained from Agilent 6540 Liquid Chromatography - Electrospray Ionization Quadrupole-Time-of-Flight Mass Spectrometer or Waters Synapt G2-Si Ion Mobility Quadrupole MS and the chemical shifts were determined with tetramethylsilane (TMS) or solvents in parts per million (ppm).

4.4.2. Synthesis & Characterization

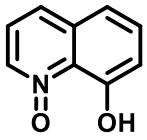

M1-1

Compound M1-1 To the solution of quinoline-8-ol (10.02 g, 68.5 mmol, 1 equiv.) in 300 mL dichloromethane, meta-chloroperoxybenzoic acid (27.8 g, 137 mmol, 2 equiv.) was added under ice temperature. The reaction mixture was then stirred overnight under nitrogen atmosphere. The solvent was then removed, and residue was diluted with ethyl acetate. The organic extracts were then washed with sodium bicarbonate solution (3X), brine (2X), dried over anhydrous sodium sulphate and dried under reduced pressure to obtain pale yellow solids. The crude was then loaded to column chromatography (silica gel, Hex to 50% EA/Hex, R_f = 0.3 in 20% EA/Hex). The obtained product was suspended in saturated sodium thiosulphate solution for overnight stirring. The solids was then filtered and dried to afford pale yellow solids. (5.56 g, 50%) ^{1}H NMR (400 MHz, Chloroform-*d*) δ 15.05 (s, 1H), 8.25 (dd, *J* = 5.9, 1.1 Hz, 1H), 7.79 (dd, *J* = 8.5, 1.0 Hz, 1H), 7.49 (t, *J* = 8.0 Hz, 1H), 7.25 (dd, *J* = 8.4, 6.2 Hz, 1H), 7.07 (dd, *J* = 7.9, 1.2 Hz, 1H).

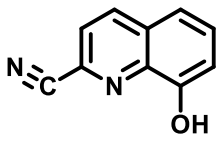

M1-2

Compound M1-2. To compound **M1-1** (2 g, 12 mmol, 1 equiv.) in 100 mL two neck flask, trimethylsilyl cyanide (4.65 mL, 36.8 mmol, 3 equiv.) was added in caution under nitrogen atmosphere. The reaction was slowly heated to 80°C for overnight reaction. Upon completion of reaction, trimethyl cyanide was removed under reduced pressure with the neutralization of base trap and cold trap. The resulting solid was then used in next step without further purification. ^{1}H NMR (400 MHz, Chloroform-*d*) δ 8.27 (d, *J*

= 8.4 Hz, 1H), 7.67 (d, *J* = 8.4 Hz, 1H), 7.59 (t, *J* = 7.9 Hz, 1H), 7.48 (dd, *J* = 8.3, 1.3 Hz, 1H), 7.28 (dd, *J* = 7.7, 1.3 Hz, 1H).

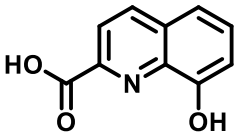

M1-3

Compound M1-2. To the crude solid of **CHT M2 – 02** (24 mmol, 1 equiv.), sodium hydroxide solution (3N, 24 mL, 3 equiv.) was added. The resulting mixture was heated to 100°C and stirred 24h for reaction. Upon completion of reaction with the indication of TLC, the reaction mixture was cooled and extracted with dichloromethane (100 mL, 3X). The obtained aqueous extract is acidified with 1N HCl until solid appears. The solution was then extracted trice with ethyl acetate (3X) and the resulting organic extracts were washed with brine, dried over anhydrous sodium sulphate, solvent removed under reduced pressure to afford brown solids. (2.23 g, 45%). ^{1}H NMR (400 MHz, DMSO-d_6) δ 10.17 (s, 1H), 8.51 (dd, *J* = 8.5, 2.1 Hz, 1H), 8.08 (dd, *J* = 8.6, 2.1 Hz, 1H), 7.68 – 7.55 (m, 1H), 7.47 (d, *J* = 8.2 Hz, 1H), 7.15 (d, *J* = 7.7 Hz, 1H). ^{13}C NMR (101 MHz, DMSO-d_6) δ 165.58, 154.29, 144.75, 138.81, 136.94, 130.92, 130.40, 120.43, 118.06, 112.47.

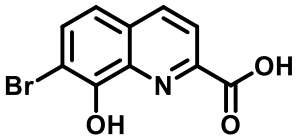

M1-4 (2b)

Compound M1-4 (2b). To the solution of t-butylamine (2.49 mL, 23.2 mmol, 2.2 equiv.) in anhydrous toluene (80 mL), N-bromosuccinimide (1.81 g, 10 mmol, 0.95 equiv.) was added under acetone/liquid nitrogen cooling bath. Upon stirring for 30 minutes, compound **M1-3** (2.02 g, 10.6 mmol, 1 equiv.) in tetrahydrofuran (30 mL) was added in dropwise manner at same temperature. The solution mixture was then slowly back to room temperature over 3 hours and stirred

overnight under room temperature. Upon completion of reaction, the mixture was then diluted with minimal ethyl acetate and methanol, filtered with thick pad of silica (5 cm) and washed with ethyl acetate. The residues bed was then eluted with 50% EA/MeOH (v/v) and the solvent was removed under reduced pressure. The residues were then uptake by ethyl acetate and precipitated in hexane to obtain semi-pure product (1.21 g, yield: 36%). ^{1}H NMR (400 MHz, DMSO-d_6) δ 8.30 (d, J = 8.4 Hz, 1H), 8.06 (d, J = 8.4 Hz, 1H), 7.64 (d, J = 8.7 Hz, 1H), 7.18 (d, J = 8.7 Hz, 1H).

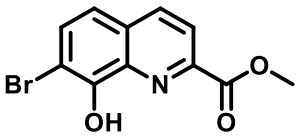

M1-5 (2b)

Compound M1-5 (2b). To the solution of **M1-4 (2b)** (2.5 g) in 150 mL fresh methanol was added concentrated sulphuric acid (1.5 mL, cat.). The resulting mixture was then heated to reflux temperature. Upon overnight reaction, the reaction crude was diluted with H_2O and the organic solvents were removed by rotatory evaporator before partition with EA/H_2O. The organic extracts were then washed trice with sat'd $NaHCO_3$, brine, dried over anhydrous sodium sulphate followed by rotatory evaporation. The obtained oil was precipitated with DCM/Hex and collected by filtration. ^{1}H NMR (400 MHz, Acetonitrile-d_3) δ 10.57 (s, 1H), 8.57 (d, J = 8.6 Hz, 1H), 8.14 (d, J = 8.5 Hz, 1H), 7.83 (d, J = 8.8 Hz, 1H), 7.50 (d, J = 8.8 Hz, 1H).

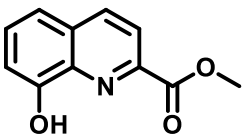

M1-4

Compound M1-4. To the suspension of compound **M1-3** (12 g, 13 mmol, 1 equiv.) in 500 mL fresh methanol was charged conc. H_2SO_4 (5 mL) in caution under nitrogen atmosphere. The resulting mixture was heated at reflux

temperature overnight before quenching of sodium bicarbonate solution. The aqueous layer was then extracted trice with ethyl acetate while the combined organic layer was washed with sodium bicarbonate solution (3X), brine (2X), drying over anhydrous sodium sulphate, solvent removed under reduced pressure to give crude solids. The crude was then loaded to column chromatography (silica gel, gradient from hex to DCM) to afford titled compounds. ^{1}H NMR (400 MHz, Chloroform-*d*) δ 8.36 (dt, *J* = 2.4, 1.2 Hz, 1H), 8.26 (d, *J* = 8.5 Hz, 1H), 8.14 (d, *J* = 8.5 Hz, 1H), 7.54 (t, *J* = 8.0 Hz, 1H), 7.36 (dd, *J* = 8.3, 1.2 Hz, 1H), 7.27 – 7.14 (m, 1H), 4.03 (s, 3H). ^{13}C NMR (101 MHz, Chloroform-*d*) δ 165.50, 153.20, 145.42, 137.74, 137.25, 130.26, 129.72, 121.65, 117.66, 110.98, 52.92.

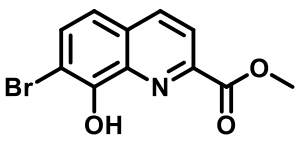

M1-5

Compound M1-5. To the slurry mixture of NBS (555 mg, 3.1 mmol, 0.95 equiv.) and t-butylamine (0.77 mL, 7.1 mmol, 2.2 equiv.) in toluene (40 mL) was added CHT – M1 – 04 (667 mg, 3.2 mmol, 1 equiv.) in dichloromethane (10 mL) in dropwise manner at -100°C in acetone/liq. N_2 bath. At the same temperature, the mixture was stirred for another 30 minutes before slowly warmed to room temperature over 2 hours. The resulting reaction mixture was then further stirred at room temperature overnight. Upon completion of reaction, the solvent was removed in rotatory evaporator and the crude was partitioned in ethyl acetate and H_2O. The aqueous layer was extracted trice with ethyl acetate while the combined organic layer was then washed H2O (3X) and brine (2X), followed by drying over anhydrous magnesium sulphate, solvent removed under reduced pressure to afford crude solids. The solids were then loaded to column chromatography (silica gel, gradient from DCM to 20% EA/DCM, R_f = 0.2 in DCM) to yield titled compounds. ^{1}H NMR (400 MHz,

Chloroform-*d*) δ 9.11 (s, 1H), 8.30 (d, *J* = 8.5 Hz, 1H), 8.20 (d, *J* = 8.5 Hz, 1H), 7.75 (d, *J* = 8.8 Hz, 1H), 7.37 – 7.22 (m, 1H, with d-$CDCl_3$), 5.31 (s, 1H), 4.08 (s, 3H).^{13}C NMR (101 MHz, Chloroform-*d*) δ 165.21, 150.85, 146.10 137.87, 137.49, 133.73, 128.71, 121.77, 118.22, 53.43, 53.08.

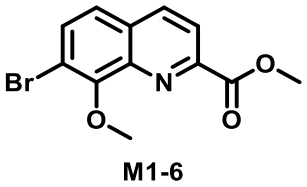

M1-6

Compound M1-6. To the suspension of compound **M1-5** (2.67 g, 9.4 mmol, 1 equiv.) and potassium carbonate (1.5732 g, 11.3 mmol, 1.2 equiv.) in 25 mL DMF was charged methyl iodide (0.66 mL, 10.3 mmol, 1.1 equiv.). The resulting mixture was stirred overnight before precipitating in 500 mL of H_2O. The titled compound was then obtained by filtration followed by washing of H_2O. ^{1}H NMR (400 MHz, DMSO-d_6) δ 8.51 (d, *J* = 8.6 Hz, 1H), 8.06 (d, *J* = 8.4 Hz, 1H), 7.81 (d, *J* = 9.0 Hz, 1H), 7.69 (d, *J* = 8.7 Hz, 1H), 4.09 (s, 3H), 3.90 (s, 3H). ^{13}C NMR (101 MHz, DMSO-d_6) δ 165.52, 162.97, 153.79, 147.59, 142.10, 138.85, 132.94, 130.27, 124.81, 121.75, 116.85, 62.65, 53.33.

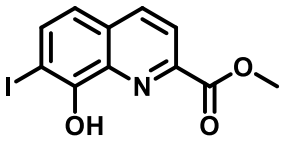

M1-5 - iodide

Compound M1-5 iodide. To the slurry mixture of NIS (1.05 g, 4.4 mmol, 0.95 equiv.) and t-butylamine (1.1 mL, 10.3 mmol, 2.2 equiv.) in toluene (250 mL) was added compound **M1-4** (1.0 g, 4.68 mmol, 1 equiv.) in 25 mL dichloromethane in dropwise manner at -100 ℃ in acetone/liq. N_2 bath. At the same temperature, the mixture was stirred for another 30 minutes before slowly warmed to room temperature over 2 hours. The resulting reaction mixture was then further stirred at room temperature overnight. Upon completion of reaction, the solvent was removed in rotatory evaporator and the crude

was partitioned in ethyl acetate and H_2O. The aqueous layer was extracted trice with ethyl acetate while the combined organic layer was then washed H2O (3X) and brine (2X), followed by drying over anhydrous magnesium sulphate, solvent removed under reduced pressure to afford crude solids. The solids were then loaded to column chromatography (silica gel, gradient from DCM to 20% EA/DCM, R_f = 0.2 in DCM) to yield titled compounds (0.8185 g, 55%). ^{1}H NMR (400 MHz, Chloroform-*d*) δ 8.23 (d, *J* = 8.5 Hz, 1H), 8.15 (d, *J* = 8.4 Hz, 1H), 7.85 (d, *J* = 8.7 Hz, 1H), 7.14 (d, *J* = 8.7 Hz, 1H), 4.02 (s, 3H).

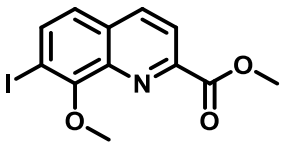

M1-6-iodide

Compound M1-6-iodide. To the suspension of compound **M1-5-iodide** (0.81 g, 2.5 mmol, 1 equiv.) and potassium carbonate (0.5158 g, 3.70 mmol, 1.5 equiv.) in 10 mL DMF was charged methyl iodide (0.19 mL, 2.95 mmol, 1.2 equiv.). The resulting mixture was stirred overnight before precipitating in 100 mL of H_2O. The titled compound was then obtained by filtration followed by washing of H_2O. (0.5351 g, 63%). ^{1}H NMR (400 MHz, Chloroform-*d*) δ 8.25 (d, *J* = 8.5 Hz, 1H), 8.16 (d, *J* = 8.5 Hz, 1H), 7.92 (d, *J* = 8.7 Hz, 1H), 7.33 (d, *J* = 8.7 Hz, 1H), 4.27 (s, 3H), 4.02 (s, 3H).

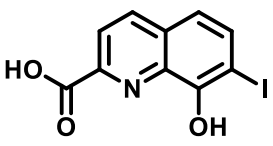

M1-9

Compound M1-9. To the Compound **M1-6-iodide** (1.6 g, 4.66 mmol, 1 equiv.) in 25 mL tetrahydrofuran was added 1N KOH (23 mL, 23.3 mmol, 5 equiv.) under room temperature and reacted for 2 days. The organic solvent was removed under rotatory evaporation followed by dilution with DCM/H_2O. The

aqueous phase was first extracted trice with DCM followed by acidification to precipitate white powder. The tilited products were then collected by simple filtration and dried under vacuum.

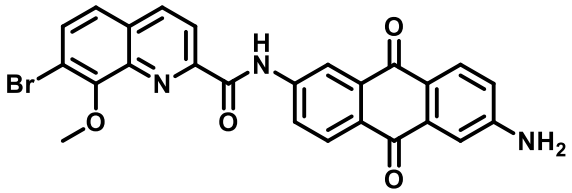

Compound M1-12-(anthraquinone)-NH_2 To the solution of **M1-12** (100 mg, 0.373 mmol, 1 equiv.) in 5 mL anhydrous N,N'-dimethylformamide was added HATU (312 mg, 0.82 mol, 2.2 equiv.). Upon 30 minutes stirring, 2,6-diaminoanthracene-9,10-dione (89 mg, 0.373 mmol, 1 equiv.) was added. With additional 30 miuntes stirring, DIPEA (142 µL, 0.82 mmol, 2.2 equiv.) was added. Upon 2 days stirring, the resulting slurry mixture was added H2O and the precipitates were collected by filtration and washed with dichloromethane. The obtaine solids were analyzed with NMR spectroscopy.

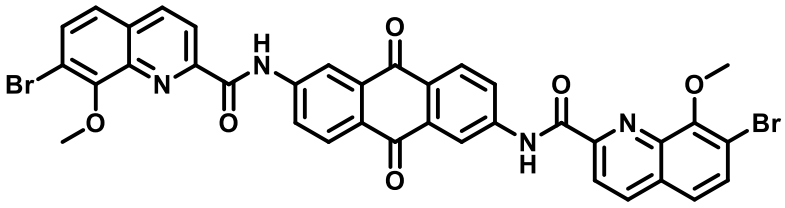

Compound M1-12-(anthraquinone)-M1-12. To the solution of compound **M1-12** (100 mg, 0.373 mmol, 1 equiv.) in 5 mL anhydrous N,N'-dimethylformamide was added HATU (312 mg, 0.82 mol, 2.2 equiv.). Upon 30 minutes stirring, mono-coupled products **M1-12-(anthraquinone)-NH_2** (1 equiv.) was added. With additional 30 miuntes stirring, DIPEA (142 µL, 0.82 mmol, 2.2 equiv.) was added. Upon 2 days stirring, the resulting slurry mixture was added H2O and the precipitates were collected by

filtration and washed with dichloromethane. The obtained solids were analyzed with NMR spectroscopy.

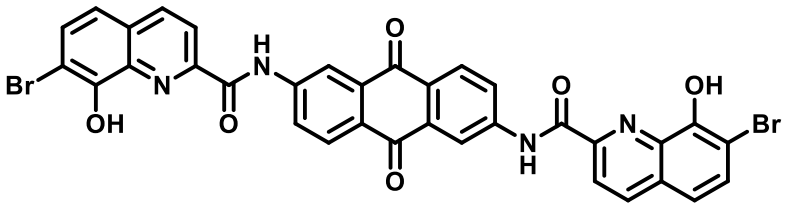

Compound HO-M1-12-(anthraquinone)-M1-12-OH To the suspeonsion of Lignad T – CHT M1 – Br – OMe (1 equiv.) in chloroform was added boron tribromide (1.0 M in DCM, 2 equiv.) under nitrogen atmosphere. Upon 2 days reaction, the reactio mixture was precipitated with H2O and the precipitates were collected by filtration and analyzed with NMR spectroscopy.

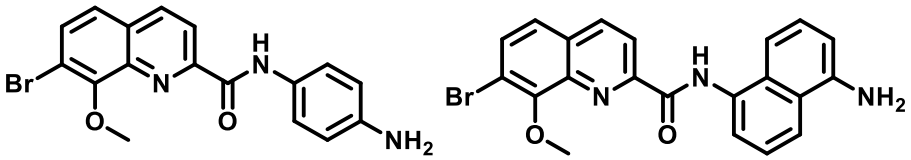

Compound M1-12-(phenylene)-NH_2 & M1-12-(napthalene)-NH_2. To the solution of compound **M1-12** (100 mg, 0.375 mmol, 1 equiv.) in 5 mL anhydrous N,N'-dimethylformamide was added HATU (157 mg, 0.412 mmol, 2.2 equiv.). Upon 30 minutes stirring, benzene-1,4-diamine or naphthalene-1,5-diamine (20.3 or 29.7 mg, 0.188 mmol, 1 equiv.) was added. With additional 30 miuntes stirring, DIPEA (72 μL, 0.412 mmol, 2.2 equiv.) was added. Upon 2 days stirring, the resulting slurry mixture was added H_2O and the precipitates were collected by filtration and washed with dichloromethane. The obtaine solids were analyzed with NMR spectroscopy.

4.5. Reference

1. Wei, C.; Wei, H.; Yan, W.; Zhao, Z.; Cai, Z.; Sun, B.; Meng, Z.; Liu, Z.; Bian, Z.; Huang, C., Water-Soluble and Highly Luminescent Europium(III) Complexes with Favorable Photostability and Sensitive pH Response Behavior. *55* **2016,** *20*, 10645-10653.

2. A.Kitchen, J., Lanthanide-based self-assemblies of 2,6-pyridyldicarboxamide ligands: Recent advances and applications as next-generation luminescent and magnetic materials. *Coordin Chem Rev* **2017,** *340*, 232-246.

3. Yim, K.-H.; Yeung, C.-T.; Probert, M. R.; Chan, W. T. K.; Mackenzie, L. E.; Pal, R.; Wong, W.-T.; Law, G.-L., Helicate-to-tetrahedron transformation of chiral lanthanide supramolecular complexes induced by ionic radii effect and linker length. *Communications Chemistry* **2021,** (116).

4. Li, X. Z.; Tian, C. B.; Sun, Q. F., Coordination-Directed Self-Assembly of Functional Polynuclear Lanthanide Supramolecular Architectures. *Chem Rev* **2022,** *122* (6), 6374-6458.

5. Comby, S.; Imbert, D.; Chauvin, A. S.; Bunzli, J. C., Stable 8-hydroxyquinolinate-based podates as efficient sensitizers of lanthanide near-infrared luminescence. *Inorg Chem* **2006,** *45* (2), 732-43.

6. Artizzu, F.; Deplano, P.; Marchio, L.; Mercuri, M. L.; Pilia, L.; Serpe, A.; Quochi, F.; Orru, R.; Cordella, F.; Meinardi, F.; Tubino, R.; Mura, A.; Bongiovanni, G., Structure and emission properties of Er3Q9 (Q = 8-quinolinolate). *Inorg Chem* **2005,** *44* (4), 840-2.

7. Albrecht, M.; Osetska, O.; Frohlich, R.; Bunzli, J. C.; Aebischer, A.; Gumy, F.; Hamacek, J., Highly efficient near-IR emitting Yb/Yb and Yb/Al helicates. *J Am Chem Soc* **2007,** *129* (46), 14178-9.

8. Van Deun, R.; Fias, P.; Nockemann, P.; Schepers, A.; Parac-Vogt, T. N.; Van Hecke, K.; Van Meervelt, L.; Binnemans, K., Rare-earth quinolinates: infrared-emitting molecular

materials with a rich structural chemistry. *Inorg Chem* **2004,** *43* (26), 8461-9.

9. Deun, R. V.; Fias, P.; Driesen, K.; Binnemans, K.; Görller-Walranda, C., Halogen substitution as an efficient tool to increase the near-infrared photoluminescence intensity of erbium(iii) quinolinates in non-deuterated DMSO. *Phys. Chem. Chem. Phys.* **2003,** *5*, 2754-2757.

10. Albrecht, M.; Osetska, O.; Fröhlich, R., Synthesis of Homo- and Heteroditopic 8-Hydroxyquinoline Ligands. *Eur. J. Org. Chem.* **2007**, 4902–4908.

11. Feng, X. S.; Li, X. Z.; Hu, S. J.; Yan, D. N.; Zhou, L. P.; Sun, Q. F., Base- and Metal-Dependent Self-Assembly of Lathanide-Organic Coordination Polymers or Macrocycles with Tetradentate Acylhydrazone-based Ditopic Ligands. *Chem Asian J* **2021,** *16* (11), 1392-1397.

12. Deraeve, C.; Boldron, C.; Maraval, A.; Mazarguil, H.; Gornitzka, H.; Vendier, L.; Pitie, M.; Meunier, B., Preparation and study of new poly-8-hydroxyquinoline chelators for an anti-Alzheimer strategy. *Chemistry* **2008,** *14* (2), 682-96.

13. Liang, S. H.; Southon, A. G.; Fraser, B. H.; Krause-Heuer, A. M.; Zhang, B.; Shoup, T. M.; Lewis, R.; Volitakis, I.; Han, Y.; Greguric, I.; Bush, A. I.; Vasdev, N., Novel Fluorinated 8-Hydroxyquinoline Based Metal Ionophores for Exploring the Metal Hypothesis of Alzheimer's Disease. *ACS Med Chem Lett* **2015,** *6* (9), 1025-9.

14. Schertzer, B. M.; Baker, S. N.; Diver, S. T.; Baker, G. A., A general, modular approach to a new family of amine-substituted arylboronic acid saccharide chemosensors. *Aust J Chem* **2006,** *59* (9), 633-639.

15. Kwit, M.; Gawronski, J., A circular dichroism detection of stereostructural change due to amine protonation. *Tetrahedron Lett* **2003,** *44* (45), 8311-8314.

16. Schonleber, M.; Hilgraf, R.; Pfaltz, A., Chiral Bis(N-arylamino)phosphine-oxazolines: Synthesis and application in asymmetric catalysis. *Adv Synth Catal* **2008,** *350* (13), 2033-2038.

17. Forkosh, H.; Vershinin, V.; Reiss, H.; Pappo, D., Stereoselective Synthesis of Optically Pure 2-Amino-2'-hydroxy-1,1'-binaphthyls. *Org Lett* **2018,** *20* (8), 2459-2463.

18. Al-Busafi, S. N.; Suliman, F. E. O.; Al-Alawi, Z. R., Synthesis, characterization and electronic effects investigations of new 5,7-disubstituted tris(8-quinolinolate)Al(III) complexes. *Dyes Pigments* **2014,** *103*, 138-144.

19. Kappaun, S.; Rentenberger, S.; Pogantsch, A.; Zojer, E.; Mereiter, K.; Trimmel, G.; Saf, R.; Moller, K. C.; Stelzer, F.; Slugovc, C., Organoboron quinolinolates with extended conjugated chromophores: Synthesis, structure, and electronic and electroluminescent properties. *Chem Mater* **2006,** *18* (15), 3539-3547.

20. Sarmah, B. K.; Konwar, M.; Bhattacharyya, D.; Adhikari, P.; Das, A., Regioselective Cyanation of Six-Membered N-Heteroaromatic Compounds Under Metal-, Activator-, Base- and Solvent-Free Conditions. *Adv Synth Catal* **2019,** *361* (24), 5616-5625.

21. Xu, F.; Li, Y.; Huang, X.; Fang, X.; Li, Z.; Jiang, H.; Qiao, J.; Chu, W.; Sun, Z., Hypervalent Iodine(III)-Mediated Regioselective Cyanation of Quinoline N-Oxides with Trimethylsilyl Cyanide. *Adv Synth Catal* **2018,** *361* (3), 520-525.

22. Pearson, D. E.; Wysong, R. D.; Breder, C. V., Ortho bromination of phenols. *Journal of Organic Chemistry* **1967,** *32* (7), 2358-2360.

Chapter 5: Appendix

5.1. Appendix of Chapter 2

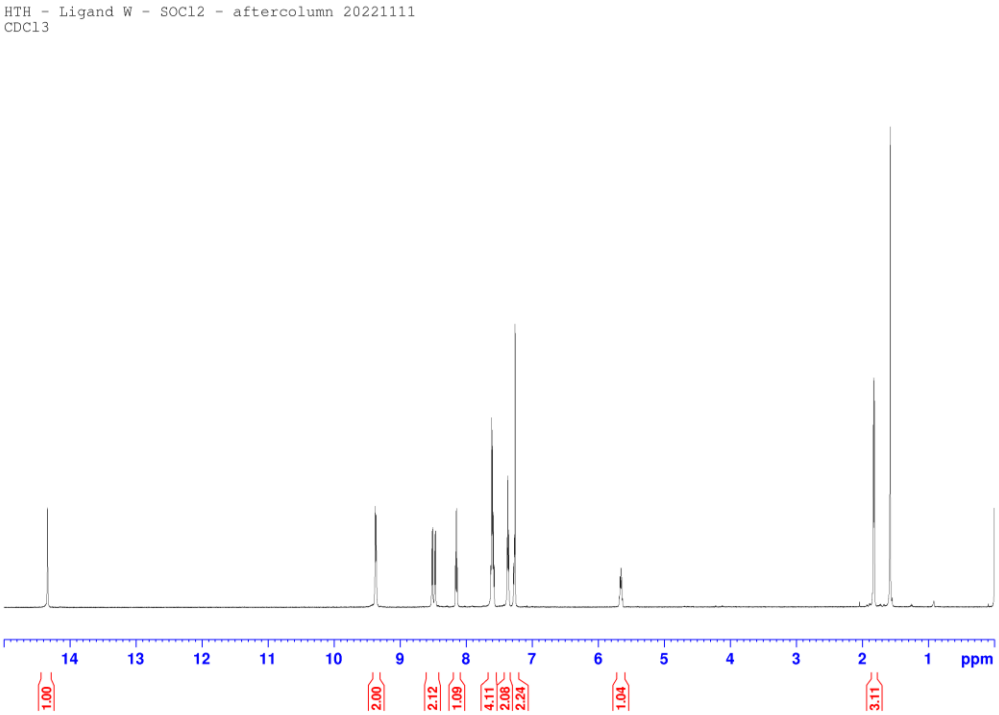

Spectrum S2-37: ^{1}H NMR spectrum of ligand **1b**

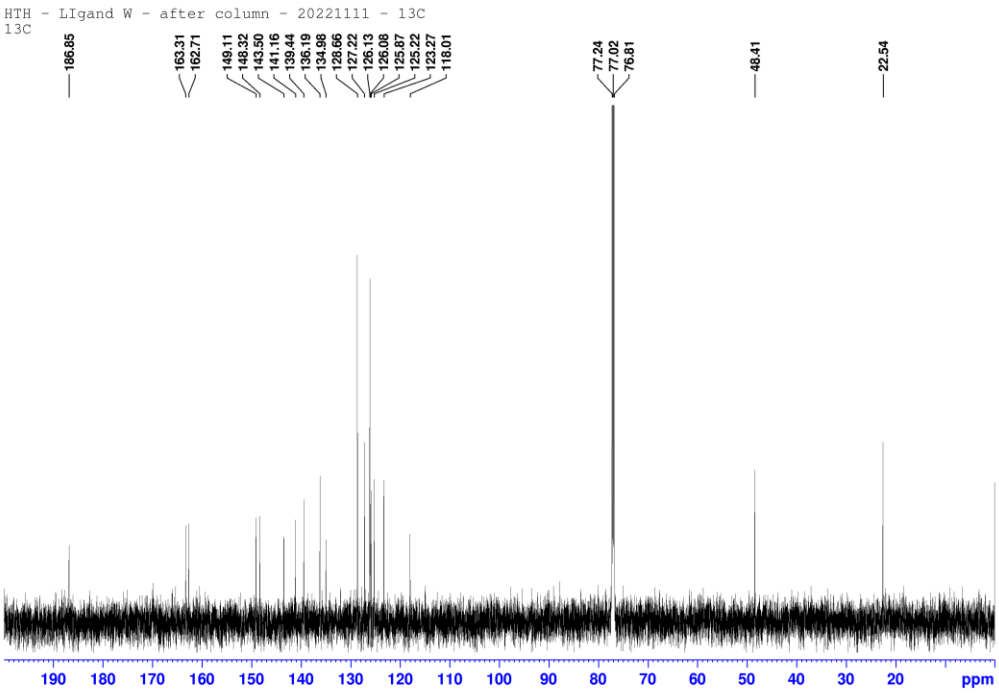

Spectrum S2-38: ^{13}C NMR spectrum of ligand **1b**

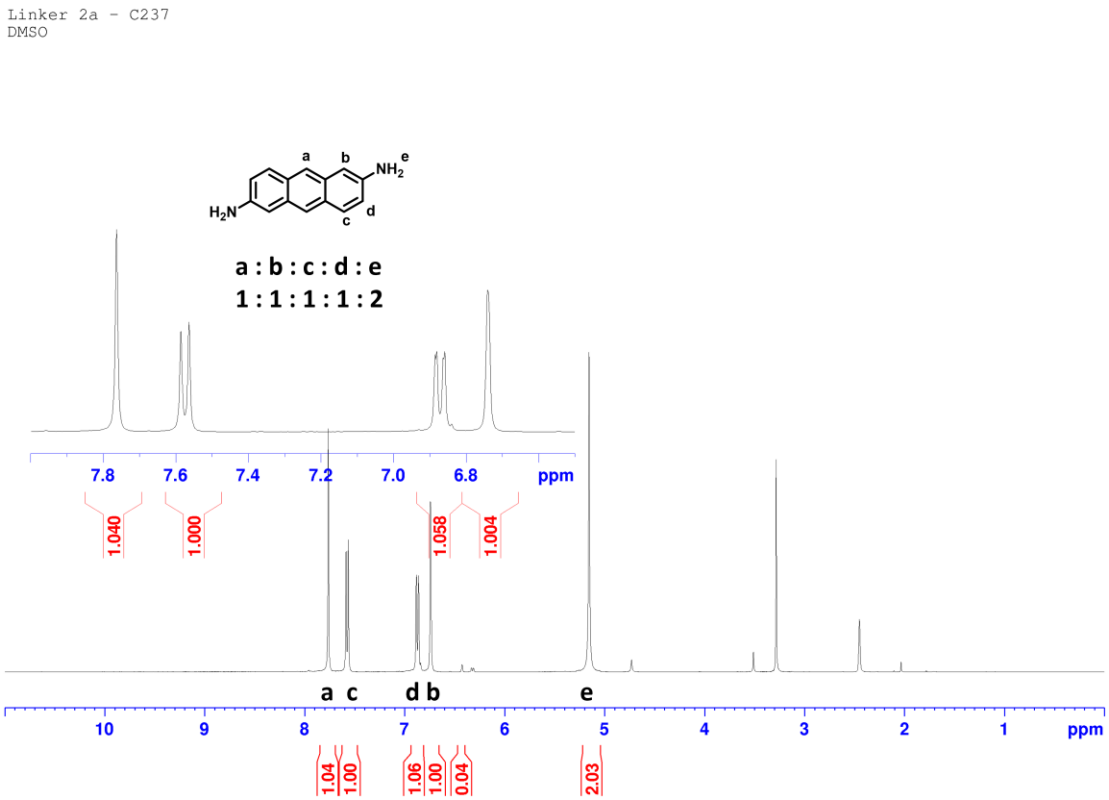

Spectrum S2-39: ^{1}H NMR spectrum of Linker **2a**

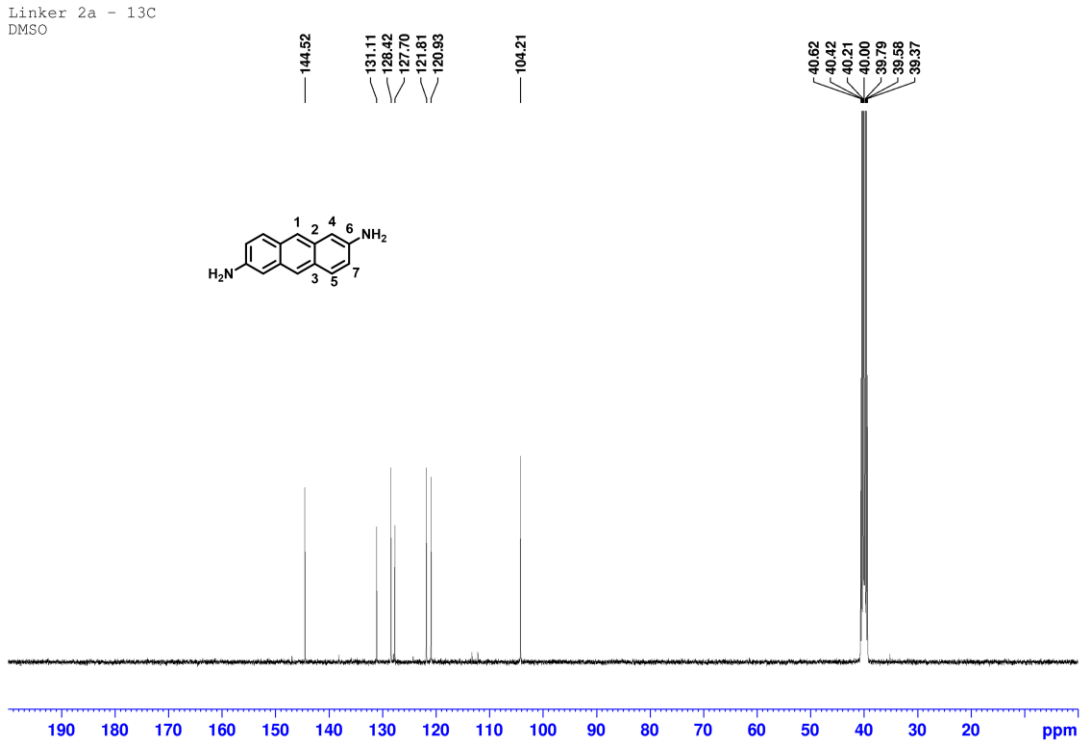

Spectrum S2-40: ^{13}C NMR spectrum of Linker **2a**

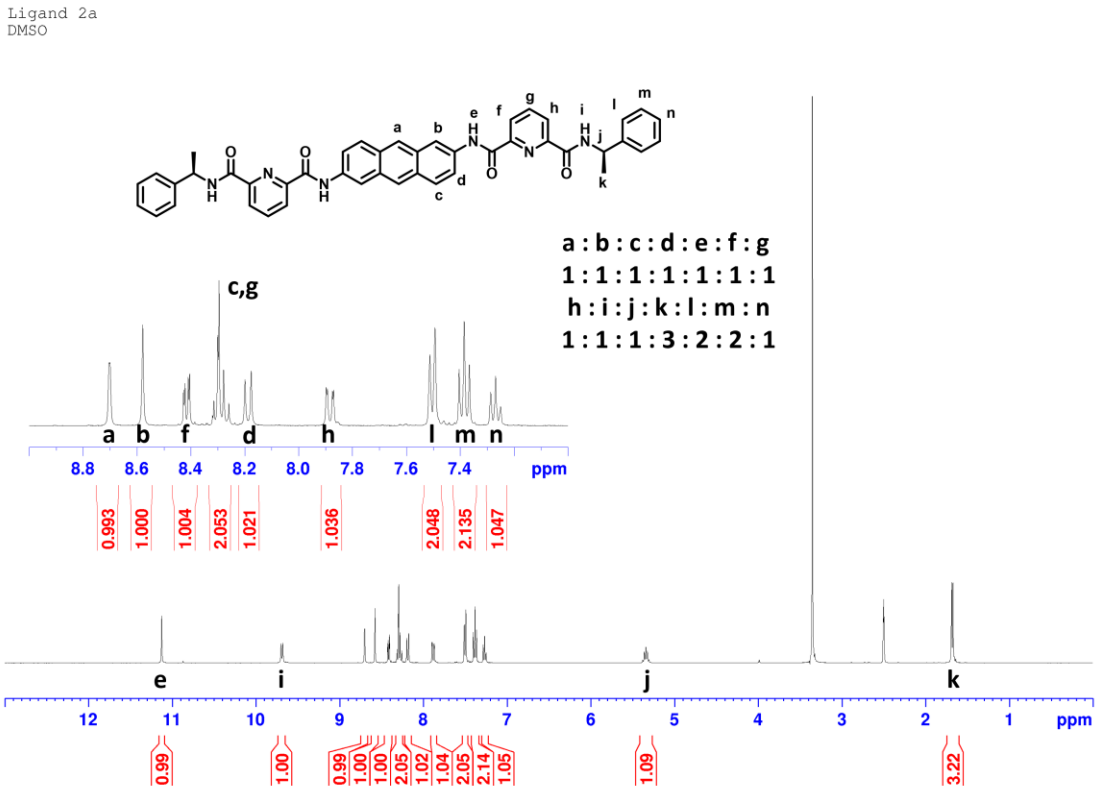

Spectrum S2-41: ^{1}H NMR spectrum of Ligand $\mathbf{L_{2a}}$

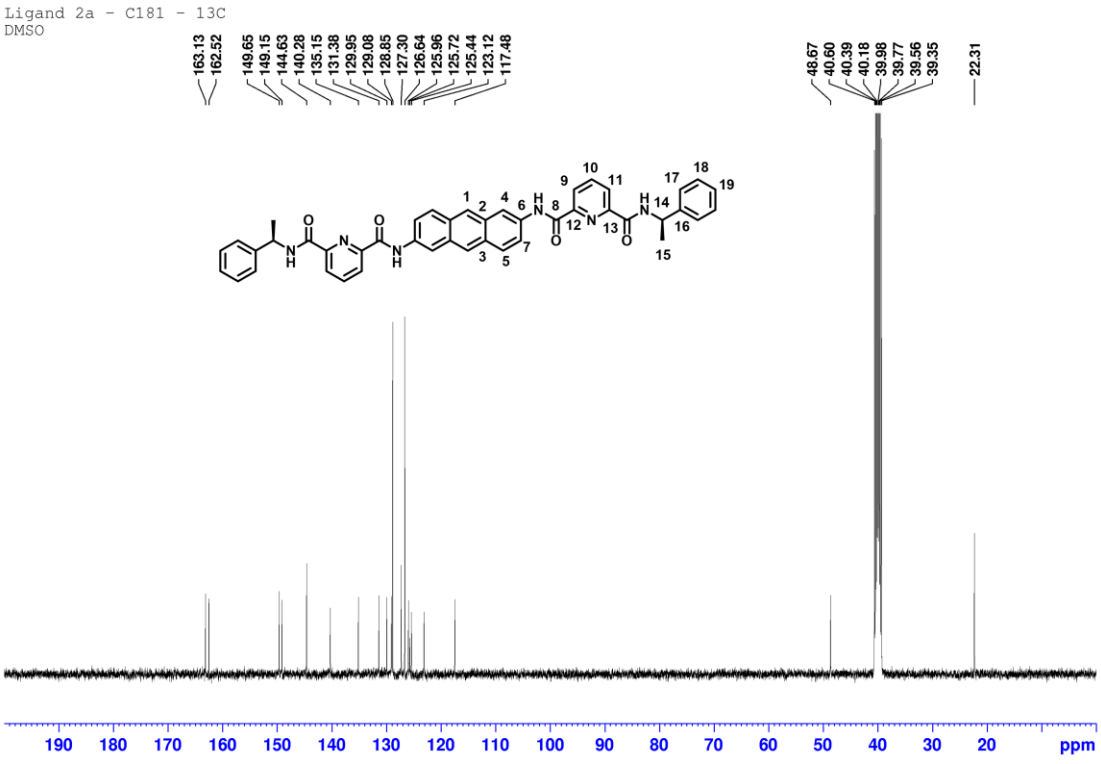

Spectrum S2-42: ^{13}C NMR spectrum of Ligand L_{2a}

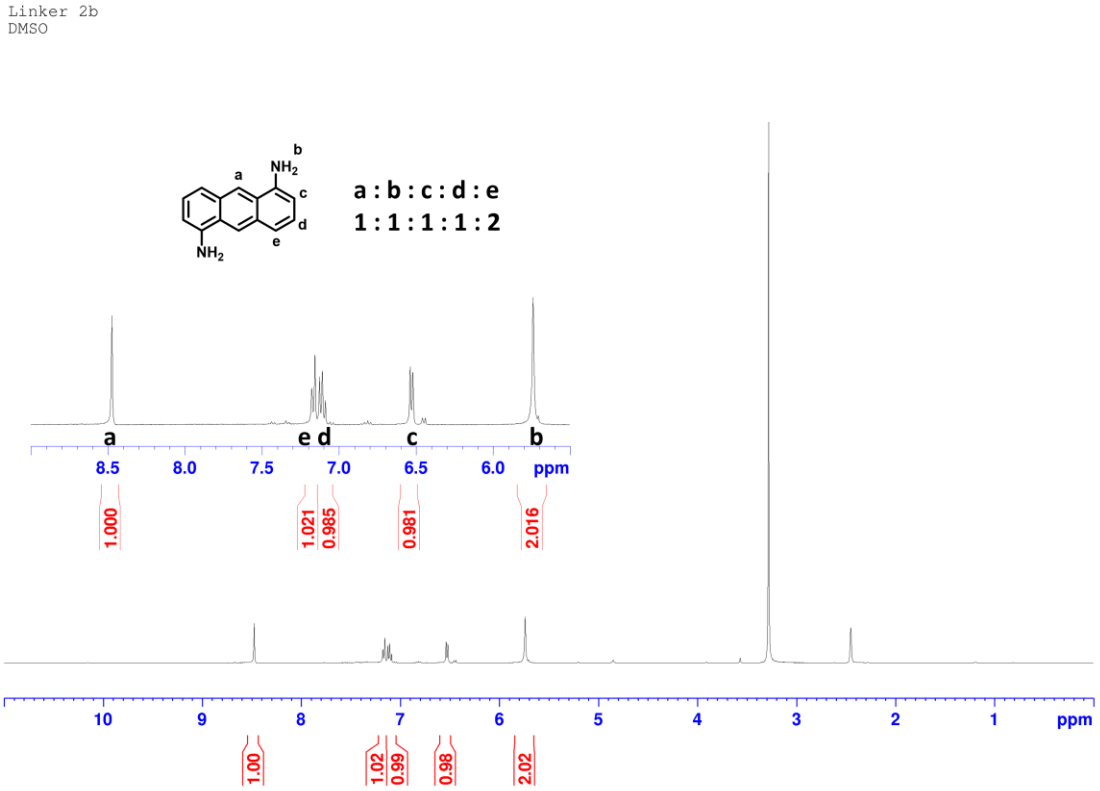

Spectrum S2-43: ^{1}H NMR spectrum of Linker **2b**

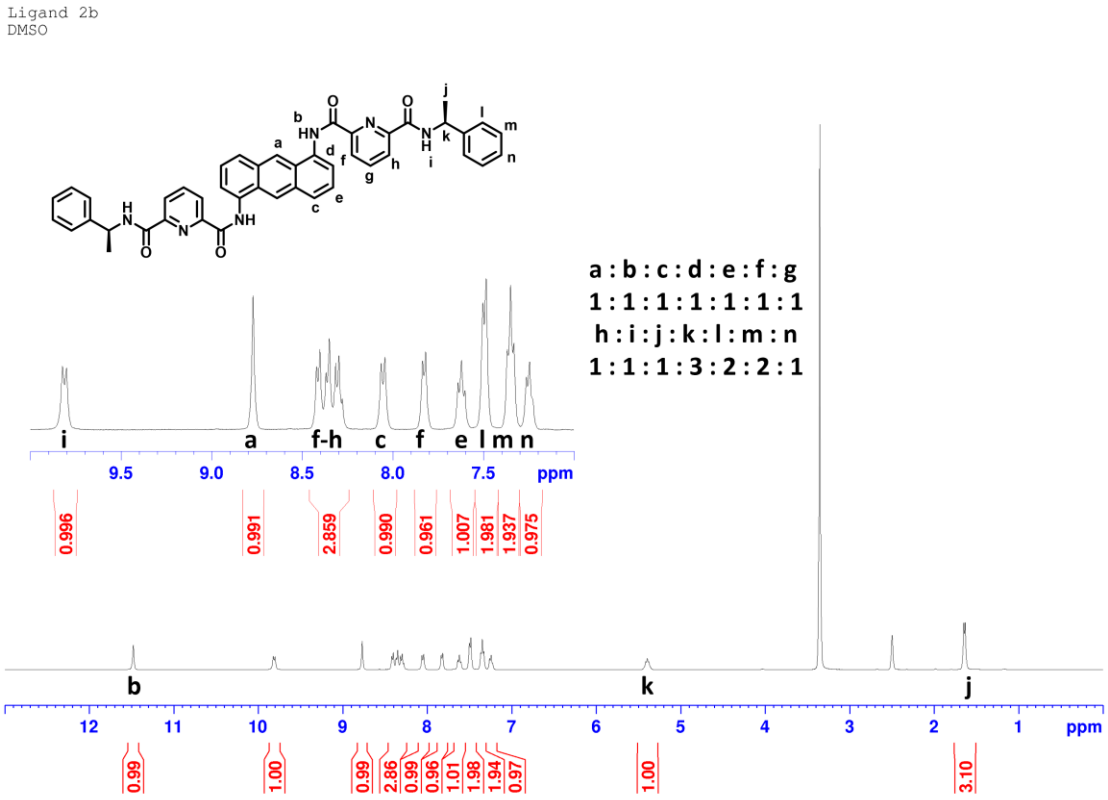

Spectrum S2-44: ^{1}H NMR spectrum of Ligand $\mathbf{L_{2b}}$

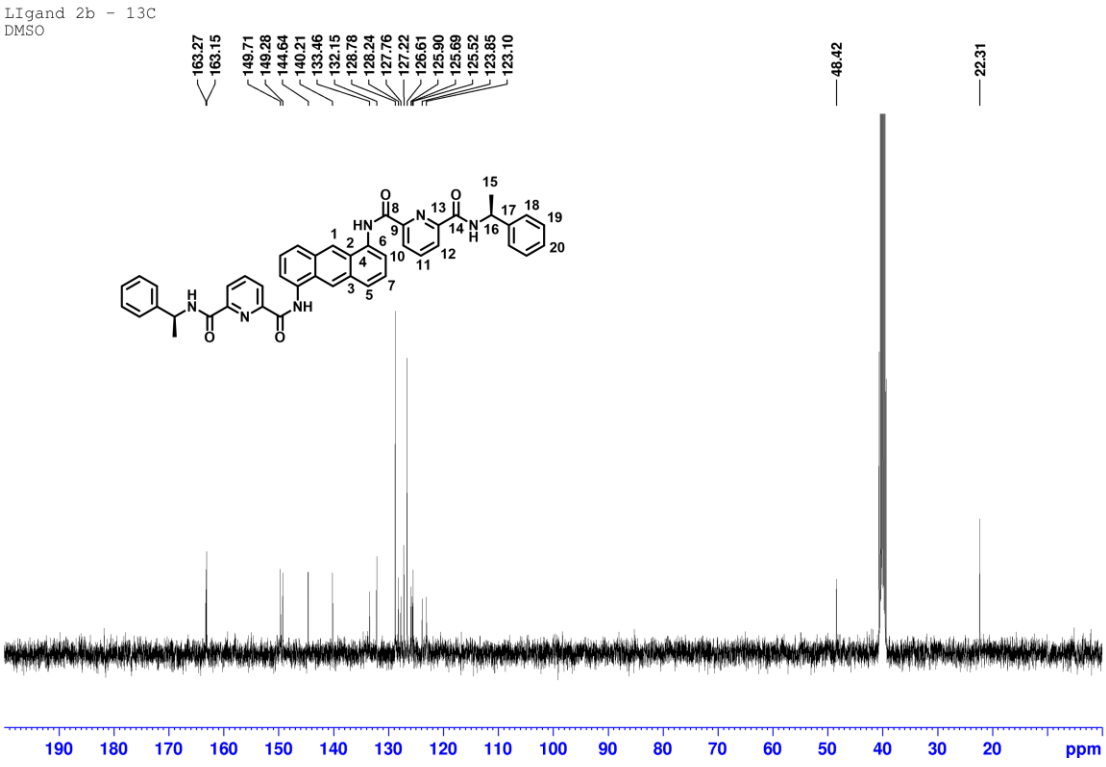

Spectrum S2-45: ^{13}C NMR spectrum of Ligand $\mathbf{L_{2b}}$

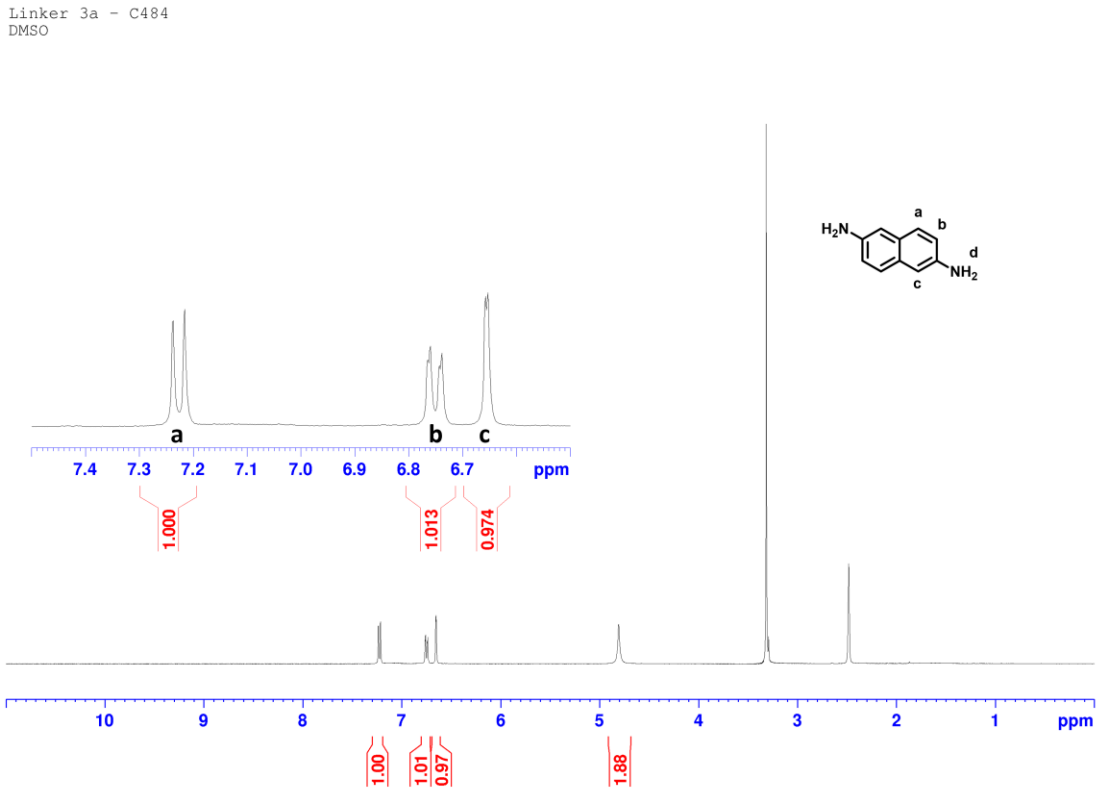

Spectrum S2-46: ^{1}H NMR spectrum of Linker **3a**

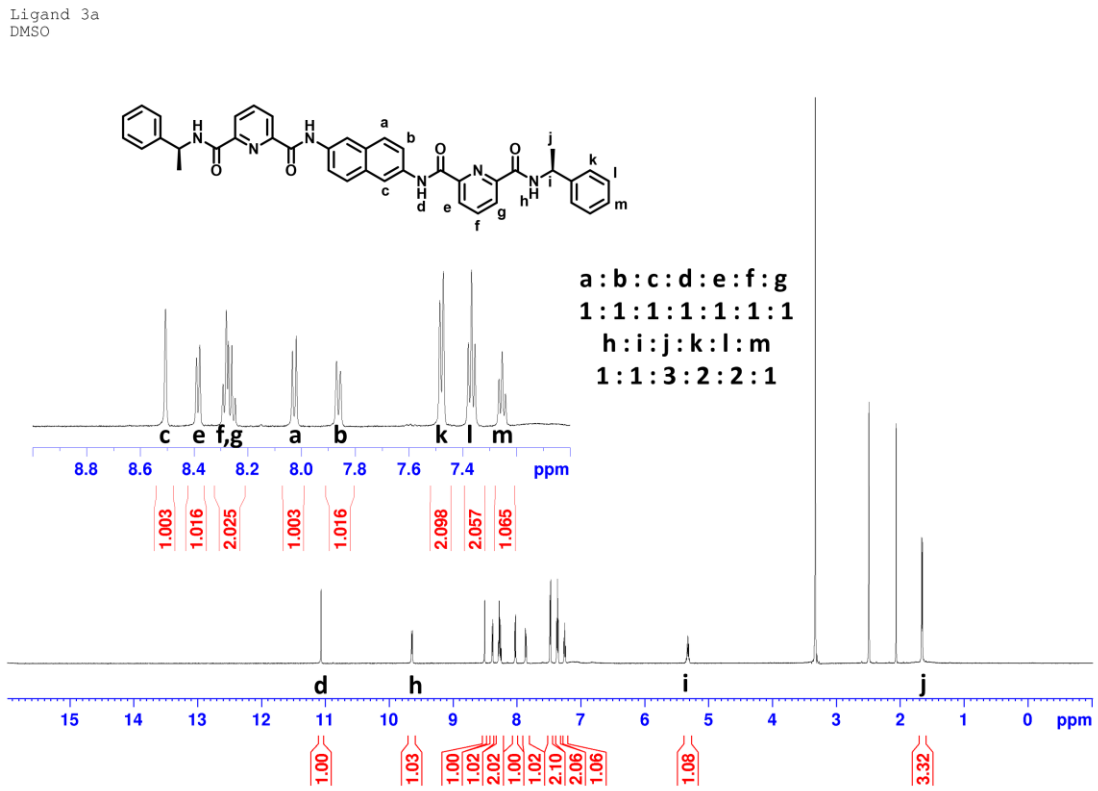

Spectrum S2-47: ^{1}H NMR spectrum of Ligand $\mathbf{L_{3a}}$

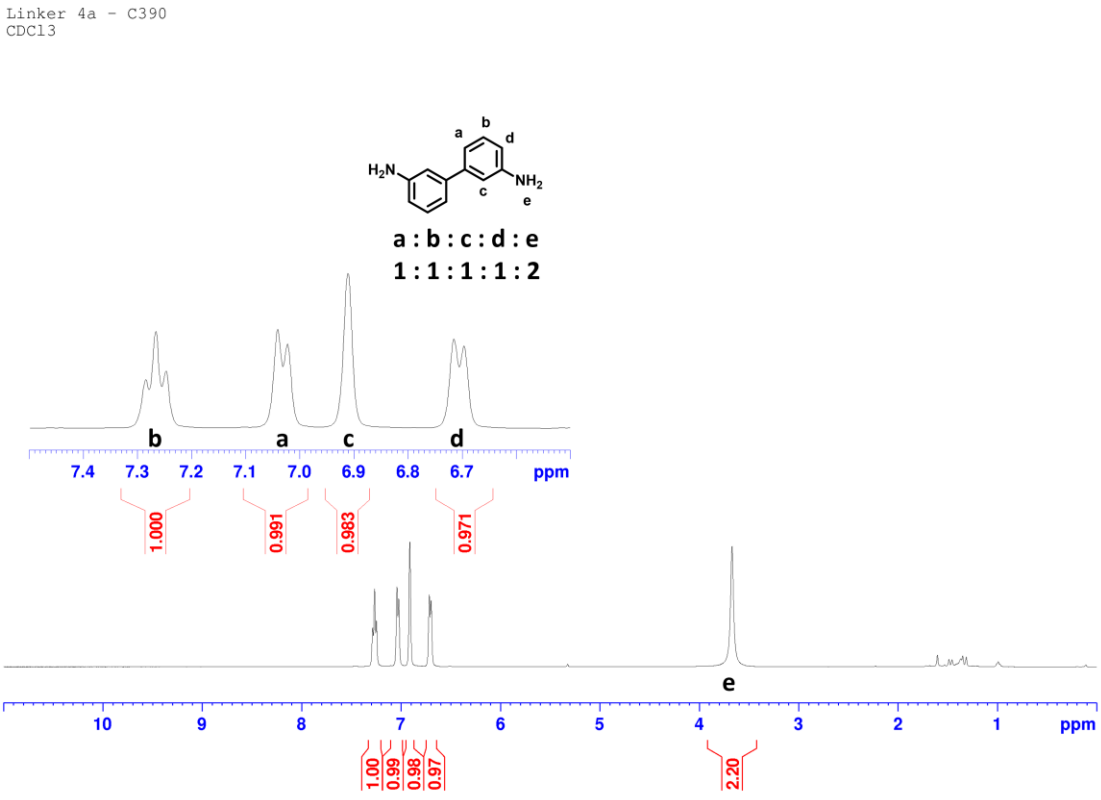

Spectrum S2-48: ^{1}H NMR spectrum of Linker **4b**

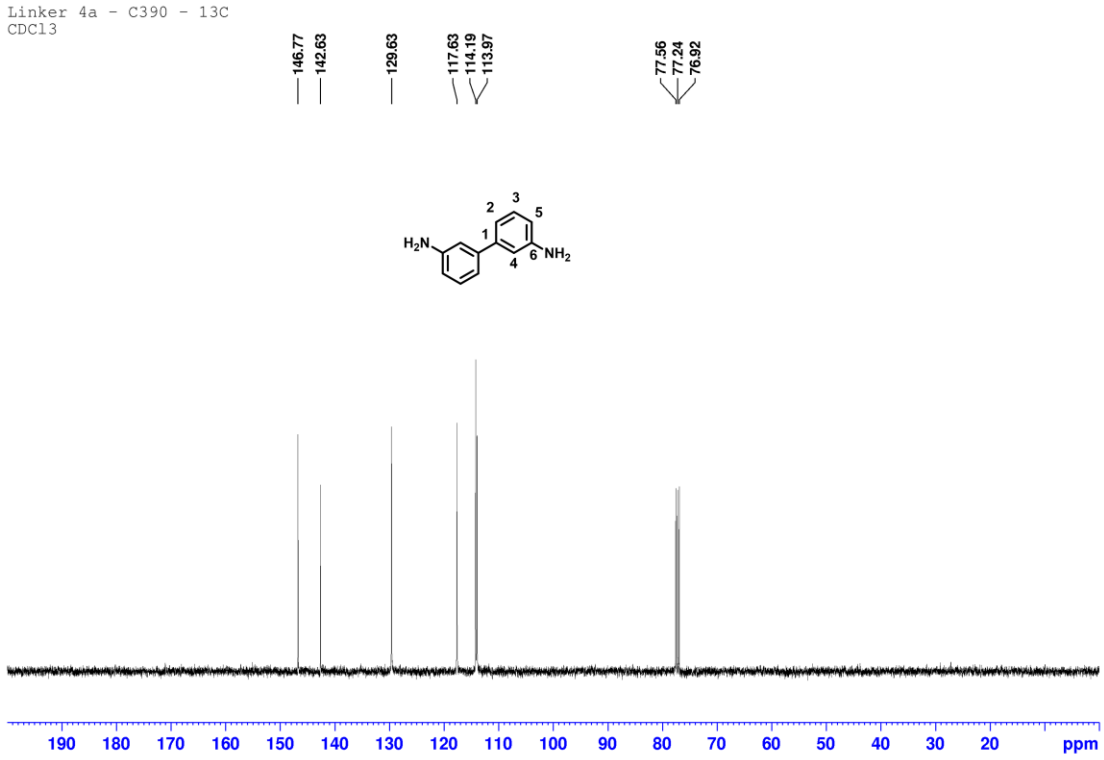

Spectrum S2-49: ^{13}C NMR spectrum of Linker **4b**

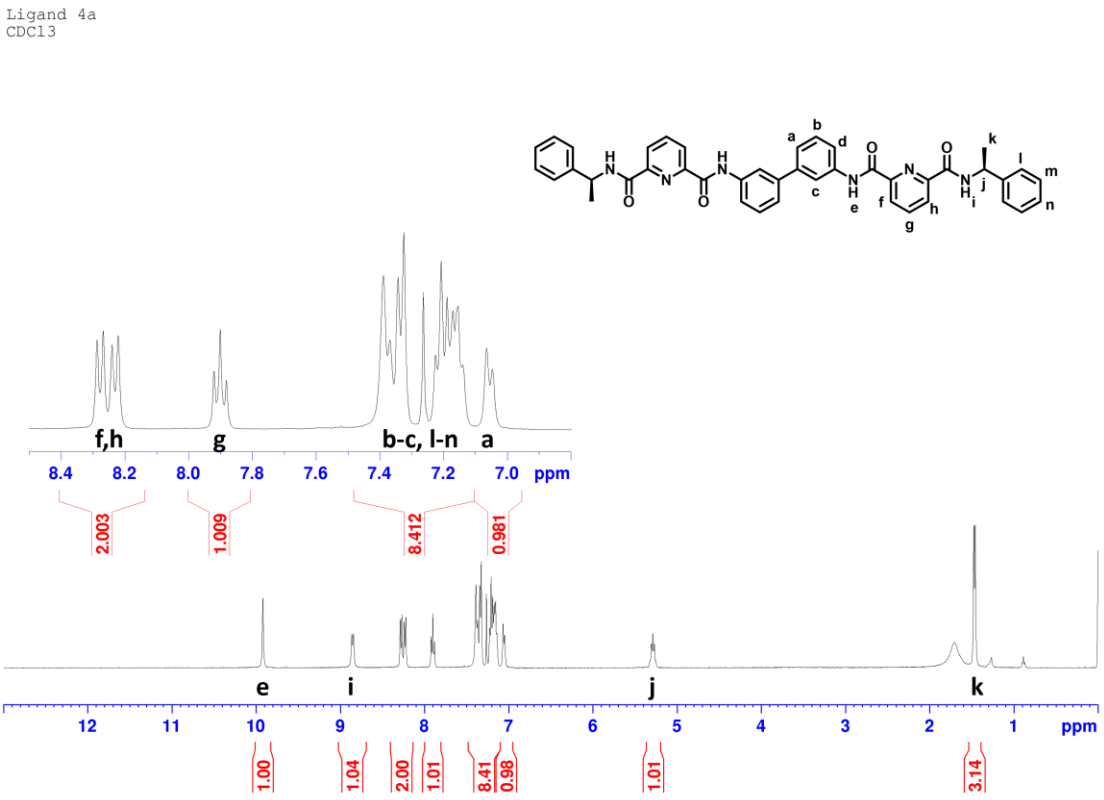

Spectrum S2-50: ^{1}H NMR spectrum of Ligand $\mathbf{L_{4b}}$

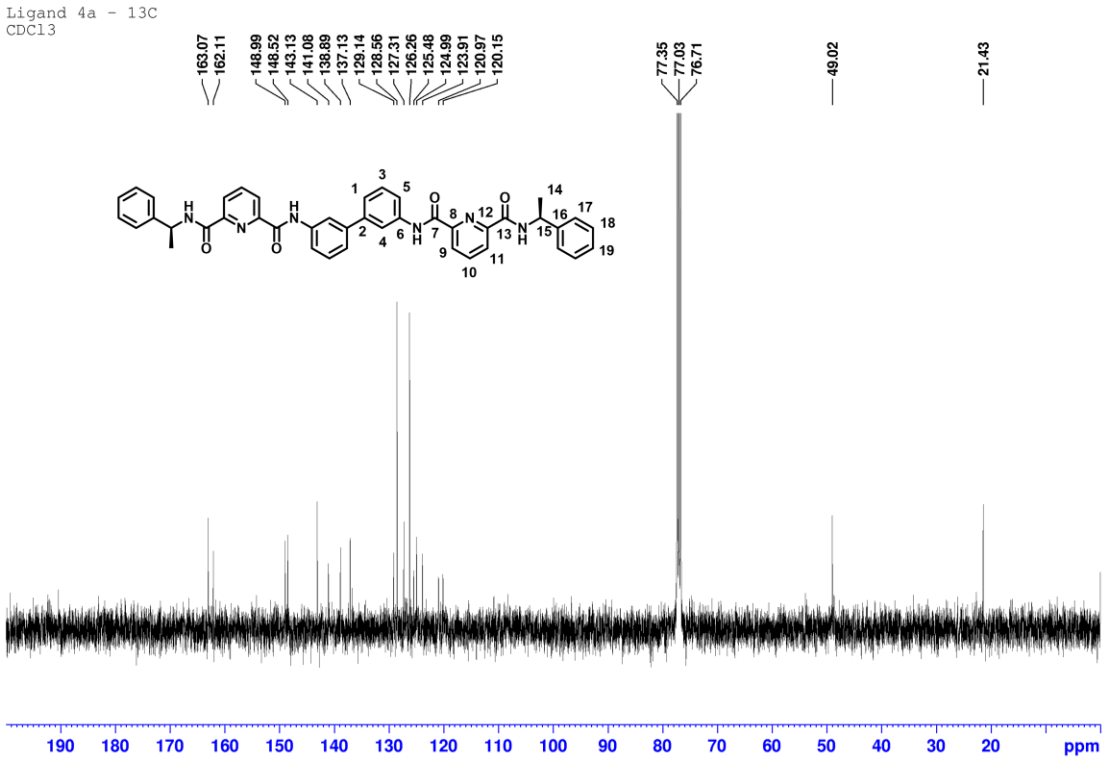

Spectrum S2-51: ^{13}C NMR spectrum of Ligand $\mathbf{L_{4b}}$

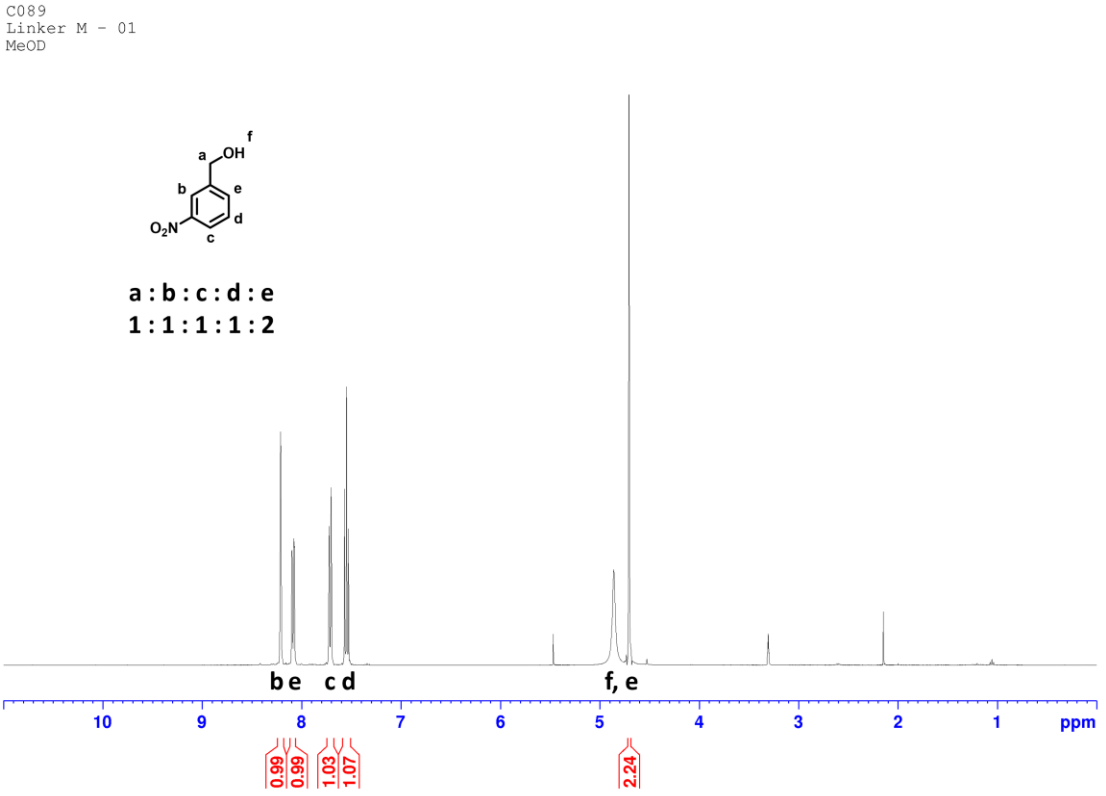

Spectrum S2-52: ^{1}H NMR spectrum of Linker **5a-1**

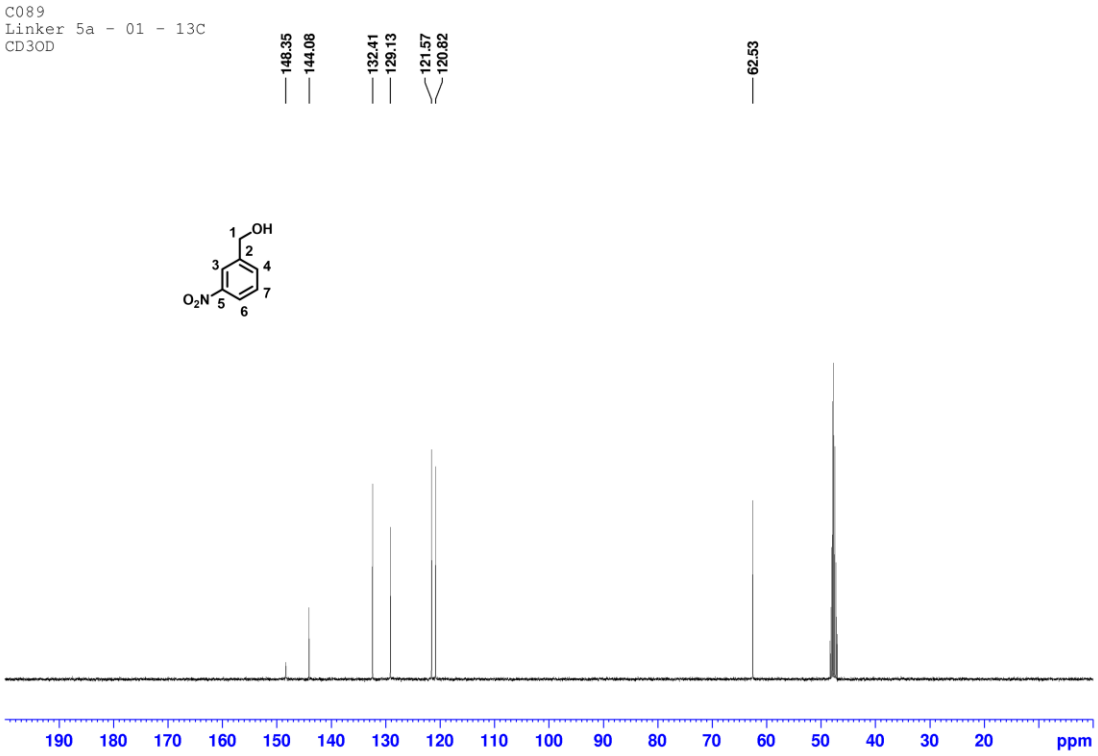

Spectrum S2-53: ^{13}C NMR spectrum of Linker **5a-1**

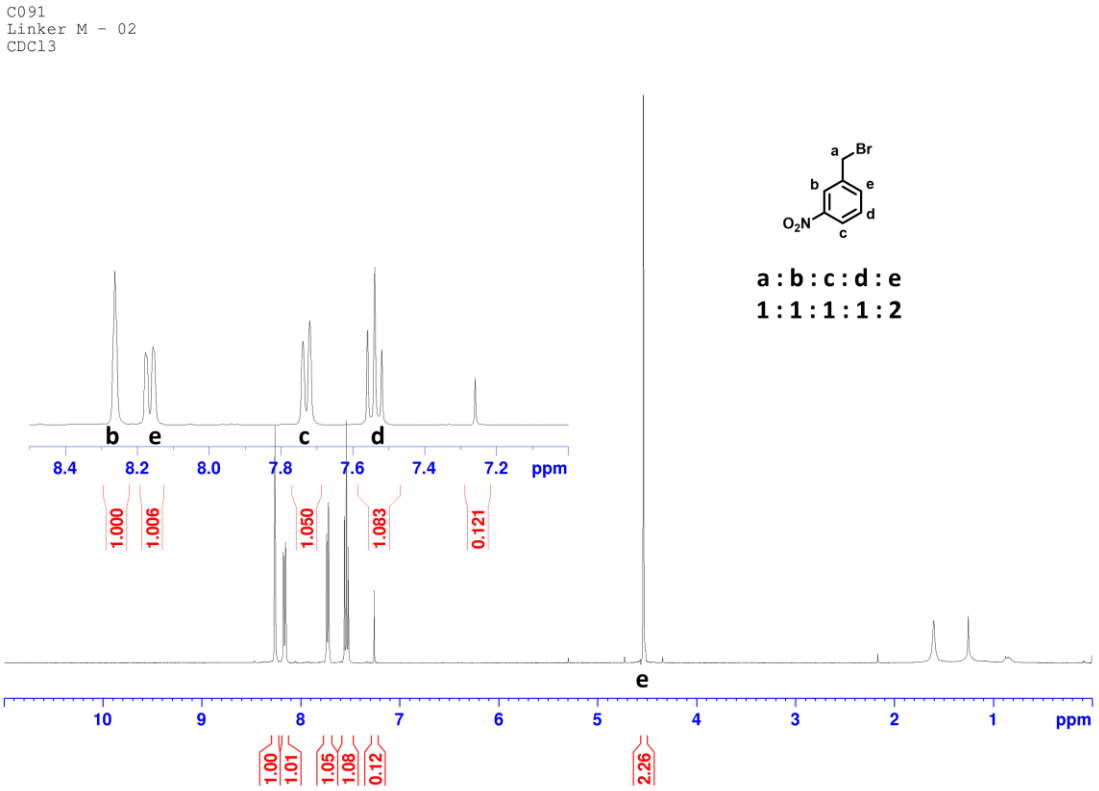

Spectrum S2-54: ^{1}H NMR spectrum of Linker **5a-2**

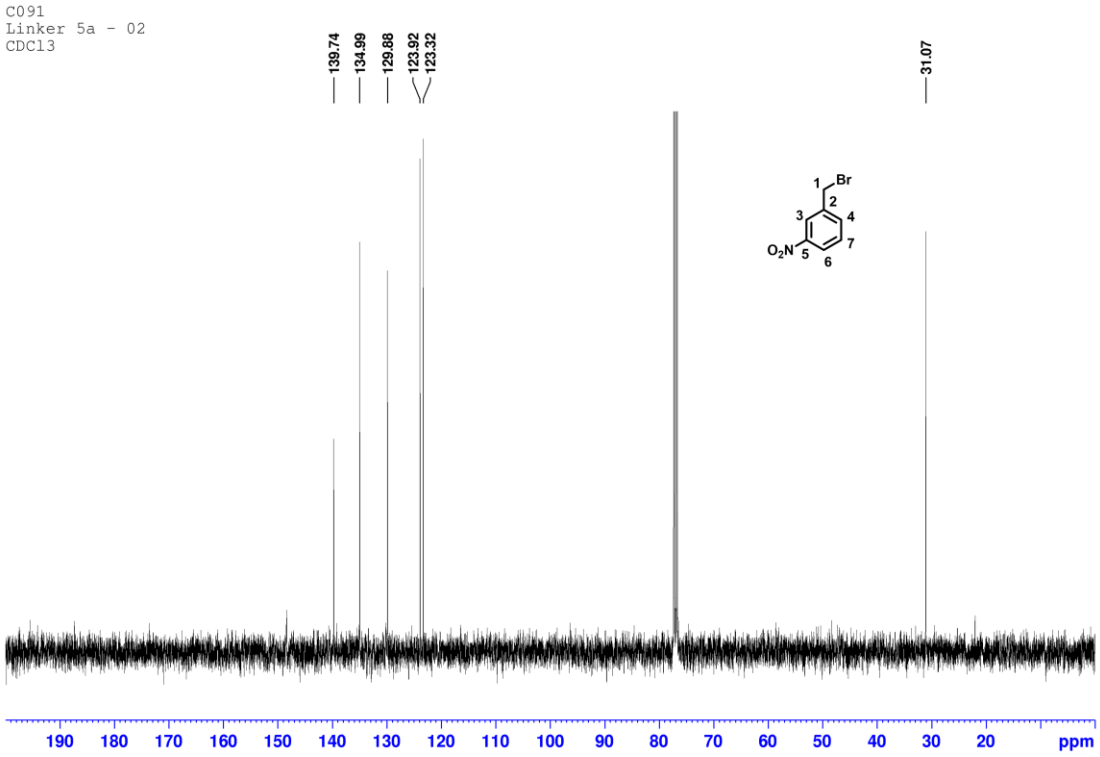

Spectrum S2-55: ^{13}C NMR spectrum of Linker **5a-2**

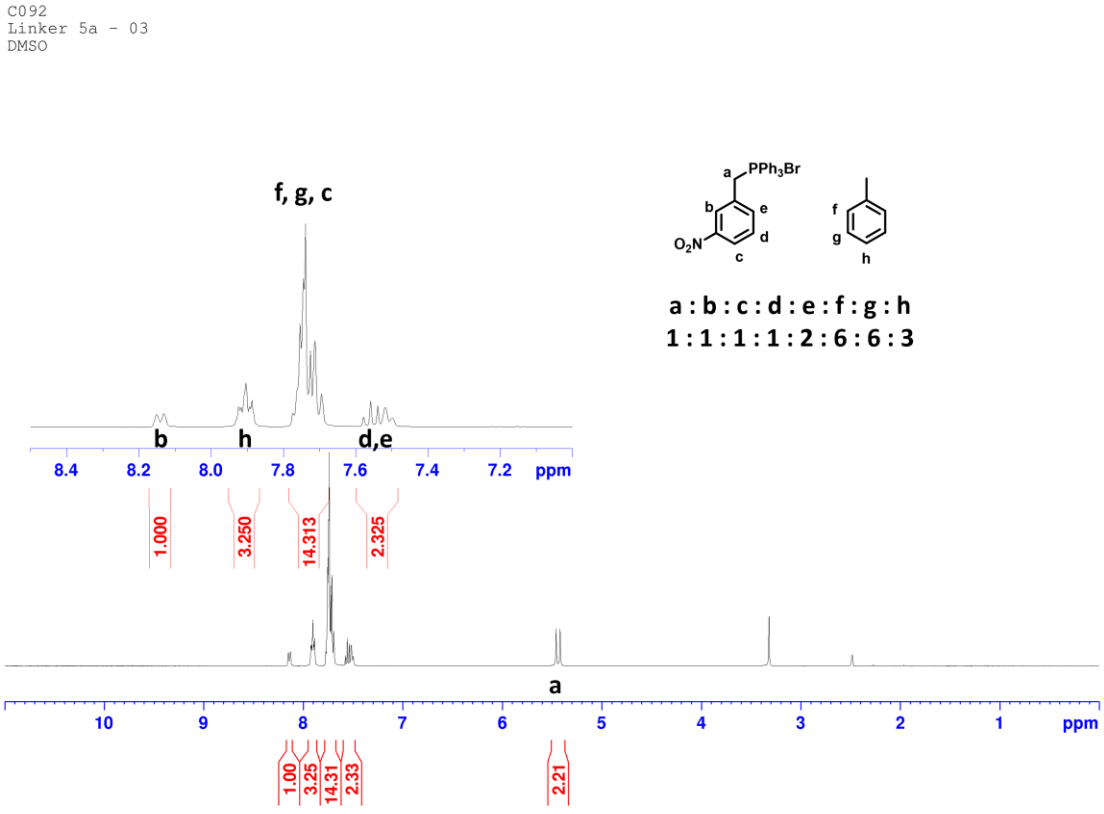

Spectrum S2-56: ^{1}H NMR spectrum of Linker **5a-3**

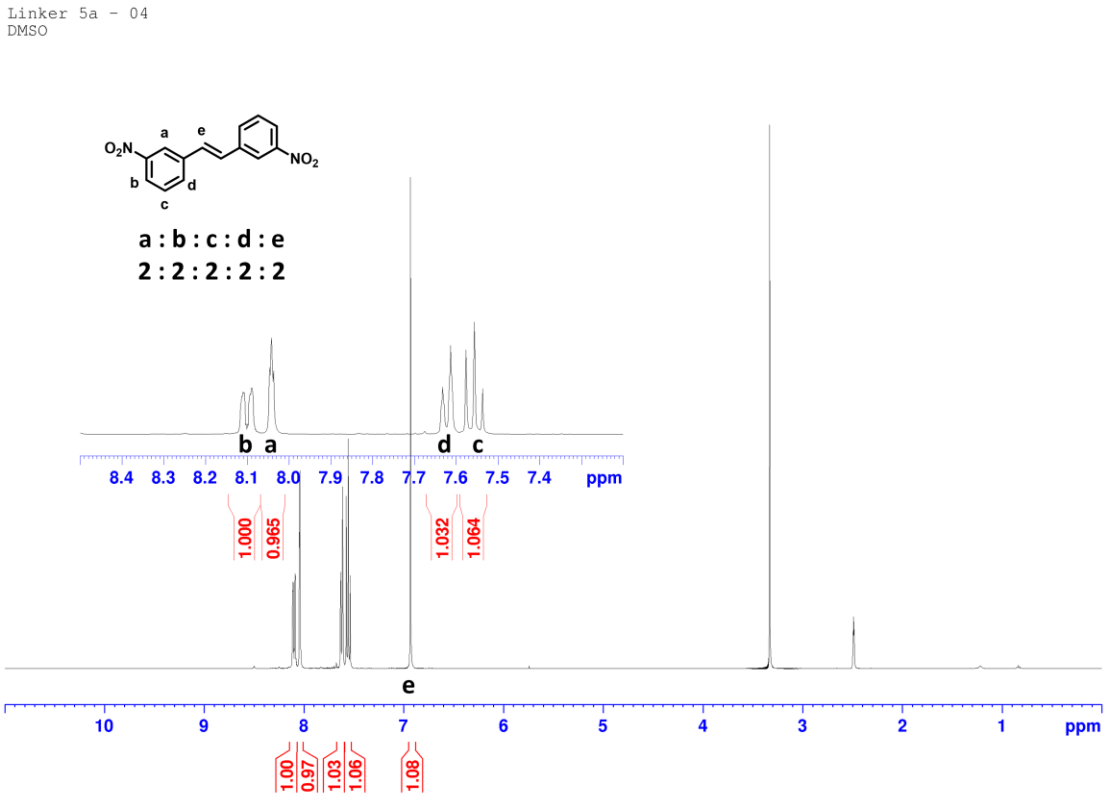

Spectrum S2-57: ^{1}H NMR spectrum of Linker **5a-4**

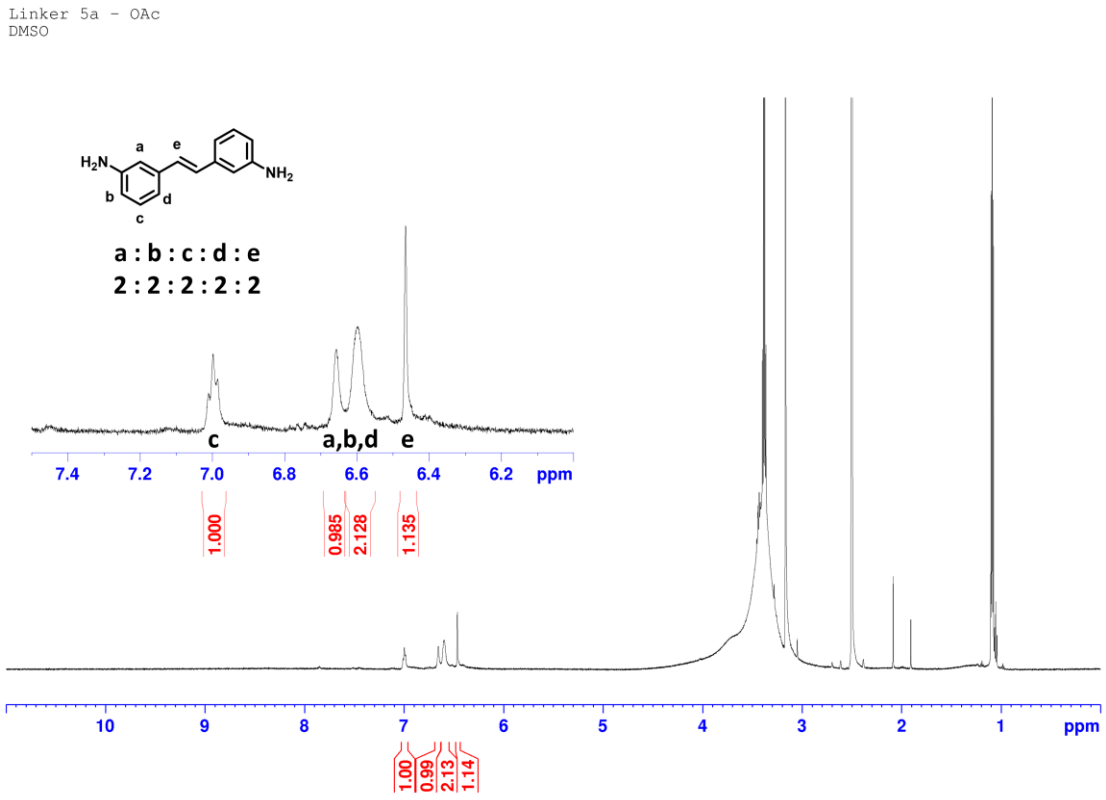

Spectrum S2-58: ^{1}H NMR spectrum of Linker **5a**

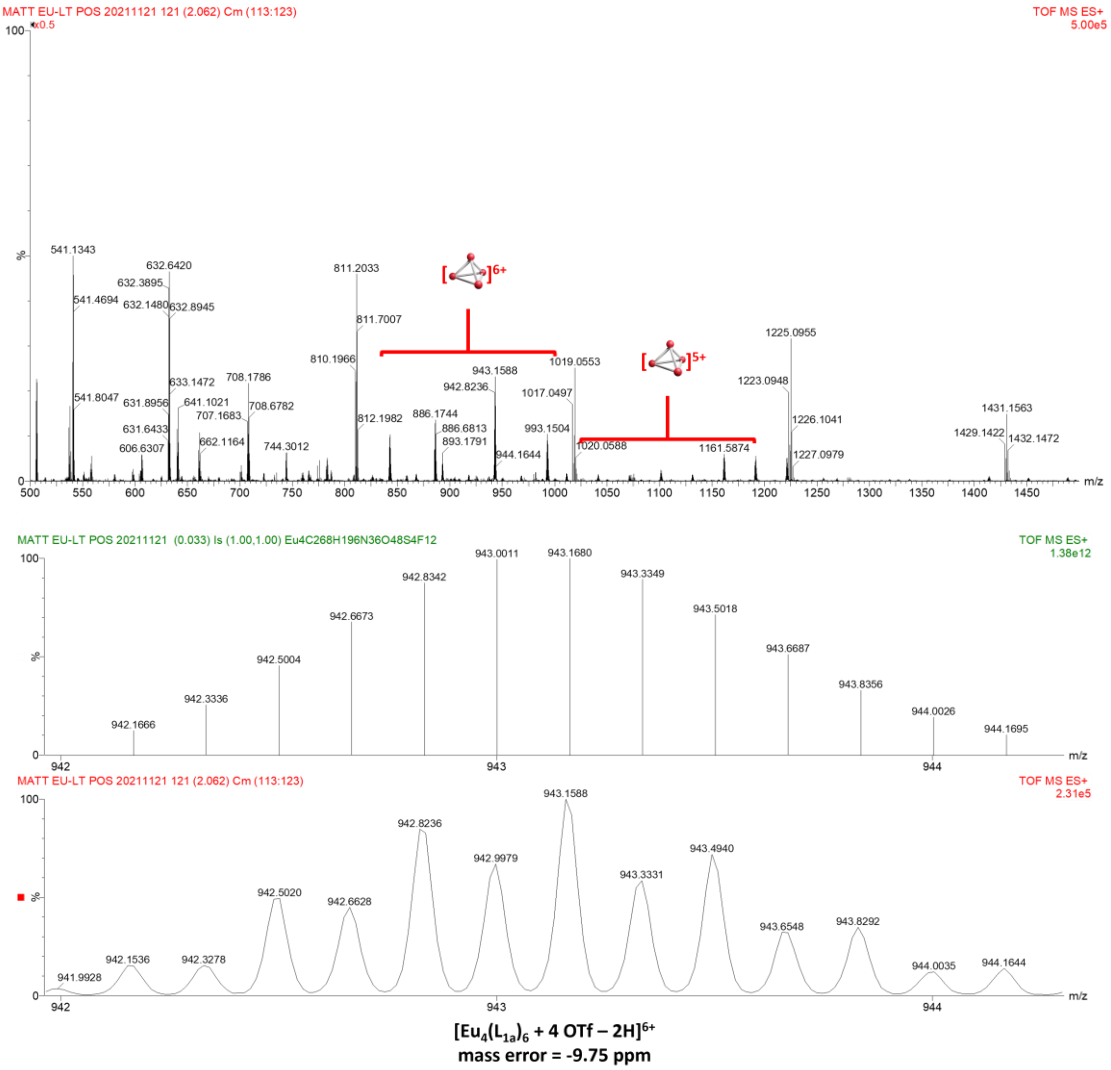

$[Eu_4(L_{1a})_6 + 4\ OTf - 2H]^{6+}$
mass error = -9.75 ppm

Spectrum S2-59: (top) ESI-HRMS spectrum of Complex **EuL_{1a}** & (bot) isotopic distribution of selected species

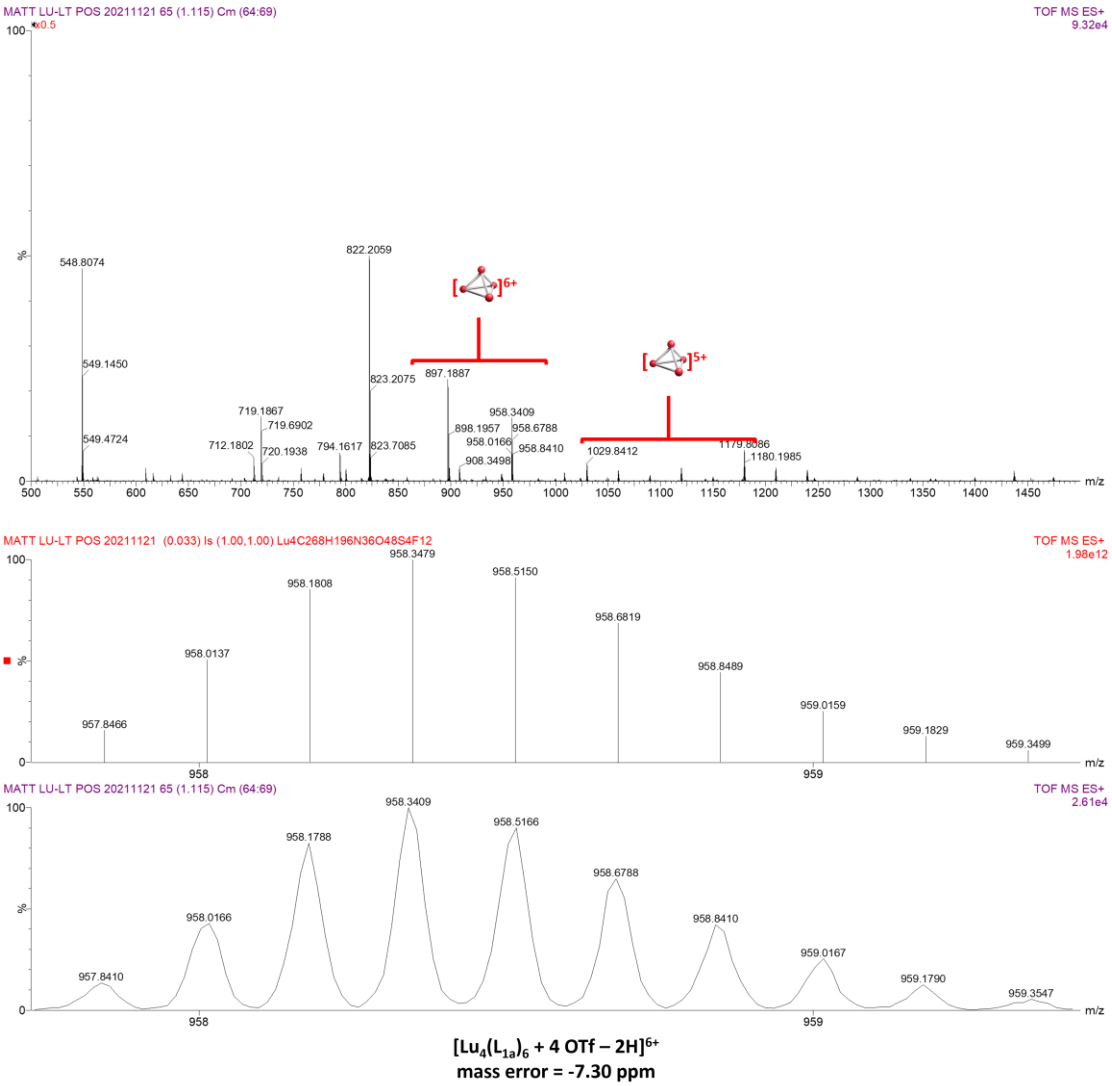

$[Lu_4(L_{1a})_6 + 4\ OTf - 2H]^{6+}$
mass error = -7.30 ppm

Spectrum S2-60: (top) ESI-HRMS spectrum of Complex **LuL_{1a}** & (bot) isotopic distribution of selected species

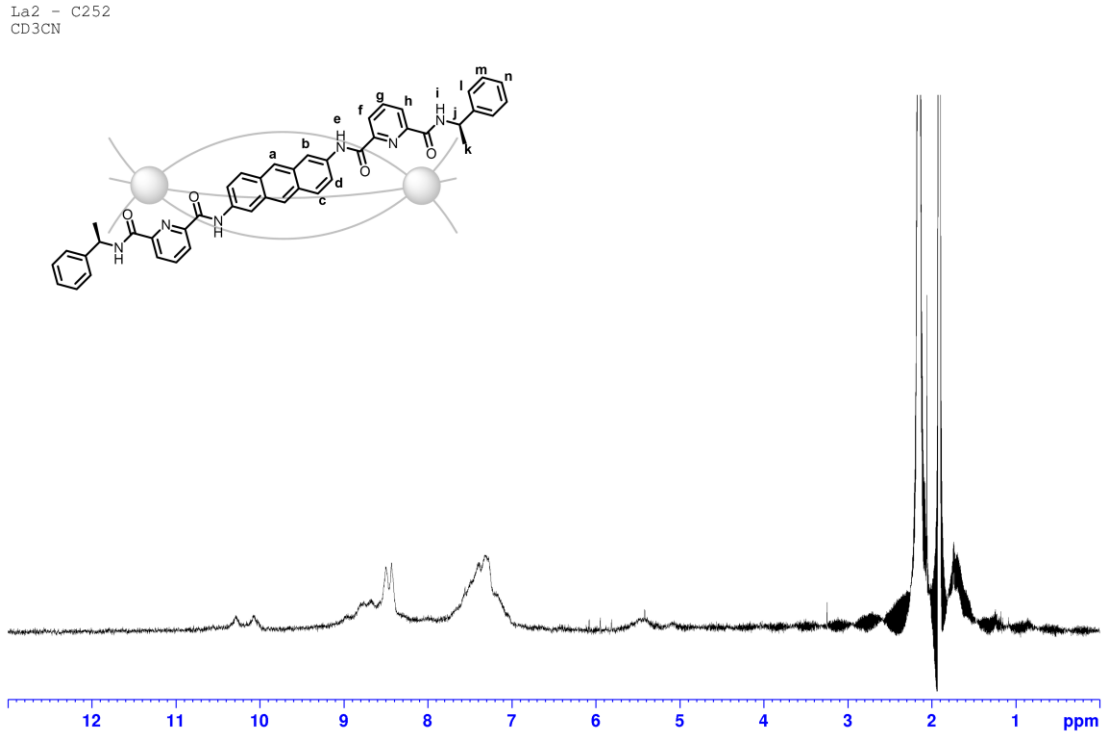

Spectrum S2-61: ^{1}H NMR spectrum of Complex $\mathbf{LaL_{2a}}$

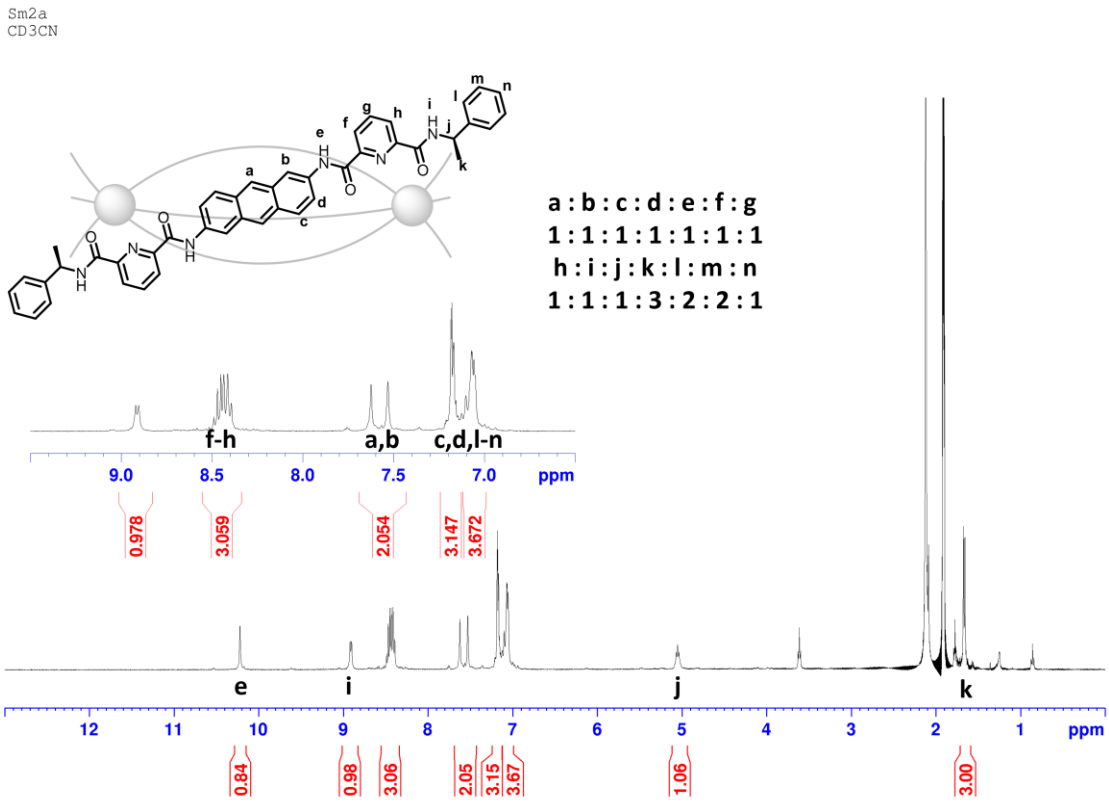

Spectrum S2-62: ^{1}H NMR spectrum of Complex $\mathbf{SmL_{2a}}$

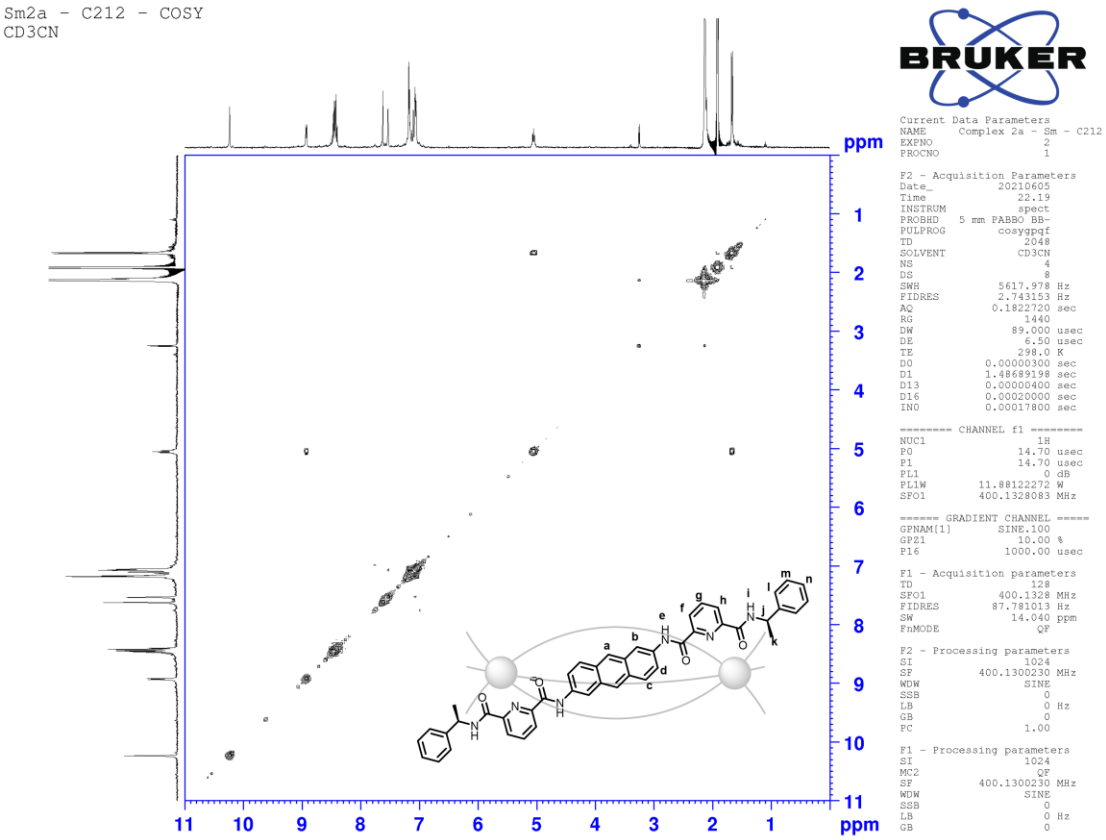

Spectrum S2-63: ^{1}H-^{1}H COSY NMR spectrum of Complex **SmL$_{2a}$**

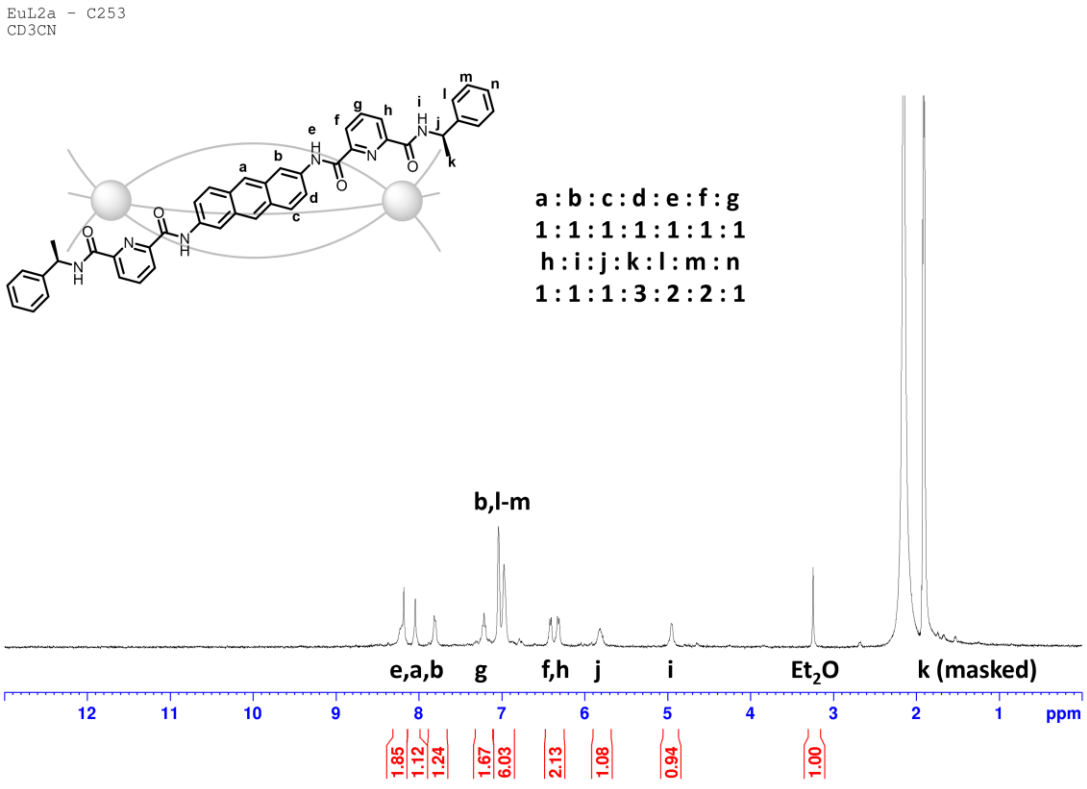

Spectrum S2-64: ^{1}H NMR spectrum of Complex **EuL$_{2a}$**

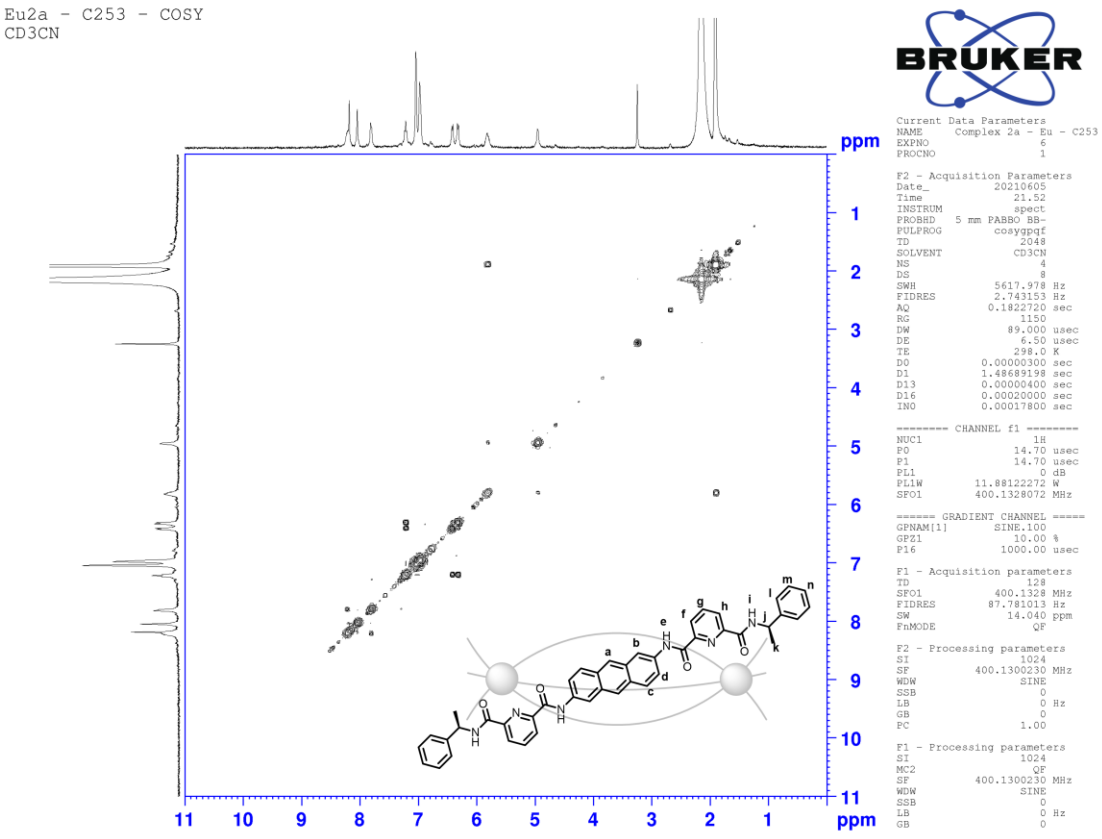

Spectrum S2-65: ^{1}H-^{1}H COSY NMR spectrum of Complex **EuL$_{2a}$**

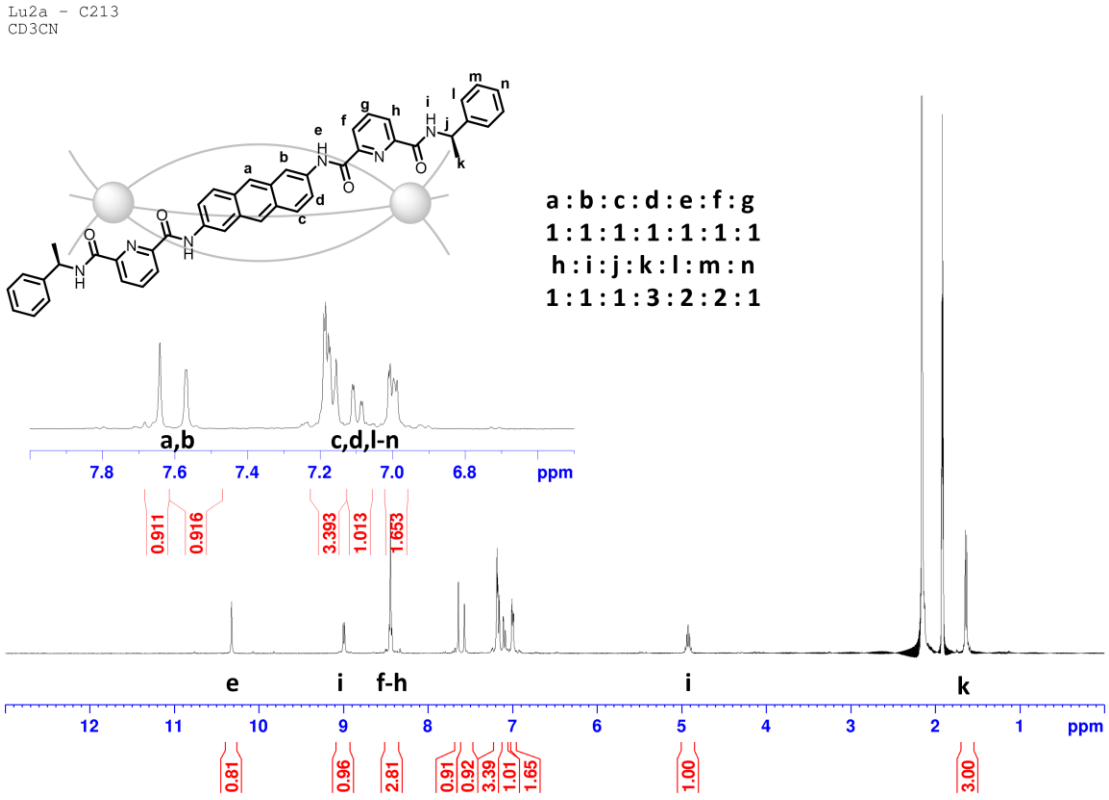

Spectrum S2-66: ^{1}H NMR spectrum of Complex **LuL$_{2a}$**

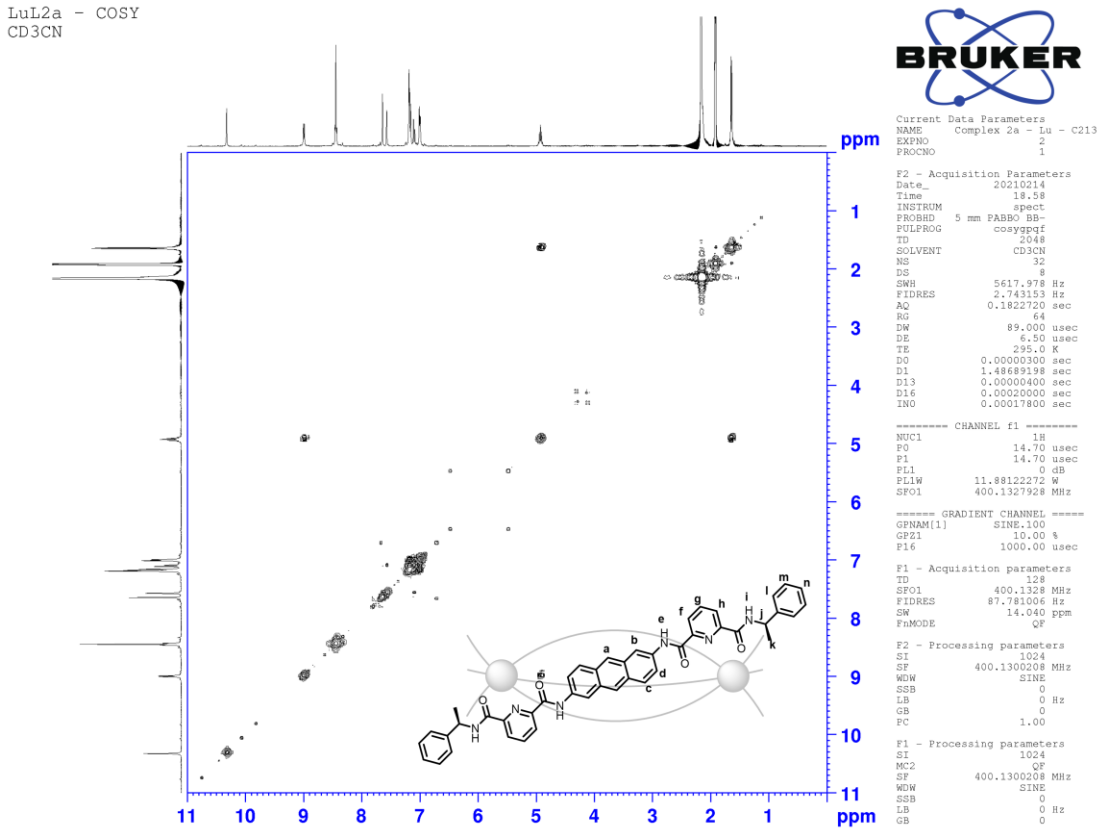

Spectrum S2-67: ^{1}H-^{1}H COSY NMR spectrum of Complex **LuL$_{2a}$**

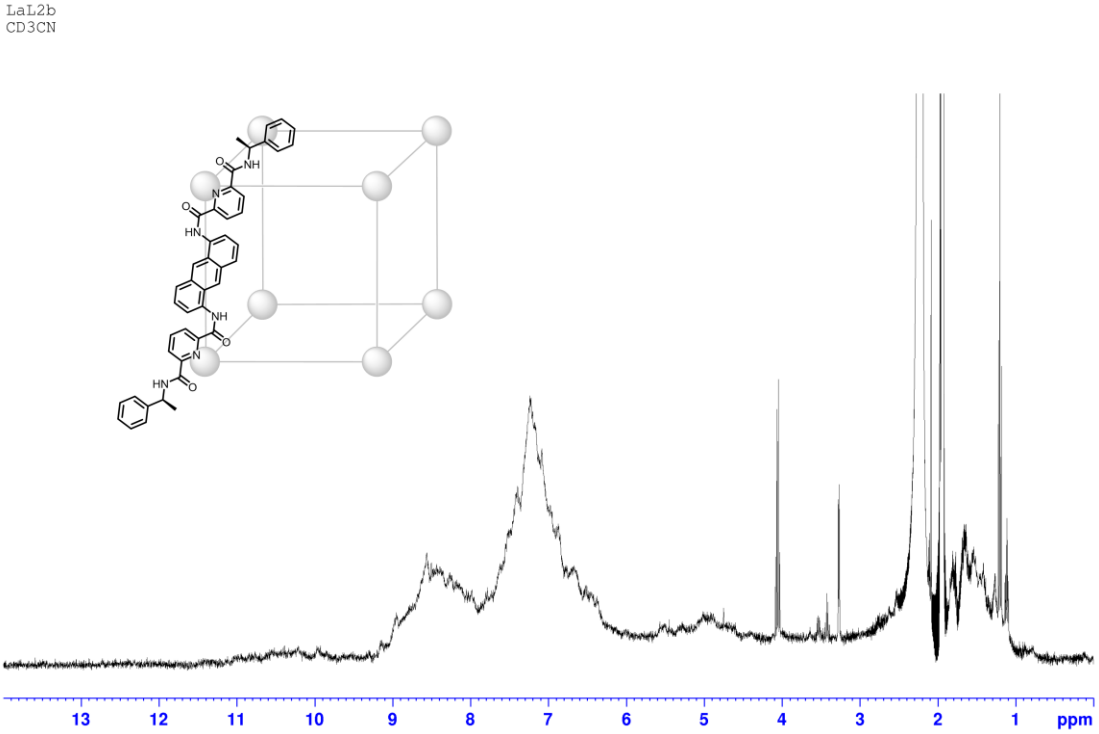

Spectrum S2-68: ^{1}H NMR spectrum of Complex **LaL$_{2b}$**

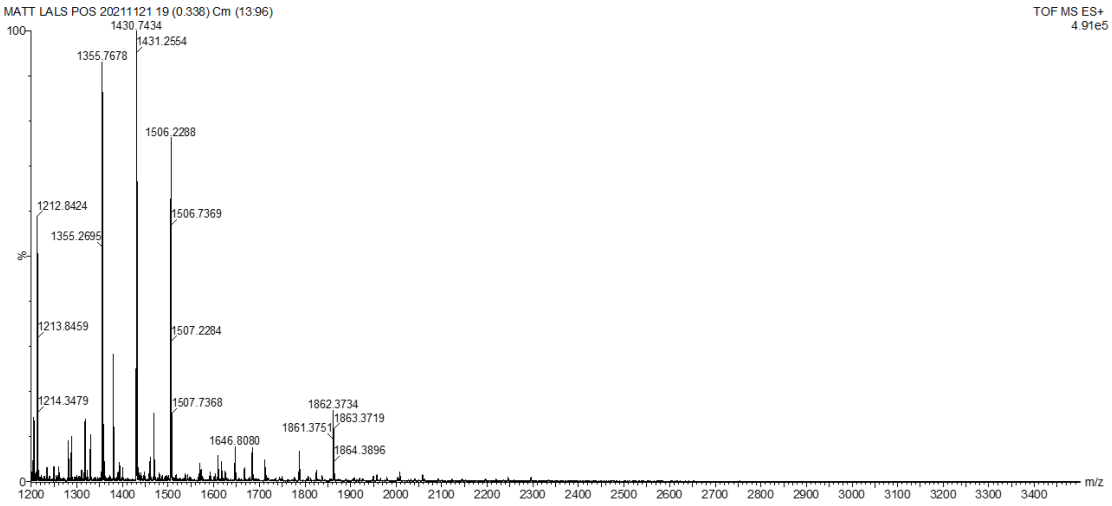

Spectrum S2-69: ESI-HRMS spectrum of Complex **LaL_{2b}**

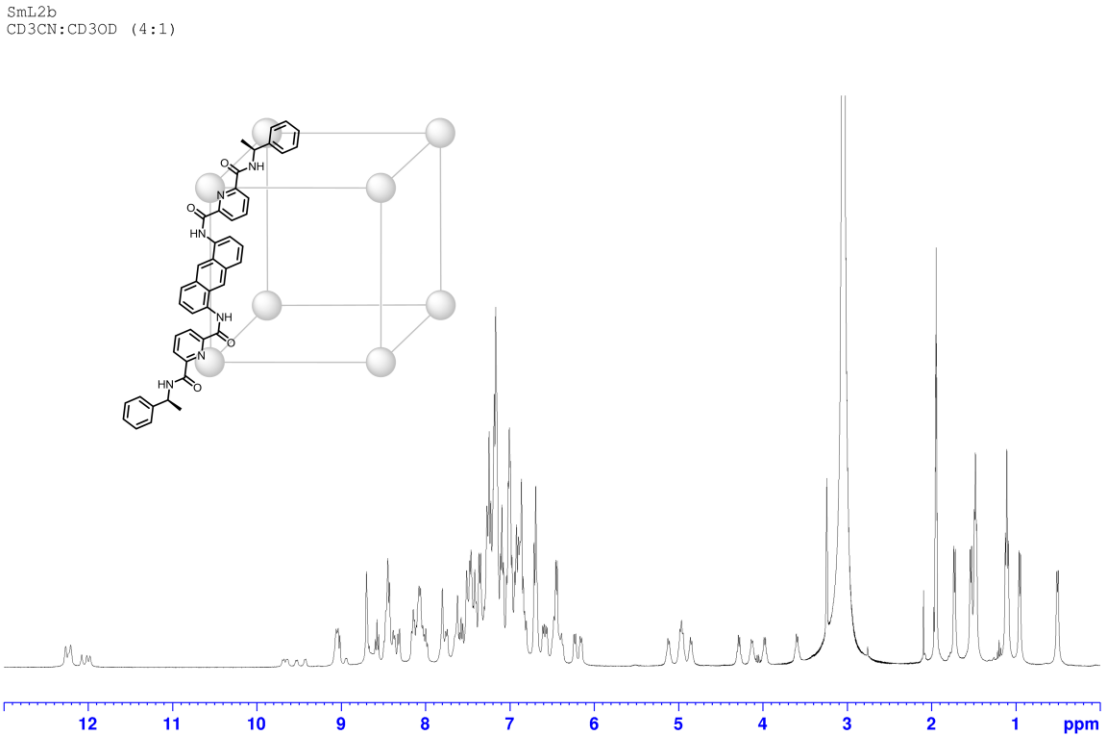

Spectrum S2-70: ^{1}H NMR spectrum of Complex **SmL_{2b}**

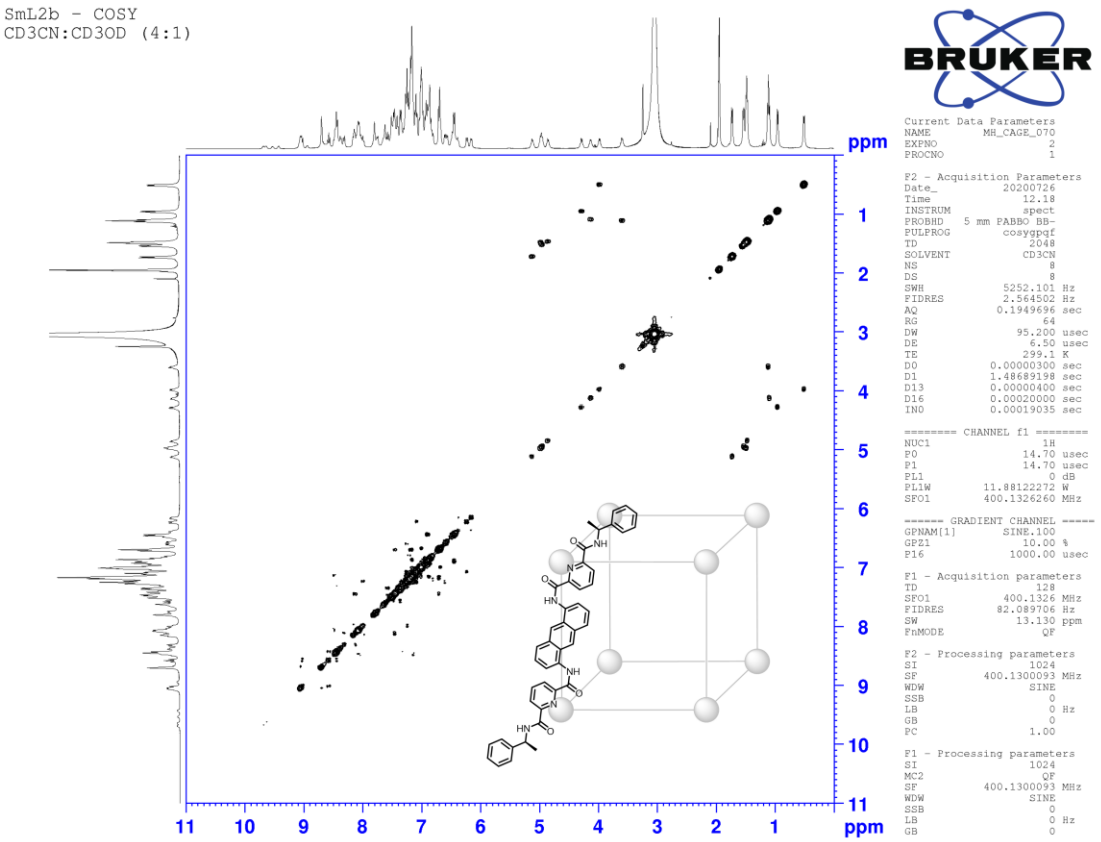

Spectrum S2-71: ^{1}H-^{1}H COSY NMR spectrum of Complex **SmL$_{2b}$**

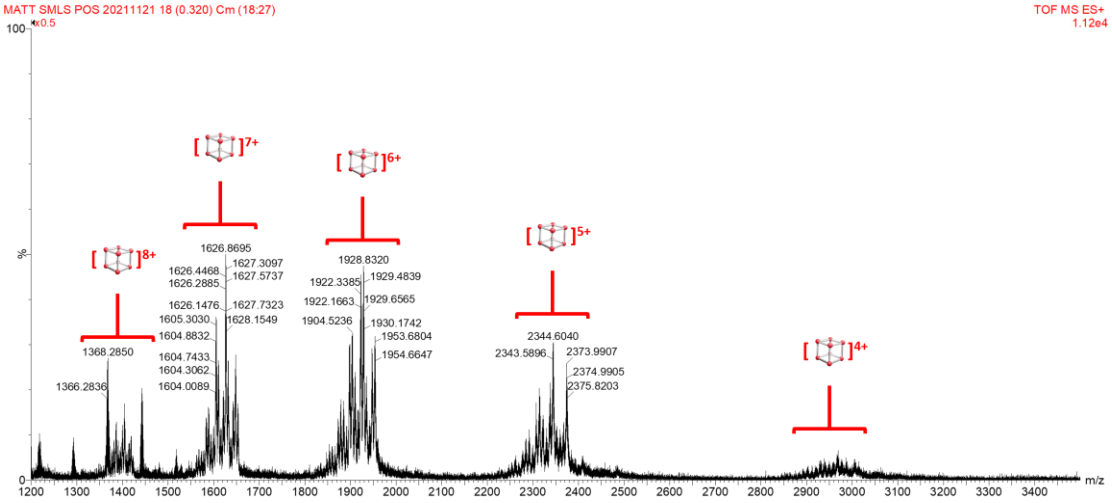

Spectrum S2-72: ESI-HRMS spectrum of Complex **SmL$_{2b}$**

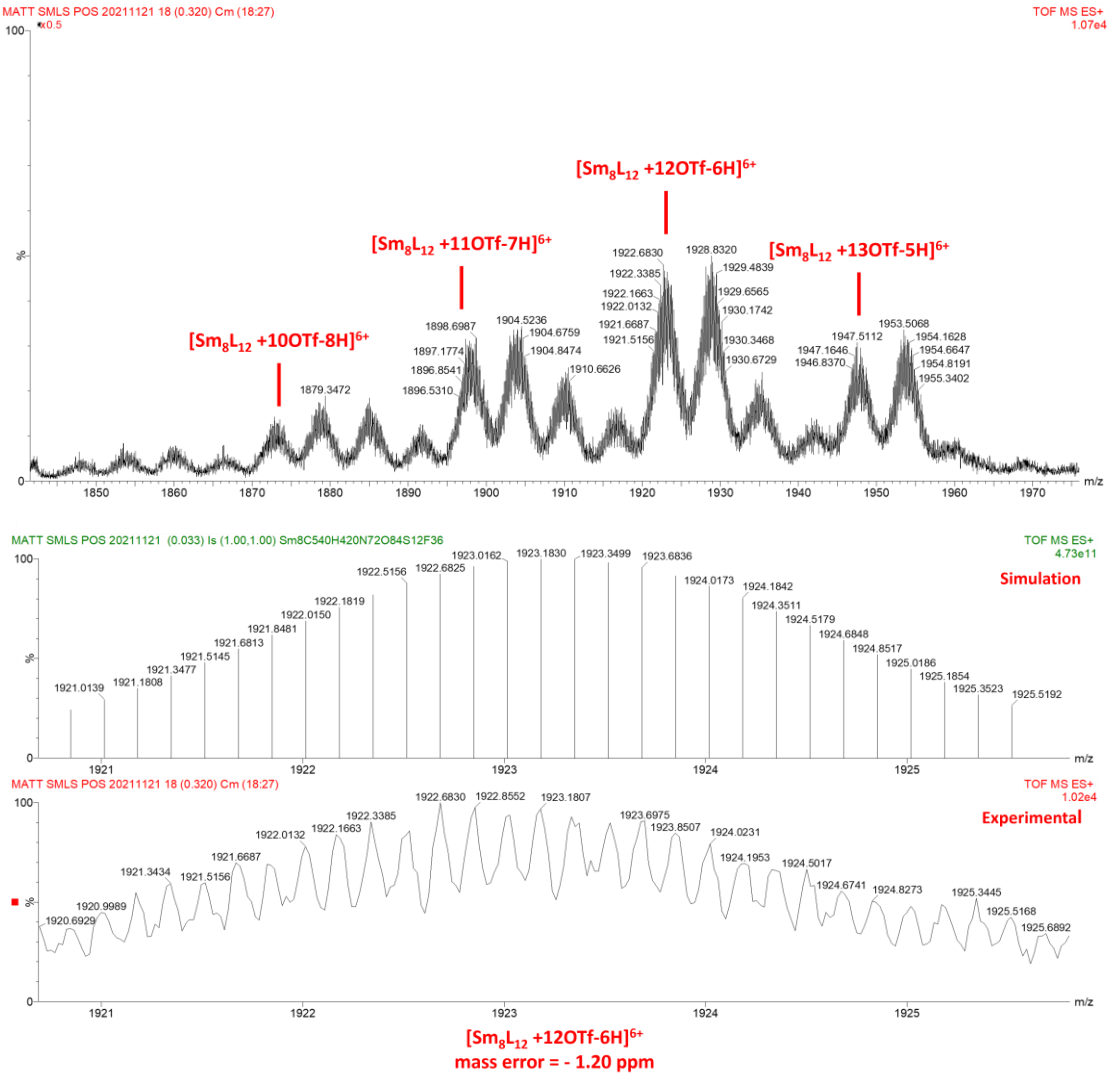

Spectrum S2-73: (top) expanded ESI-HRMS spectrum of species $[Sm_8(L_{2b})_{12}]^{6+}$ (bot) isotopic distribution of $[Sm_8(L_{2b})_{12}+12OTf-6H]^{6+}$

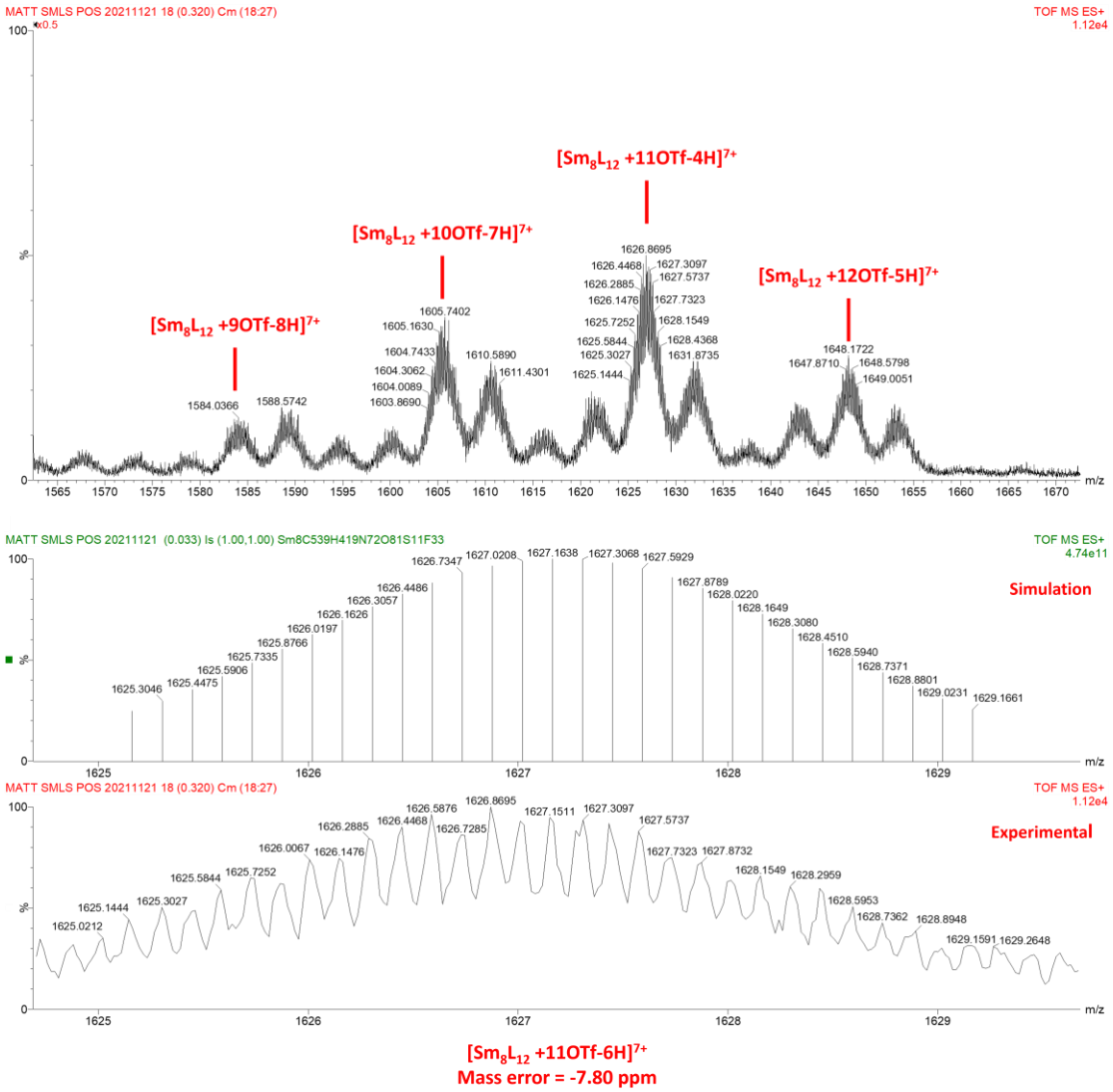

Spectrum S2-74: (top) expanded ESI-HRMS spectrum of species $[Sm_8(L_{2b})_{12}]^{7+}$ (bot) isotopic distribution of $[Sm_8(L_{2b})_{12}+11OTf-6H]^{7+}$

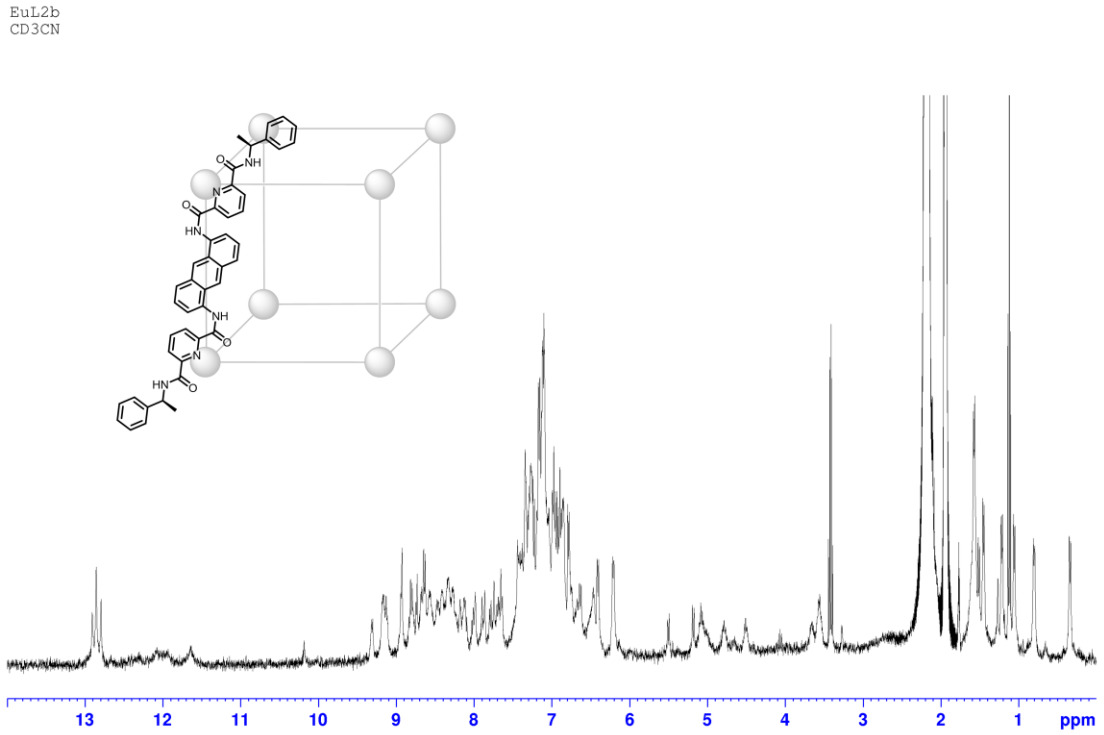

Spectrum S2-75: ^{1}H NMR spectrum of Complex **EuL$_{2b}$**

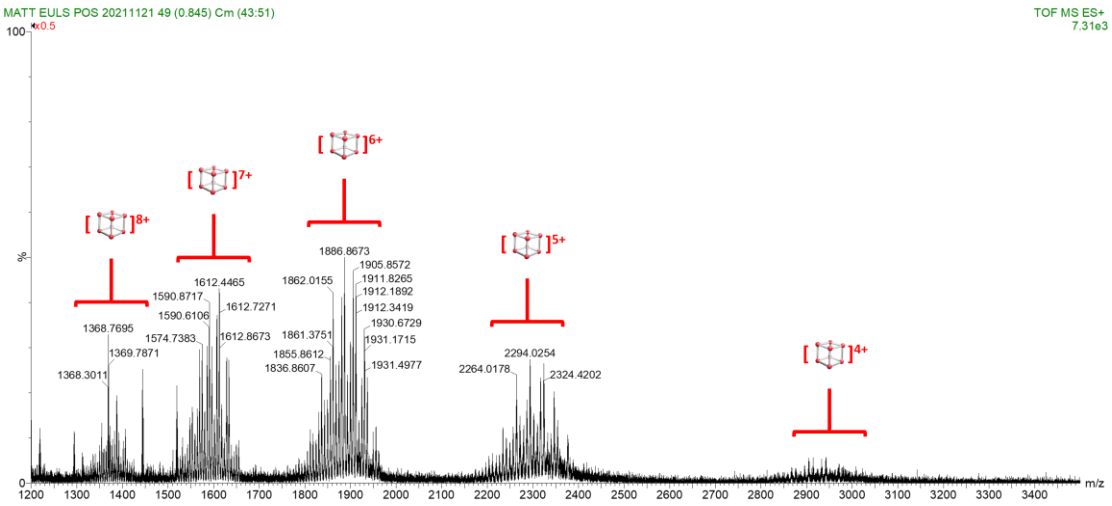

Spectrum S2-76: ESI-HRMS spectrum of Complex **EuL$_{2b}$**

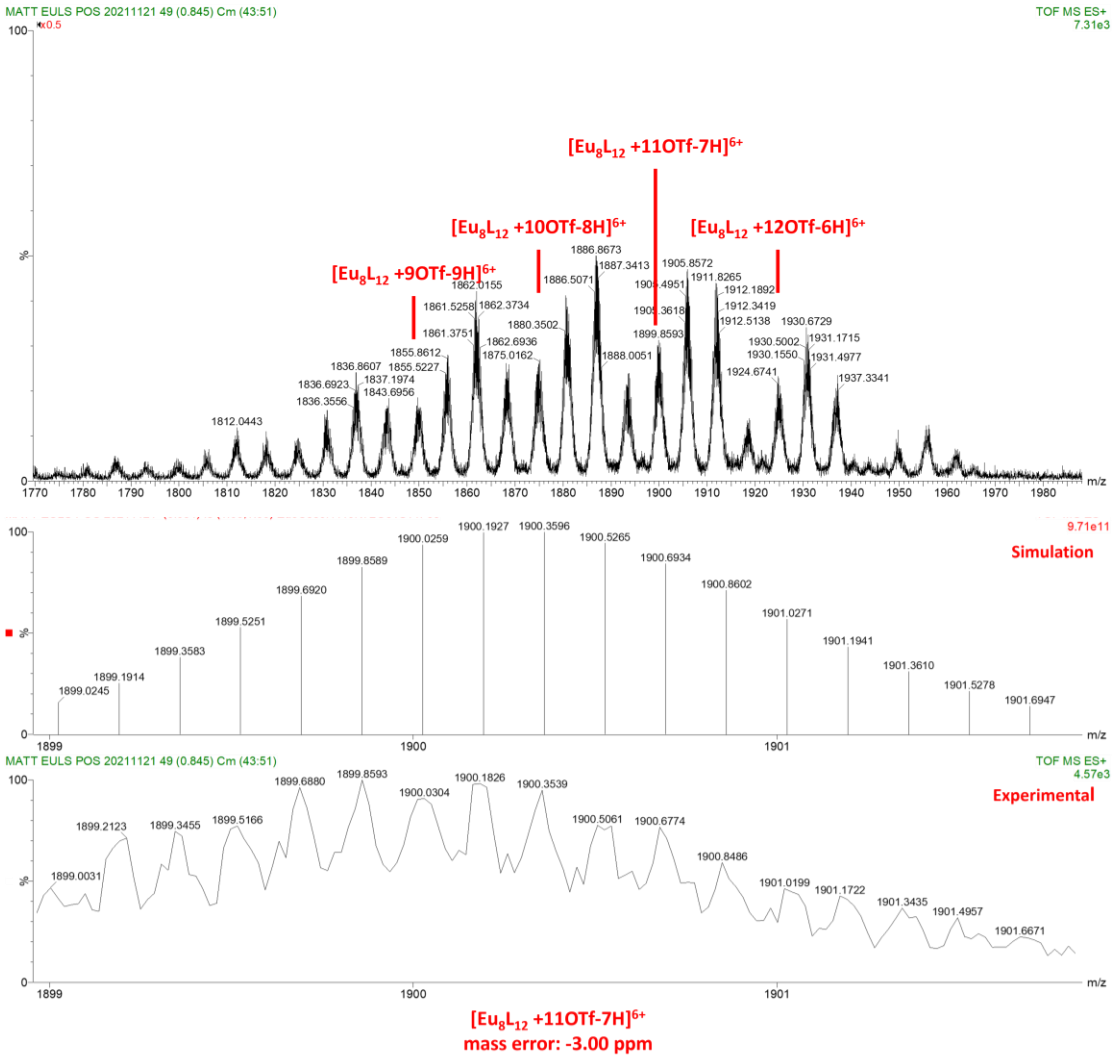

Spectrum S2-77: (top) expanded ESI-HRMS spectrum of species $[Eu_8(L_{2b})_{12}]^{6+}$ (bot) isotopic distribution of $[Eu_8(L_{2b})_{12}+11OTf-7H]^{6+}$

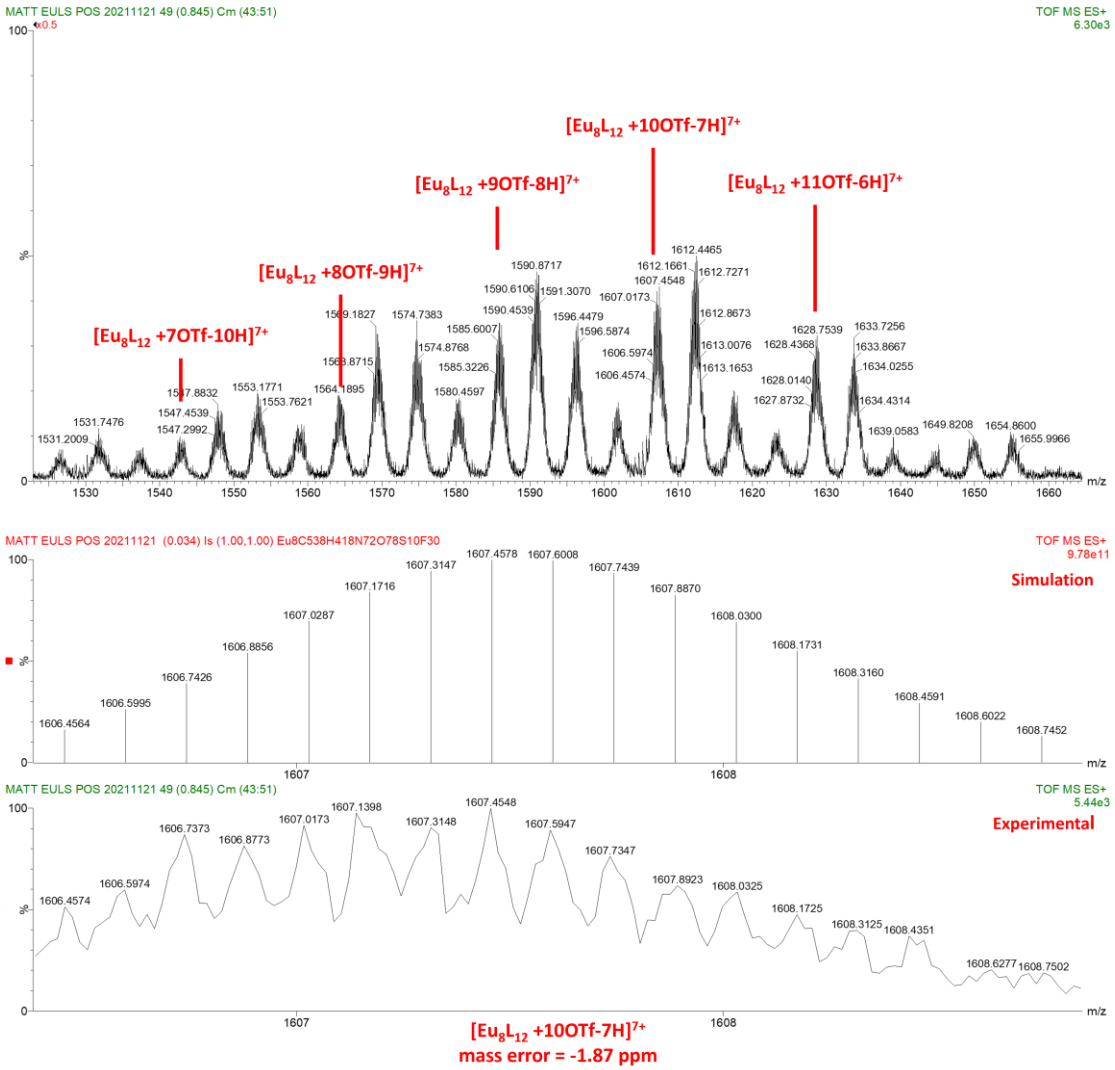

Spectrum S2-78: (top) expanded ESI-HRMS spectrum of species $[Eu_8(L_{2b})_{12}]^{7+}$ (bot) isotopic distribution of $[Eu_8(L_{2b})_{12}+10OTf-7H]^{7+}$

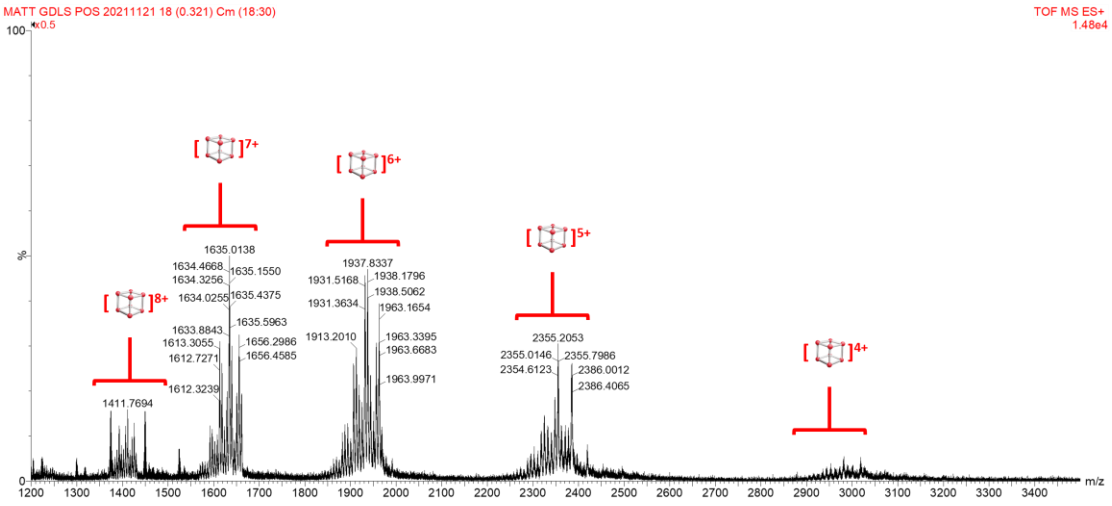

Spectrum S2-79: ESI-HRMS spectrum of Complex **GdL_{2b}**

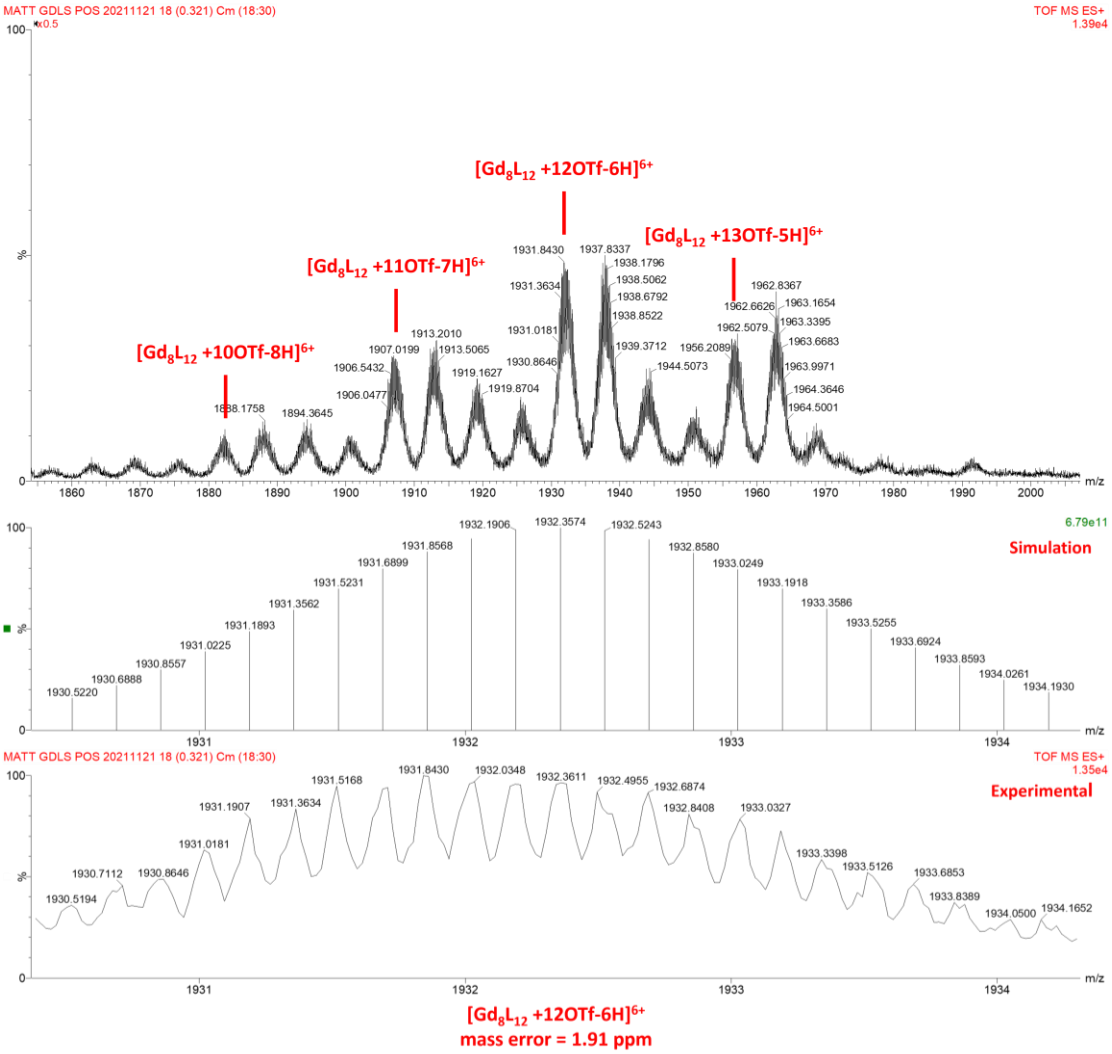

Spectrum S2-80: (top) expanded ESI-HRMS spectrum of species **$[Gd_8(L_{2b})_{12}]^{6+}$** (bot) isotopic distribution of **$[Gd_8(L_{2b})_{12}$ +12OTf – 6H$]^{6+}$**

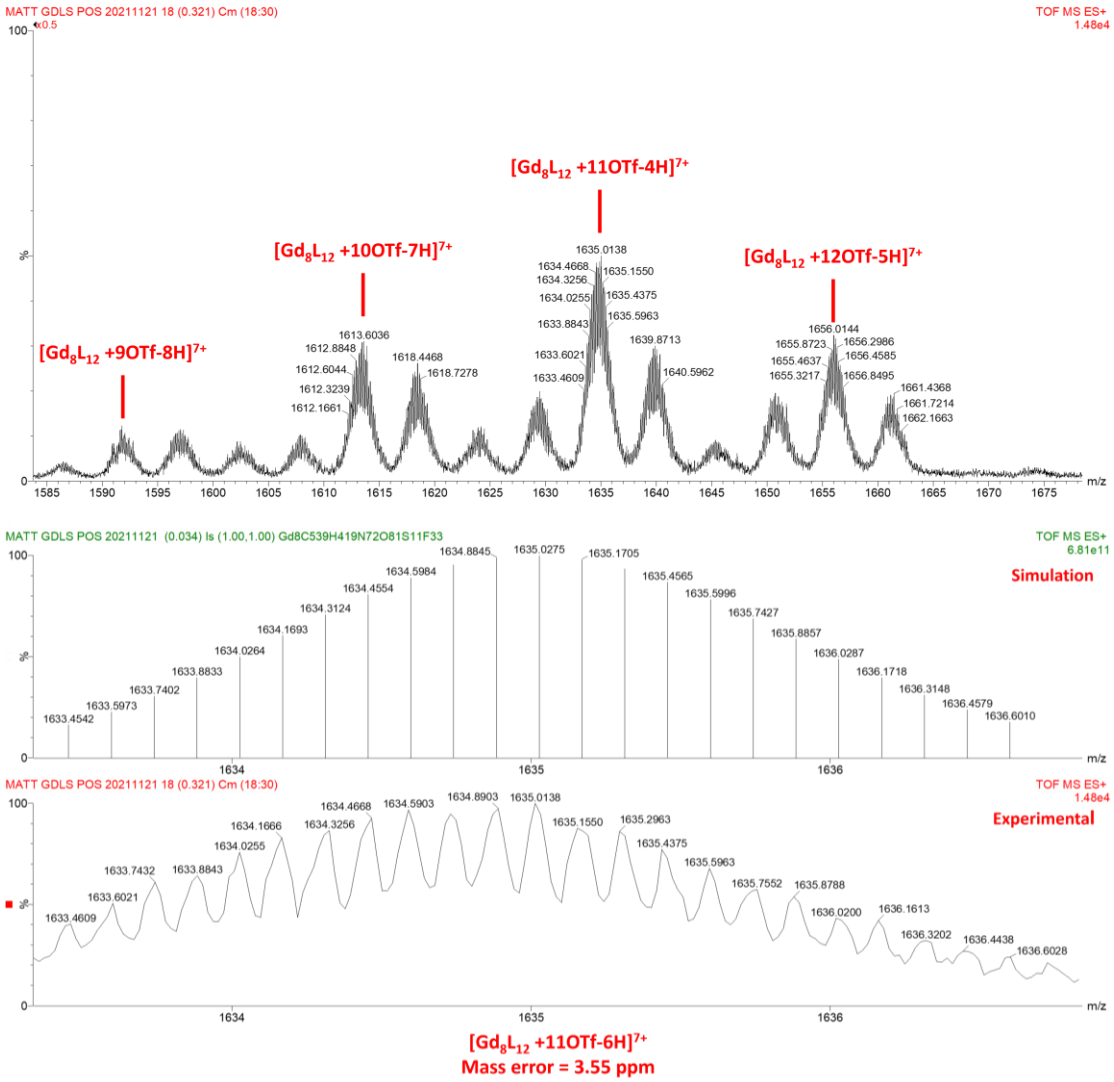

Spectrum S2-81: (top) expanded ESI-HRMS spectrum of species $[Gd_8(L_{2b})_{12}]^{7+}$ (bot) isotopic distribution of $[Gd_8(L_{2b})_{12}+11OTf-6H]^{7+}$

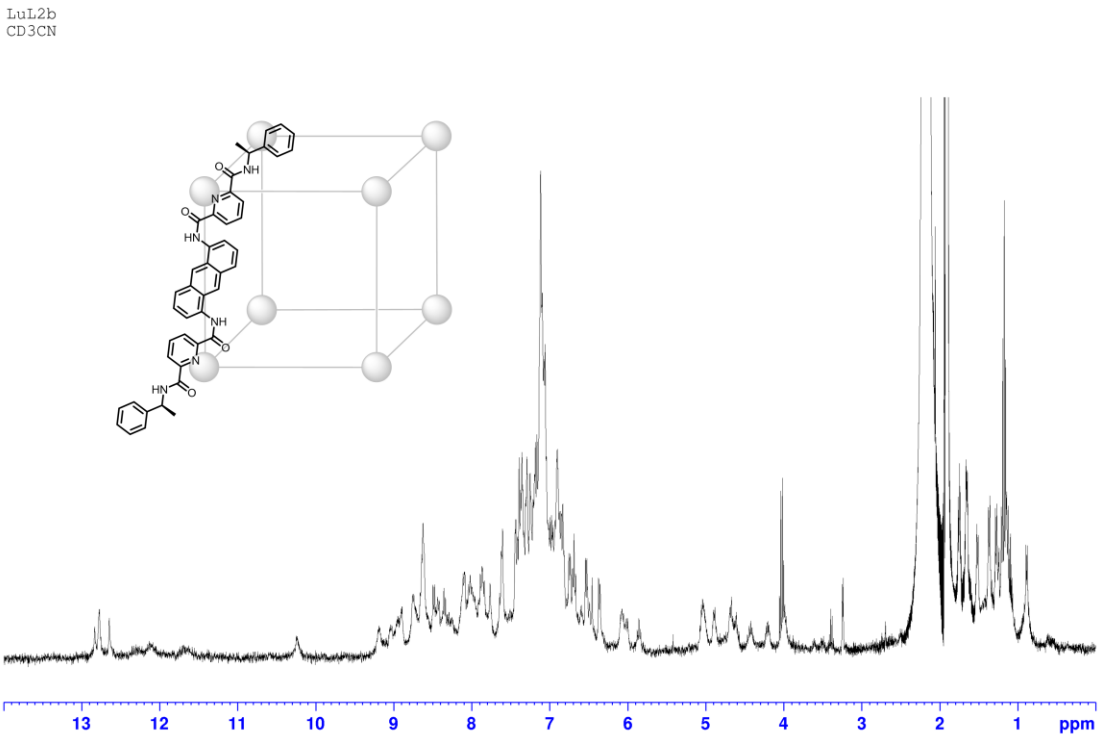

Spectrum S2-82: ^{1}H NMR spectrum of Complex **LuL$_{2b}$**

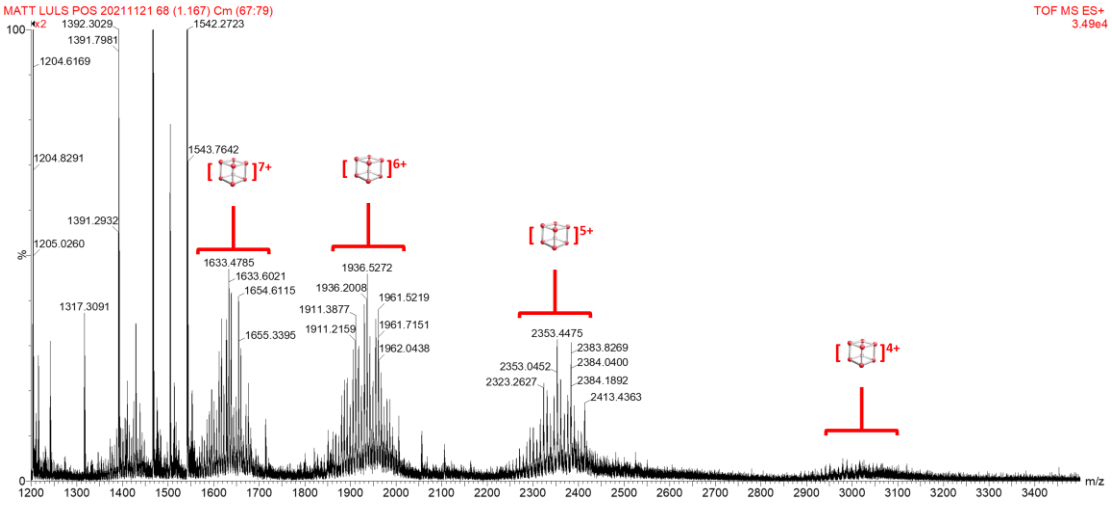

Spectrum S2-83: ESI-HRMS spectrum of Complex **LuL$_{2b}$**

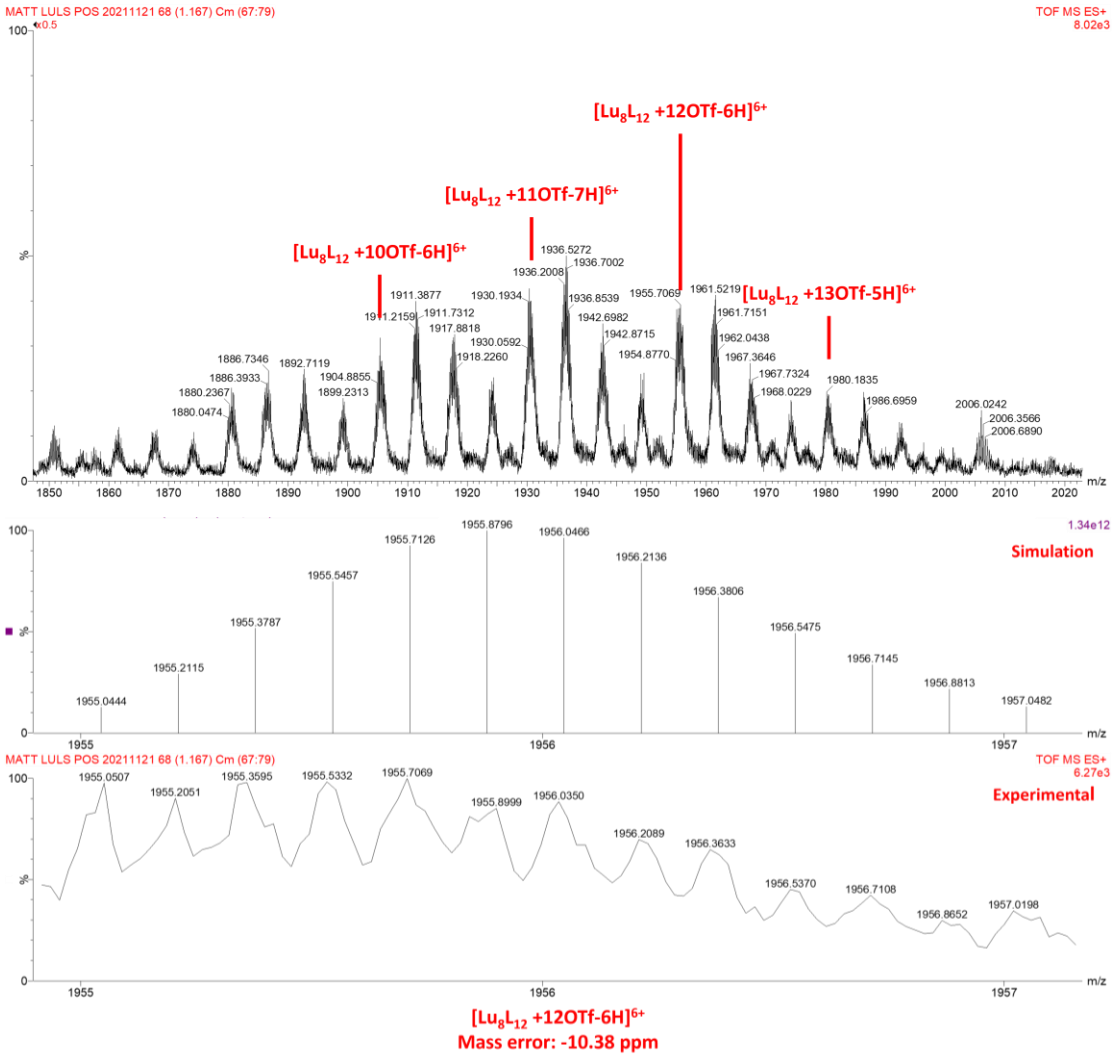

Spectrum S2-84: (top) expanded ESI-HRMS spectrum of species $[Lu_8(L_{2b})_{12}]^{6+}$ (bot) isotopic distribution of $[Lu_8(L_{2b})_{12}+12OTf-6H]^{6+}$

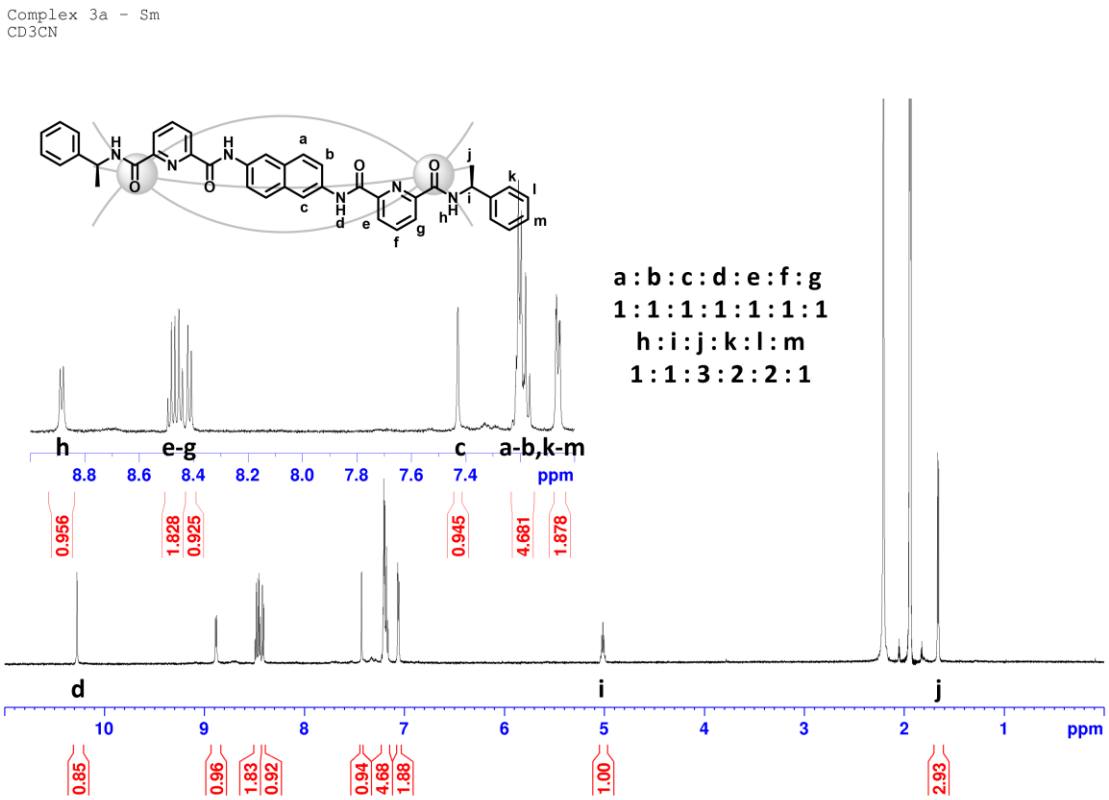

Spectrum S2-85: ^{1}H NMR spectrum of Complex **SmL$_{3a}$**

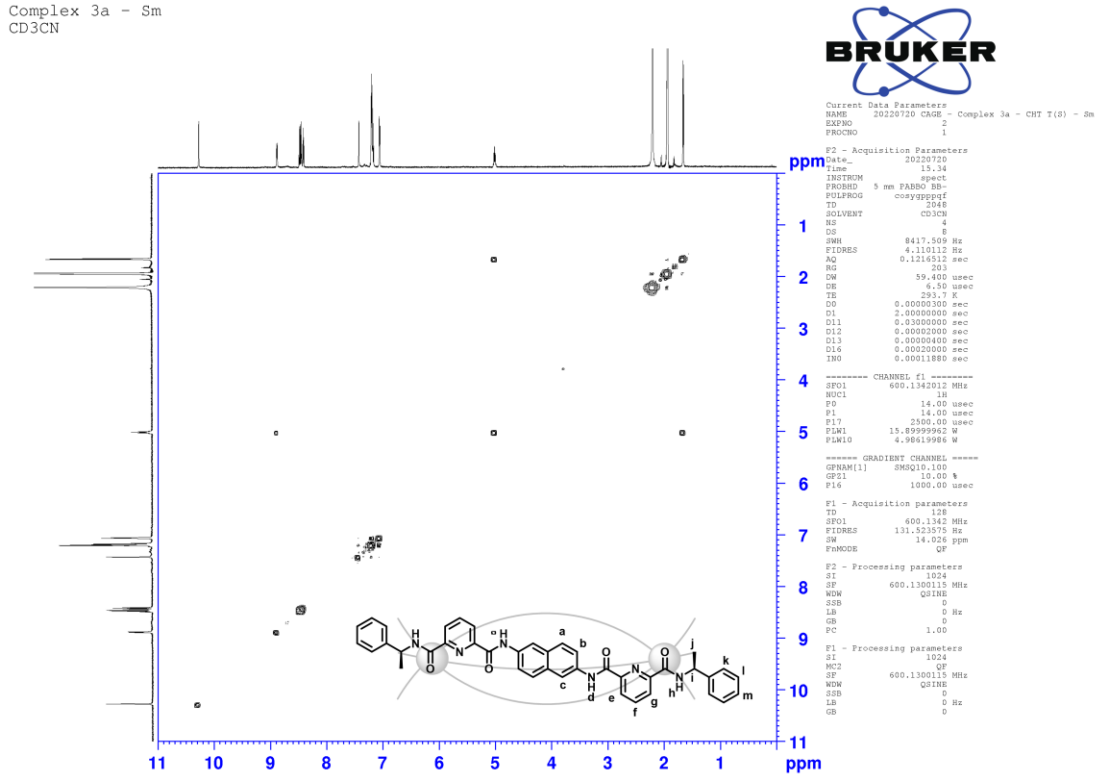

Spectrum S2-86: ^{1}H-^{1}H COSY NMR spectrum of Complex **SmL$_{3a}$**

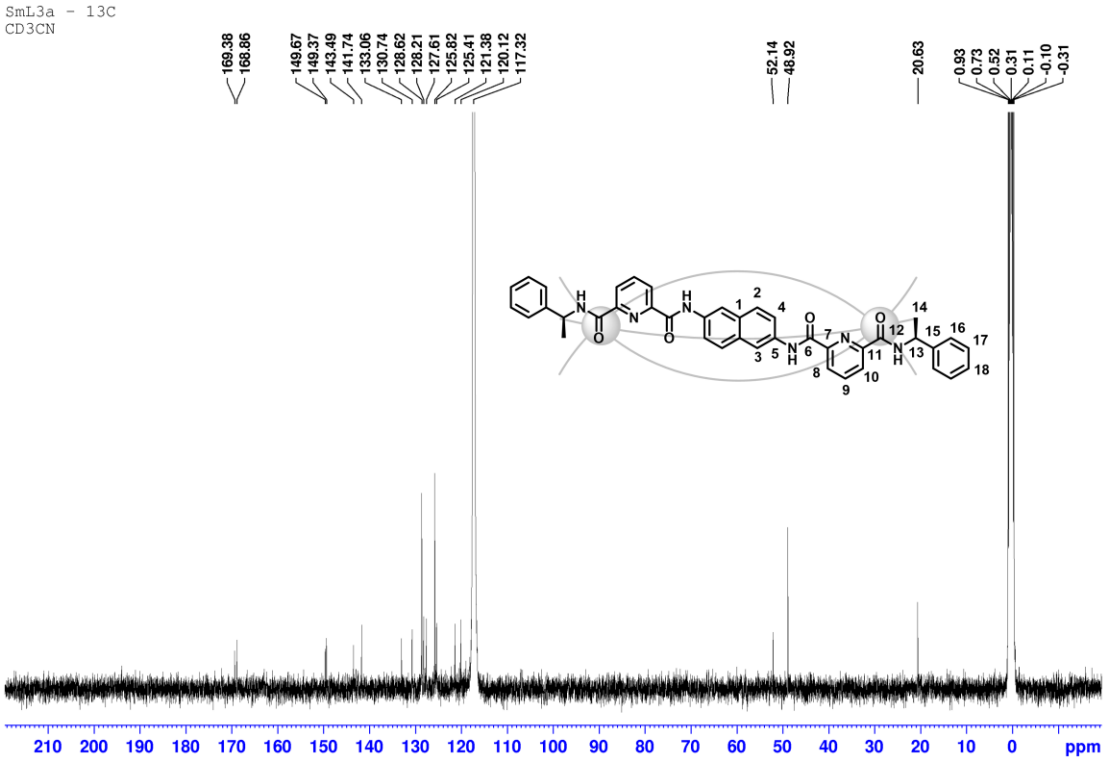

Spectrum S2-87: ^{13}C NMR spectrum of Complex **SmL$_{3a}$**

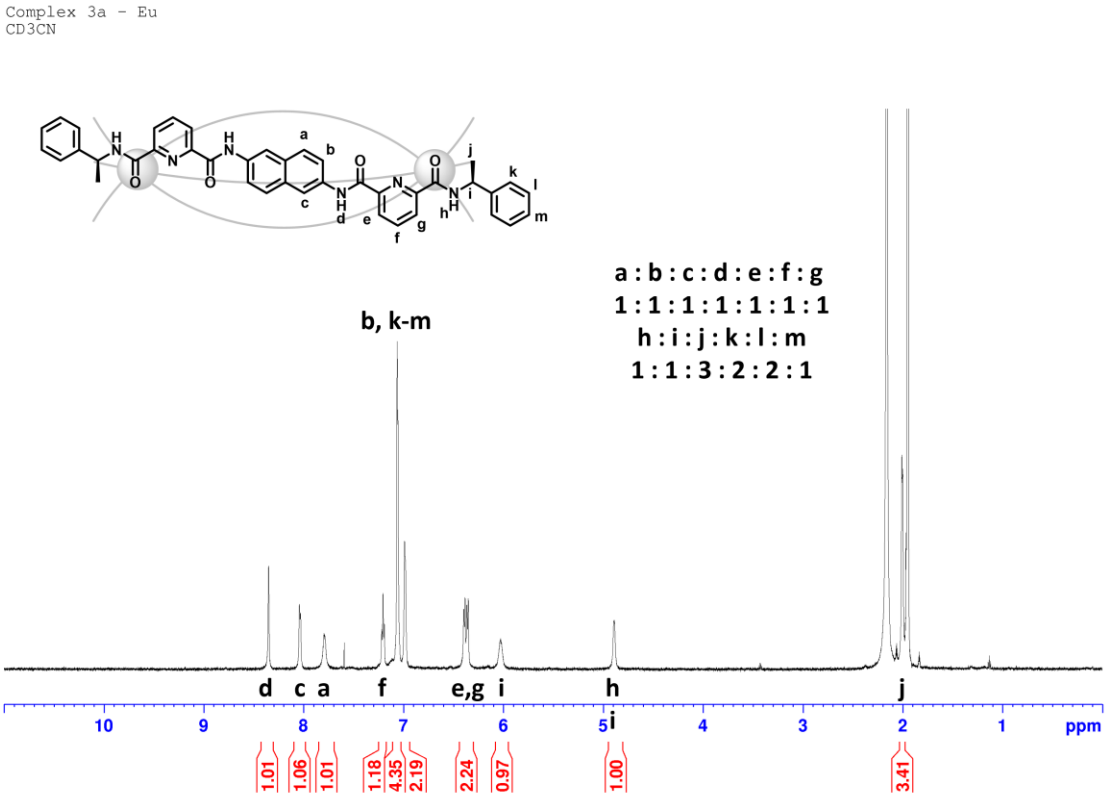

Spectrum S2-88: ^{1}H NMR spectrum of Complex **EuL$_{3a}$**

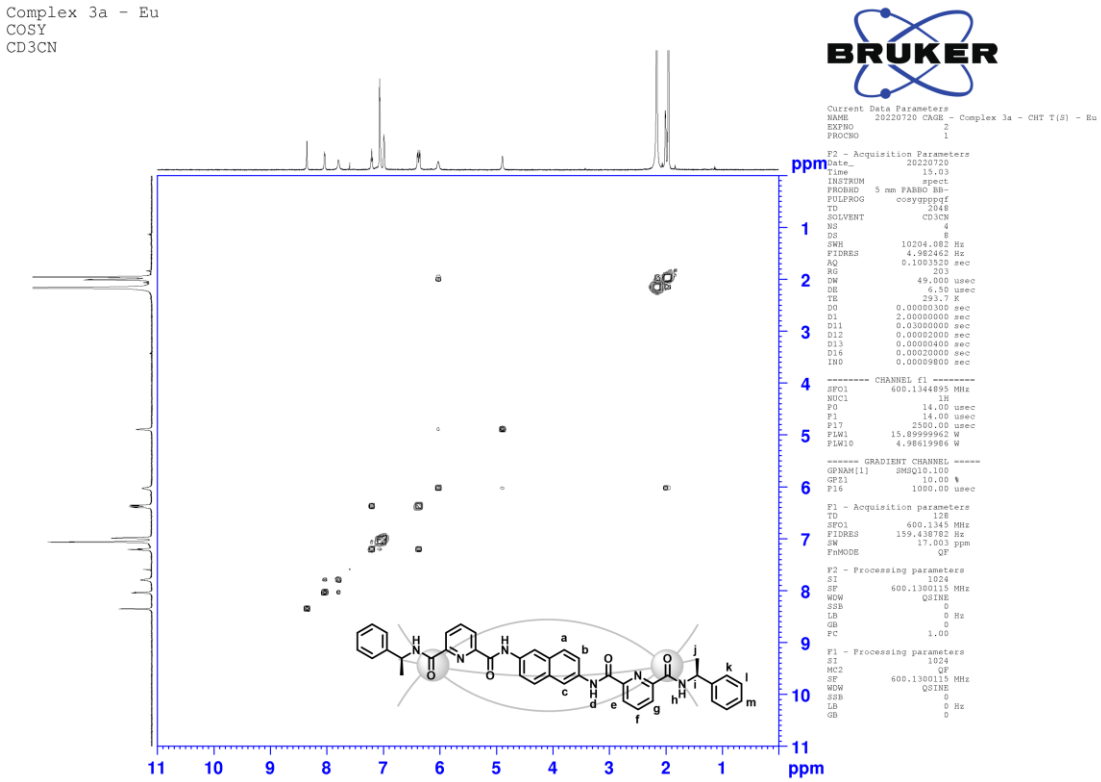

Spectrum S2-89: ^{1}H-^{1}H COSY NMR spectrum of Complex **EuL$_{3a}$**

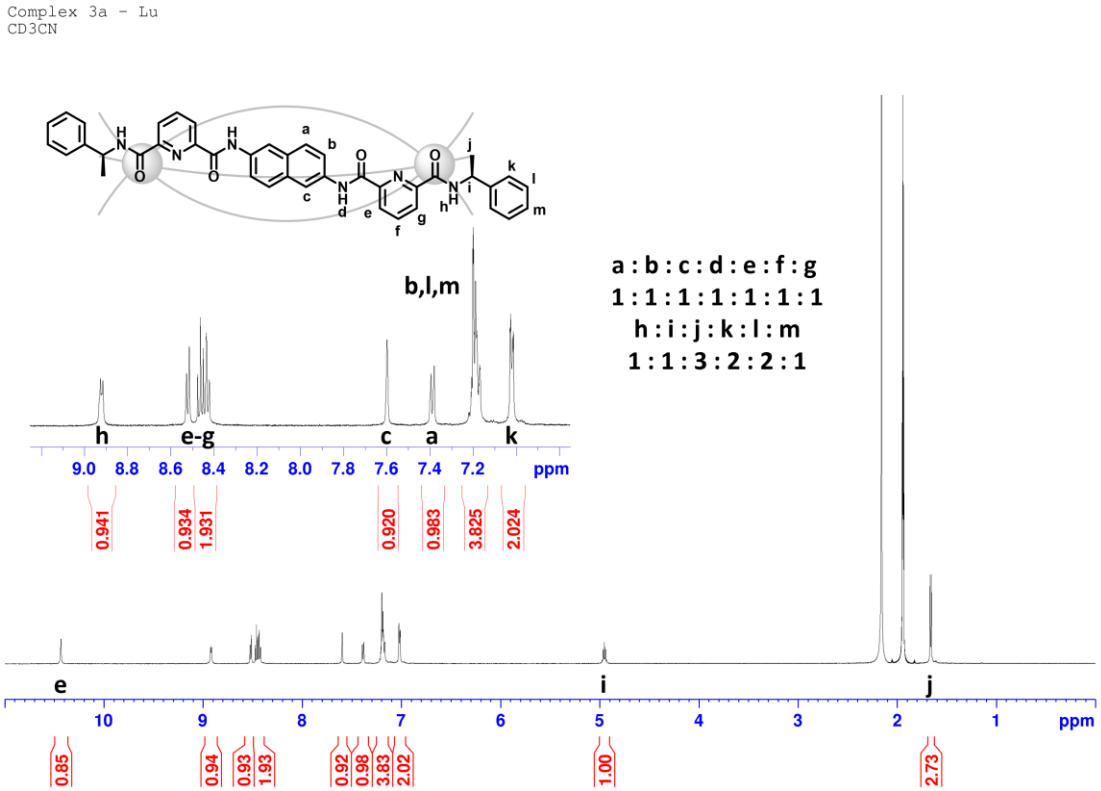

Spectrum S2-90: ^{1}H NMR spectrum of Complex **LuL$_{3a}$**

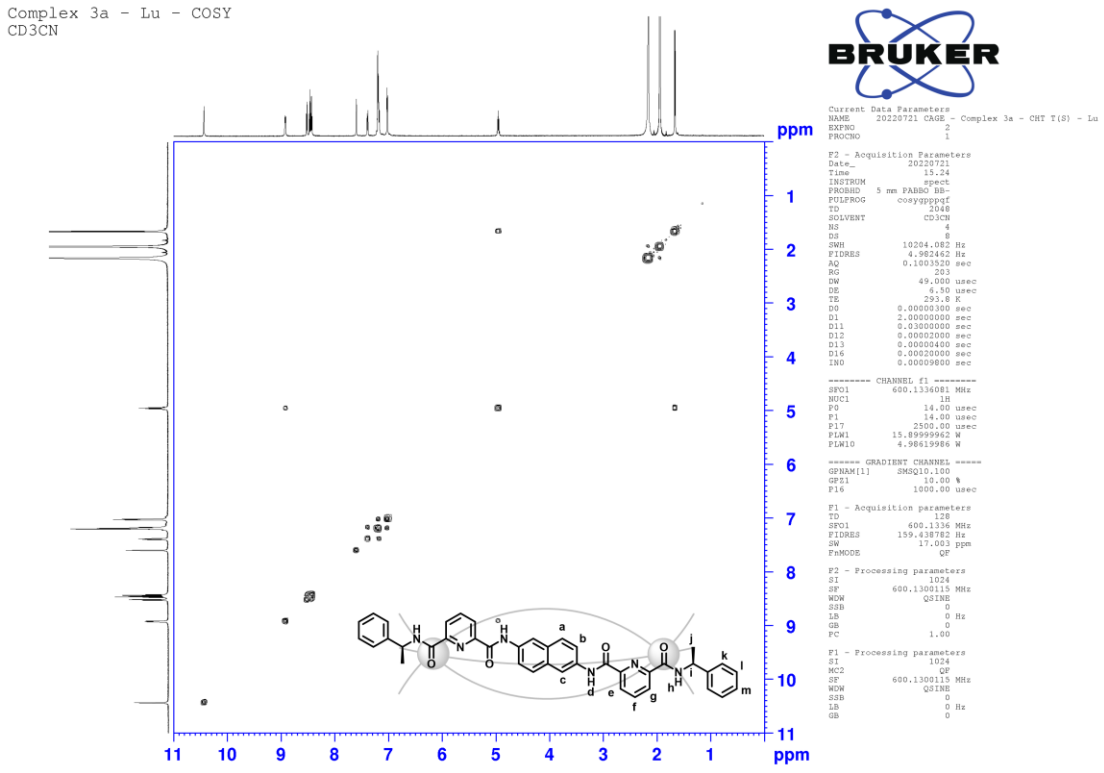

Spectrum S2-91: ^{1}H-^{1}H COSY NMR spectrum of Complex **LuL$_{3a}$**

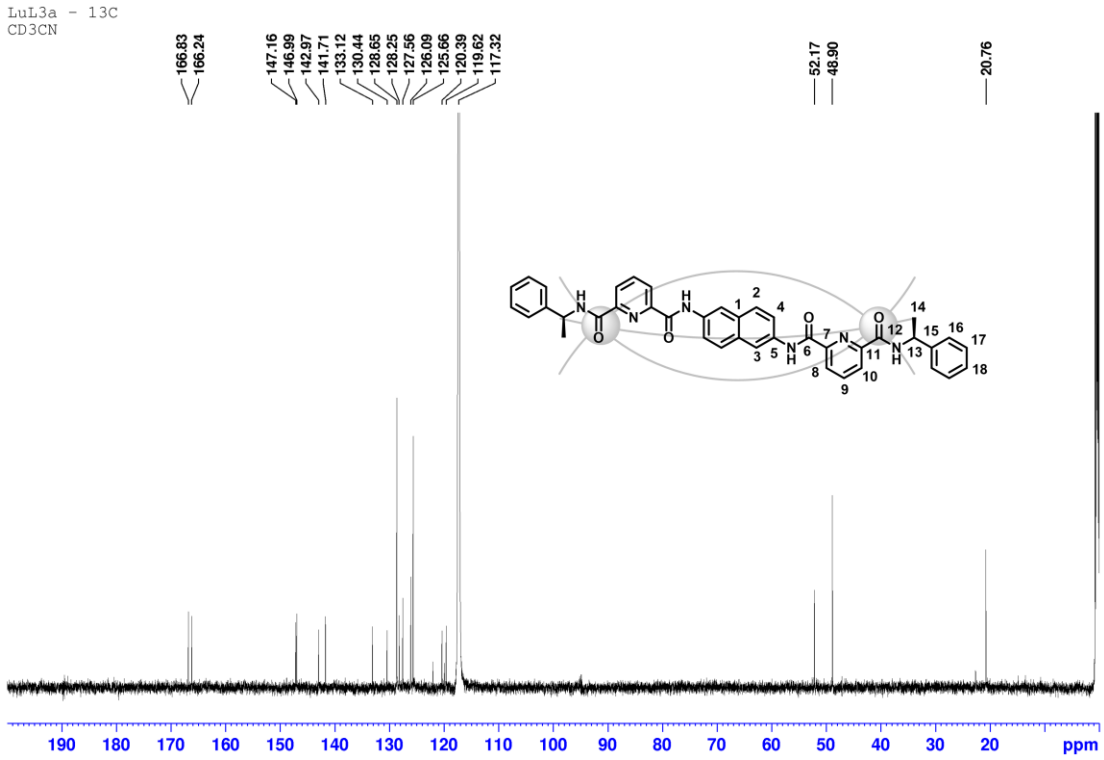

Spectrum S2-92: ^{13}C NMR spectrum of Complex **LuL$_{3a}$**

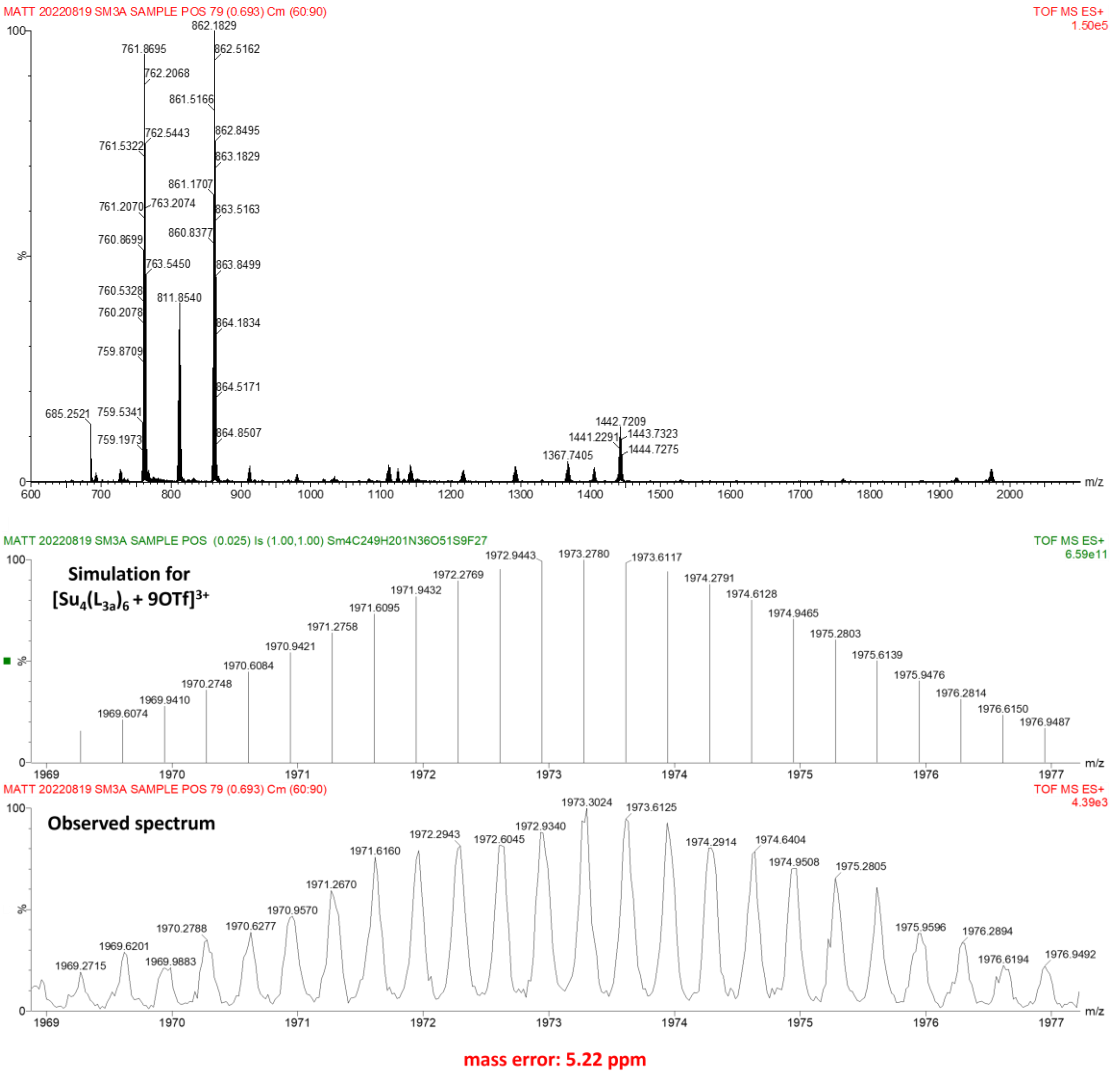

mass error: 5.22 ppm

Spectrum S2-93: (top) ESI-HRMS spectrum of complex **SmL_{3a}** (bot) isotopic distribution of **$[Sm_4(L_{3a})_6 + 9OTf]^{3+}$**

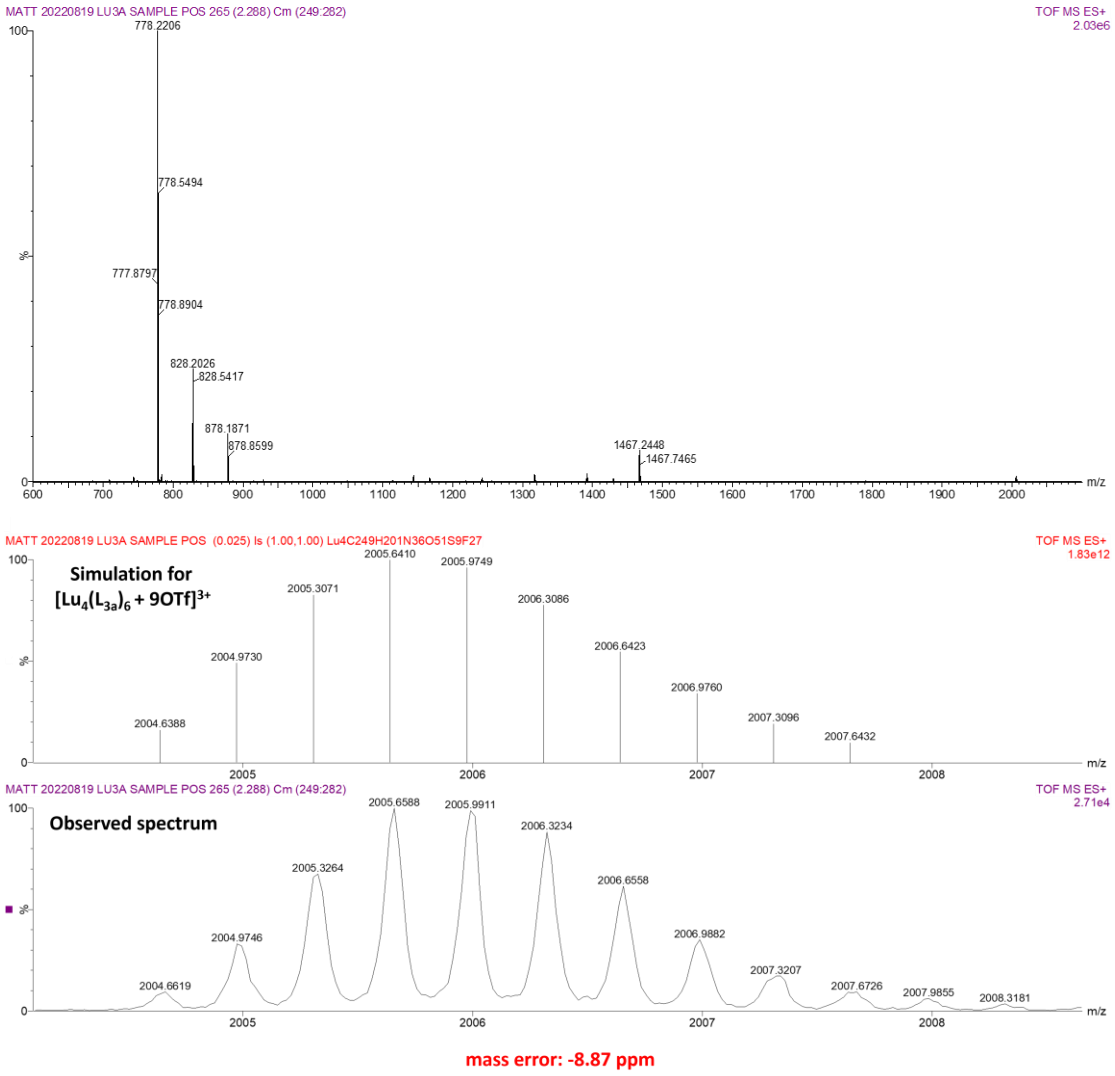

mass error: -8.87 ppm

Spectrum S2-94: (top) ESI-HRMS spectrum of complex **LuL_{3a}** (bot) isotopic distribution of **$[Lu_4(L_{3a})_6 + 9OTf]^{3+}$**

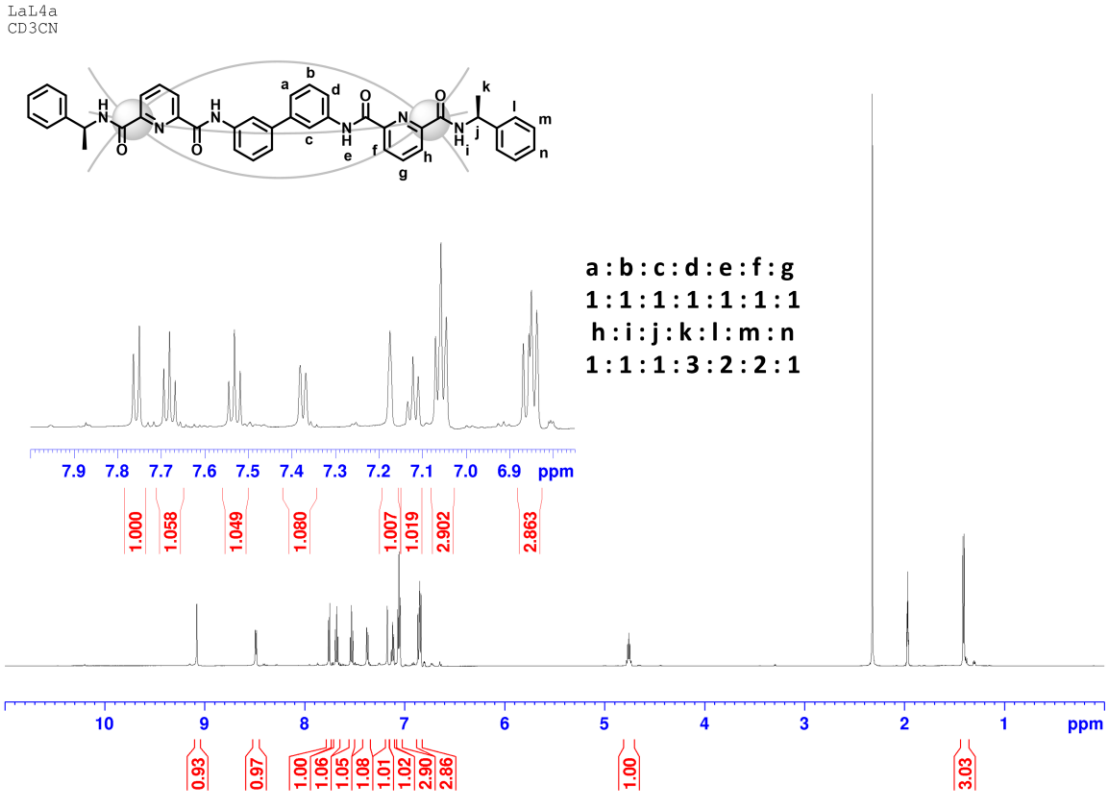

Spectrum S2-95: ^{1}H NMR spectrum of Complex **LaL$_{4b}$**

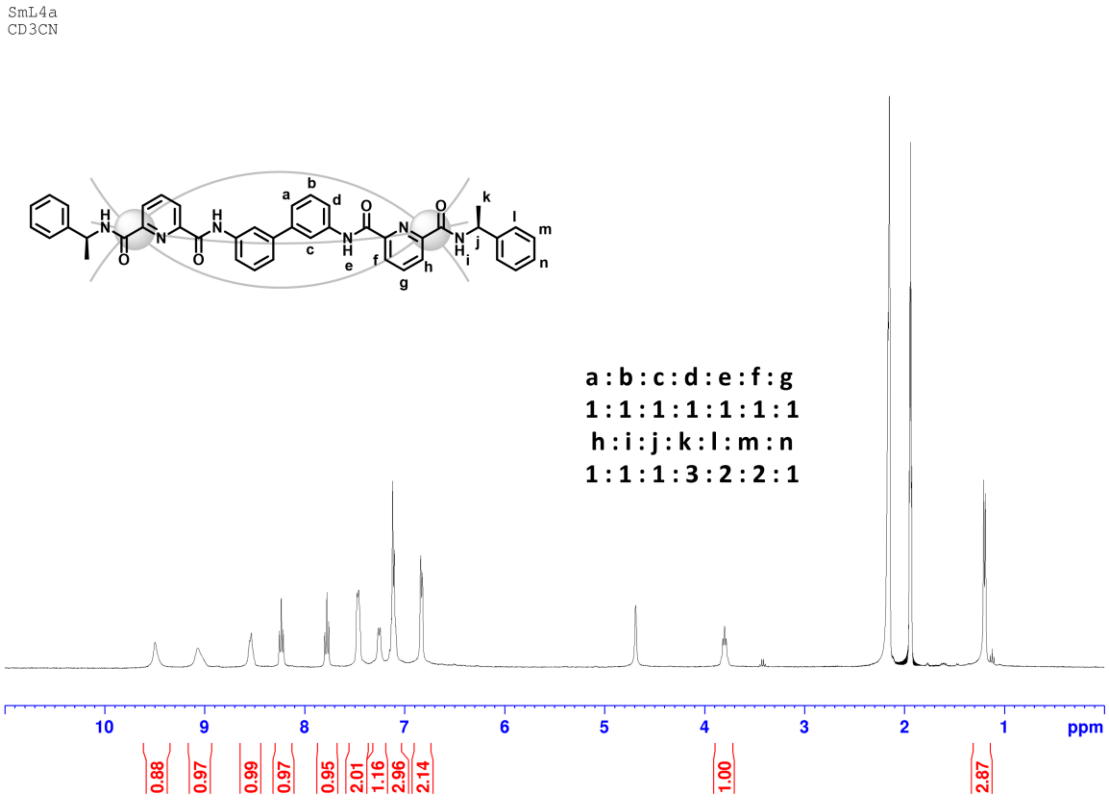

Spectrum S2-96: ^{1}H NMR spectrum of Complex **SmL$_{4b}$**

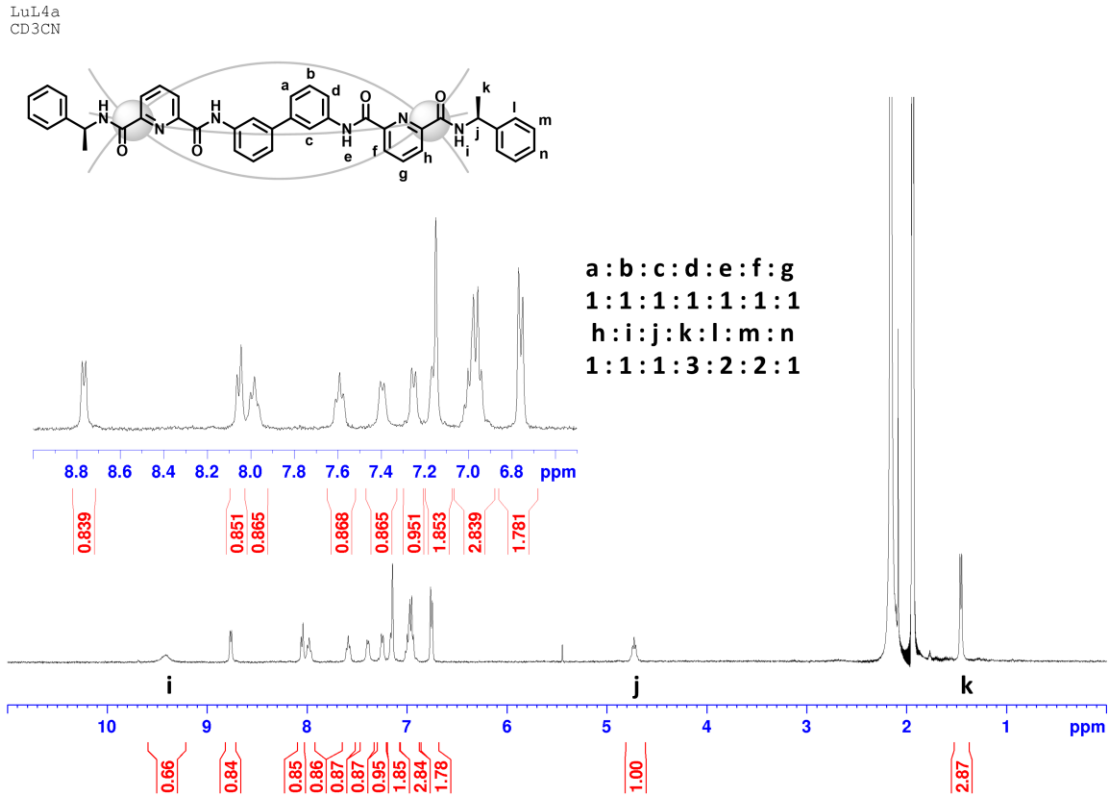

Spectrum S2-97: ^{1}H NMR spectrum of Complex **LuL$_{4b}$**

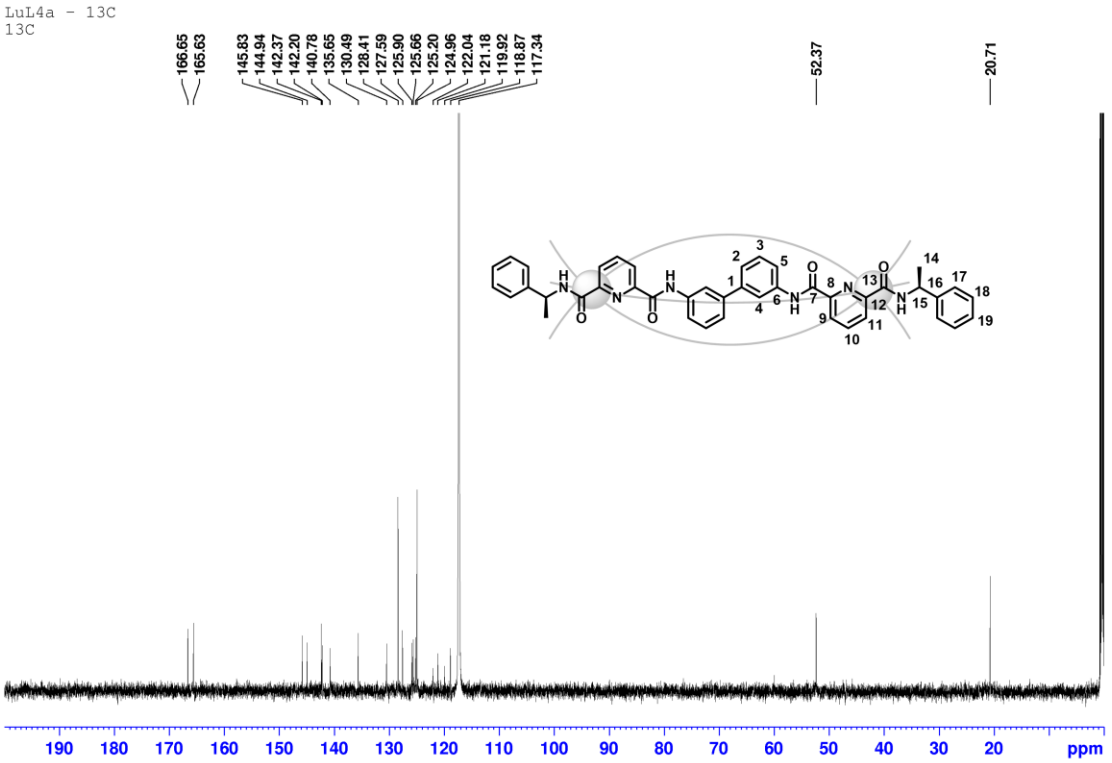

Spectrum S2-98: ^{13}C NMR spectrum of Complex **LuL$_{4b}$**

SUMMARY OF PM7 CALCULATION

MOPAC v22.0.4 Windows

Wed Nov 2 11:47:01 2022

Empirical Formula: C18 H14 N2 O4 = 38 atoms

PM7 PRECISE CHARGE=0 EF LET AUX XYZ BONDS GNORM=0.0100 CHARGE=0

Linker1a.mop

GEOMETRY OPTIMISED USING EIGENVECTOR FOLLOWING (EF).

SCF FIELD WAS ACHIEVED

HEAT OF FORMATION = -77.60902 KCAL/MOL = -324.71613 KJ/MOL

GRADIENT NORM = 425.10822 = 68.96166 PER ATOM

DIPOLE = 2.15655 DEBYE POINT GROUP: C2h

NO. OF FILLED LEVELS = 60

IONIZATION POTENTIAL = 9.148965 EV

HOMO LUMO ENERGIES (EV) = -9.149 -1.621

MOLECULAR WEIGHT = 322.3196

COSMO AREA = 333.22 SQUARE ANGSTROMS

COSMO VOLUME = 358.23 CUBIC ANGSTROMS

MOLECULAR DIMENSIONS (Angstroms)

Atom Atom Distance

H 38 H 35 16.73086

H 28 H 27 6.15388

H 37 H 36 1.77817

SCF CALCULATIONS = 35

WALL-CLOCK TIME = 2.918 SECONDS

COMPUTATION TIME = 17.406 SECONDS

FINAL GEOMETRY OBTAINED

PM7 PRECISE CHARGE=0 EF LET AUX XYZ BONDS GNORM=0.0100 CHARGE=0

Linker1a.mop

C -0.01622639 +1 -0.16692171 +1 -0.00000524 +1

C 1.39267054 +1 -0.15089238 +1 -0.00002965 +1

C 2.02829825 +1 1.11411756 +1 -0.00010219 +1

C 1.30764476 +1 2.30832991 +1 -0.00023358 +1

C -0.09134460 +1 2.20871697 +1 -0.00008571 +1

C -0.70950277 +1 0.96845522 +1 0.00002396 +1

C 2.10213640 +1 3.56665101 +1 -0.00066981 +1

C 1.27995508 +1 4.85449822 +1 -0.00093480 +1

C -0.11317113 +1 4.71186799 +1 -0.00052014 +1

C -0.88043996 +1 3.51284918 +1 -0.00010186 +1

C 1.89623816 +1 6.03991740 +1 -0.00154474 +1

C 1.18929660 +1 7.24844828 +1 -0.00177519 +1

C -0.15471576 +1 7.13464139 +1 -0.00126201 +1

C -0.85158625 +1 5.94091004 +1 -0.00065041 +1

O -2.10779608 +1 3.47174946 +1 0.00021305 +1

O 3.26090472 +1 3.57529373 +1 -0.00083999 +1

N -1.11894682 +1 8.32830860 +1 -0.00112437 +1

C -0.76378178 +1 9.62661120 +1 -0.00306707 +1

N 2.27218759 +1 -1.18783533 +1 0.00014515 +1

C 1.97069269 +1 -2.57622001 +1 -0.00107669 +1

C 3.18604391 +1 -3.43645084 +1 -0.00073735 +1

O 0.75366059 +1 -2.99238401 +1 -0.00220526 +1

C -2.00201963 +1 10.49169725 +1 -0.00263614 +1

O 0.41603460 +1 10.04731774 +1 -0.00485818 +1

H -0.53279282 +1 -1.16810649 +1 -0.00002585 +1

H 3.16265258 +1 1.18411865 +1 -0.00011630 +1

H -1.86050060 +1 0.96612195 +1 0.00014043 +1

H 3.05649183 +1 6.08940202 +1 -0.00190289 +1

H 1.71284734 +1 8.21778104 +1 -0.00233131 +1

H -1.98375616 +1 5.86117689 +1 -0.00027492 +1

H -2.07793015 +1 8.02799657 +1 -0.00011476 +1

H 3.24770559 +1 -0.97748322 +1 0.00059434 +1

H 3.80079749 +1 -3.23759866 +1 -0.88817854 +1

H 3.79825648 +1 -3.24028514 +1 0.88903072 +1

H 2.93155211 +1 -4.50658769 +1 -0.00275560 +1

H -2.61375625 +1 10.28540715 +1 -0.89024978 +1

H -2.61057776 +1 10.28884890 +1 0.88792196 +1

H -1.74879534 +1 11.55629426 +1 -0.00518644 +1

SUMMARY OF PM7 CALCULATION

MOPAC v22.0.4 Windows

Wed Nov 2 13:39:52 2022

Empirical Formula: C18 H14 N2 O4 = 38 atoms

PM7 PRECISE CHARGE=0 EF LET AUX XYZ BONDS GNORM=0.0100 CHARGE=0

Linker1b.mop

GEOMETRY OPTIMISED USING EIGENVECTOR FOLLOWING (EF).

SCF FIELD WAS ACHIEVED

HEAT OF FORMATION = -58.60994 KCAL/MOL = -245.22399 KJ/MOL

GRADIENT NORM = 618.14926 = 100.27705 PER ATOM

DIPOLE = 1.77738 DEBYE POINT GROUP: C2

NO. OF FILLED LEVELS = 60

IONIZATION POTENTIAL = 9.259763 EV

HOMO LUMO ENERGIES (EV) = -9.260 -2.189

MOLECULAR WEIGHT = 322.3196

COSMO AREA = 318.43 SQUARE ANGSTROMS

COSMO VOLUME = 352.16 CUBIC ANGSTROMS

MOLECULAR DIMENSIONS (Angstroms)

Atom Atom Distance

H 38 H 35 13.31264

H 29 H 25 7.84592

H 33 H 32 2.14859

SCF CALCULATIONS = 25

WALL-CLOCK TIME = 2.215 SECONDS

COMPUTATION TIME = 13.141 SECONDS

FINAL GEOMETRY OBTAINED

PM7 PRECISE CHARGE=0 EF LET AUX XYZ BONDS GNORM=0.0100 CHARGE=0

Linker2b.mop

C -0.04300501 +1 -0.18949526 +1 -0.01112951 +1

C 1.35046579 +1 -0.16533846 +1 -0.02438728 +1

C 2.10457660 +1 1.02402130 +1 -0.02063702 +1

C 1.44107319 +1 2.23620819 +1 0.00237077 +1

C -0.03760016 +1 2.29280766 +1 -0.02169181 +1

C -0.74236979 +1 1.03379307 +1 -0.01822453 +1

C 2.06999506 +1 3.54826817 +1 0.03362097 +1

C 1.35611578 +1 4.77530806 +1 -0.02109628 +1

C -0.11581682 +1 4.80059216 +1 -0.12209466 +1

C -0.81265914 +1 3.48595054 +1 -0.08593150 +1

C 2.04371587 +1 6.00202061 +1 -0.01674811 +1

C 1.35756225 +1 7.23669007 +1 -0.12446043 +1

C -0.03217276 +1 7.20524717 +1 -0.25329755 +1

C -0.79595193 +1 6.03448178 +1 -0.25676137 +1

O -1.99150278 +1 3.43444658 +1 -0.12172305 +1

O 3.33905732 +1 3.61867720 +1 0.09932529 +1

N -2.11878134 +1 6.05182838 +1 -0.44643794 +1

C -3.06670115 +1 7.01592294 +1 -0.23489616 +1

N 3.47596798 +1 0.95878851 +1 -0.08979679 +1

C 4.46248981 +1 0.05417349 +1 0.21101106 +1

C 3.98117286 +1 -1.17343627 +1 1.07128553 +1

O 5.49535865 +1 0.18563073 +1 -0.07185861 +1

C -2.74048764 +1 8.26506342 +1 0.57260664 +1

O -4.25639330 +1 6.83247297 +1 -0.66491778 +1

H -0.60255368 +1 -1.09580459 +1 -0.01150045 +1

H 1.85471238 +1 -1.15736891 +1 -0.08495445 +1

H -1.82408517 +1 1.07531094 +1 -0.03927761 +1

H 3.13442095 +1 5.97309378 +1 0.05528701 +1

H 1.91456729 +1 8.14129001 +1 -0.12033276 +1

H -0.52668624 +1 8.19427593 +1 -0.40174066 +1

H -2.57295075 +1 5.09022595 +1 -0.73517395 +1

H 3.92963859 +1 1.93284800 +1 -0.38934003 +1

H 3.19991192 +1 -0.92336721 +1 1.79740740 +1

H 3.63443727 +1 -2.00257504 +1 0.44067665 +1

H 4.85161012 +1 -1.55499540 +1 1.63971507 +1

H -2.02540466 +1 8.04416988 +1 1.36931319 +1

H -2.34193570 +1 9.06054134 +1 -0.06762842 +1

H -3.65795595 +1 8.66561052 +1 1.04567437 +1

SUMMARY OF PM7 CALCULATION

MOPAC v22.0.4 Windows

Wed Nov 2 12:00:36 2022

Empirical Formula: C18 H16 N2 O2 = 38 atoms

PM7 PRECISE CHARGE=0 EF LET AUX XYZ BONDS GNORM=0.0100 CHARGE=0

Linker2a.mop

GEOMETRY OPTIMISED USING EIGENVECTOR FOLLOWING (EF).

SCF FIELD WAS ACHIEVED

HEAT OF FORMATION = -6.27546 KCAL/MOL = -26.25653 KJ/MOL

GRADIENT NORM = 365.06485 = 59.22134 PER ATOM

DIPOLE = 0.56607 DEBYE POINT GROUP: C2h

NO. OF FILLED LEVELS = 55

IONIZATION POTENTIAL = 7.928705 EV

HOMO LUMO ENERGIES (EV) = -7.929 -0.919

MOLECULAR WEIGHT = 292.3366

COSMO AREA = 324.02 SQUARE ANGSTROMS

COSMO VOLUME = 344.23 CUBIC ANGSTROMS

MOLECULAR DIMENSIONS (Angstroms)

Atom Atom Distance

H 38 H 35 16.68357

H 25 H 28 6.14161

H 33 H 34 1.78989

SCF CALCULATIONS = 24

WALL-CLOCK TIME = 1.902 SECONDS

COMPUTATION TIME = 11.281 SECONDS

FINAL GEOMETRY OBTAINED

PM7 PRECISE CHARGE=0 EF LET AUX XYZ BONDS GNORM=0.0100

CHARGE=0

Linker2a.mop

C -0.05578948 +1 -0.21785328 +1 -0.00009923 +1

C 1.45536985 +1 -0.07140333 +1 -0.00021125 +1

C 2.03213133 +1 1.11624963 +1 -0.00029340 +1

C 1.36091930 +1 2.34032804 +1 -0.00007983 +1

C -0.07446478 +1 2.32994789 +1 0.00034637 +1

C -0.76954971 +1 0.99243930 +1 0.00019196 +1

C 2.04607379 +1 3.51635506 +1 -0.00008132 +1

C 1.23354305 +1 4.74853855 +1 0.00051664 +1

C -0.12689369 +1 4.67500402 +1 0.00113321 +1

C -0.81406032 +1 3.48965508 +1 0.00100966 +1

C 1.96914635 +1 6.04934437 +1 0.00054496 +1

C 1.21591636 +1 7.22849175 +1 0.00148193 +1

C -0.19725896 +1 7.15784837 +1 0.00243855 +1

C -0.85959835 +1 5.90049573 +1 0.00214150 +1

N -1.04242634 +1 8.21757136 +1 0.00427136 +1

C -0.75941567 +1 9.63300791 +1 0.00455957 +1

N 2.27004628 +1 -1.18119166 +1 0.00040833 +1

C 1.90941439 +1 -2.57123031 +1 0.00000442 +1

C 3.18738002 +1 -3.42503594 +1 0.00329053 +1

O 0.76386669 +1 -2.97712953 +1 -0.00222107 +1

C -1.96666831 +1 10.43931376 +1 0.00904914 +1

O 0.44743569 +1 10.01185855 +1 0.00152997 +1

H -0.51797239 +1 -1.16051310 +1 -0.00019515 +1

H 3.15582686 +1 1.17774095 +1 -0.00039880 +1

H -1.85638148 +1 0.98153714 +1 0.00035057 +1

H 3.10064612 +1 3.57541999 +1 -0.00040567 +1

H -1.90144828 +1 3.45804366 +1 0.00148192 +1

H 3.06102167 +1 6.05563204 +1 -0.00012413 +1

H 1.73081582 +1 8.20802276 +1 0.00155208 +1

H -1.95224819 +1 5.86352044 +1 0.00286949 +1

H -2.07081510 +1 8.01127942 +1 0.00610787 +1

H 3.25836800 +1 -0.97081253 +1 0.00150742 +1

H 3.80474610 +1 -3.20786525 +1 -0.88885686 +1

H 3.79756597 +1 -3.21073098 +1 0.90103224 +1

H 2.93866159 +1 -4.49798993 +1 0.00051350 +1

H -2.59695549 +1 10.23858899 +1 -0.88021543 +1

H -2.58840887 +1 10.24043796 +1 0.90475076 +1

H -1.73346383 +1 11.51801925 +1 0.00677703 +1

SUMMARY OF PM7 CALCULATION

MOPAC v22.0.4 Windows

Wed Nov 2 13:39:56 2022

Empirical Formula: C18 H16 N2 O2 = 38 atoms

PM7 PRECISE CHARGE=0 EF LET AUX XYZ BONDS GNORM=0.0100 CHARGE=0

Linker2b.mop

GEOMETRY OPTIMISED USING EIGENVECTOR FOLLOWING (EF).

SCF FIELD WAS ACHIEVED

HEAT OF FORMATION = 0.07035 KCAL/MOL = 0.29432 KJ/MOL

GRADIENT NORM = 462.27429 = 74.99079 PER ATOM

DIPOLE = 0.81052 DEBYE POINT GROUP: C2h

NO. OF FILLED LEVELS = 55

IONIZATION POTENTIAL = 7.823330 EV

HOMO LUMO ENERGIES (EV) = -7.823 -1.038

MOLECULAR WEIGHT = 292.3366

COSMO AREA = 318.44 SQUARE ANGSTROMS

COSMO VOLUME = 343.38 CUBIC ANGSTROMS

MOLECULAR DIMENSIONS (Angstroms)

Atom Atom Distance

H 37 H 34 13.89942

H 29 H 23 9.17926

H 35 H 36 1.78067

SCF CALCULATIONS = 25

WALL-CLOCK TIME = 2.273 SECONDS

COMPUTATION TIME = 13.406 SECONDS

FINAL GEOMETRY OBTAINED

PM7 PRECISE CHARGE=0 EF LET AUX XYZ BONDS GNORM=0.0100 CHARGE=0

Linker2b.mop

C -0.04571299 +1 -0.14953506 +1 0.00003004 +1

C 1.41051499 +1 -0.14992534 +1 0.00005206 +1

C 2.08392385 +1 1.03084231 +1 0.00004172 +1

C 1.38526978 +1 2.29149067 +1 0.00015874 +1

C -0.06840080 +1 2.28283741 +1 0.00012004 +1

C -0.69755434 +1 1.00868645 +1 0.00000806 +1

C 1.99148258 +1 3.55763495 +1 0.00035564 +1

C 1.36029027 +1 4.72909538 +1 0.00037697 +1

C -0.10130341 +1 4.72254547 +1 0.00028215 +1

C -0.70018509 +1 3.44614776 +1 0.00022117 +1

C	2.00871256 +1	5.98118233 +1	0.00050430 +1
C	1.31953877 +1	7.18212605 +1	0.00062731 +1
C	-0.10925042 +1	7.19138512 +1	0.00053022 +1
C	-0.81842629 +1	5.95722778 +1	0.00029193 +1
N	3.45443735 +1	1.19479864 +1	-0.00072779 +1
N	-2.16292242 +1	5.82462326 +1	-0.00055001 +1
C	-3.19465478 +1	6.87523726 +1	0.00199663 +1
C	4.47867435 +1	0.07355889 +1	0.00198630 +1
O	-2.89950292 +1	8.07080108 +1	0.00554378 +1
C	-4.55450716 +1	6.27130731 +1	-0.00062832 +1
O	4.19520916 +1	-1.00255477 +1	0.00502778 +1
C	5.84678865 +1	0.73939487 +1	-0.00063941 +1
H	-0.54468026 +1	-1.12661869 +1	-0.00004422 +1
H	1.92716029 +1	-1.12611305 +1	0.00003437 +1
H	-1.83197898 +1	1.01589492 +1	-0.00008580 +1
H	3.14167350 +1	3.59830680 +1	0.00057364 +1
H	-1.84977977 +1	3.41526314 +1	0.00031995 +1
H	3.11889014 +1	5.99660175 +1	0.00052350 +1
H	1.83561852 +1	8.13891404 +1	0.00072394 +1
H	-0.63460302 +1	8.13520819 +1	0.00059426 +1
H	3.84892385 +1	2.11622658 +1	-0.00268959 +1
H	-2.55788742 +1	4.89651068 +1	-0.00266395 +1
H	-4.73268282 +1	5.63987998 +1	0.88644583 +1
H	-5.32562100 +1	7.06007282 +1	0.00320027 +1

H -4.73253582 +1 5.64854456 +1 -0.89384162 +1

H 6.02192119 +1 1.37126316 +1 0.88678279 +1

H 6.61796196 +1 -0.04941424 +1 0.00296592 +1

H 6.02182195 +1 1.36314246 +1 -0.89381938 +1

SUMMARY OF PM7 CALCULATION

MOPAC v22.0.4 Windows

Wed Nov 2 13:56:07 2022

Empirical Formula: C14 H14 N2 O2 = 32 atoms

PM7 PRECISE CHARGE=0 EF LET AUX XYZ BONDS GNORM=0.0100 CHARGE=0

Linker3a.mop

GEOMETRY OPTIMISED USING EIGENVECTOR FOLLOWING (EF).

SCF FIELD WAS ACHIEVED

HEAT OF FORMATION = -15.69393 KCAL/MOL = -65.66342 KJ/MOL

GRADIENT NORM = 534.43104 = 94.47495 PER ATOM

DIPOLE = 0.94800 DEBYE POINT GROUP: C2h

NO. OF FILLED LEVELS = 46

IONIZATION POTENTIAL = 8.589788 EV

HOMO LUMO ENERGIES (EV) = -8.590 -0.624

MOLECULAR WEIGHT = 242.2768

COSMO AREA = 277.39 SQUARE ANGSTROMS

COSMO VOLUME = 288.19 CUBIC ANGSTROMS

MOLECULAR DIMENSIONS (Angstroms)

Atom Atom Distance

H 32 H 28 14.35749

H 22 H 21 5.47949

H 31 H 30 1.78598

SCF CALCULATIONS = 27

WALL-CLOCK TIME = 1.508 SECONDS

COMPUTATION TIME = 8.984 SECONDS

FINAL GEOMETRY OBTAINED

PM7 PRECISE CHARGE=0 EF LET AUX XYZ BONDS GNORM=0.0100 CHARGE=0

linker3a.mop

C -0.01603551 +1 -0.12660551 +1 -0.00005234 +1

C 1.46338925 +1 -0.02525964 +1 -0.00002336 +1

C 2.08259400 +1 1.14947536 +1 -0.00006508 +1

C 1.31191827 +1 2.43315750 +1 -0.00028031 +1

C -0.10307445 +1 2.29263313 +1 -0.00034027 +1

C -0.72270093 +1 1.05060495 +1 -0.00013624 +1

C 1.94364968 +1 3.69407948 +1 -0.00052166 +1

C 1.26059209 +1 4.76302241 +1 -0.00095948 +1

C -0.15390161 +1 4.72796416 +1 -0.00109789 +1

C -0.83810240 +1 3.49445717 +1 -0.00071506 +1

N	2.21646251 +1	-1.22035201 +1	0.00017496 +1
C	1.92983445 +1	-2.49950290 +1	-0.00045726 +1
C	3.16925768 +1	-3.41317598 +1	0.00069689 +1
O	0.79541334 +1	-2.91963103 +1	-0.00159463 +1
N	-1.04177563 +1	5.91199982 +1	-0.00146791 +1
C	-0.63621756 +1	7.19638343 +1	-0.00262980 +1
C	-1.93291703 +1	8.10011393 +1	-0.00196672 +1
O	0.39903187 +1	7.60394153 +1	-0.00372615 +1
H	-0.50325708 +1	-1.12215946 +1	0.00001754 +1
H	3.15577755 +1	1.24559884 +1	0.00001457 +1
H	-1.82385912 +1	1.00988541 +1	-0.00007628 +1
H	3.05975574 +1	3.67595063 +1	-0.00032195 +1
H	1.74984162 +1	5.80542485 +1	-0.00125881 +1
H	-1.91939695 +1	3.45117457 +1	-0.00074648 +1
H	3.30467607 +1	-0.93323551 +1	0.00084898 +1
H	3.78300983 +1	-3.19468099 +1	-0.88794006 +1
H	3.77907575 +1	-3.19747804 +1	0.89259248 +1
H	2.91388339 +1	-4.45261532 +1	-0.00157323 +1
H	-2.03866594 +1	5.62092312 +1	-0.00082754 +1
H	-2.55670931 +1	7.89489772 +1	-0.89329390 +1
H	-2.55295864 +1	7.89840967 +1	0.89268719 +1
H	-1.67385545 +1	9.15216533 +1	-0.00463747 +1

SUMMARY OF PM7 CALCULATION

MOPAC v22.0.4 Windows

Wed Nov 2 13:39:17 2022

Empirical Formula: C14 H14 N2 O2 = 32 atoms

PM7 PRECISE CHARGE=0 EF LET AUX XYZ BONDS GNORM=0.0100 CHARGE=0

Linker3b.mop

GEOMETRY OPTIMISED USING EIGENVECTOR FOLLOWING (EF).

SCF FIELD WAS ACHIEVED

HEAT OF FORMATION = -57.32892 KCAL/MOL = -239.86420 KJ/MOL

GRADIENT NORM = 0.00988 = 0.00175 PER ATOM

DIPOLE = 2.81500 DEBYE POINT GROUP: C2

NO. OF FILLED LEVELS = 46

IONIZATION POTENTIAL = 8.320379 EV

HOMO LUMO ENERGIES (EV) = -8.320 -0.646

MOLECULAR WEIGHT = 242.2768

COSMO AREA = 270.96 SQUARE ANGSTROMS

COSMO VOLUME = 285.82 CUBIC ANGSTROMS

MOLECULAR DIMENSIONS (Angstroms)

Atom Atom Distance

H 32 H 28 12.77209

H 19 H 23 7.15562

O 18 H 27 1.71715

SCF CALCULATIONS = 219

WALL-CLOCK TIME = 13.277 SECONDS

COMPUTATION TIME = 1 MINUTE AND 17.922 SECONDS

FINAL GEOMETRY OBTAINED

PM7 PRECISE CHARGE=0 EF LET AUX XYZ BONDS GNORM=0.0100 CHARGE=0

Linker3b.mop

C 0.06955231 +1 -0.12757169 +1 0.04047244 +1

C 1.47711038 +1 -0.07525790 +1 0.10607758 +1

C 2.11938207 +1 1.14509295 +1 0.14196740 +1

C 1.36454734 +1 2.37271680 +1 0.10877846 +1

C -0.04560108 +1 2.29559660 +1 0.10832508 +1

C -0.67558210 +1 1.02317452 +1 0.05074646 +1

C 1.99457220 +1 3.64517054 +1 0.05238186 +1

C 1.24943724 +1 4.79591769 +1 0.04234529 +1

C -0.15816218 +1 4.74356853 +1 0.10705127 +1

C -0.80046561 +1 3.52320053 +1 0.14183645 +1

N 3.52678450 +1 1.23381390 +1 0.24829751 +1

C 4.41467668 +1 0.24607931 +1 -0.18775565 +1

C 5.86590220 +1 0.59600924 +1 -0.00069568 +1

O	4.03650198 +1	-0.79421092 +1	-0.67068807 +1
N	-2.20791627 +1	3.43437225 +1	0.24738492 +1
C	-3.09566584 +1	4.42258156 +1	-0.18788872 +1
C	-4.54695443 +1	4.07253963 +1	-0.00150007 +1
O	-2.71735442 +1	5.46334800 +1	-0.66968564 +1
H	-0.41293482 +1	-1.10384055 +1	-0.01568440 +1
H	2.03604535 +1	-1.01380437 +1	0.12198489 +1
H	-1.75840155 +1	0.95561944 +1	-0.01106135 +1
H	3.07742951 +1	3.71275821 +1	-0.00869962 +1
H	1.73195781 +1	5.77222389 +1	-0.01289704 +1
H	-0.71708833 +1	5.68211770 +1	0.12318069 +1
H	3.90017999 +1	2.10285006 +1	0.61515040 +1
H	6.16268135 +1	1.45960460 +1	-0.61062227 +1
H	6.11234193 +1	0.80981714 +1	1.04718763 +1
H	6.49850789 +1	-0.25164319 +1	-0.31543207 +1
H	-2.58147619 +1	2.56497805 +1	0.61323703 +1
H	-4.84369725 +1	3.20965150 +1	-0.61244108 +1
H	-4.79361179 +1	3.85759835 +1	1.04610271 +1
H	-5.17943514 +1	4.92059255 +1	-0.31541075 +1

SUMMARY OF PM7 CALCULATION

MOPAC v22.0.4 Windows

Wed Nov 2 14:00:10 2022

Empirical Formula: C16 H16 N2 O2 = 36 atoms

PM7 PRECISE CHARGE=0 EF LET AUX XYZ BONDS GNORM=0.0100 CHARGE=0

linker4b-cis.mop

GEOMETRY OPTIMISED USING EIGENVECTOR FOLLOWING (EF).

SCF FIELD WAS ACHIEVED

HEAT OF FORMATION = -11.81515 KCAL/MOL = -49.43459 KJ/MOL

GRADIENT NORM = 411.31242 = 68.55207 PER ATOM

DIPOLE = 7.73663 DEBYE POINT GROUP: C2v

NO. OF FILLED LEVELS = 51

IONIZATION POTENTIAL = 8.168319 EV

HOMO LUMO ENERGIES (EV) = -8.168 -0.184

MOLECULAR WEIGHT = 268.3146

COSMO AREA = 307.25 SQUARE ANGSTROMS

COSMO VOLUME = 320.92 CUBIC ANGSTROMS

MOLECULAR DIMENSIONS (Angstroms)

Atom		Atom		Distance
H	31	O	20	11.83697
H	35	H	23	8.73330
H	36	H	32	1.81939

SCF CALCULATIONS = 29

WALL-CLOCK TIME = 1.992 SECONDS

COMPUTATION TIME = 11.906 SECONDS

FINAL GEOMETRY OBTAINED

PM7 PRECISE CHARGE=0 EF LET AUX XYZ BONDS GNORM=0.0100 CHARGE=0

linker4b-cis.mop

C -0.08782493 +1 -0.00221386 +1 -0.00199088 +1

C 1.45120634 +1 -0.04543185 +1 -0.00061144 +1

C -0.72754241 +1 1.16526281 +1 -0.00052099 +1

C 0.00548327 +1 2.37512983 +1 0.00110483 +1

C 1.39888556 +1 2.38325863 +1 0.00118646 +1

C 2.09365435 +1 1.20481677 +1 0.00059231 +1

C -2.19336421 +1 1.17715411 +1 -0.00084675 +1

C -2.97552349 +1 2.25839506 +1 -0.01517663 +1

C -4.38912594 +1 2.27311522 +1 -0.01607779 +1

C -5.05209394 +1 0.96760731 +1 -0.00060829 +1

C -2.80863351 +1 -0.10250675 +1 0.01531117 +1

C -4.25185326 +1 -0.21724142 +1 0.01472458 +1

N 1.90184338 +1 -1.30224941 +1 -0.00111840 +1

C 3.37320353 +1 -1.68179375 +1 -0.00093475 +1

C	3.49063571 +1	-3.15515208 +1	-0.00411895 +1
O	4.19277383 +1	-0.86229736 +1	0.00115811 +1
N	-4.70799129 +1	-1.49783684 +1	0.02972698 +1
C	-6.08210206 +1	-1.97377813 +1	0.03478511 +1
C	-6.16434284 +1	-3.44298133 +1	0.05478098 +1
O	-7.04016969 +1	-1.16715279 +1	0.02302878 +1
H	-0.53453659 +1	-0.94674506 +1	-0.00408282 +1
H	-0.54519397 +1	3.36549642 +1	0.00257207 +1
H	1.92540979 +1	3.31935520 +1	0.00165752 +1
H	3.20293015 +1	1.18371786 +1	0.00093811 +1
H	-2.50301798 +1	3.31537278 +1	-0.02874224 +1
H	-4.96898856 +1	3.12283355 +1	-0.02661374 +1
H	-6.12003557 +1	0.91966300 +1	-0.00087706 +1
H	-2.27055955 +1	-0.99830978 +1	0.02800906 +1
H	1.29048562 +1	-2.07965146 +1	-0.00244858 +1
H	3.04956595 +1	-3.63756740 +1	0.88463809 +1
H	4.57608825 +1	-3.44217234 +1	-0.00310159 +1
H	3.05251149 +1	-3.63301164 +1	-0.89687241 +1
H	-4.02072166 +1	-2.23643803 +1	0.03986197 +1
H	-5.69289355 +1	-3.89760359 +1	-0.82621317 +1
H	-7.23138913 +1	-3.78643176 +1	0.05756371 +1
H	-5.69627839 +1	-3.87288238 +1	0.94996566 +1

SUMMARY OF PM7 CALCULATION

MOPAC v22.0.4 Windows

Wed Nov 2 13:38:44 2022

Empirical Formula: C16 H16 N2 O2 = 36 atoms

PM7 PRECISE CHARGE=0 EF LET AUX XYZ BONDS GNORM=0.0100 CHARGE=0

linker 4b - trans.mop

GEOMETRY OPTIMISED USING EIGENVECTOR FOLLOWING (EF).

SCF FIELD WAS ACHIEVED

HEAT OF FORMATION = -17.73992 KCAL/MOL = -74.22382 KJ/MOL

GRADIENT NORM = 378.32128 = 63.05355 PER ATOM

DIPOLE = 0.48332 DEBYE POINT GROUP: C2h

NO. OF FILLED LEVELS = 51

IONIZATION POTENTIAL = 8.847141 EV

HOMO LUMO ENERGIES (EV) = -8.847 -0.750

MOLECULAR WEIGHT = 268.3146

COSMO AREA = 308.61 SQUARE ANGSTROMS

COSMO VOLUME = 323.71 CUBIC ANGSTROMS

MOLECULAR DIMENSIONS (Angstroms)

Atom Atom Distance

H 35 H 31 15.13727

H 28 H 23 7.56465

H 34 H 36 1.77406

SCF CALCULATIONS = 38

WALL-CLOCK TIME = 2.609 SECONDS

COMPUTATION TIME = 15.516 SECONDS

FINAL GEOMETRY OBTAINED

PM7 PRECISE CHARGE=0 EF LET AUX XYZ BONDS GNORM=0.0100 CHARGE=0

linker 4b - trans.mop

C 0.01918073 +1 -0.10450121 +1 -0.00252339 +1

C 1.41328324 +1 -0.07710307 +1 -0.00136825 +1

C -0.73927216 +1 1.16594467 +1 0.00326880 +1

C 0.00389915 +1 2.31598205 +1 0.00707728 +1

C 1.34403018 +1 2.33723280 +1 0.00489305 +1

C 2.11406837 +1 1.14023911 +1 0.00140992 +1

C -2.18382615 +1 1.07212543 +1 0.00106132 +1

C -2.85192890 +1 2.28441832 +1 -0.03564259 +1

C -4.38741416 +1 2.21032514 +1 -0.03703572 +1

C -5.03387514 +1 1.03853259 +1 -0.00833372 +1

C	-2.91154197 +1	-0.21458018 +1	0.03424510 +1
C	-4.32042475 +1	-0.19415800 +1	0.02685877 +1
N	-4.94389702 +1	3.49767122 +1	-0.07190229 +1
C	-6.25547044 +1	3.83772632 +1	-0.08556629 +1
C	-6.48241355 +1	5.36515646 +1	-0.12702326 +1
O	-7.15911775 +1	3.01690883 +1	-0.06719448 +1
N	1.97994163 +1	-1.33126175 +1	-0.00345561 +1
C	3.32271775 +1	-1.71990802 +1	-0.00518478 +1
C	3.56080597 +1	-3.18291136 +1	-0.00929869 +1
O	4.24684686 +1	-0.81769677 +1	-0.00357200 +1
H	-0.52580902 +1	-1.03142202 +1	-0.00809274 +1
H	-0.55188918 +1	3.28041620 +1	0.01207134 +1
H	1.91221592 +1	3.30330503 +1	0.00581832 +1
H	3.21233969 +1	1.16536990 +1	0.00086598 +1
H	-2.41074958 +1	3.17225781 +1	-0.06092430 +1
H	-6.12473846 +1	0.99835273 +1	-0.01117961 +1
H	-2.37830754 +1	-1.10084119 +1	0.06166012 +1
H	-4.81909438 +1	-1.12013057 +1	0.04849599 +1
H	-4.23158239 +1	4.29856739 +1	-0.08990300 +1
H	-6.02571077 +1	5.82646433 +1	0.74939432 +1
H	-7.53162597 +1	5.59396775 +1	-0.13698749 +1
H	-6.01920290 +1	5.77908912 +1	-1.02343020 +1
H	1.31638028 +1	-2.12130016 +1	-0.00442104 +1
H	3.10529877 +1	-3.64762323 +1	0.87684815 +1

H 4.62114022 +1 -3.42996529 +1 -0.01058530 +1

H 3.10425448 +1 -3.64259916 +1 -0.89740461 +1

SUMMARY OF PM7 CALCULATION

MOPAC v22.0.4 Windows

Wed Nov 2 13:38:56 2022

Empirical Formula: C16 H16 N2 O2 = 36 atoms

PM7 PRECISE CHARGE=0 EF LET AUX XYZ BONDS GNORM=0.0100 CHARGE=0

linker 4a.mop

GEOMETRY OPTIMISED USING EIGENVECTOR FOLLOWING (EF).

SCF FIELD WAS ACHIEVED

HEAT OF FORMATION = -12.82549 KCAL/MOL = -53.66187 KJ/MOL

GRADIENT NORM = 416.69769 = 69.44962 PER ATOM

DIPOLE = 0.58005 DEBYE POINT GROUP: C2h

NO. OF FILLED LEVELS = 51

IONIZATION POTENTIAL = 8.353665 EV

HOMO LUMO ENERGIES (EV) = -8.354 -0.704

MOLECULAR WEIGHT = 268.3146

COSMO AREA = 304.14 SQUARE ANGSTROMS

COSMO VOLUME = 321.51 CUBIC ANGSTROMS

MOLECULAR DIMENSIONS (Angstroms)

Atom Atom Distance

H 36 H 33 14.58560

H 21 H 27 6.62547

H 34 H 35 1.80823

SCF CALCULATIONS = 41

WALL-CLOCK TIME = 2.914 SECONDS

COMPUTATION TIME = 17.438 SECONDS

FINAL GEOMETRY OBTAINED

PM7 PRECISE CHARGE=0 EF LET AUX XYZ BONDS GNORM=0.0100 CHARGE=0

linker 4aSSSS.mop

C -0.10191913 +1 -0.09749257 +1 0.00032762 +1

C 1.35510465 +1 -0.10677043 +1 0.00021533 +1

C 1.96365474 +1 1.09697183 +1 -0.00014163 +1

C 1.21702676 +1 2.27648450 +1 -0.00112699 +1

C -0.06879661 +1 2.30993245 +1 -0.00117632 +1

C -0.78901597 +1 1.03432914 +1 -0.00001107 +1

C -0.88896179 +1 3.54027636 +1 -0.00262215 +1

C -2.32288276 +1 3.54289482 +1 -0.01023254 +1

C -3.06799255 +1 4.81295823 +1 -0.01184509 +1

C -2.37306227 +1 6.02459165 +1 -0.00662040 +1

C -0.93862822 +1 6.01106304 +1 0.00110127 +1

C -0.17982569 +1 4.85626485 +1 0.00368368 +1

N -2.96370522 +1 7.24521931 +1 -0.00788932 +1

N 1.94591788 +1 -1.35549301 +1 0.00087408 +1

C 3.28276594 +1 -1.79817434 +1 -0.00176780 +1

C 4.41476259 +1 -0.80351722 +1 -0.00714879 +1

O 3.47936888 +1 -2.98153985 +1 0.00016677 +1

C -4.35000086 +1 7.63219438 +1 -0.01780037 +1

C -5.42512116 +1 6.73342167 +1 -0.02941852 +1

O -4.51129067 +1 8.89915896 +1 -0.01522746 +1

H -0.62894009 +1 -1.07435446 +1 0.00076647 +1

H 3.08733355 +1 1.18040538 +1 0.00065426 +1

H 1.82047552 +1 3.24980156 +1 -0.00189138 +1

H -1.89150725 +1 1.02428355 +1 0.00062766 +1

H -2.84247069 +1 2.64832023 +1 -0.01459109 +1

H -4.08378870 +1 4.70504272 +1 -0.01666194 +1

H -0.39983261 +1 6.94513735 +1 0.00533938 +1

H 0.84187850 +1 4.85122503 +1 0.00973641 +1

H -2.31378115 +1 8.08517643 +1 -0.00086175 +1

H 1.28584350 +1 -2.19424799 +1 0.00362780 +1

H 4.40439239 +1 -0.15608615 +1 -0.90867001 +1

H 4.41279418 +1 -0.15627360 +1 0.89458098 +1

H 5.39058446 +1 -1.33913257 +1 -0.01166258 +1

H -5.43302806 +1 6.04436847 +1 -0.93437462 +1

H -5.45108502 +1 6.04281235 +1 0.87381405 +1

H -6.41484904 +1 7.22653797 +1 -0.03885105 +1

5.2. Appendix of Chapter 3

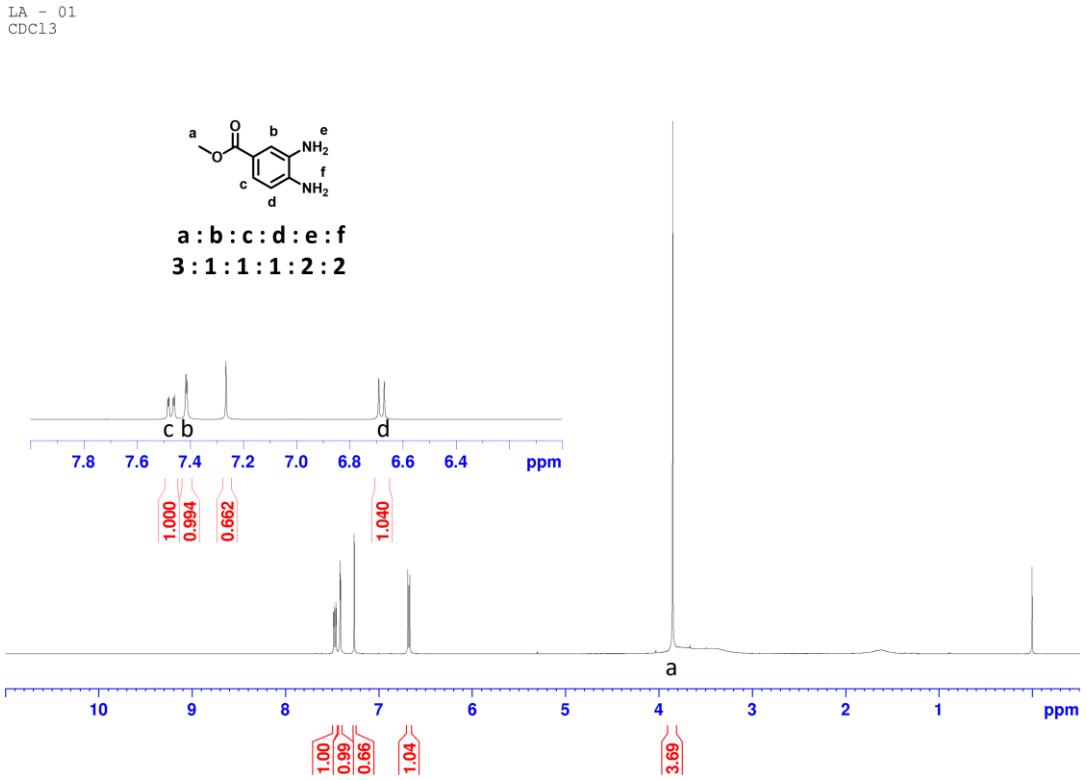

Spectrum S3-12: ^{1}H NMR spectrum of Compound **L_A-1**

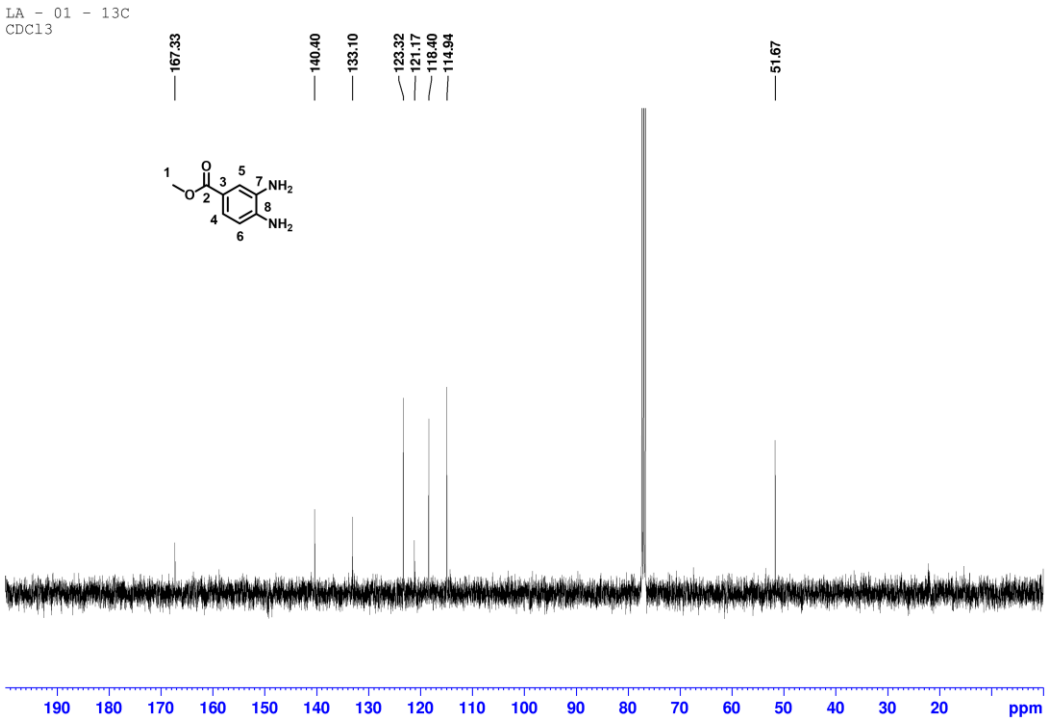

Spectrum S3-13: ^{13}C NMR spectrum of Compound **L_A-1**

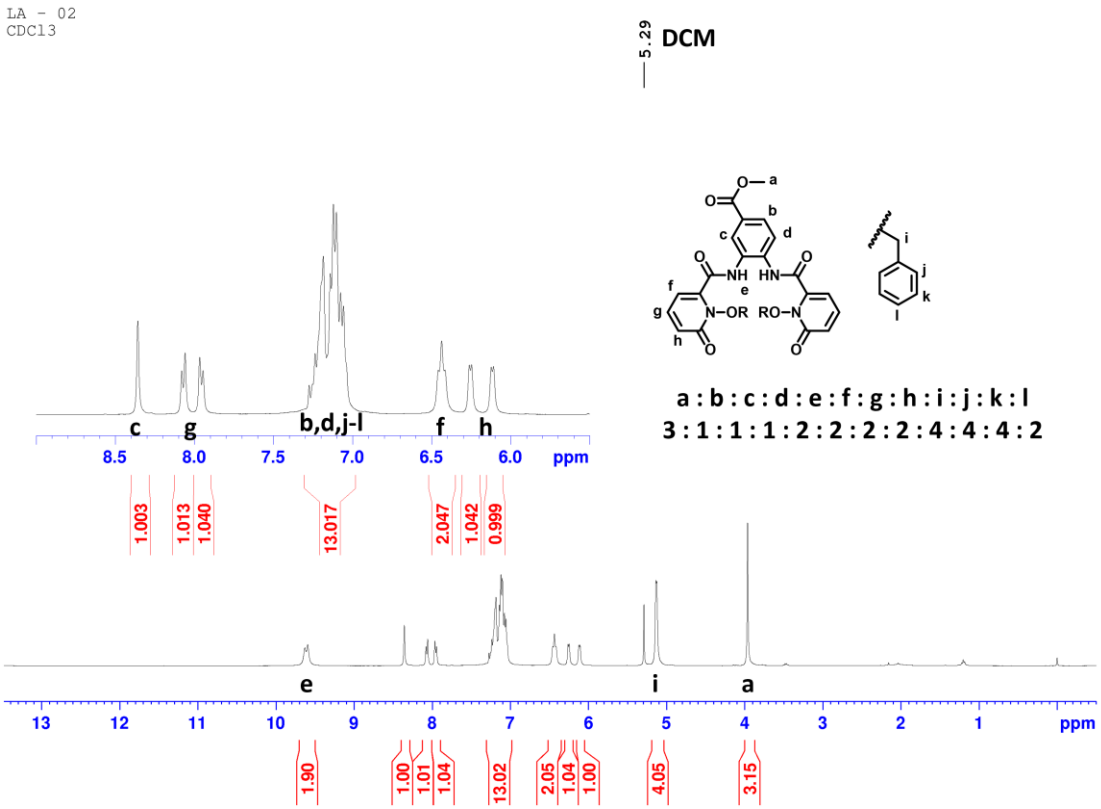

Spectrum S3-14: ^{1}H NMR spectrum of Compound **L_A-2**

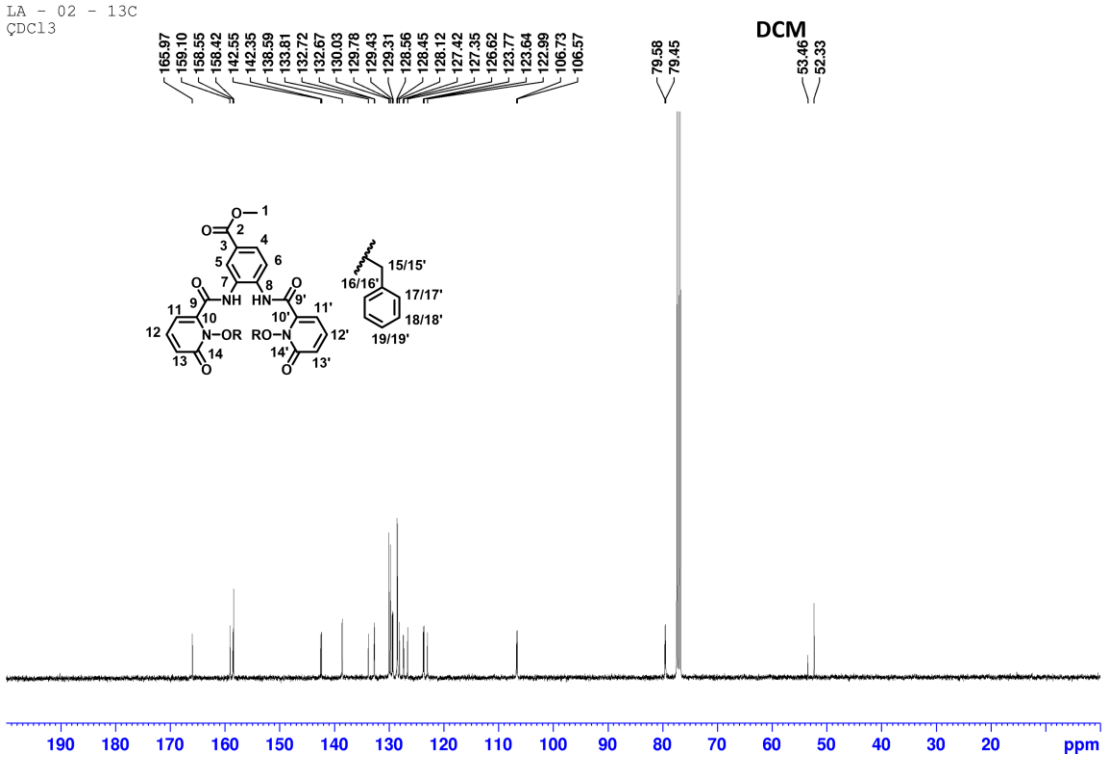

Spectrum S3-15: ^{13}C NMR spectrum of Compound **L_A-1**

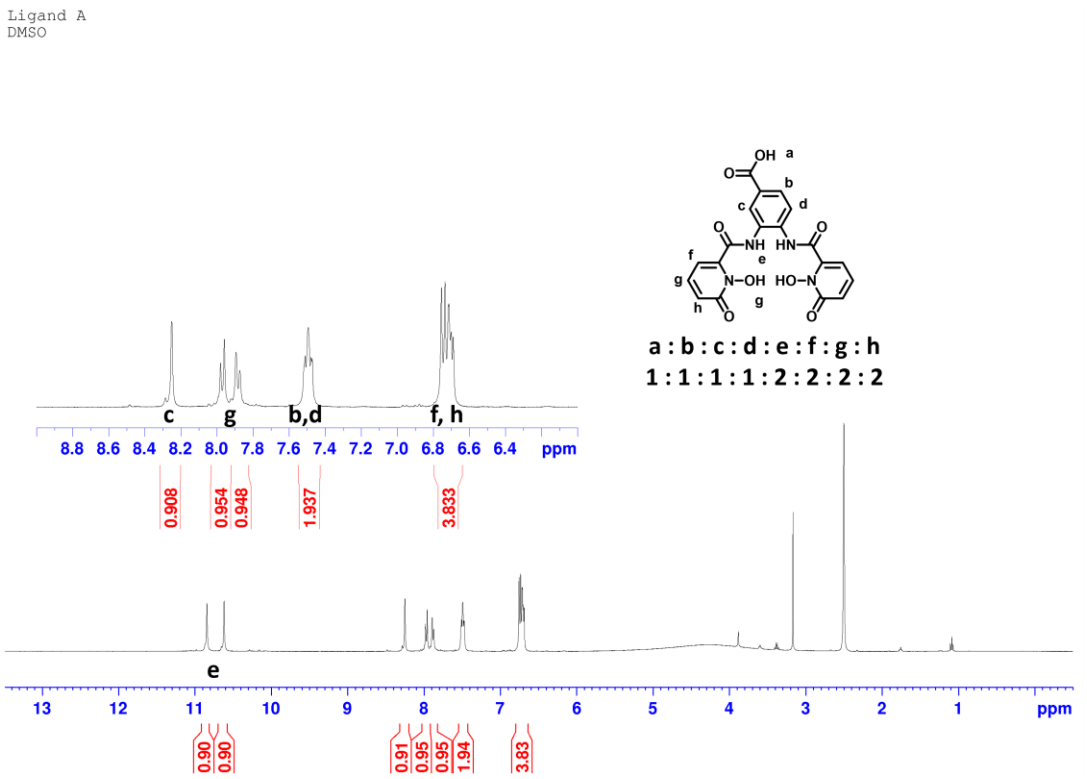

Spectrum S3-16: ^{1}H NMR spectrum of ligand $\mathbf{L_A}$

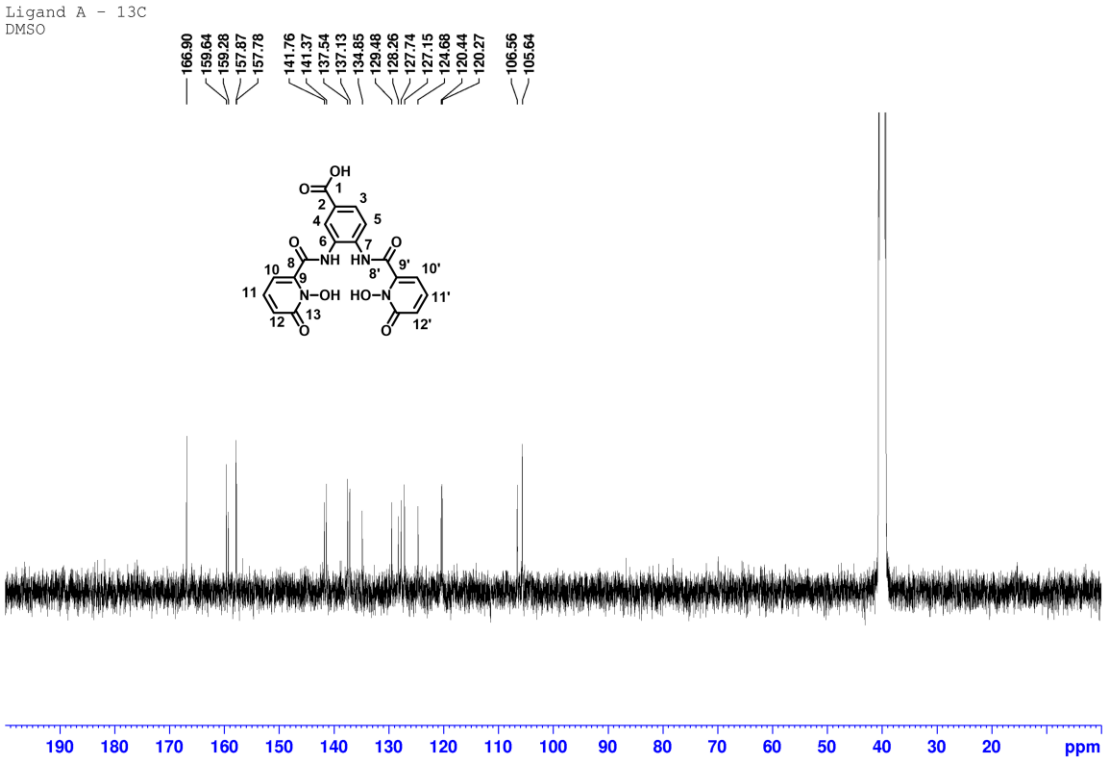

Spectrum S3-17: ^{13}C NMR spectrum of ligand $\mathbf{L_A}$

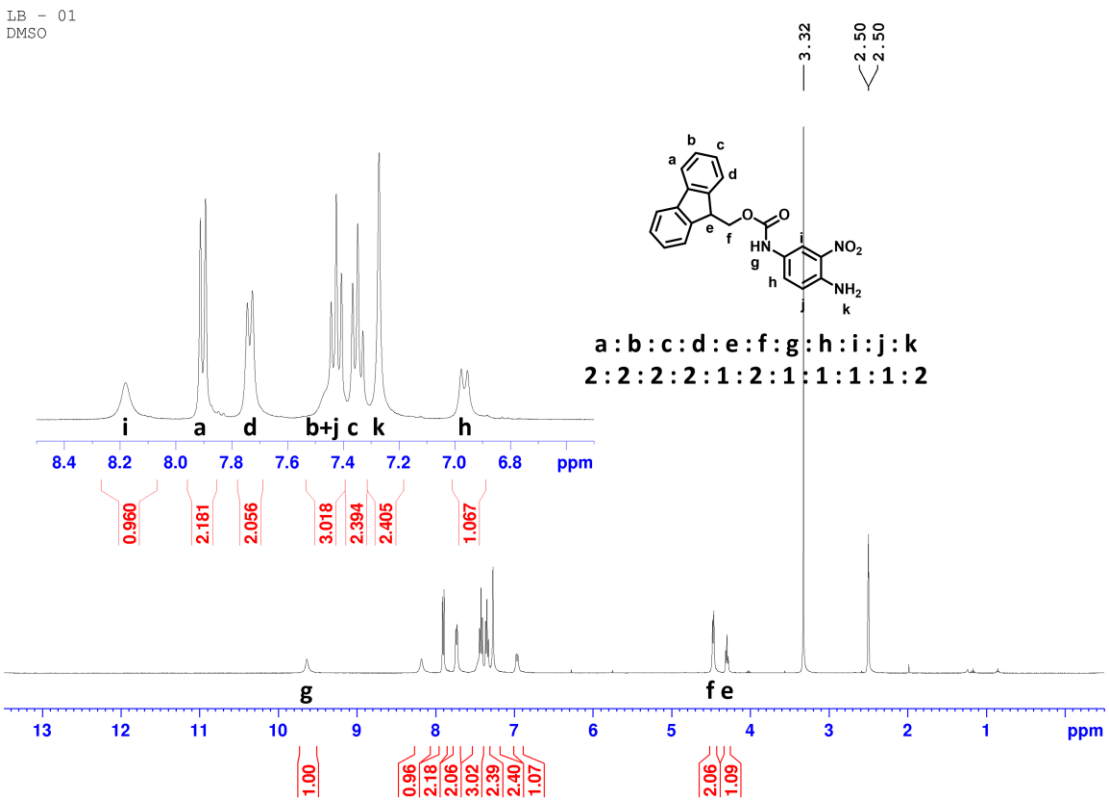

Spectrum S3-18: ^{1}H NMR spectrum of Compound **L_B-1**

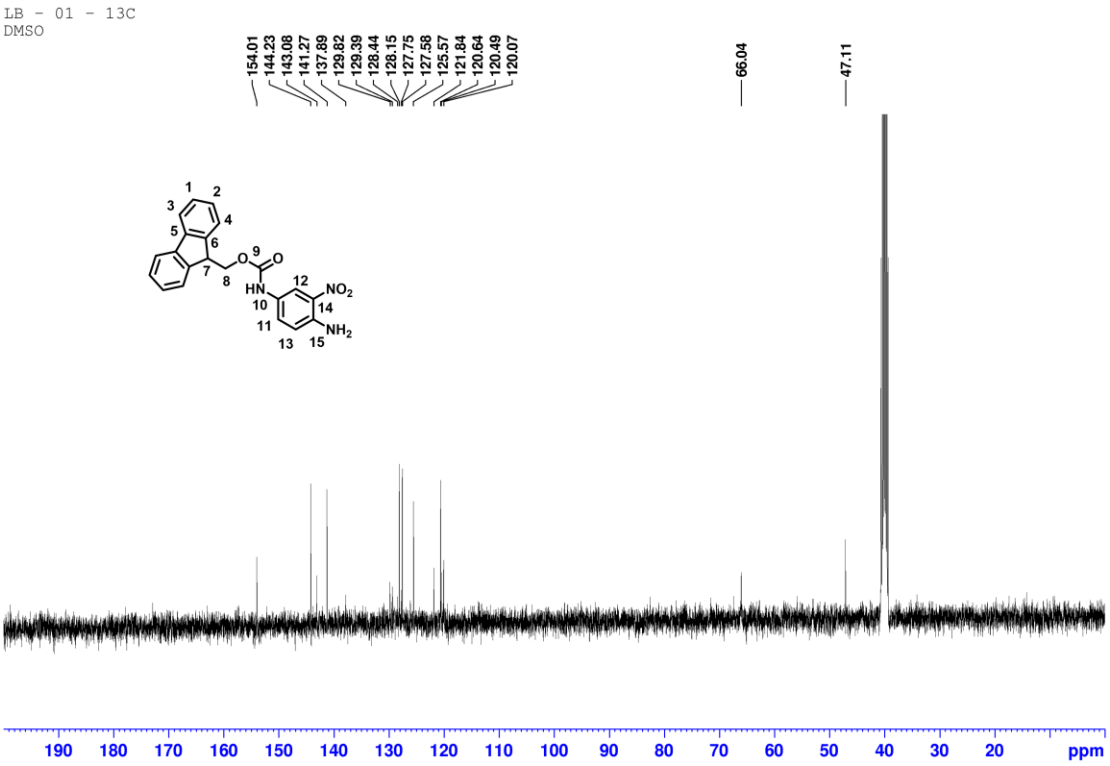

Spectrum S3-19: ^{13}C NMR spectrum of Compound **L_B-1**

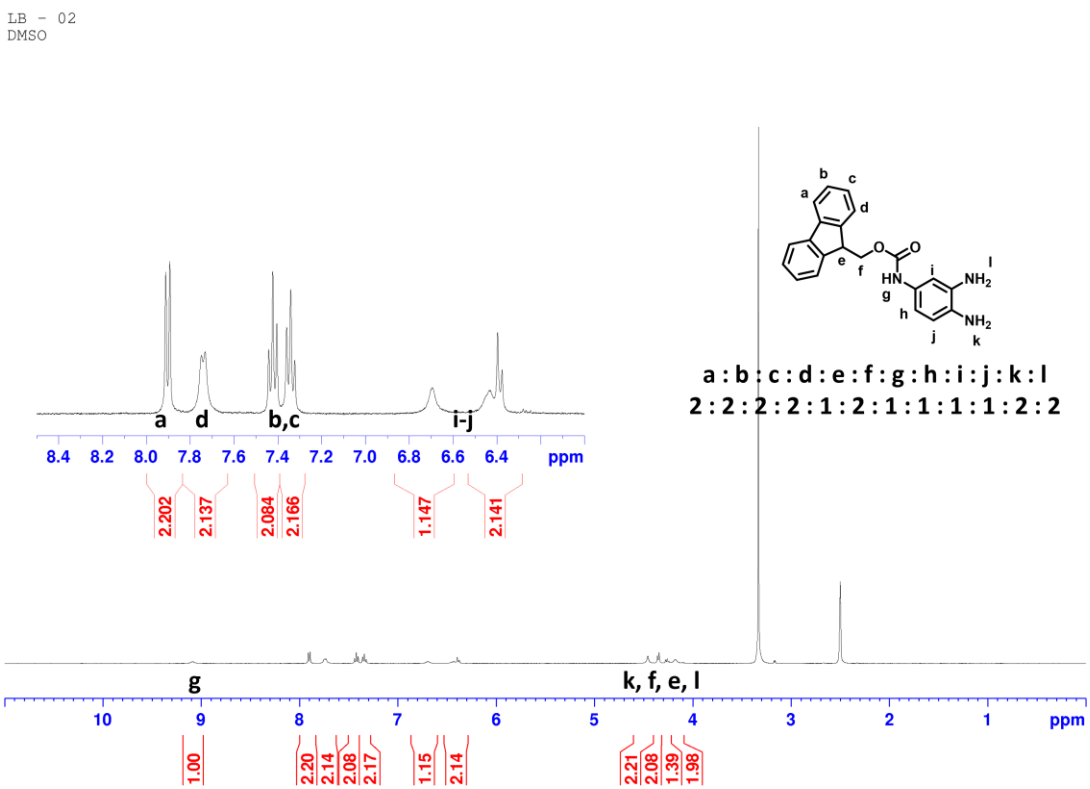

Spectrum S3-20: ^{1}H NMR spectrum of Compound **L_B-2**

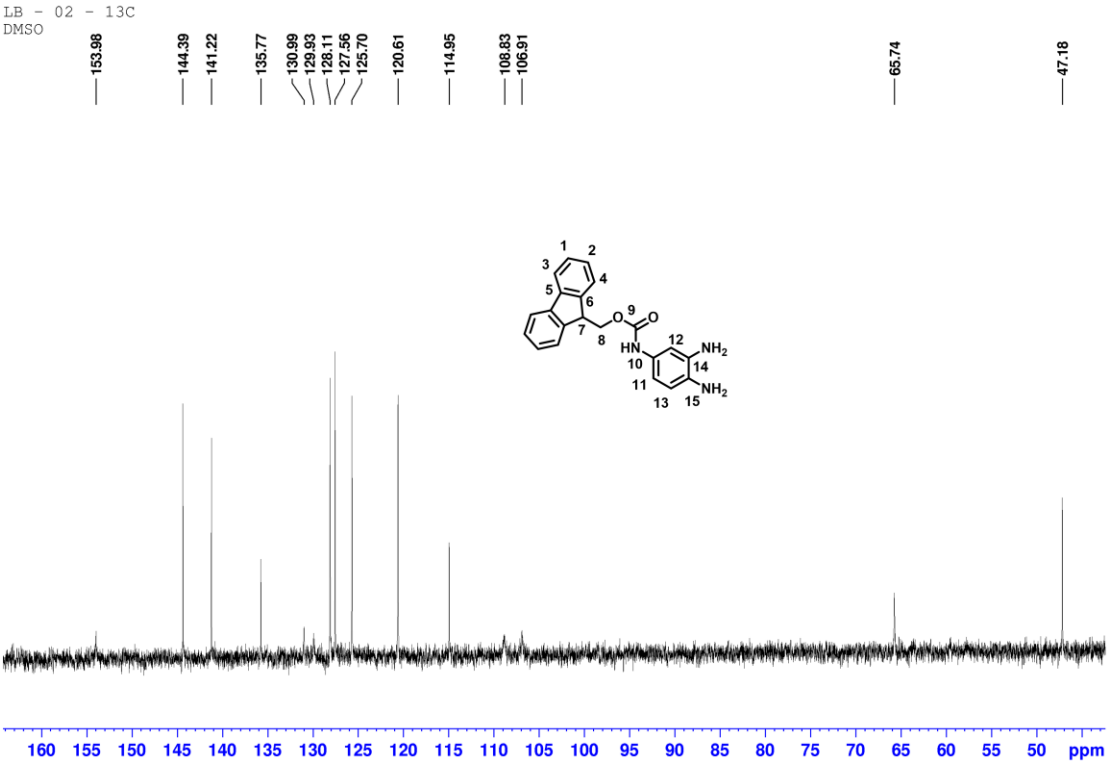

Spectrum S3-21: ^{13}C NMR spectrum of Compound **L_B-2**

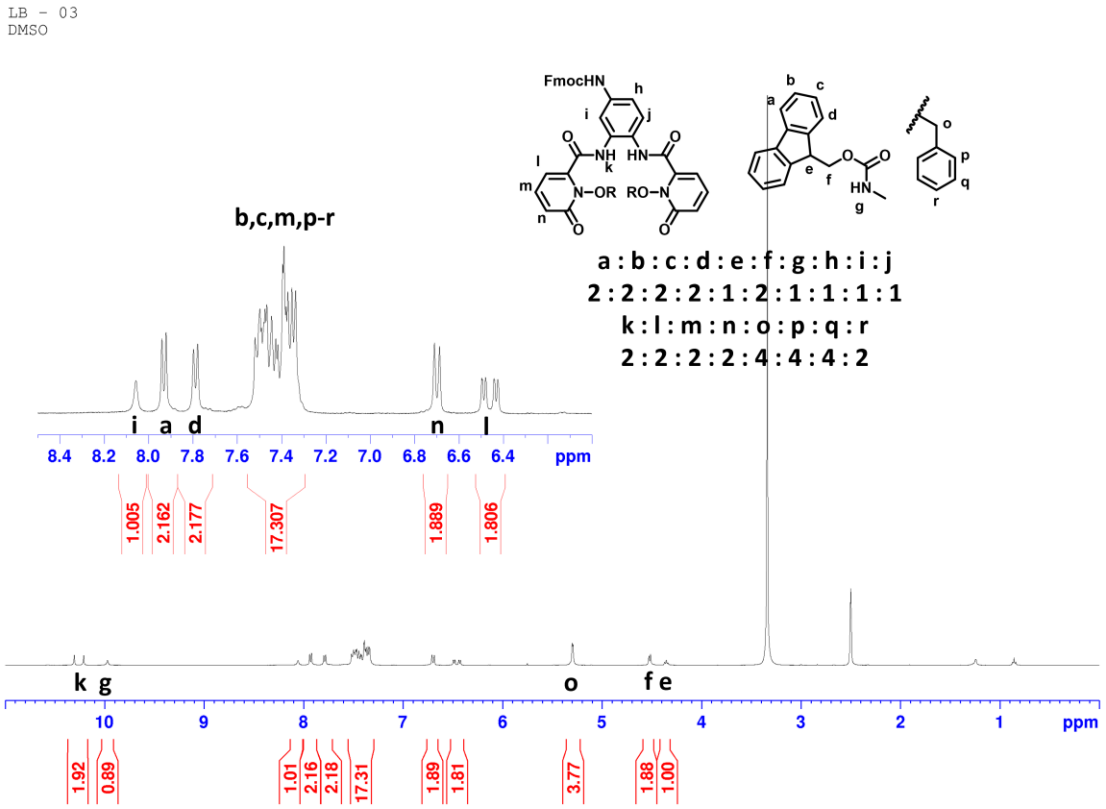

Spectrum S3-22: ^{1}H NMR spectrum of Compound **L_B-3**

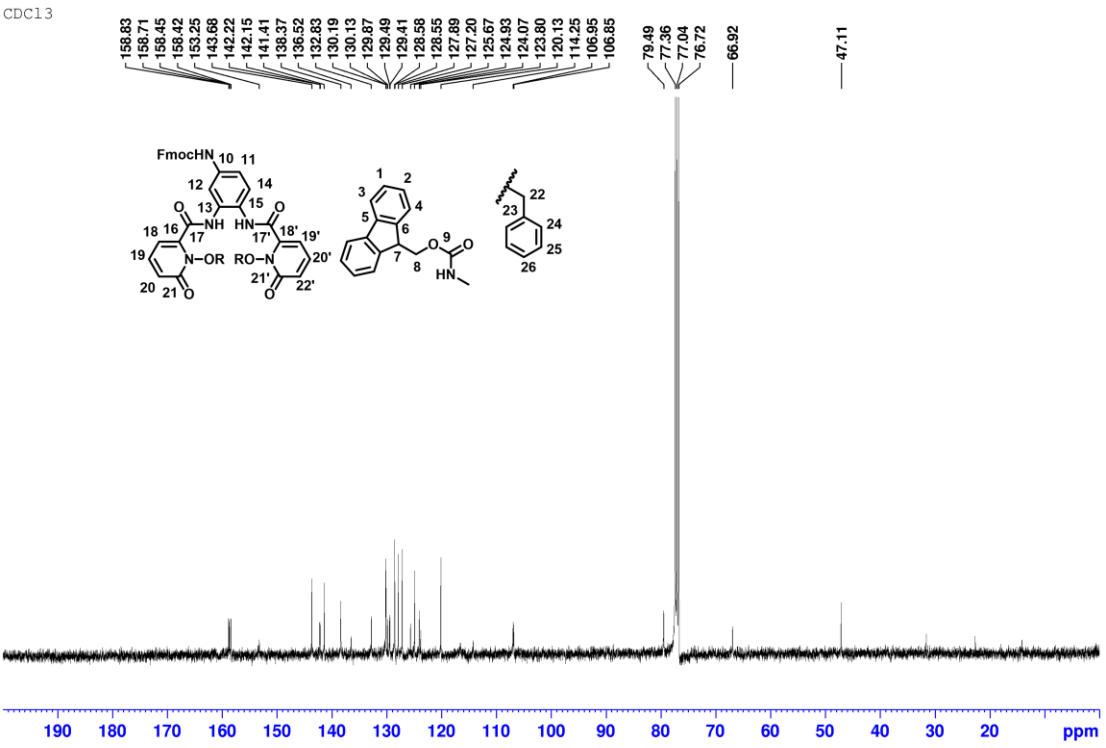

Spectrum S3-23: ^{13}C NMR spectrum of Compound **L_B-3**

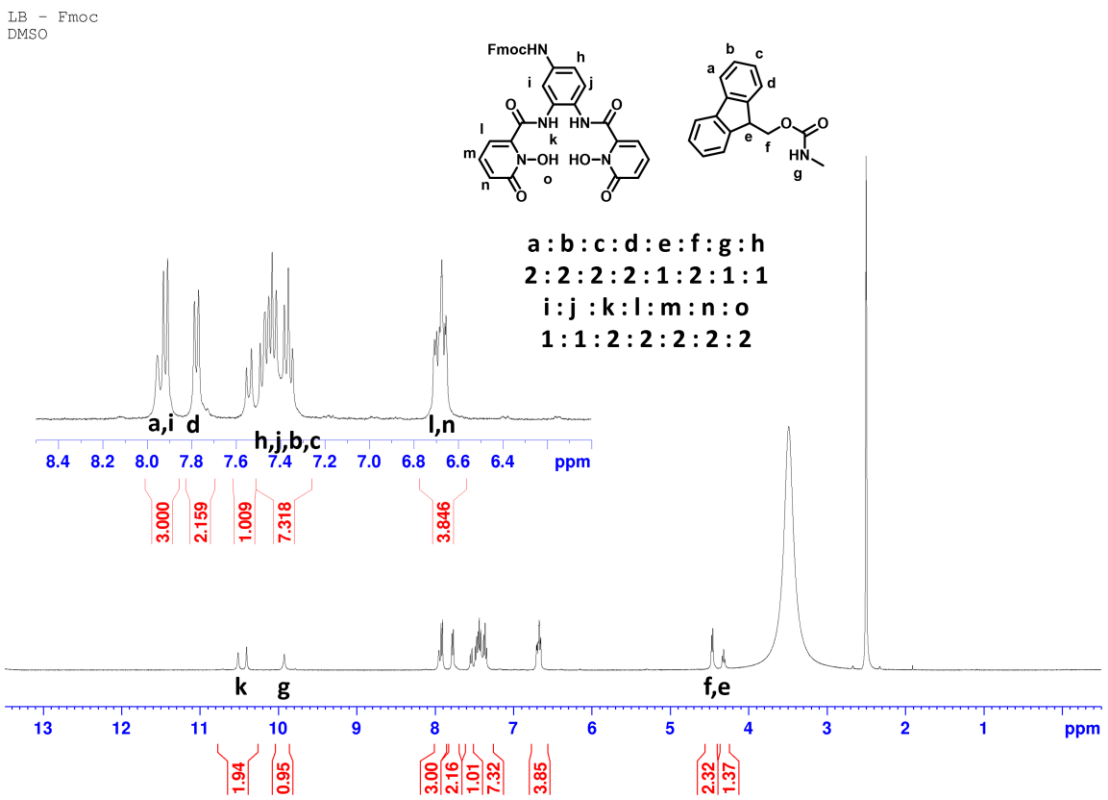

Spectrum S3-24: ^{1}H NMR spectrum of Compound **L_B-fmoc**

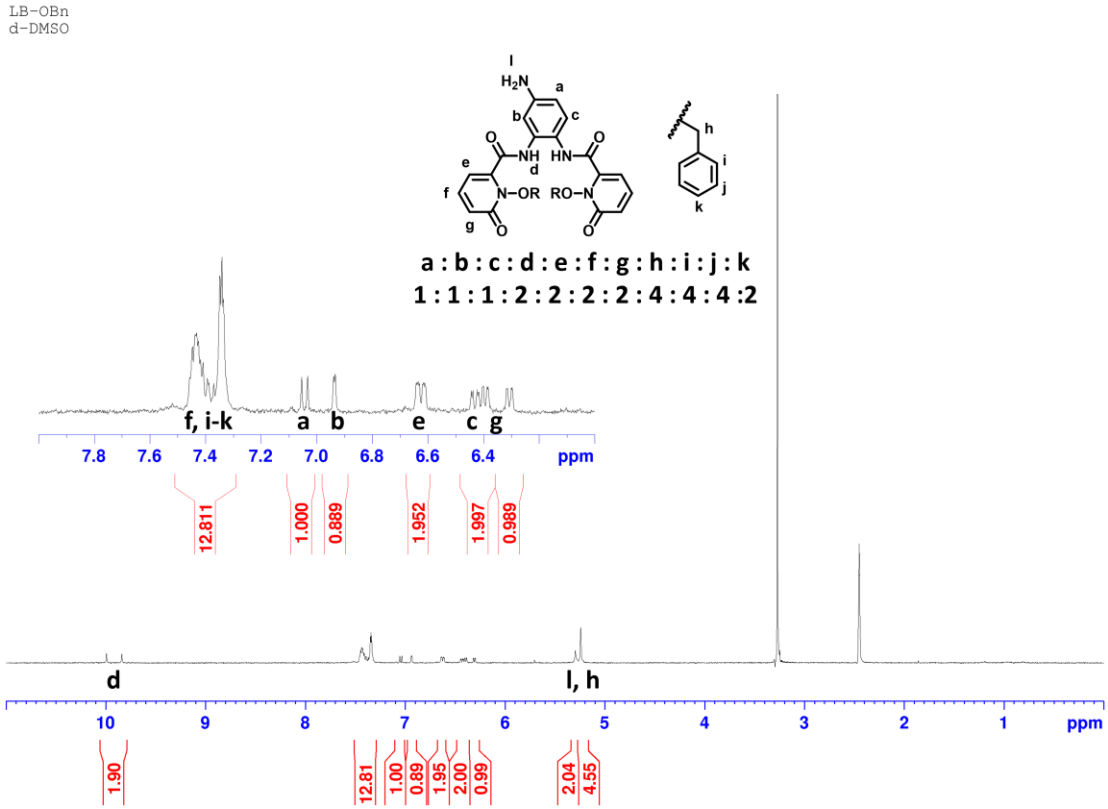

Spectrum S3-25: ^{1}H NMR spectrum of Compound **L_B-OBn**

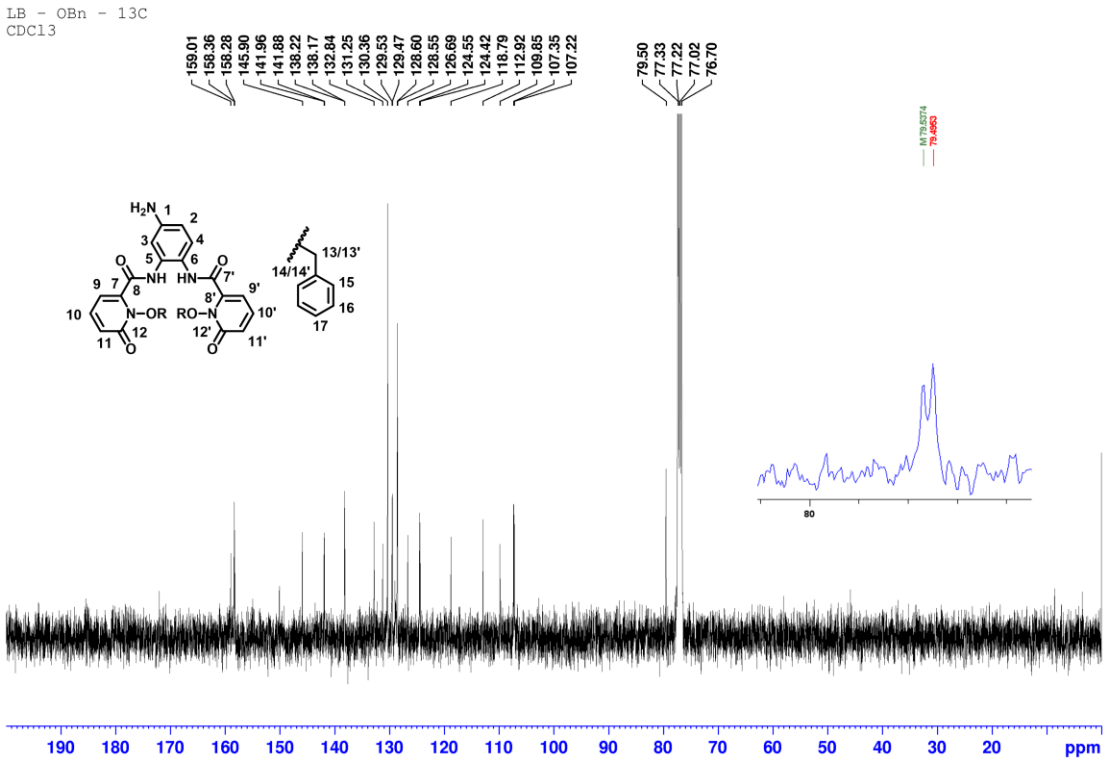

Spectrum S3-26: ^{13}C NMR spectrum of Compound **L_B-OBn**

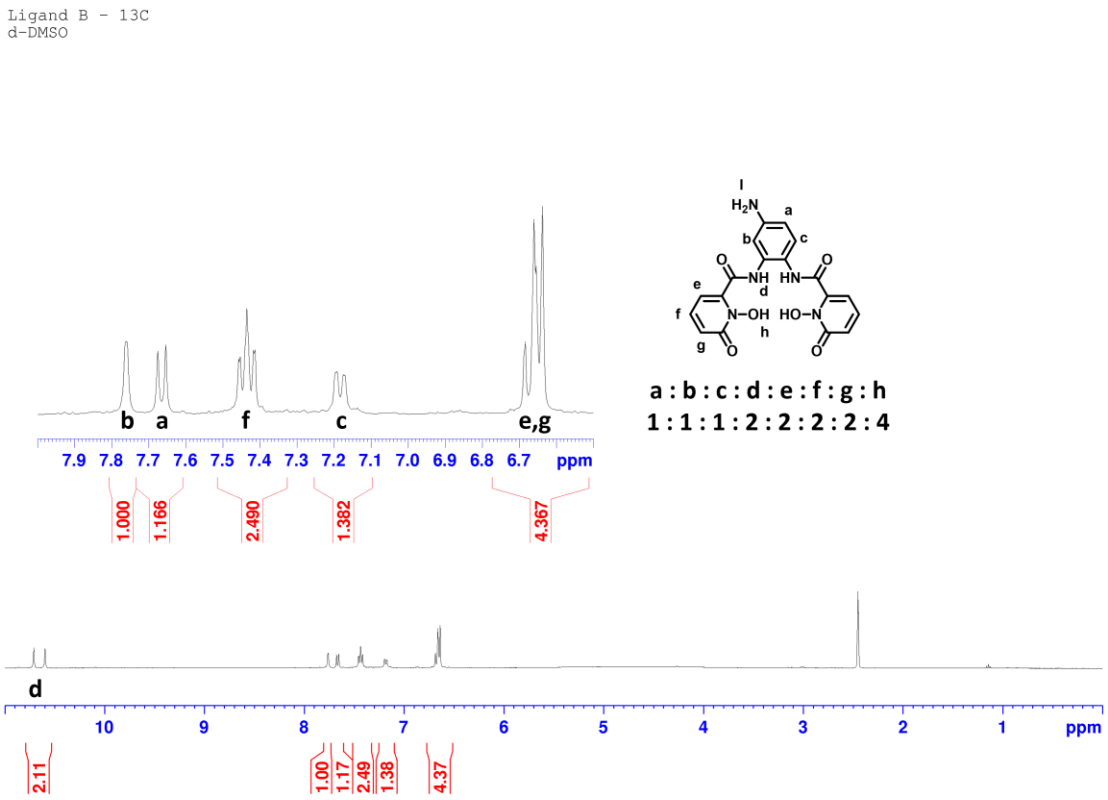

Spectrum S3-27: ^{1}H NMR spectrum of Compound **L_B**

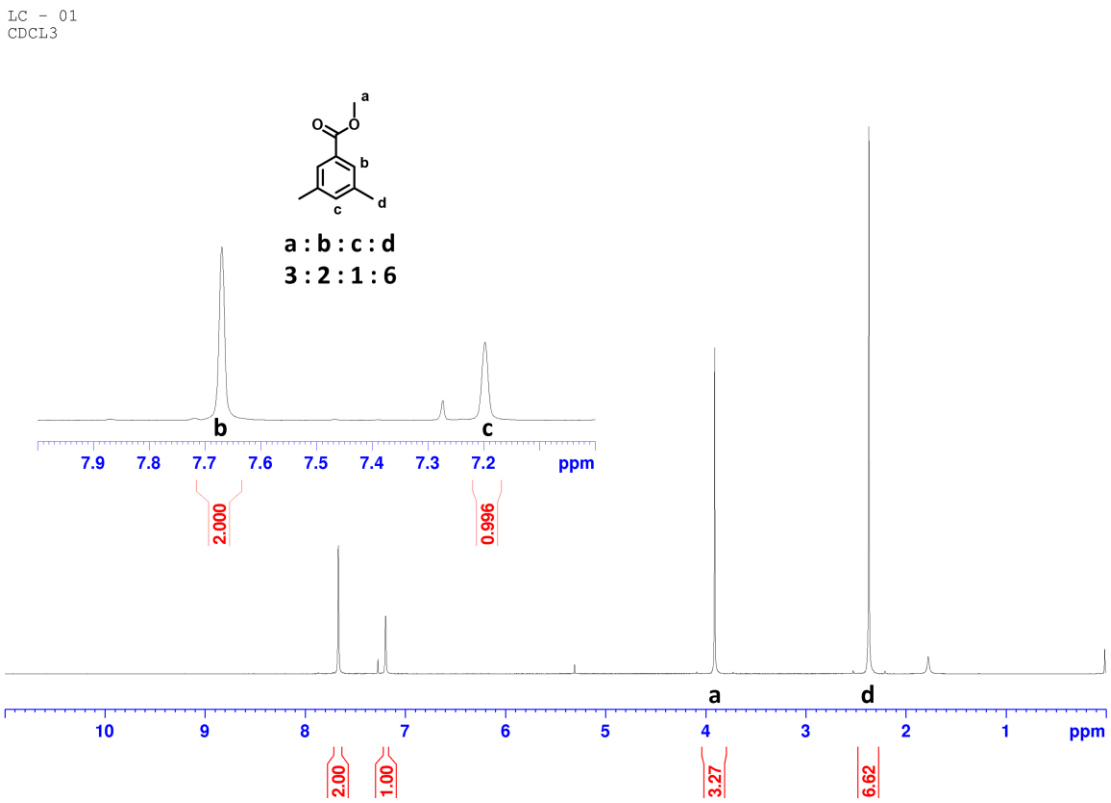

Spectrum S3-28: ^{1}H NMR spectrum of Compound **L_C-1**

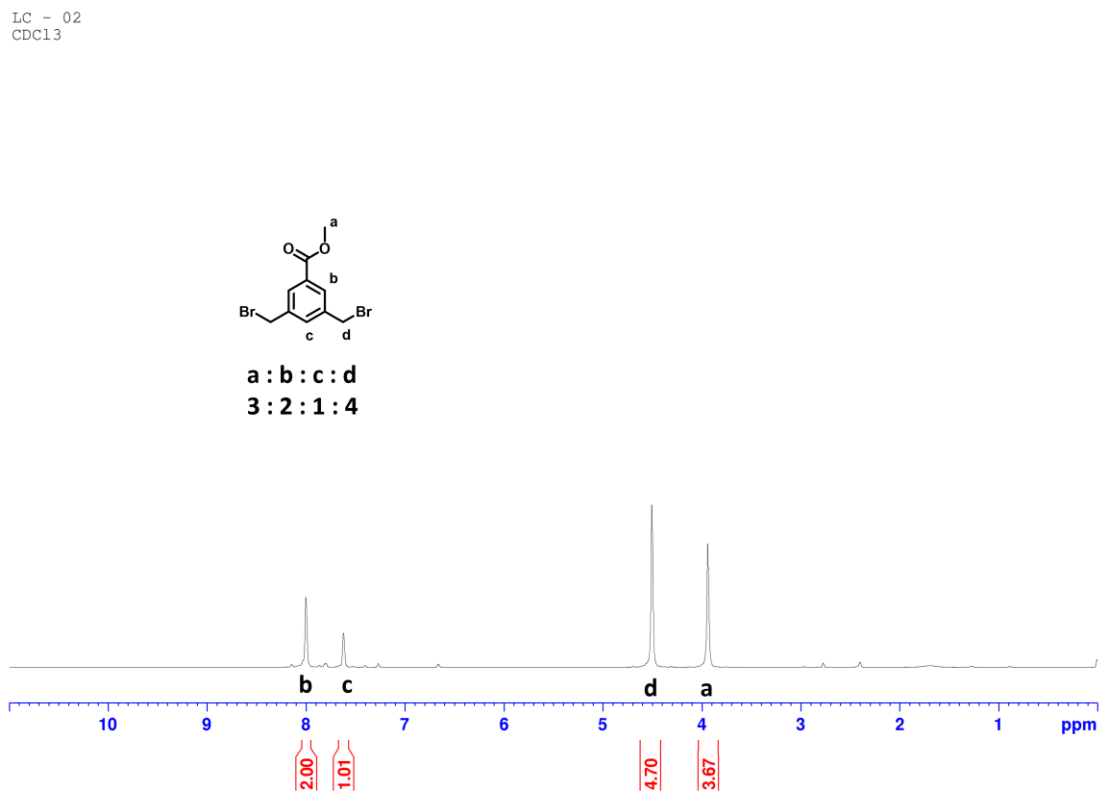

Spectrum S3-29: ^{1}H NMR spectrum of Compound **L_C-2**

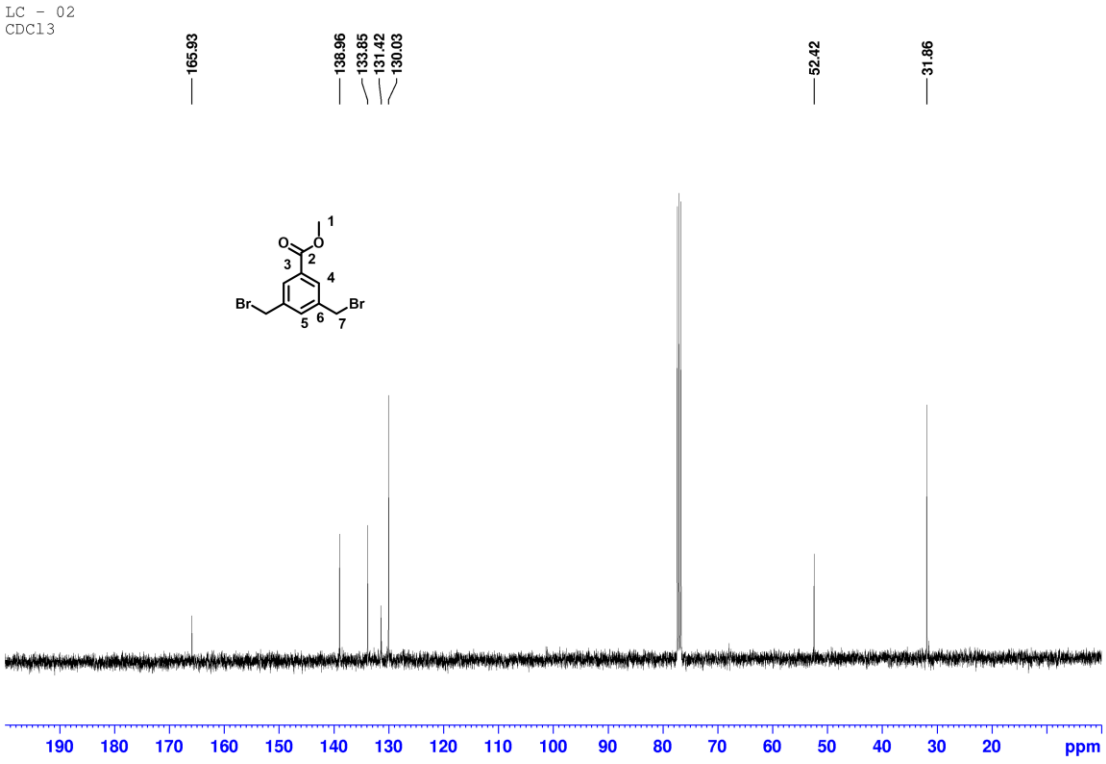

Spectrum S3-30: ^{13}C NMR spectrum of Compound **L_C-2**

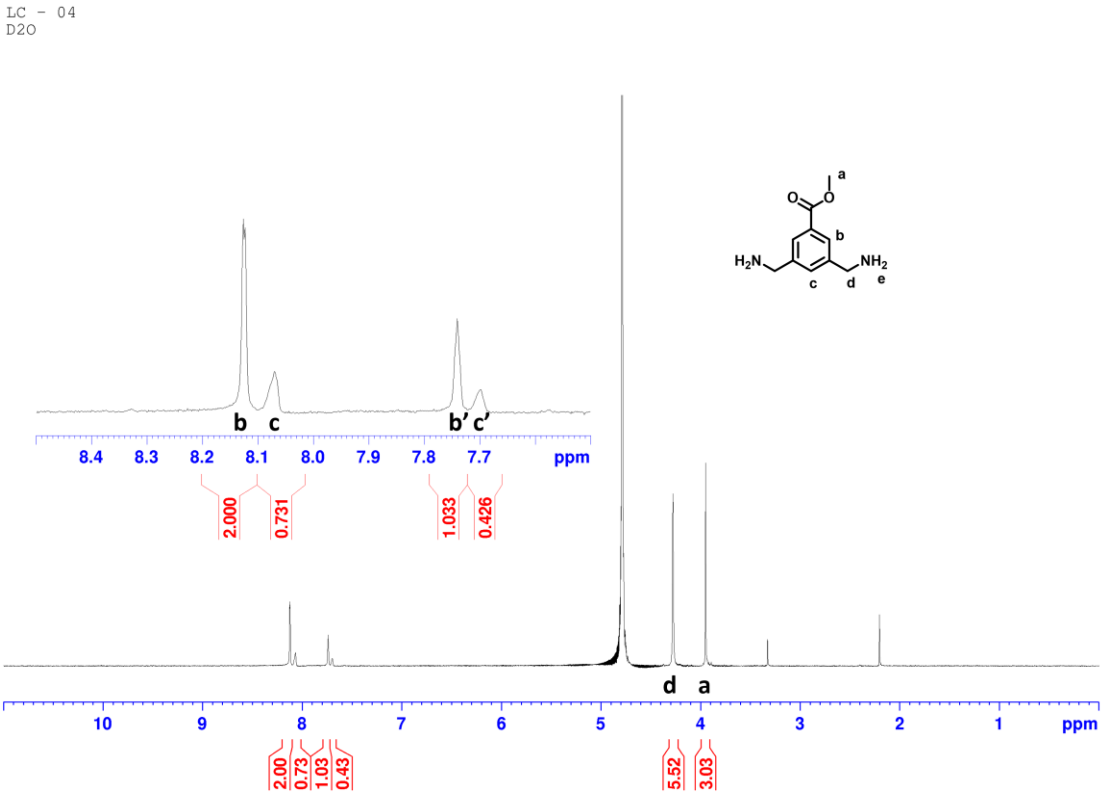

Spectrum S3-31: ^{1}H NMR spectrum of Compound **L_A-4**

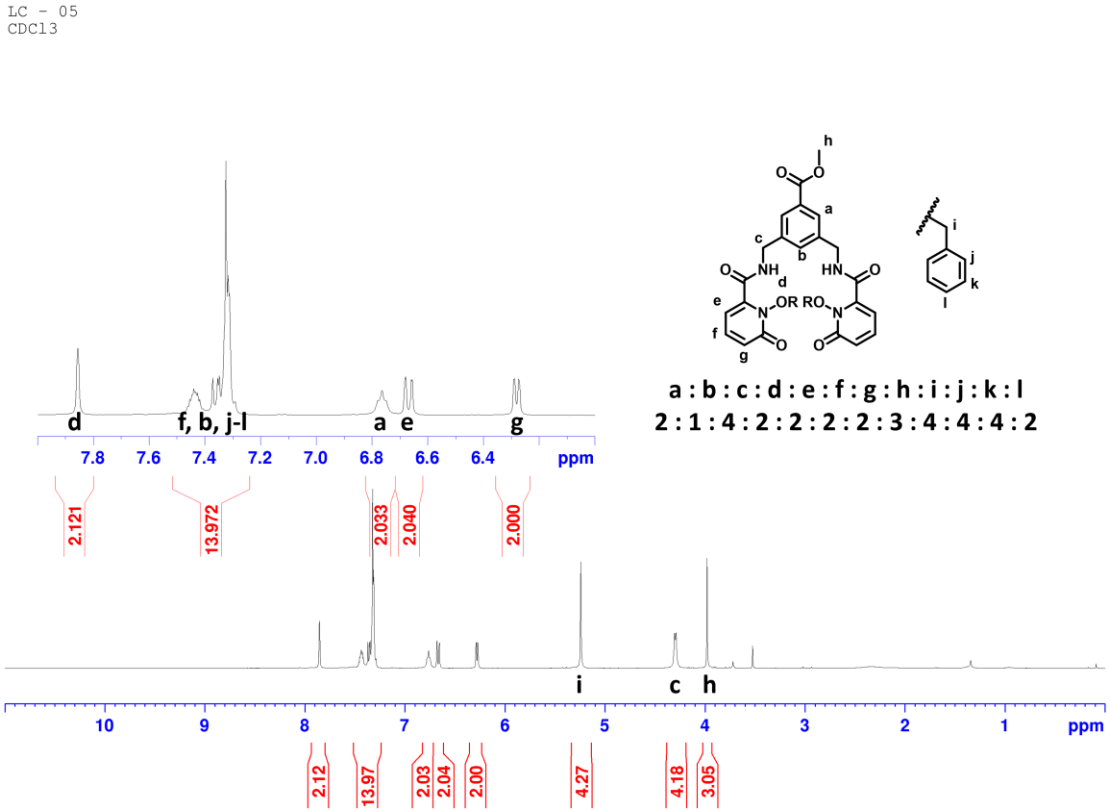

Spectrum S3-32: ^{1}H NMR spectrum of Compound **L_C-5**

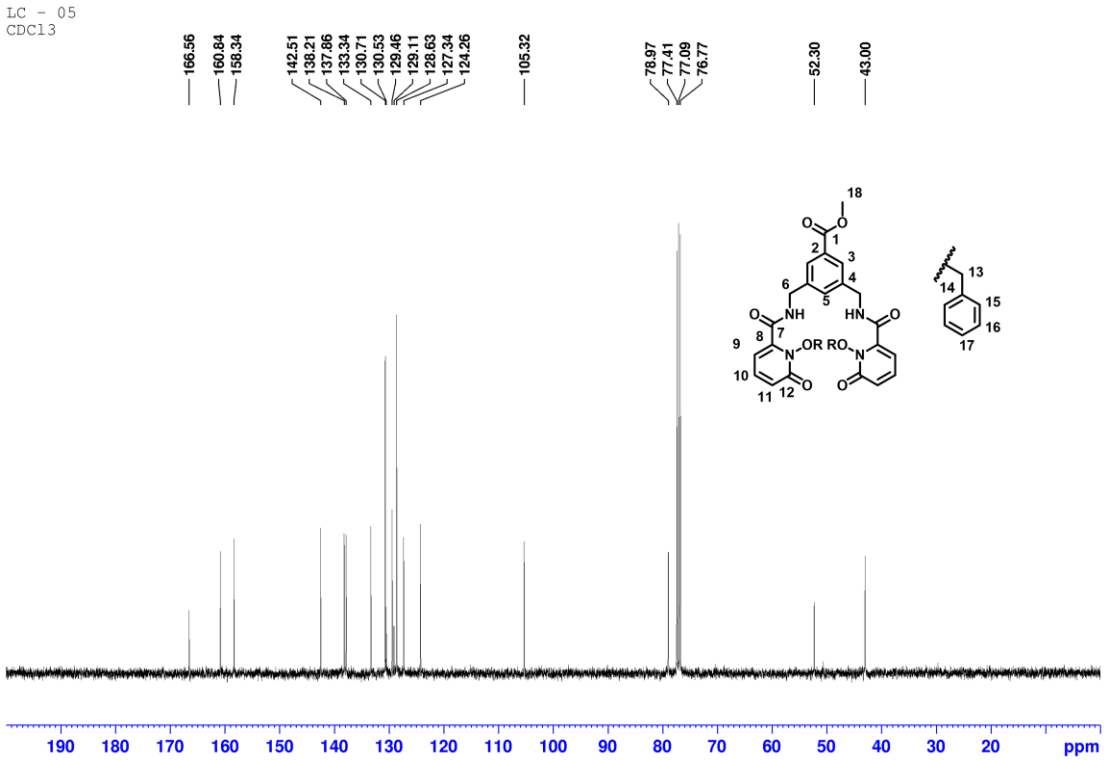

Spectrum S3-33: ^{13}C NMR spectrum of Compound **L_C-5**

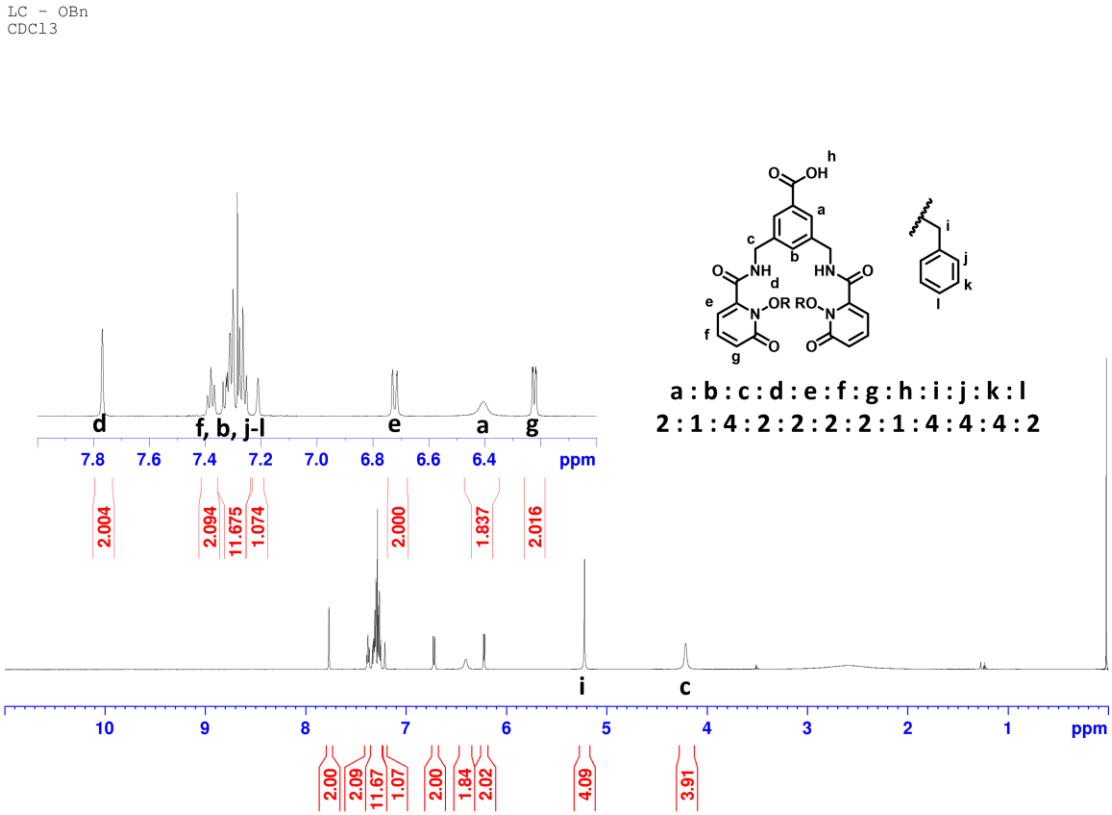

Spectrum S3-34: ^{1}H NMR spectrum of Compound **L_C-OBn**

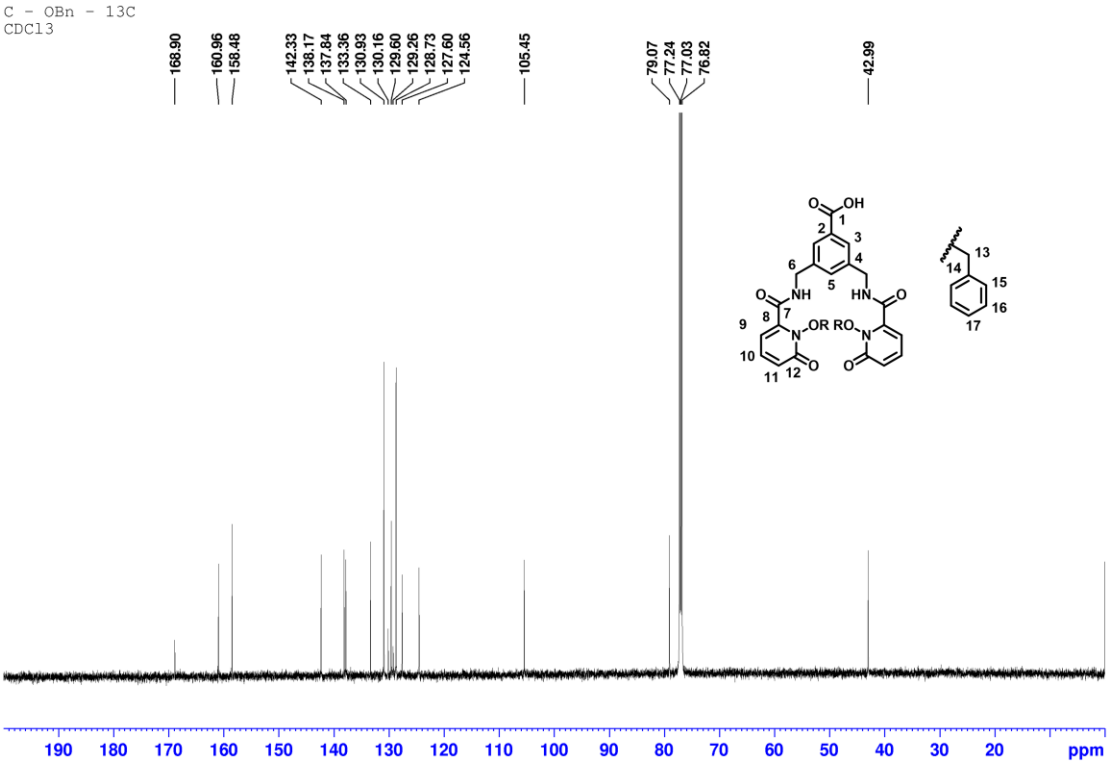

Spectrum S3-35: ^{13}C NMR spectrum of Compound **L_C-OBn**

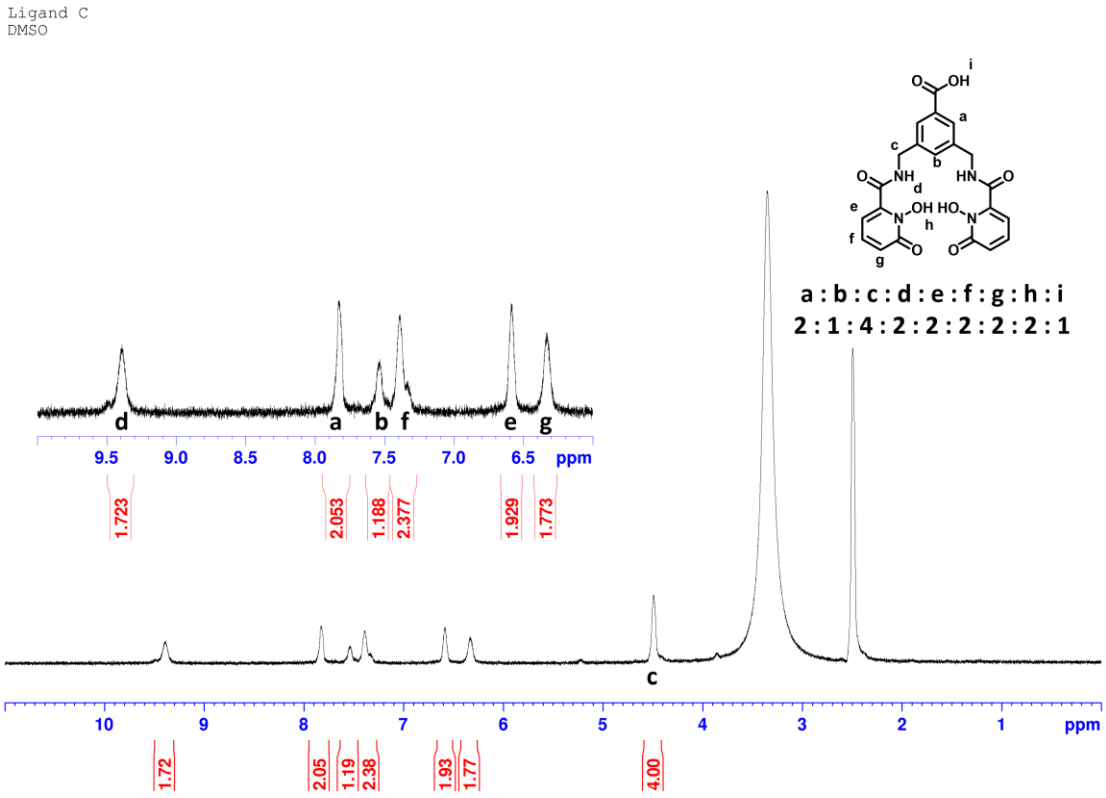

Spectrum S3-36: ^{1}H NMR spectrum of Ligand $\mathbf{L_C}$

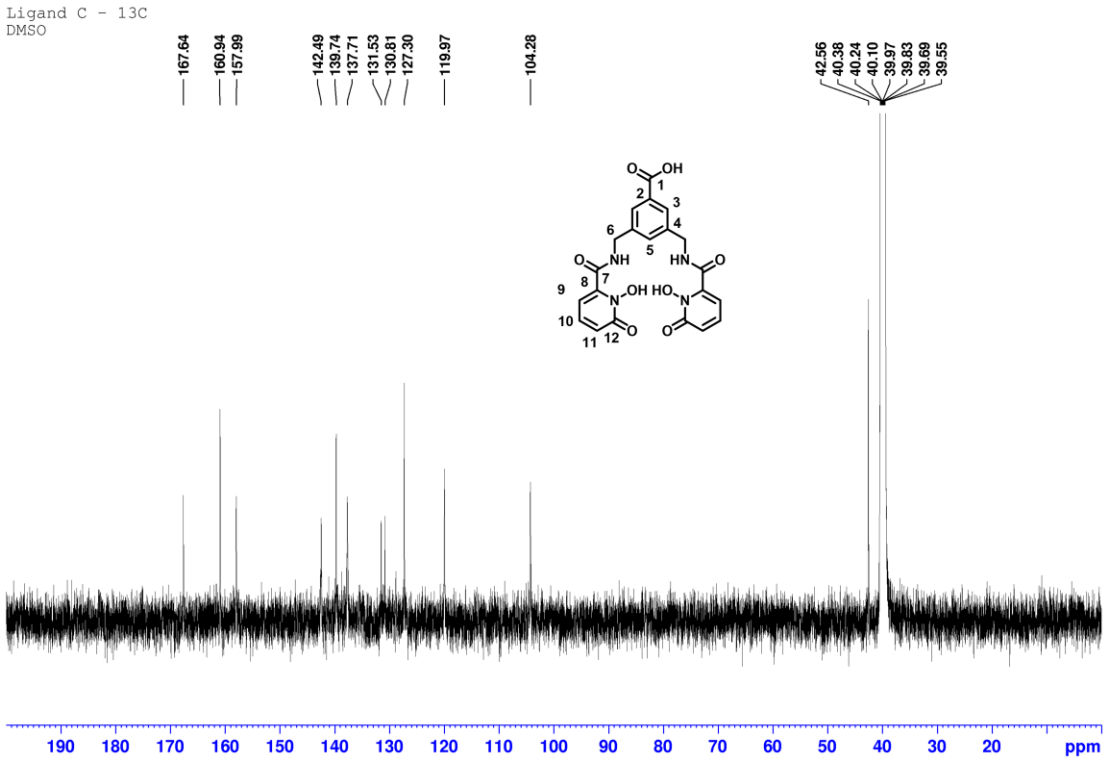

Spectrum S3-37: ^{13}C NMR spectrum of Ligand $\mathbf{L_C}$

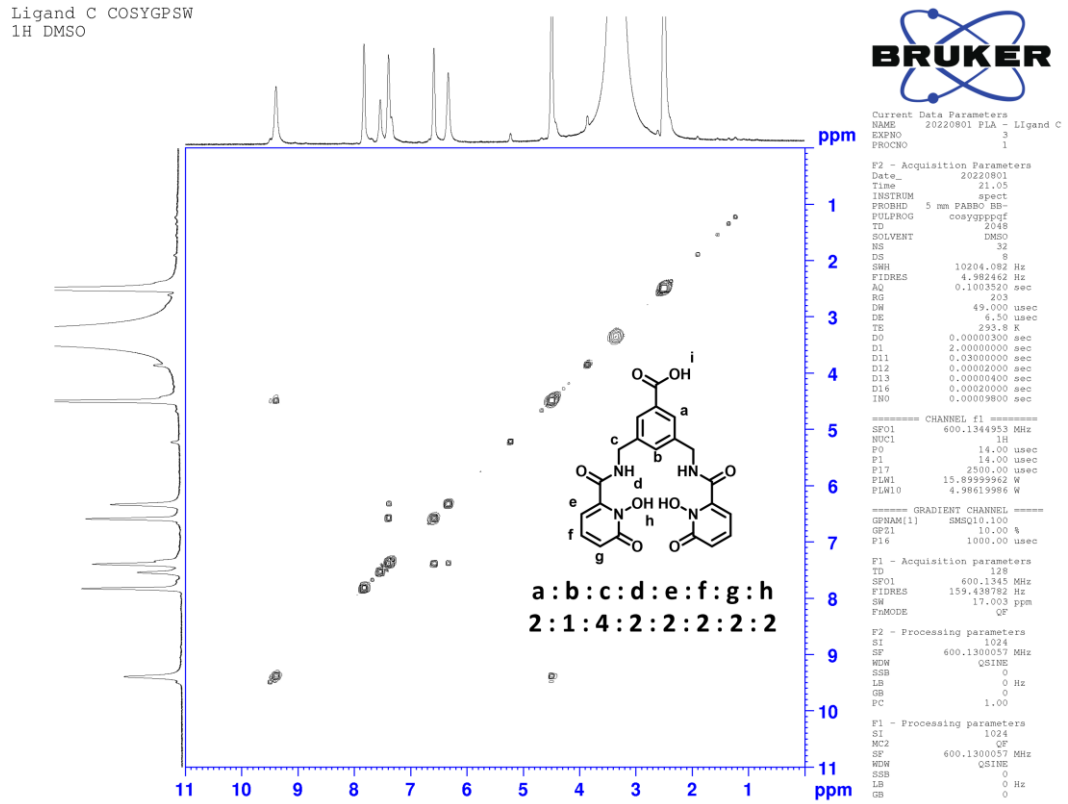

Spectrum S3-38: ^{1}H-^{1}H COSY NMR spectrum of Ligand $\mathbf{L_C}$

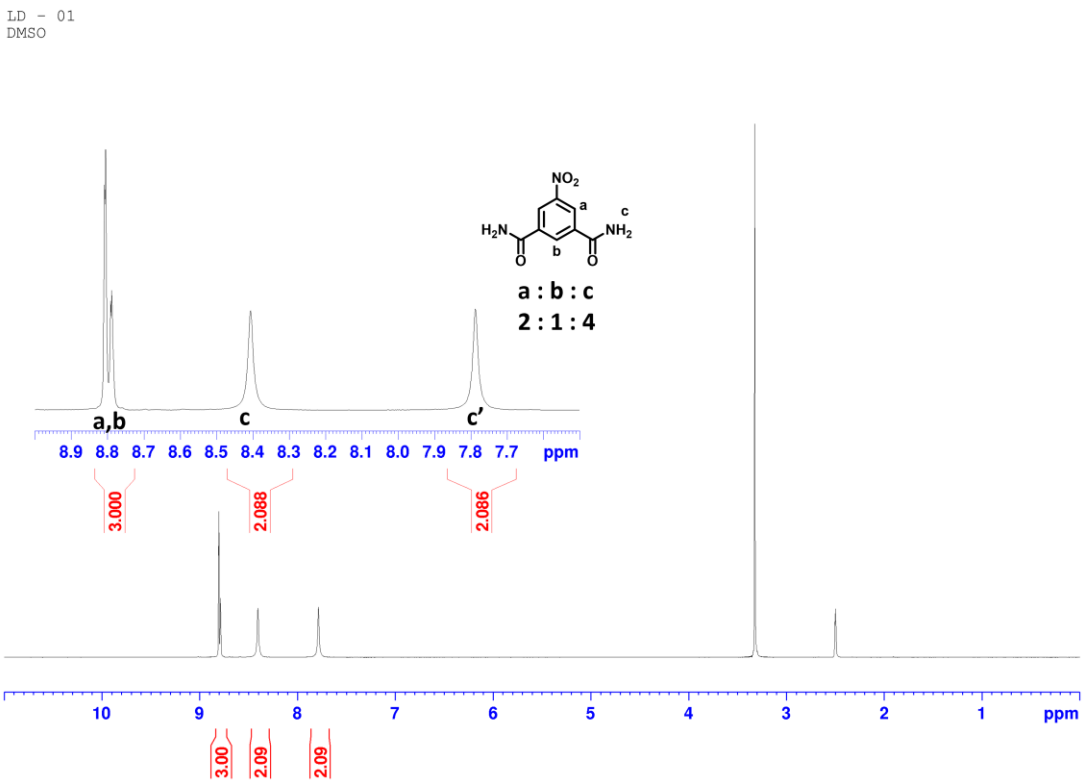

Spectrum S3-39: ^{1}H NMR spectrum of Compound $\mathbf{L_D}$**-1**

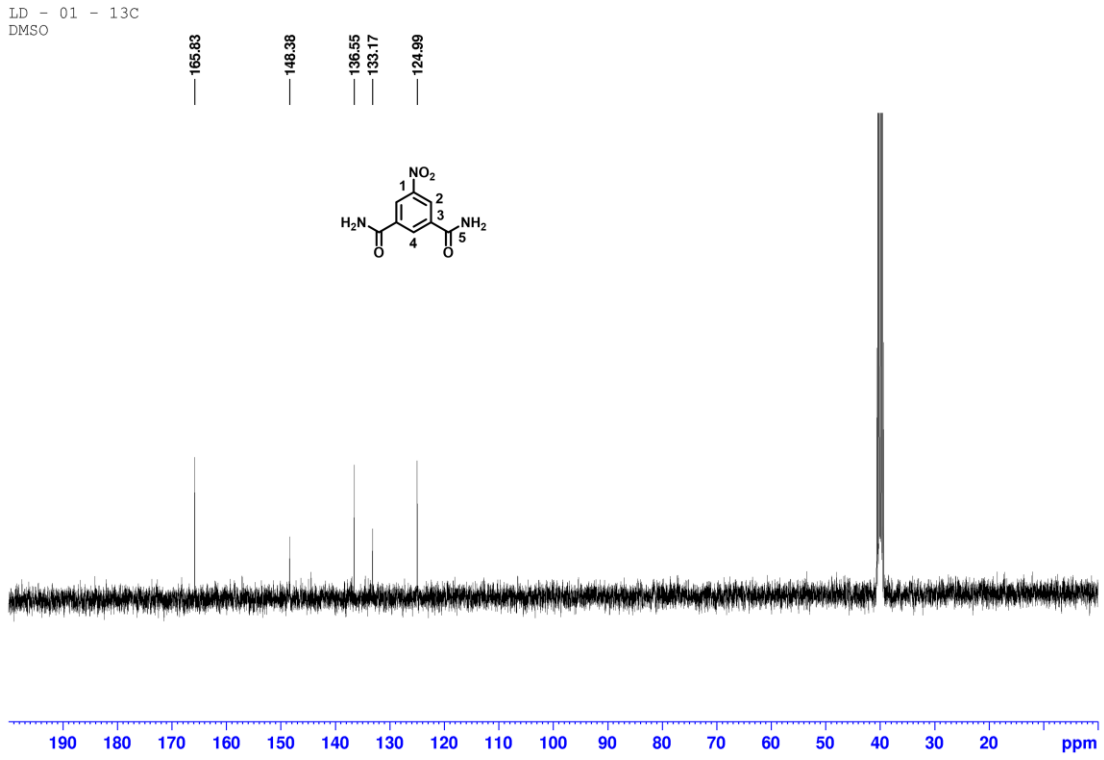

Spectrum S3-40: ^{13}C NMR spectrum of Compound **L_D-1**

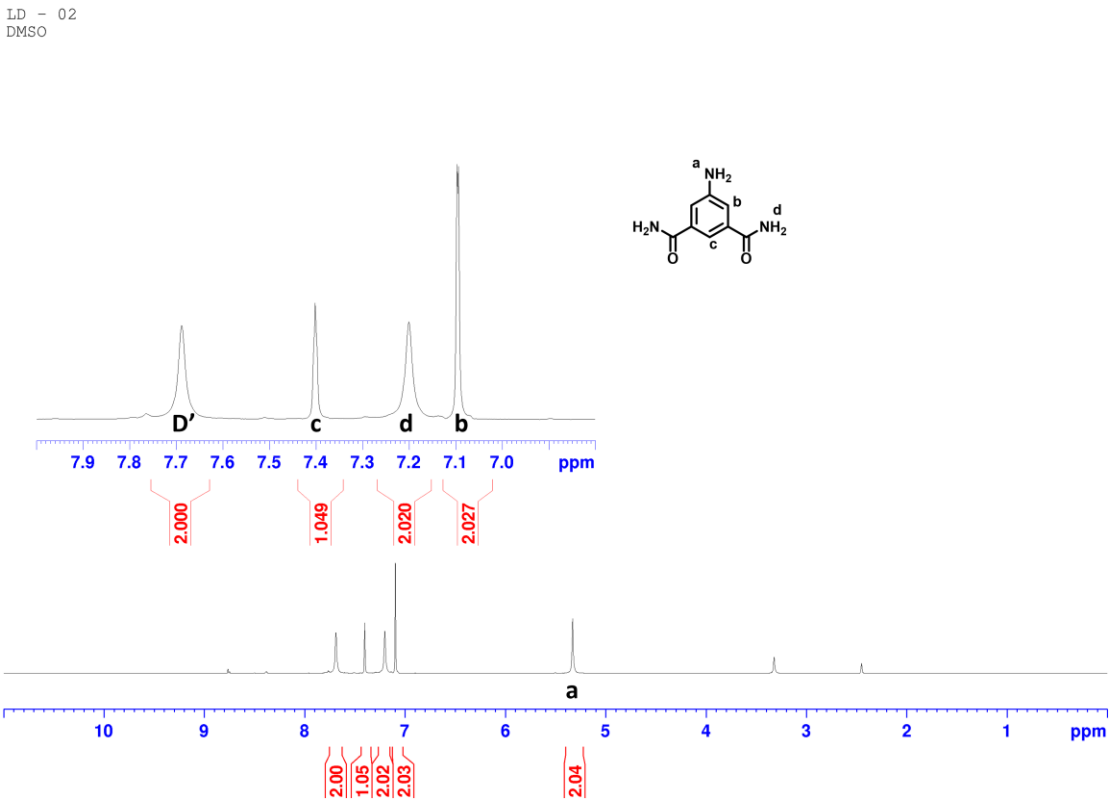

Spectrum S3-41: ^{1}H NMR spectrum of Compound **L_D-2**

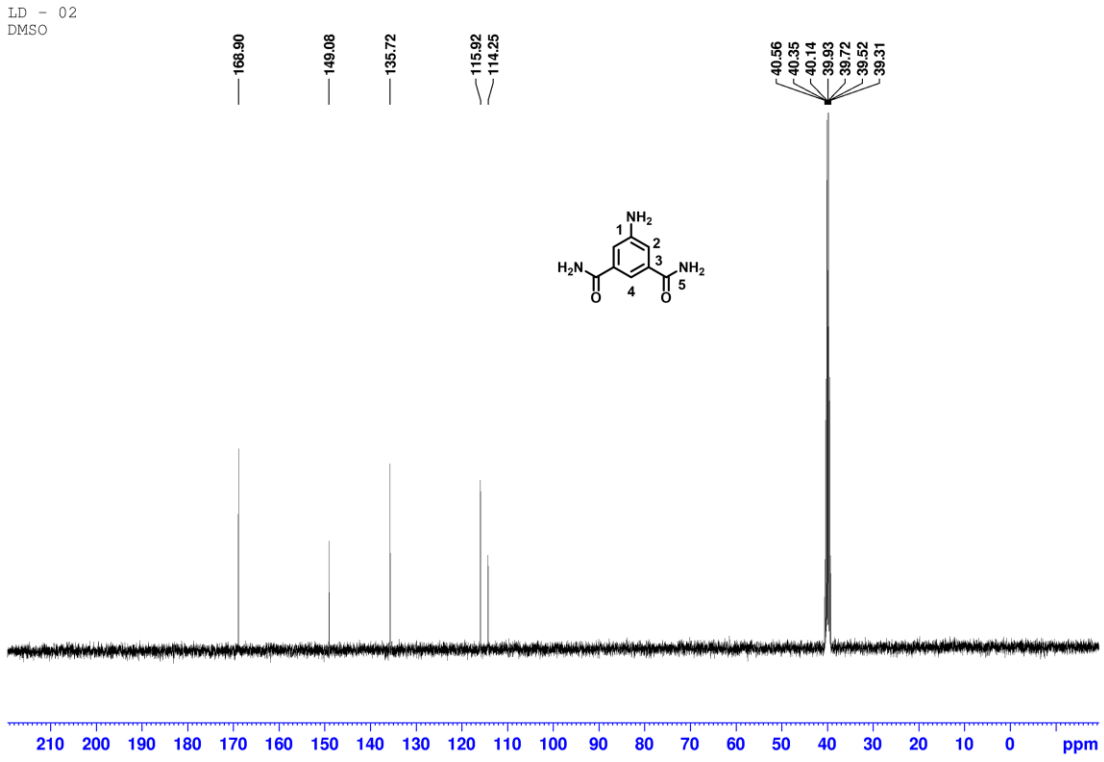

Spectrum S3-42: ^{13}C NMR spectrum of Compound **L_D-2**

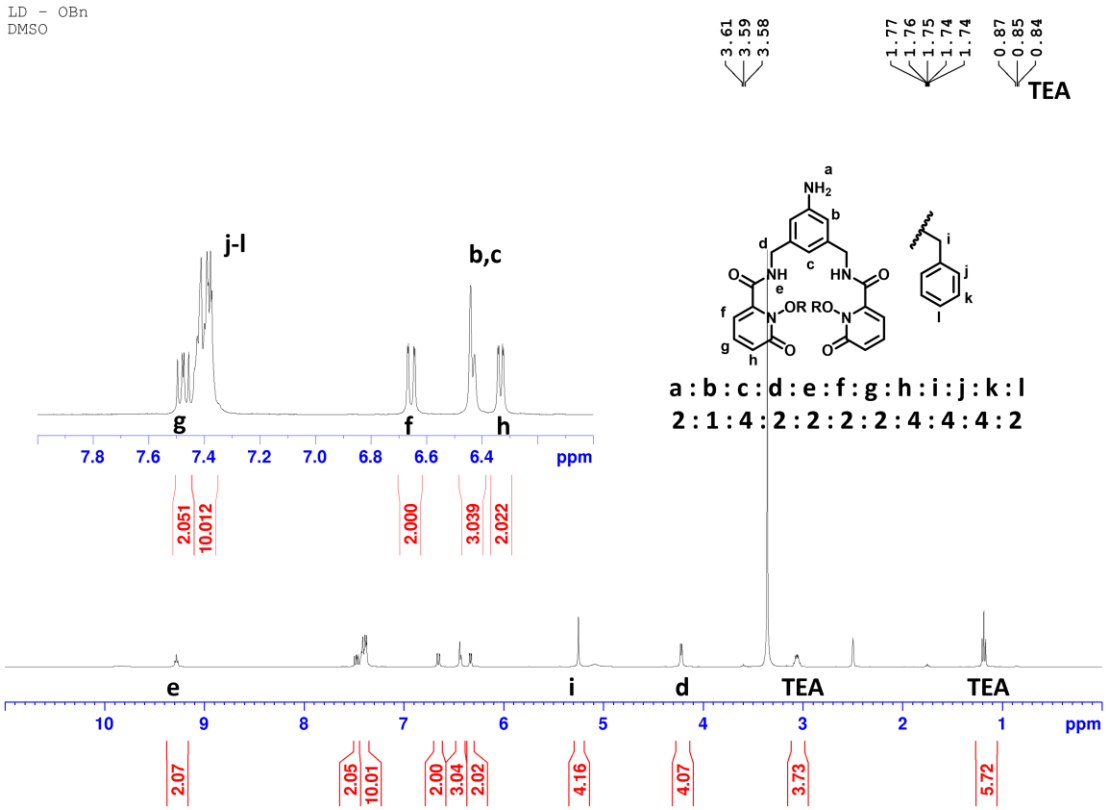

Spectrum S3-43: ^{1}H NMR spectrum of Compound **L_D-OBn**

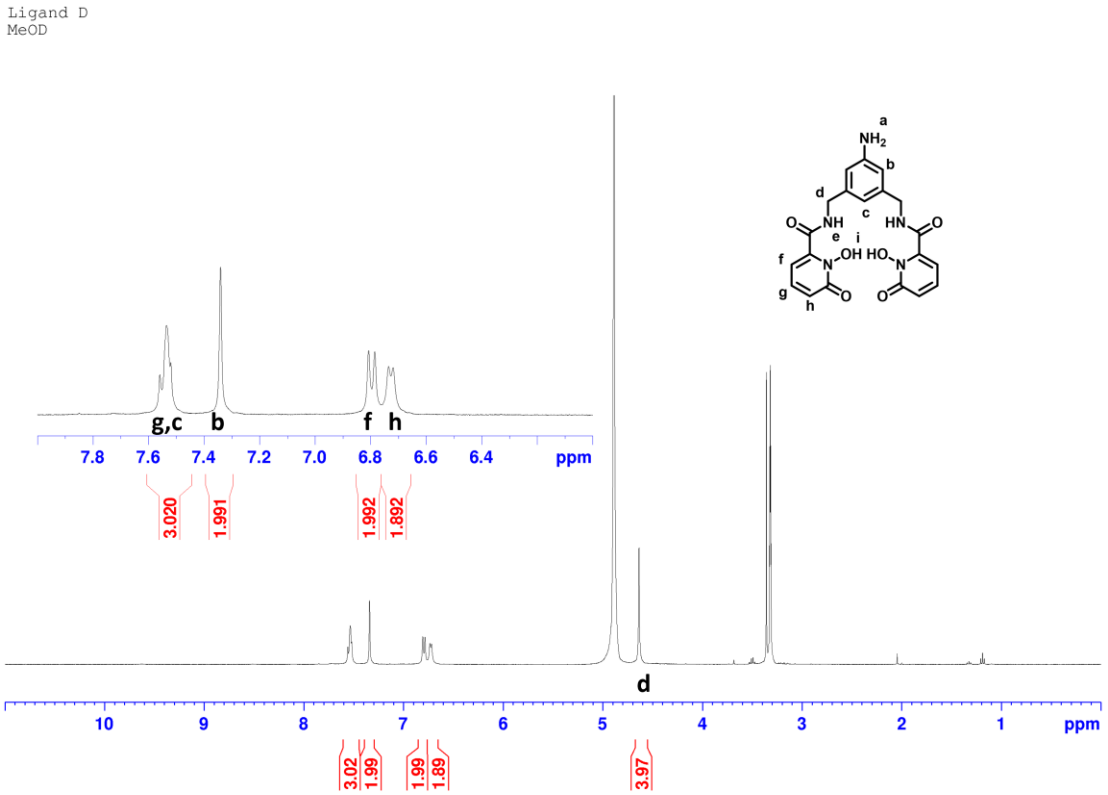

Spectrum S3-44: ^{1}H NMR spectrum of Ligand $\mathbf{L_D}$

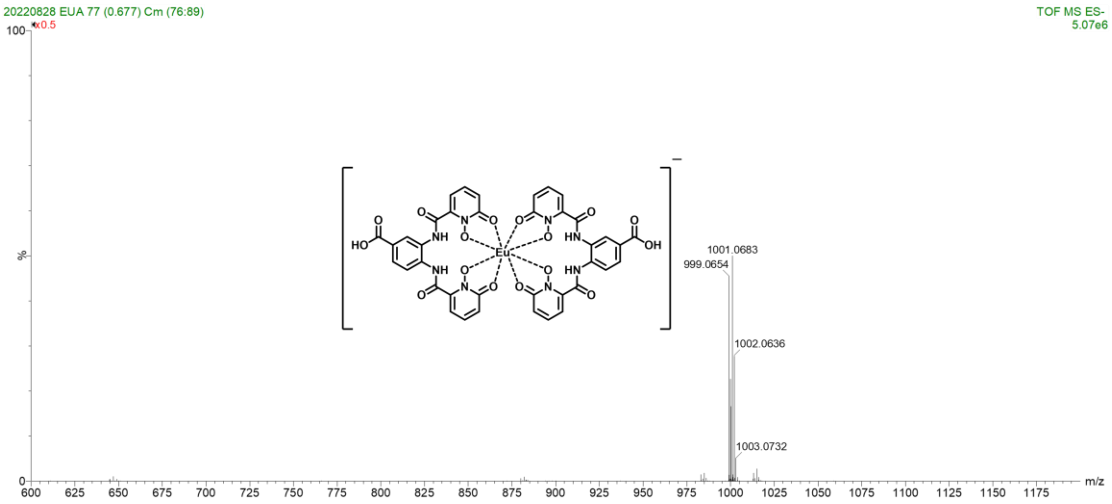

Spectrum S3-45: ESI-HRMS spectrum of complexes $\mathbf{EuL_A}$

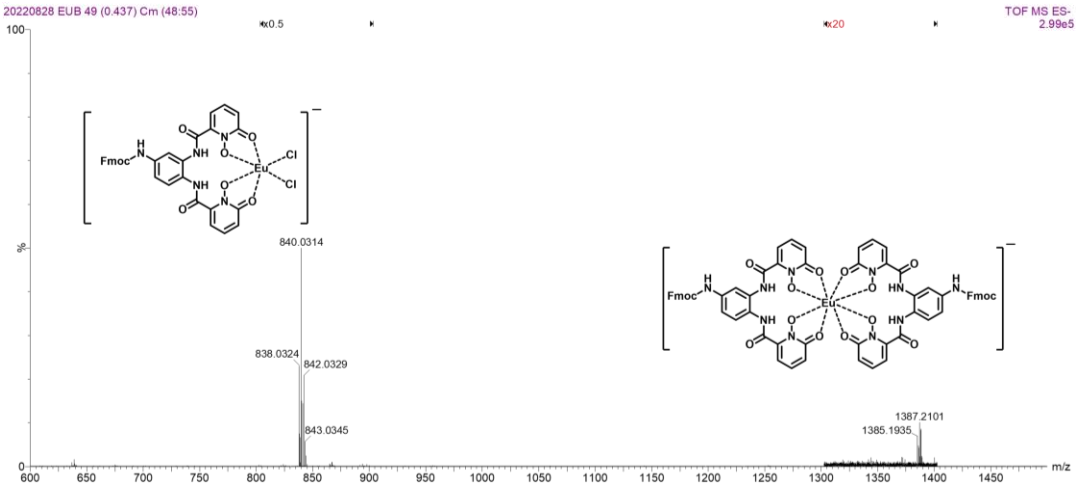

Spectrum S3-46: ESI-HRMS spectrum of complexes **EuL_B-fmoc**

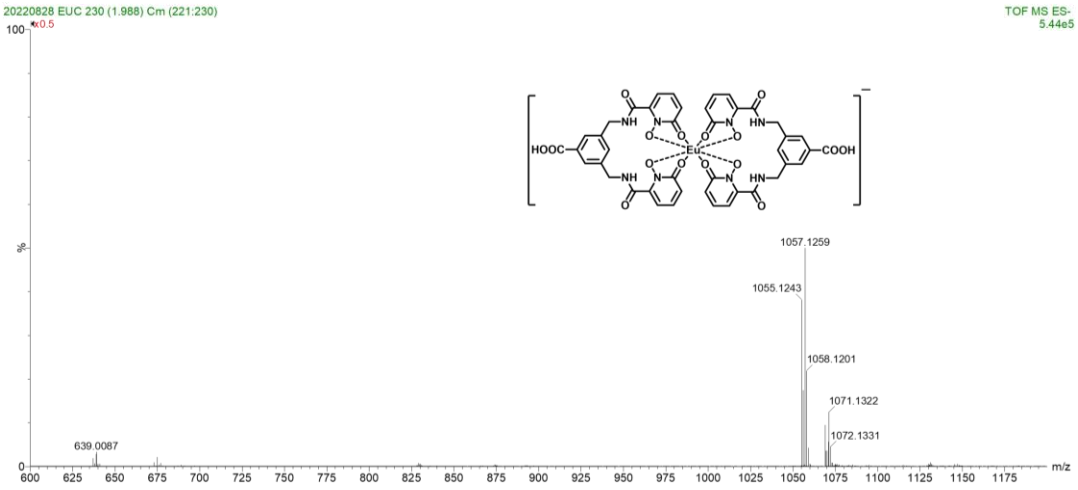

Spectrum S3-47: ESI-HRMS spectrum of complexes **EuL_C**

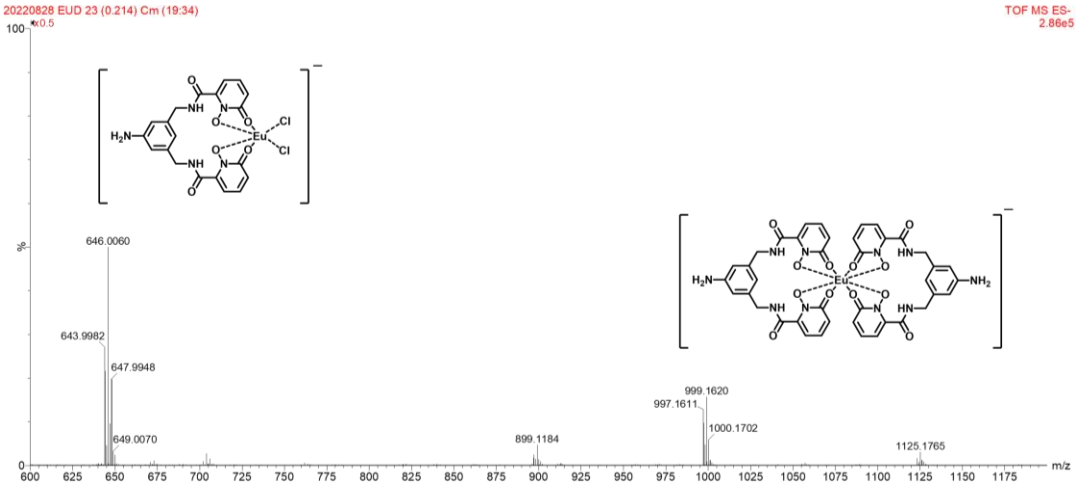

Spectrum S3-48: ESI-HRMS spectrum of complexes **EuL_D**

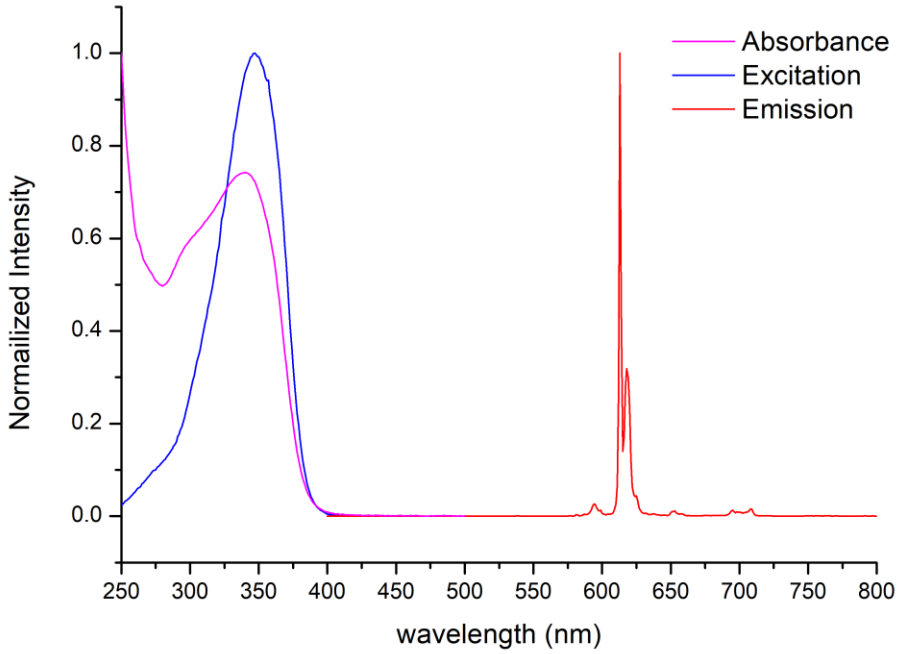

Spectrum S3-49: Combined Spectrum of complexes **EuL_A**

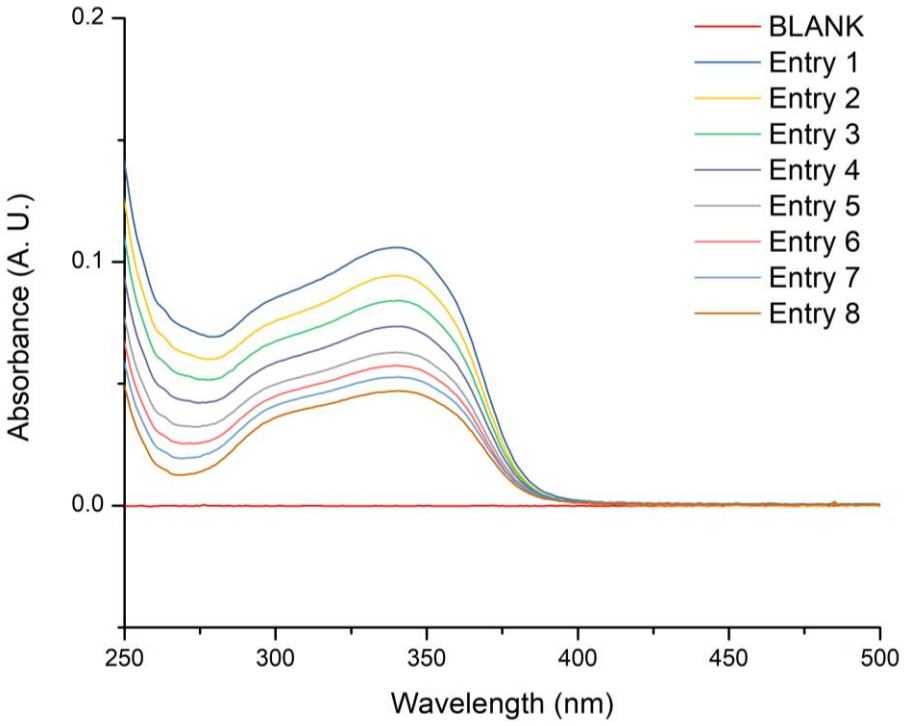

Spectrum S3-50: Absorbance spectrum of **EuL_A**

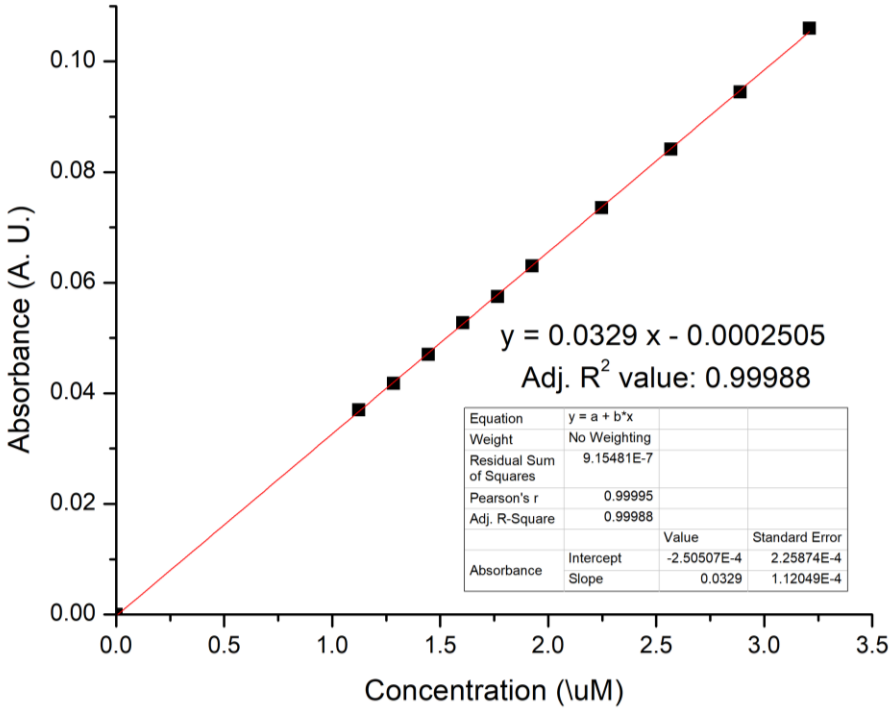

Spectrum S3-51: Absorptivity plot of **EuL_A**

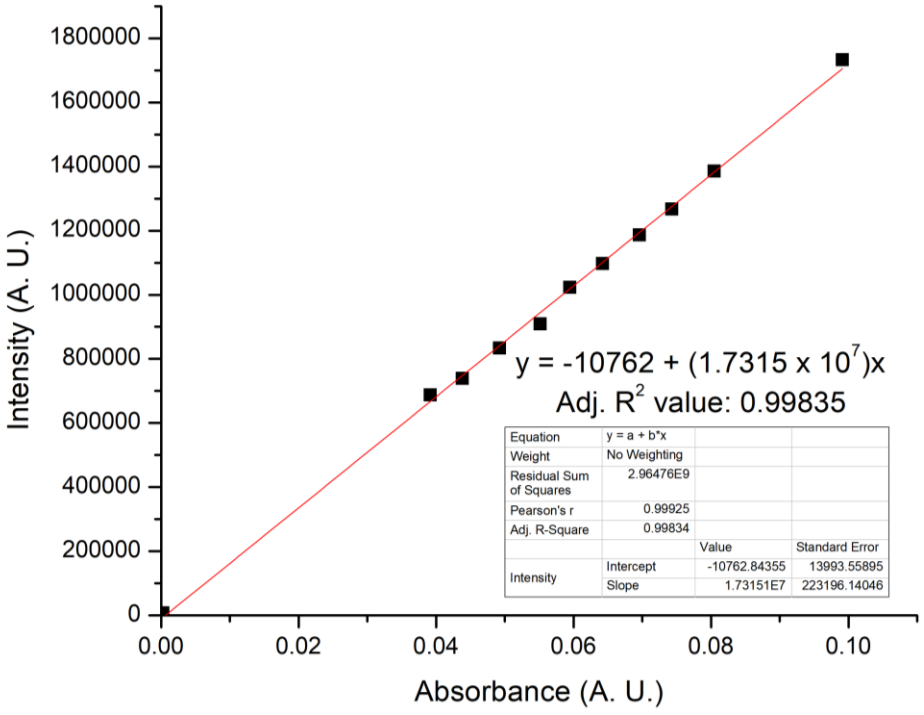

Spectrum S3-52: quantum yield linearity fit of **EuL_A**

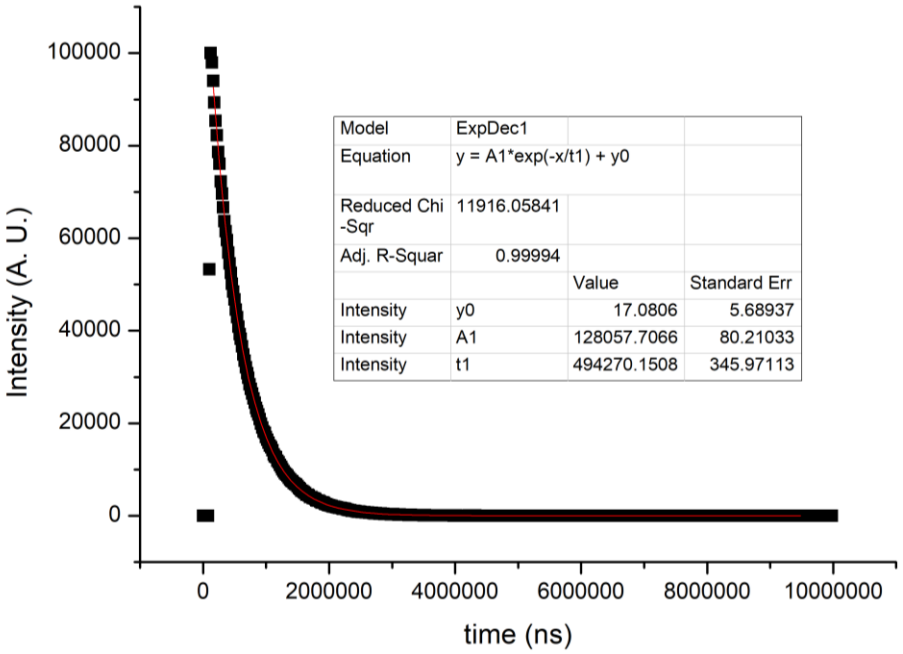

Spectrum S3-53: Decay curve of luminescence lifetime of **EuL_A** in 5% DMSO/H_2O

(mono-exponential fit)

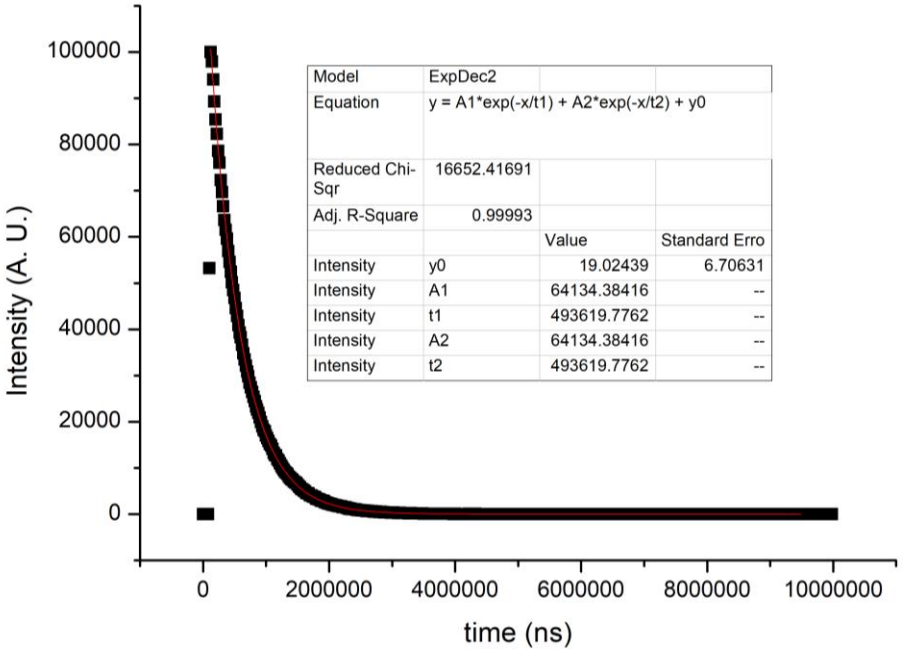

Spectrum S3-54: Decay curve of luminescence lifetime of **EuL_A** in 5% DMSO/H_2O

(Bi-exponential fit)

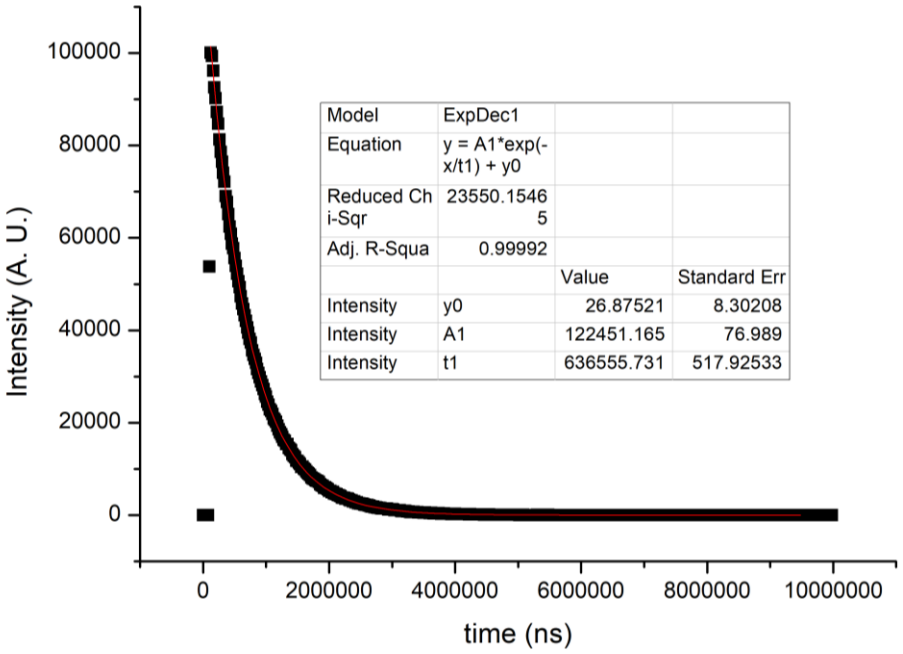

Spectrum S3-55: Decay curve of luminescence lifetime of **EuL$_A$** in 5% DMSO/D_2O

(mono-exponential fit)

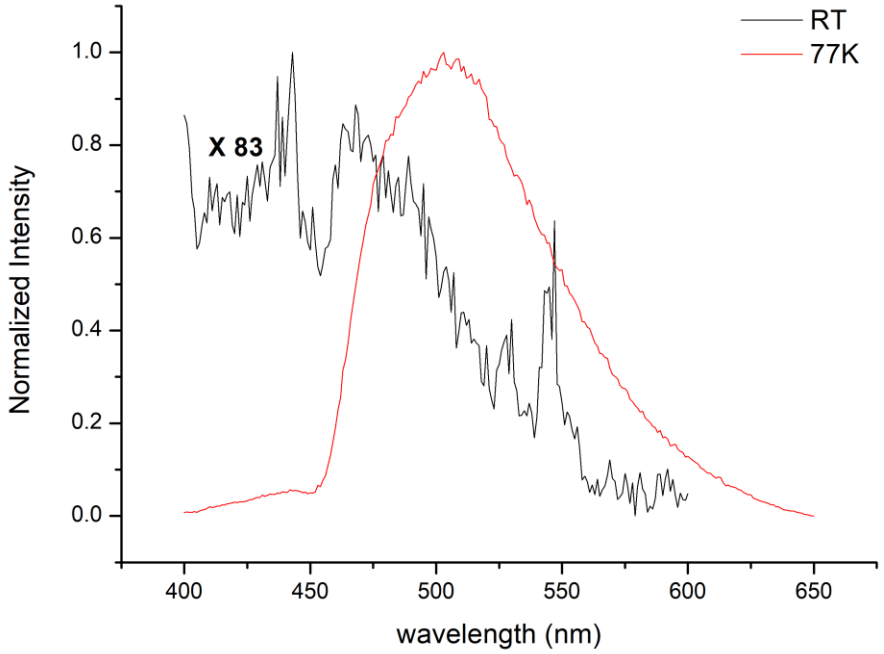

Spectrum S3-56: Normalized Emission spectrum of **GdL$_A$** (RT & 77K)

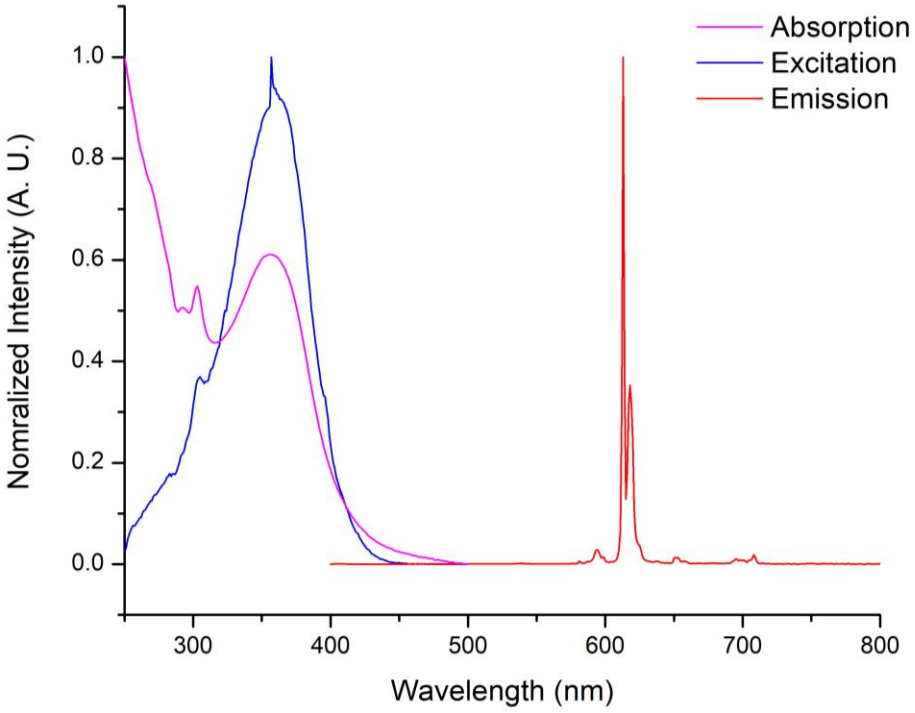

Spectrum S3-57: Combined Spectrum of complexes **EuL_B-fmoc**

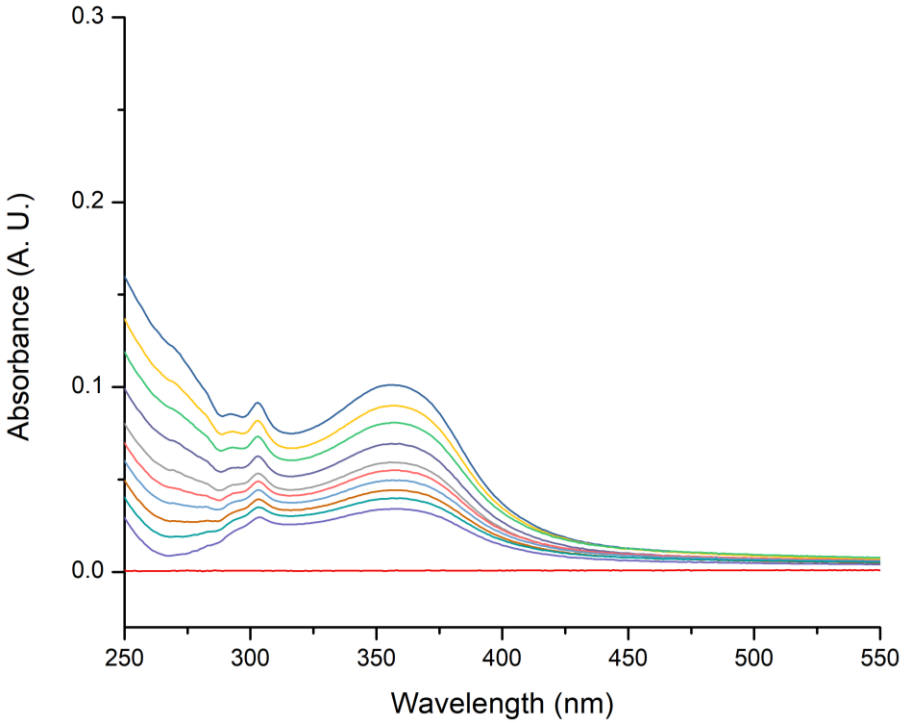

Spectrum S3-58: Absorbance spectrum of **EuL_B-fmoc**

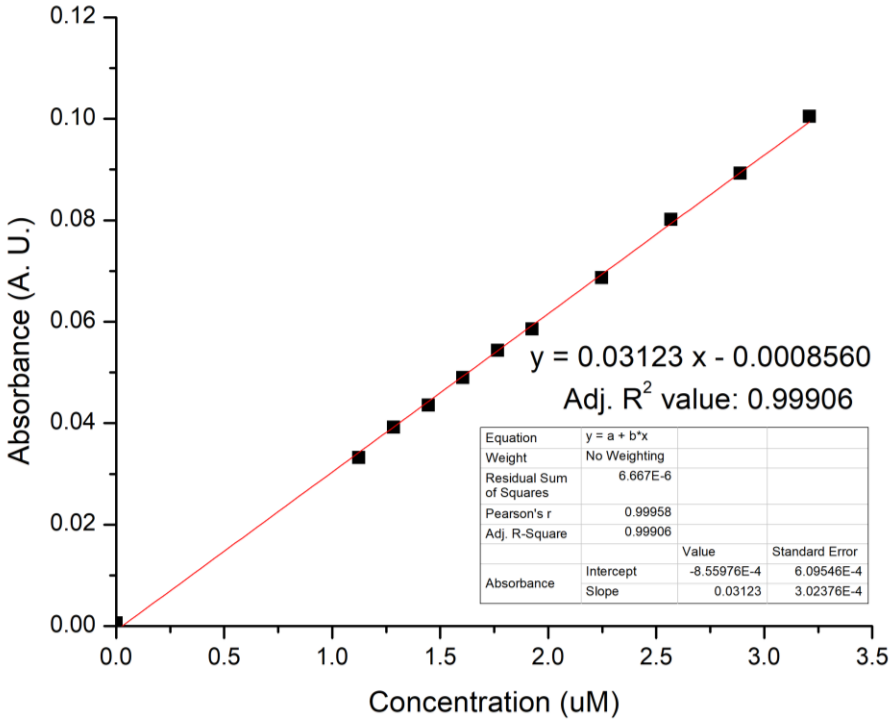

Spectrum S3-59: Absorptivity plot of **EuL_B-fmoc**

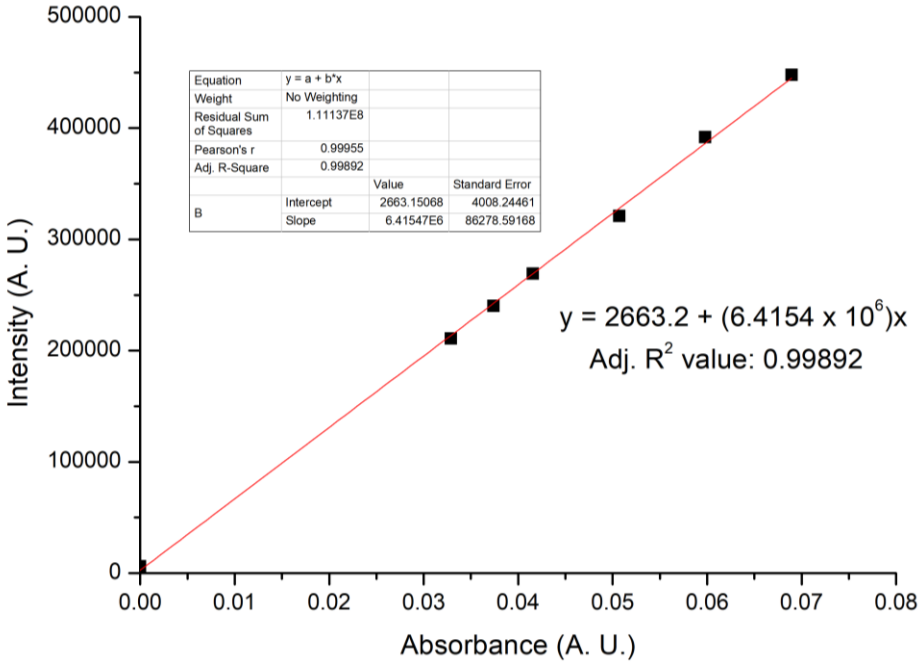

Spectrum S3-60: quantum yield linearity fit of **EuL_B-fmoc**

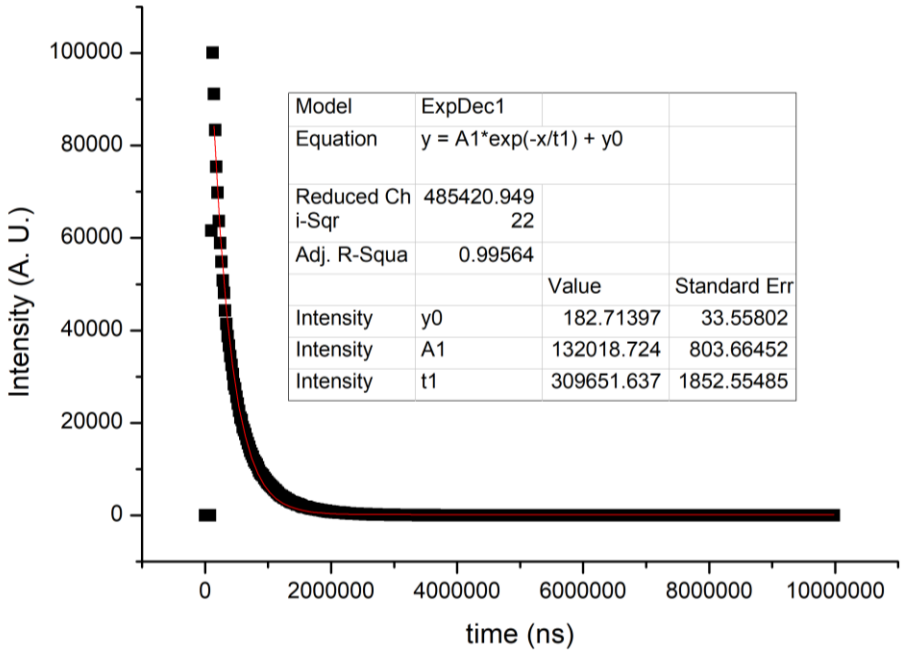

Spectrum S3-61: Decay curve of luminescence lifetime of **EuL$_B$-fmoc** in 5% DMSO/H_2O

(mono-exponential fit)

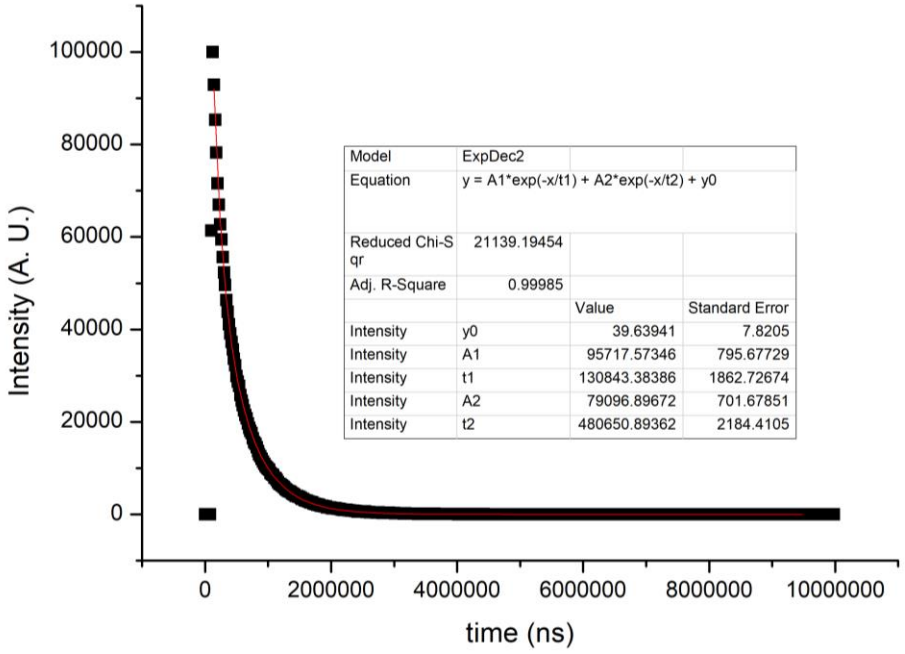

Spectrum S3-62: Decay curve of luminescence lifetime of **EuL$_B$-fmoc** in 5% DMSO/H_2O

(Bi-exponential fit)

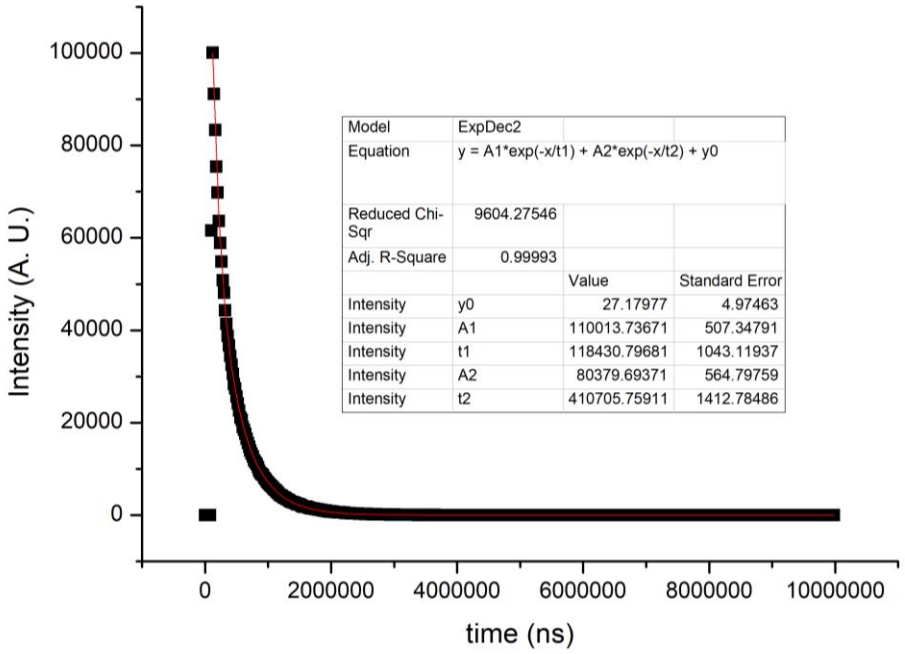

Spectrum S3-63: Decay curve of luminescence lifetime of **EuL_B-fmoc** in 5% DMSO/D_2O

(Bi-exponential fit)

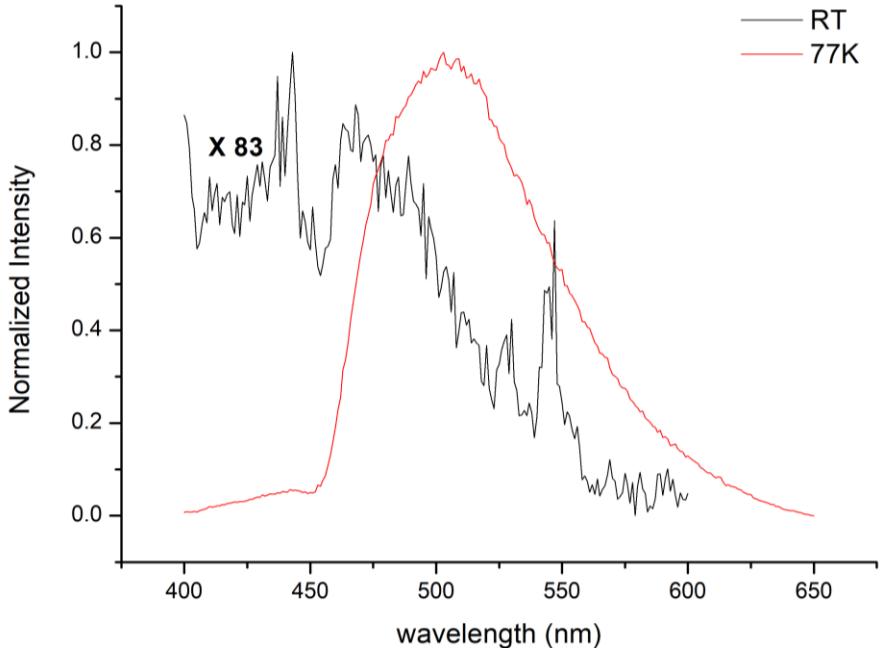

Spectrum S3-64: Normalized Emission spectrum of **GdL_B-fmoc** (RT & 77K)

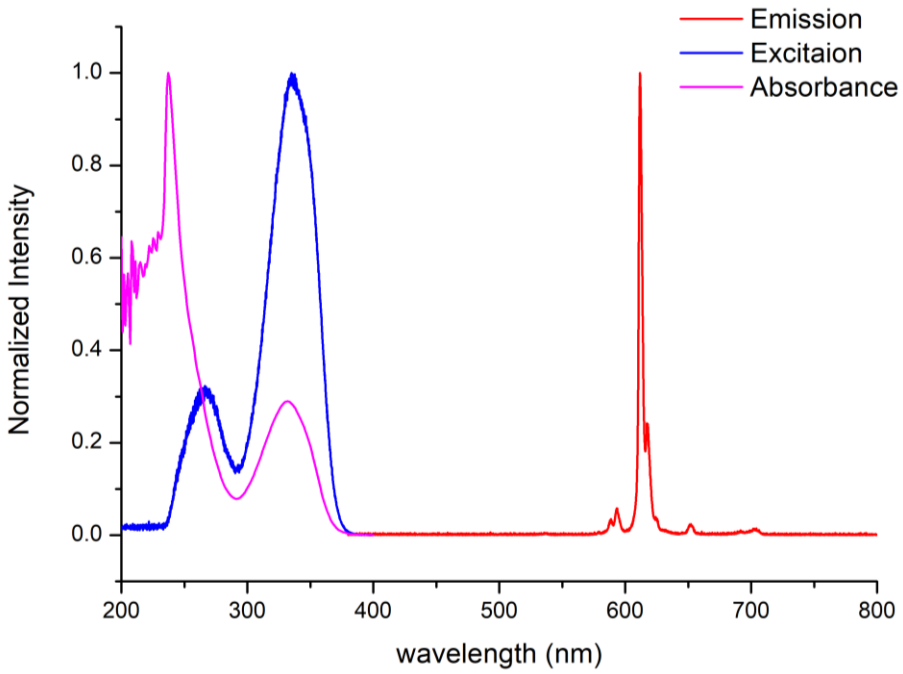

Spectrum S3-65: Combined Spectrum of complexes **EuL_C**

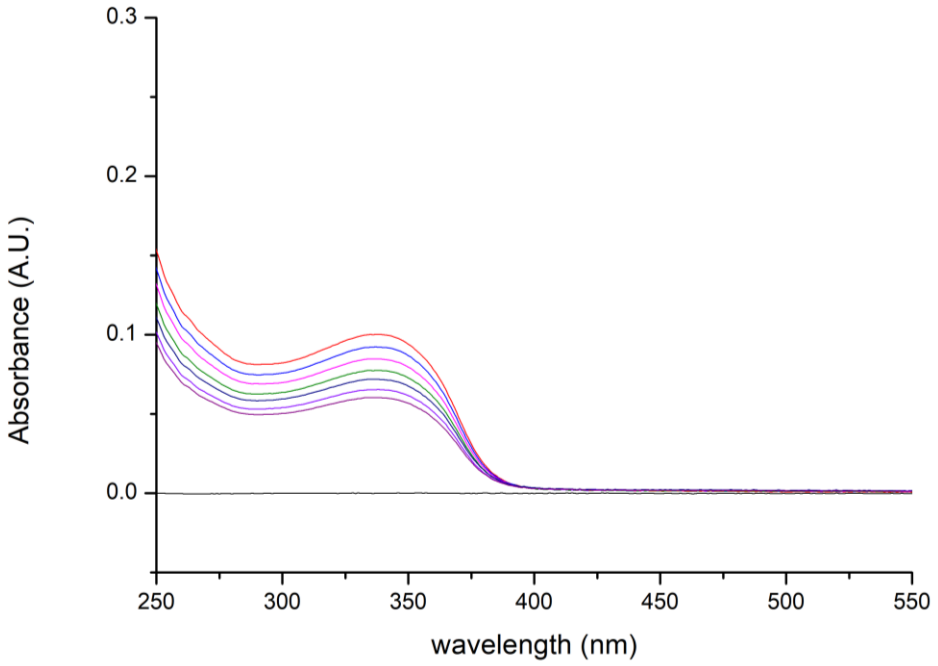

Spectrum S3-66: Absorbance spectrum of **EuL_C**

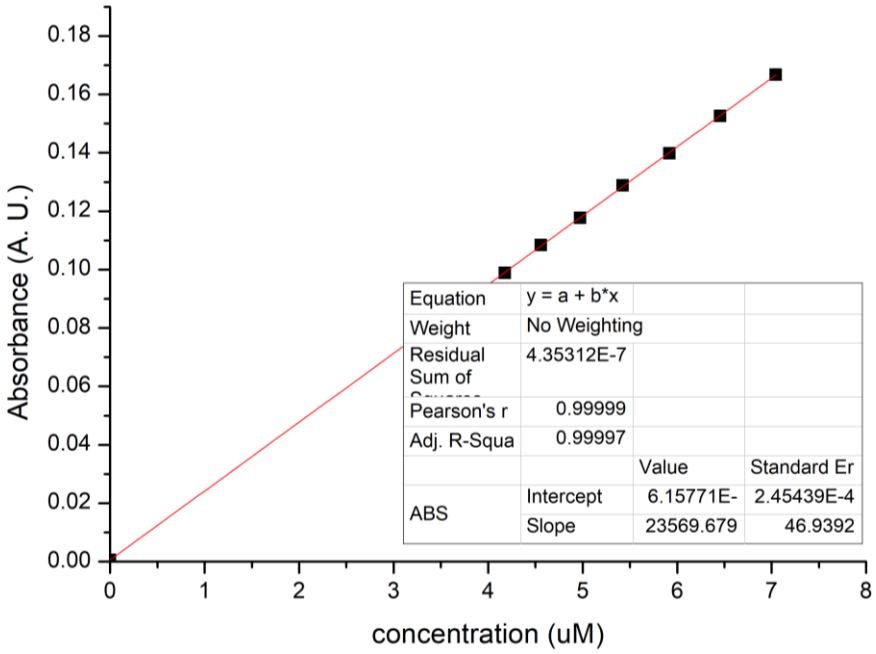

Spectrum S3-67: Absorptivity plot of **EuL_C**

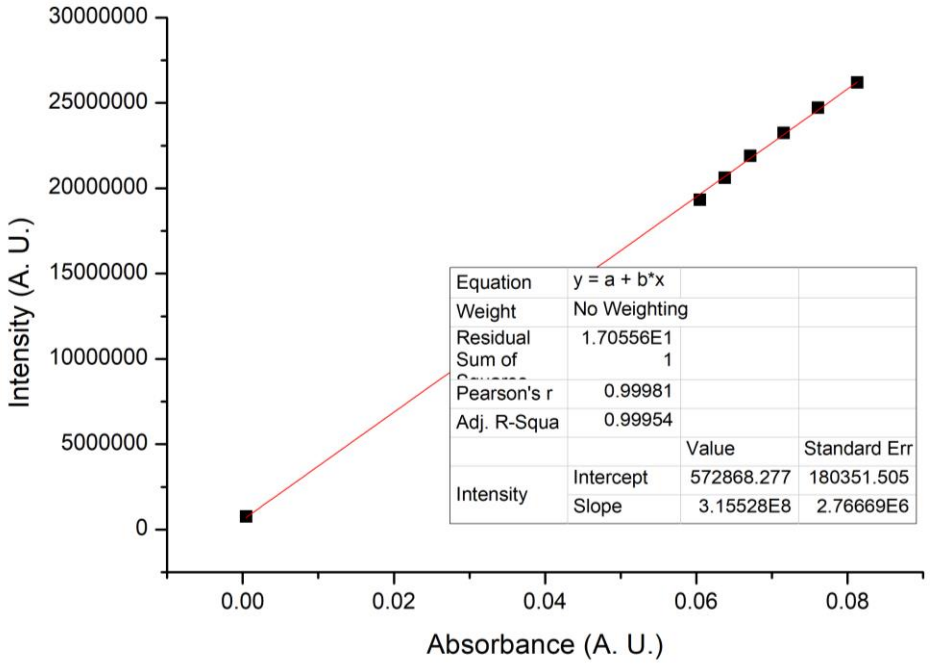

Spectrum S3-68: quantum yield linearity fit of **EuL_C**

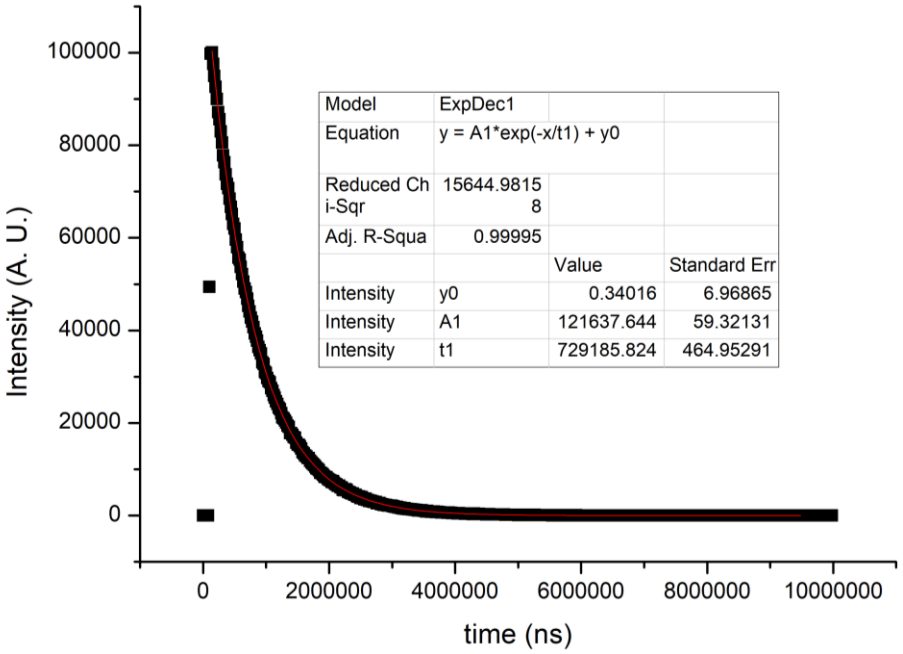

Spectrum S3-69: Decay curve of luminescence lifetime of **EuL_A** in 5% DMSO/H_2O

(mono-exponential fit)

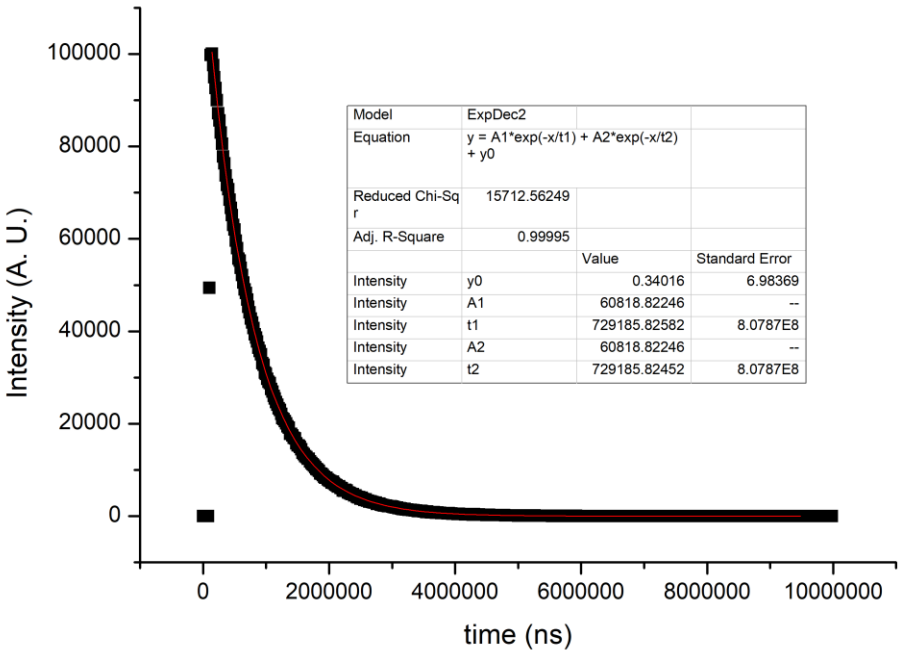

Spectrum S3-70: Decay curve of luminescence lifetime of **EuL_C** in 5% DMSO/H_2O

(Bi-exponential fit)

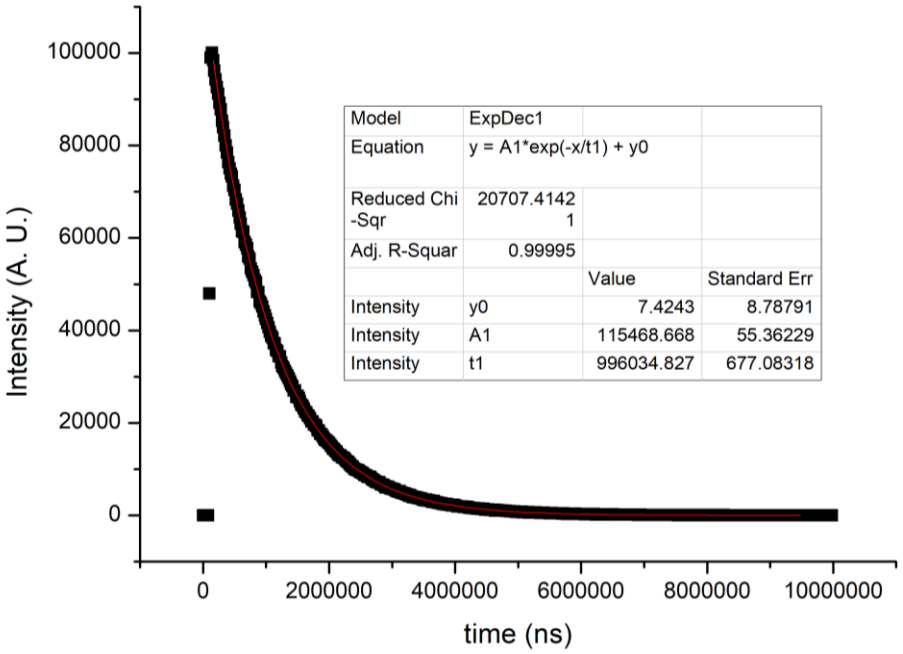

Spectrum S3-71: Decay curve of luminescence lifetime of **EuL_C** in 5% DMSO/D_2O

(mono-exponential fit)

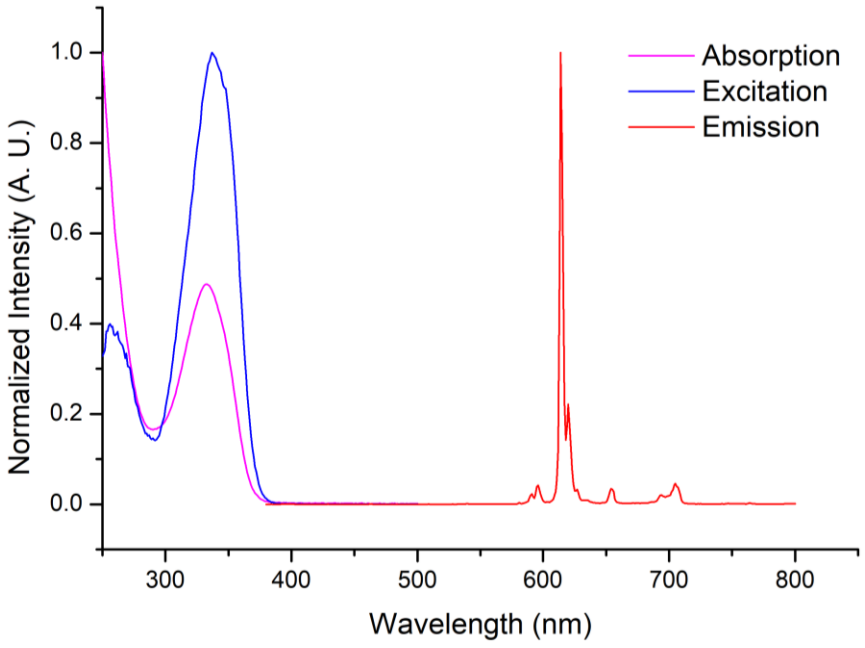

Spectrum S3-72: Combined Spectrum of complexes **EuL_D**

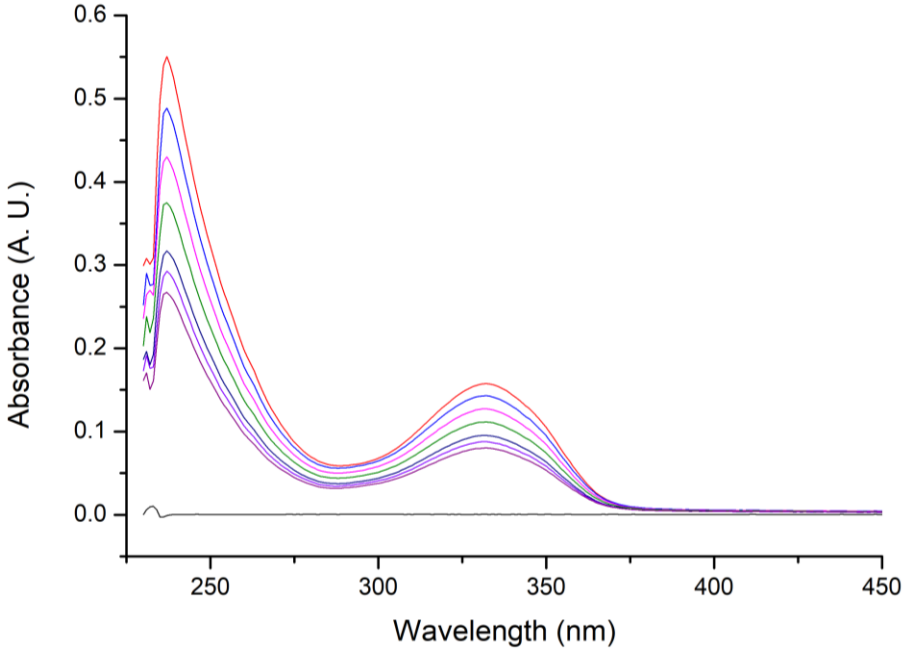

Spectrum S3-73: Absorbance spectrum of **EuL_D**

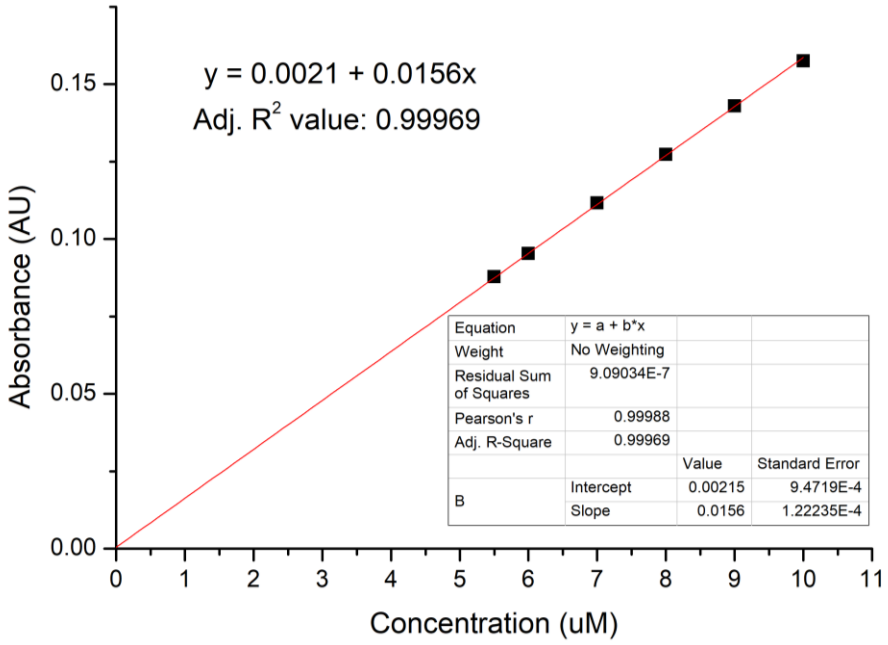

Spectrum S3-74: Absorptivity plot of **EuL_D**

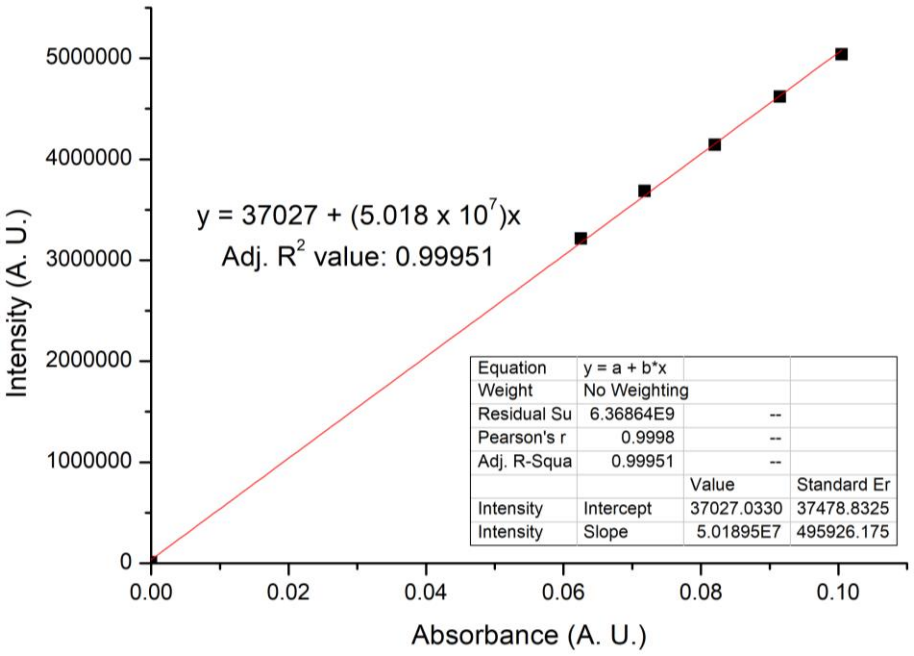

Spectrum S3-75: quantum yield linearity fit of **EuL_D**

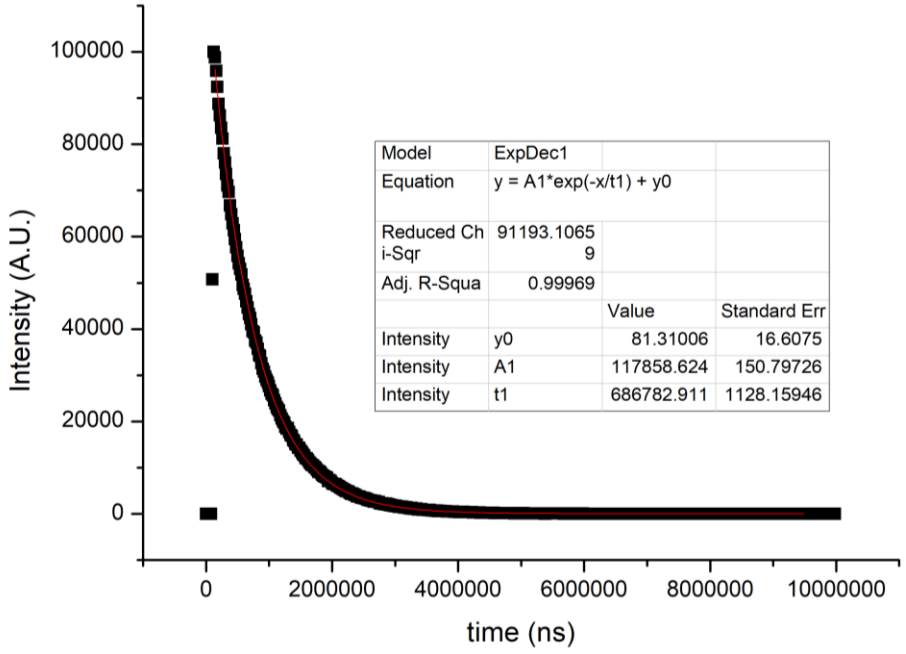

Spectrum S3-76: Decay curve of luminescence lifetime of **EuL_D** in 5% DMSO/H_2O

(mono-exponential fit)

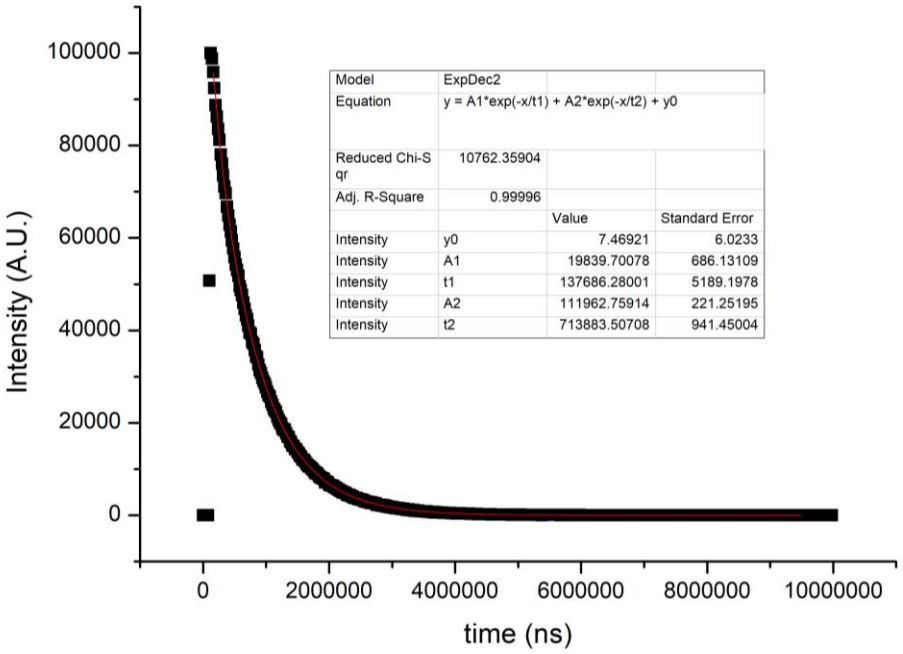

Spectrum S3-77: Decay curve of luminescence lifetime of **EuL_D** in 5% DMSO/H_2O

(Bi-exponential fit)

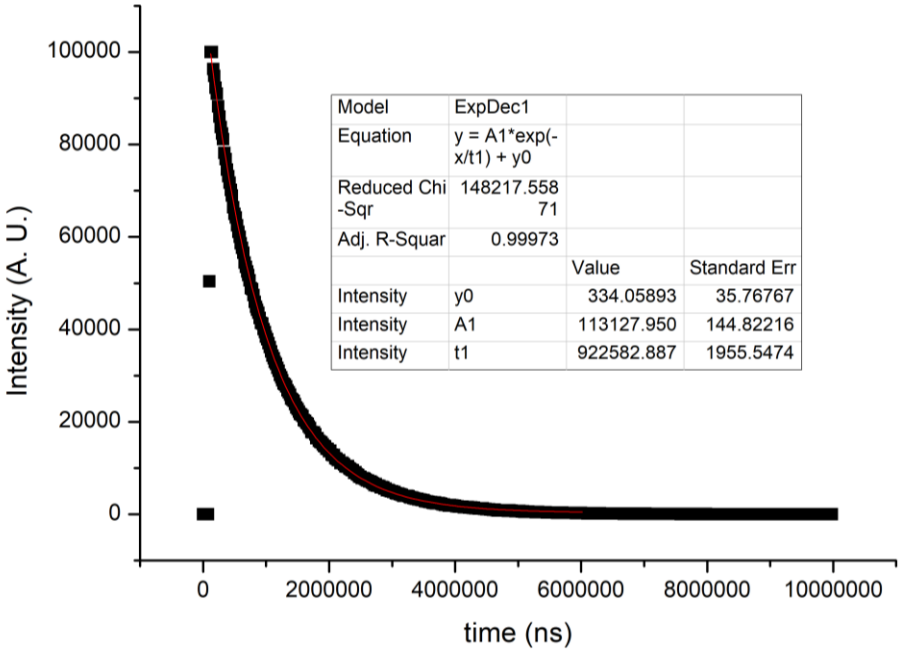

Spectrum S3-78: Decay curve of luminescence lifetime of **EuL_D** in 5% DMSO/D_2O

(mono-exponential fit)

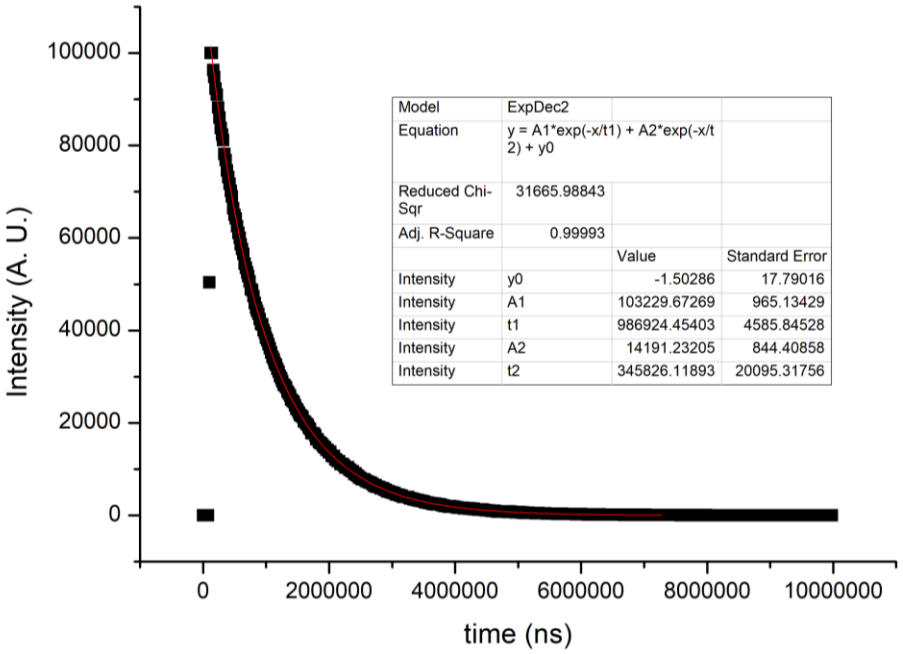

Model	ExpDec2		
Equation	y = A1*exp(-x/t1) + A2*exp(-x/t2) + y0		
Reduced Chi-Sqr	31665.98843		
Adj. R-Square	0.99993		
		Value	Standard Error
Intensity	y0	-1.50286	17.79016
Intensity	A1	103229.67269	965.13429
Intensity	t1	986924.45403	4585.84528
Intensity	A2	14191.23205	844.40858
Intensity	t2	345826.11893	20095.31756

Spectrum S3-79: Decay curve of luminescence lifetime of **EuL_D** in 5% DMSO/D_2O

(Bi-exponential fit)

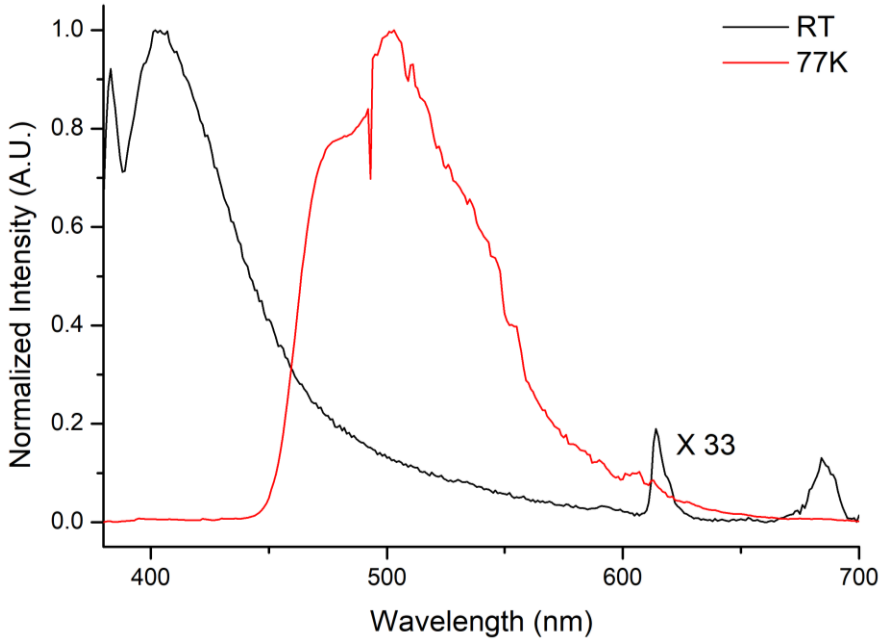

Spectrum S3-80: Normalized Emission spectrum of **GdL_D** (RT & 77K)

5.3. Appendix of Chapter 4

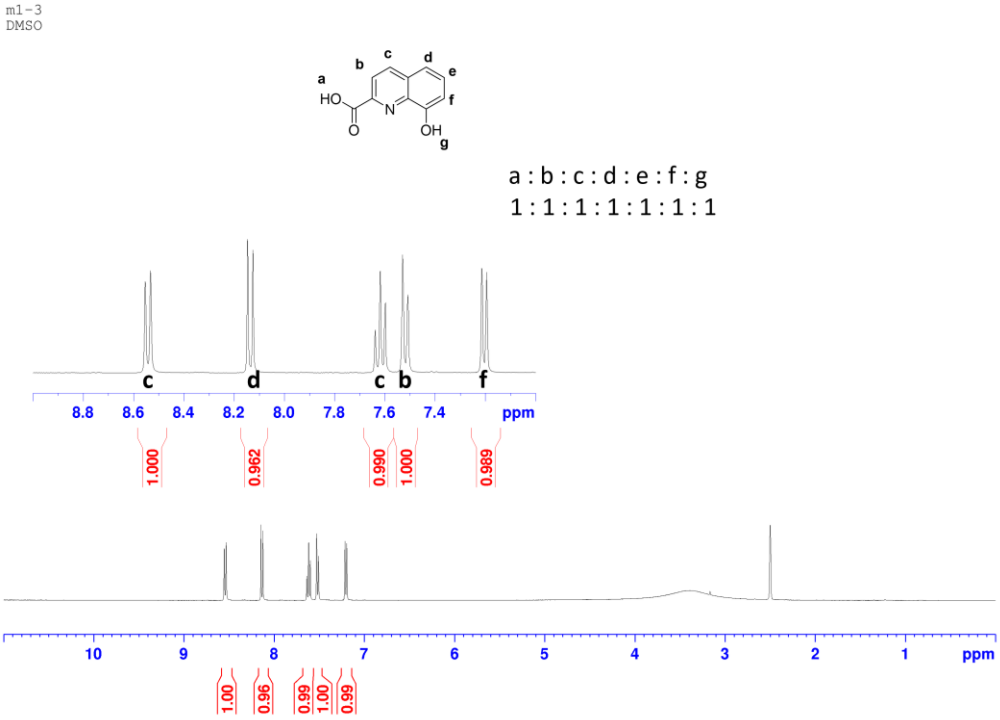

Spectrum S4-6: ^{1}H NMR spectrum of compound **M1-3**

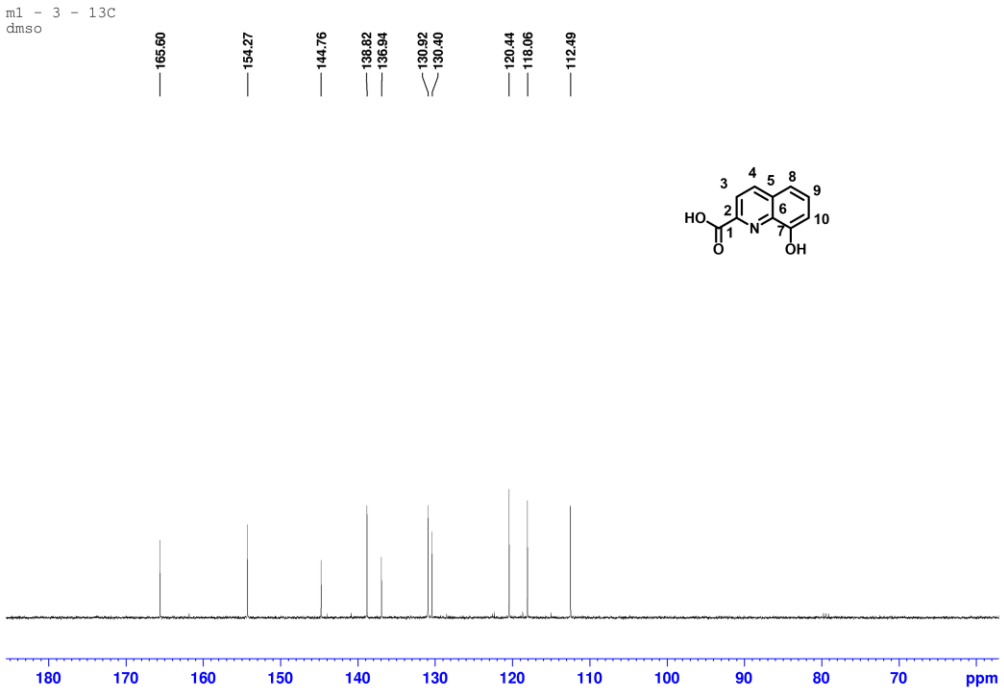

Spectrum S4-7: ^{13}C NMR spectrum of compound **M1-3**

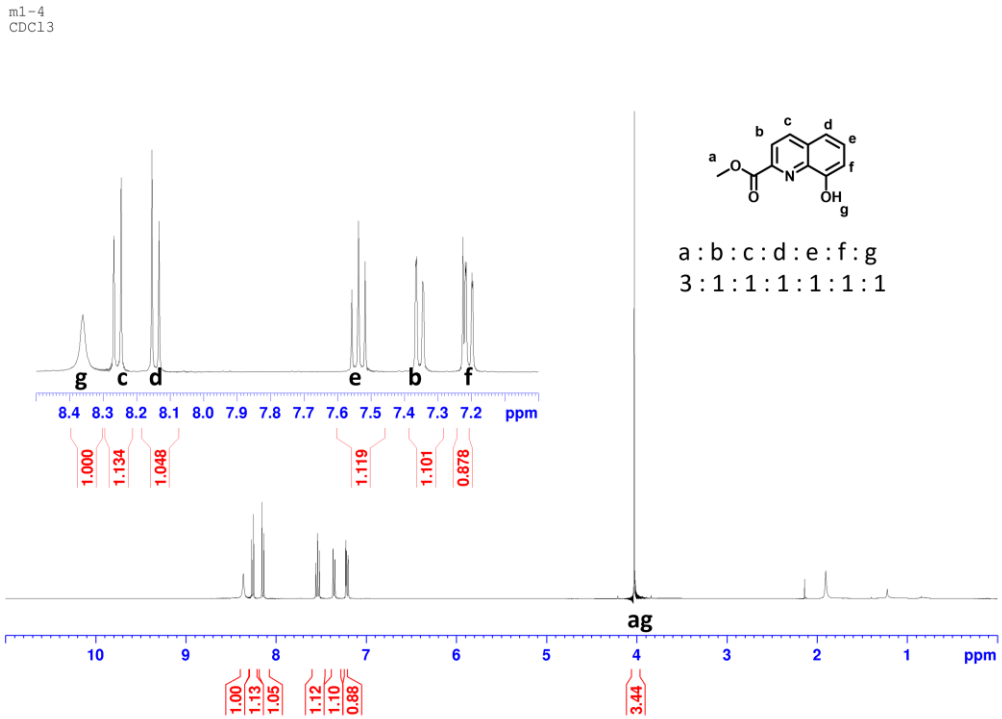

Spectrum S4-8: ^{1}H NMR spectrum of compound **M1-4**

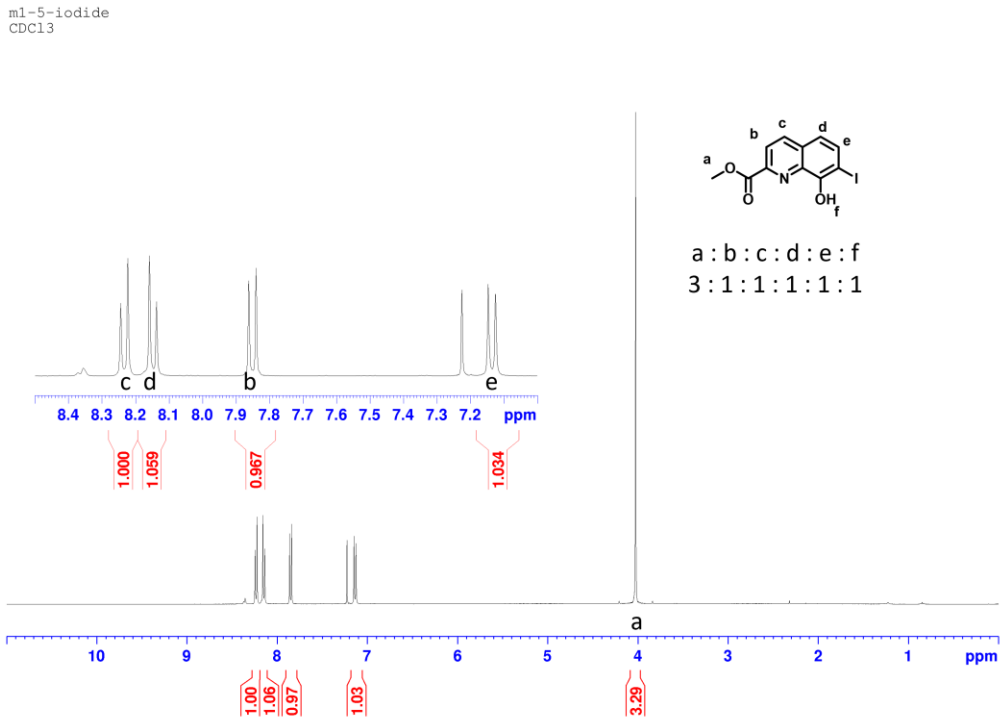

Spectrum S4-9: ^{1}H NMR spectrum of compound **M1-5-iodide**

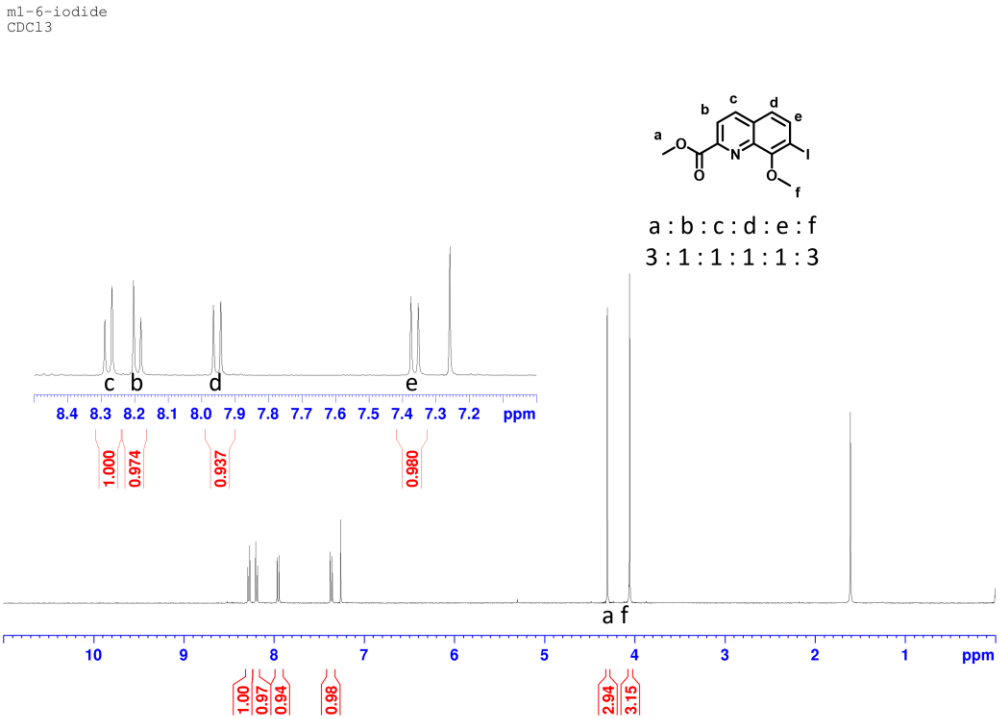

Spectrum S4-10: ^{1}H NMR spectrum of compound **M1-6-iodide**

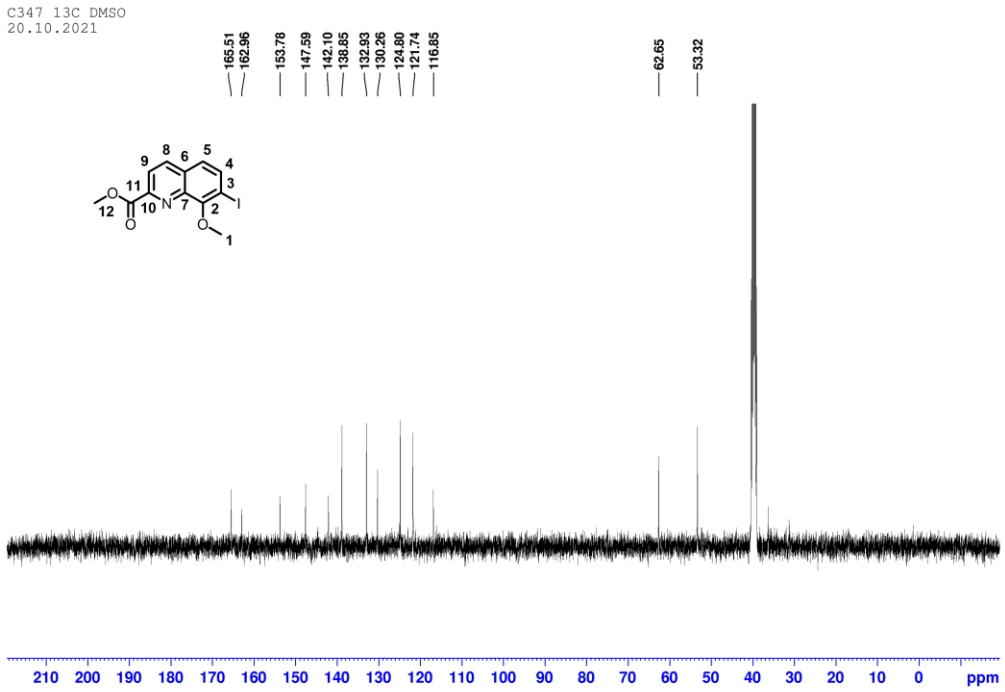

Spectrum S4-11: ^{1}H NMR spectrum of compound **M1-6-iodide**

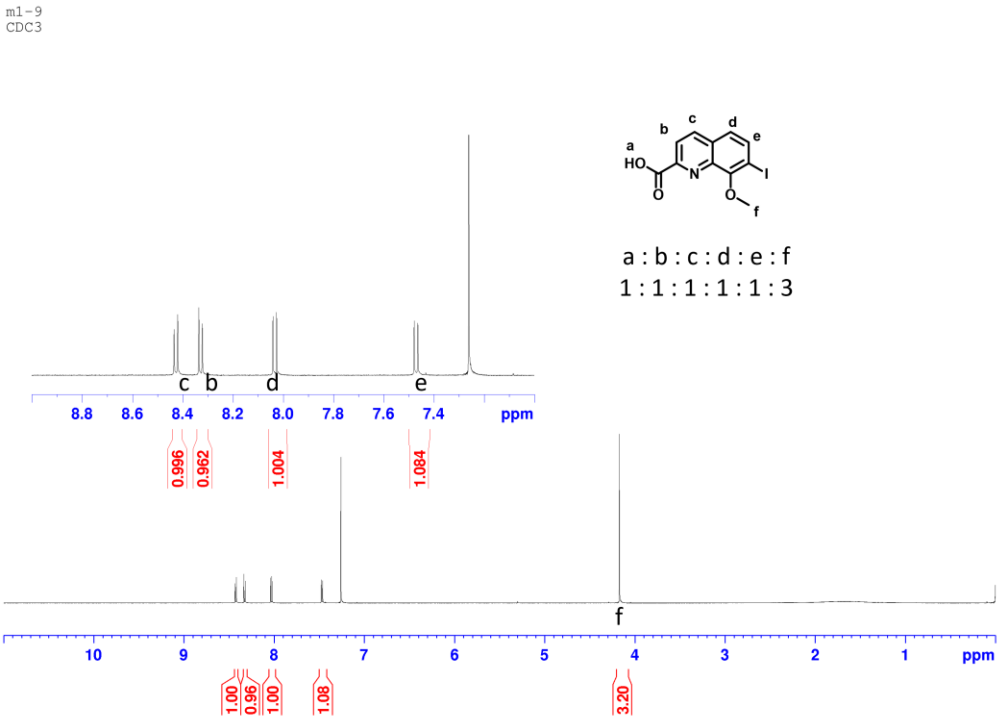

Spectrum S4-12: ^{1}H NMR spectrum of compound **M1-9**

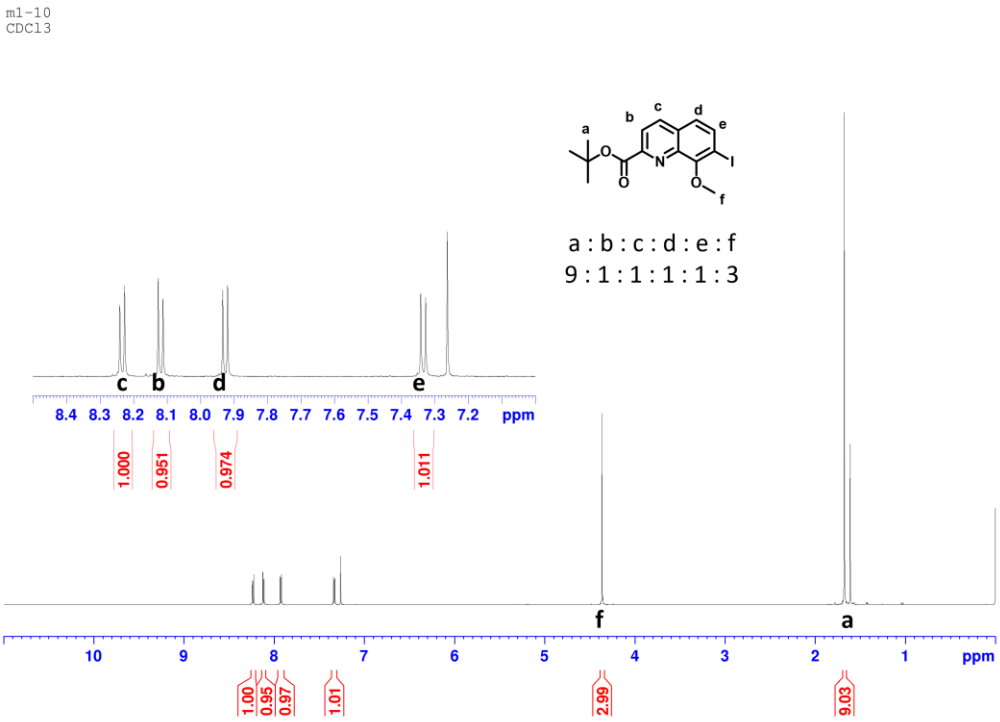

Spectrum S4-13: ^{1}H NMR spectrum of compound **M1-10**

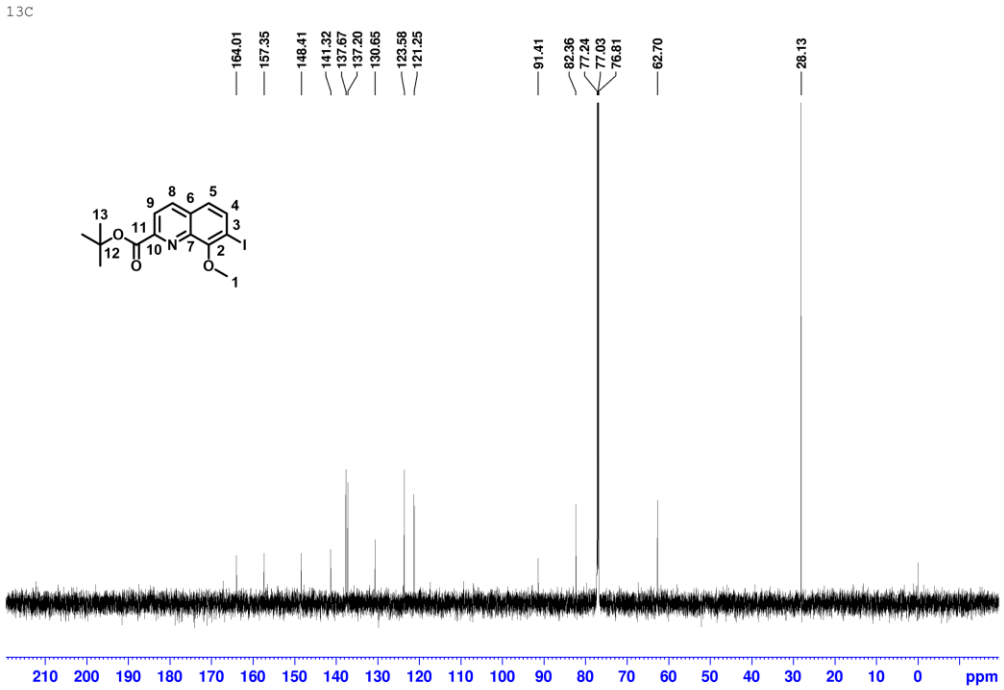

Spectrum S4-14: ^{13}C NMR spectrum of compound **M1-10**

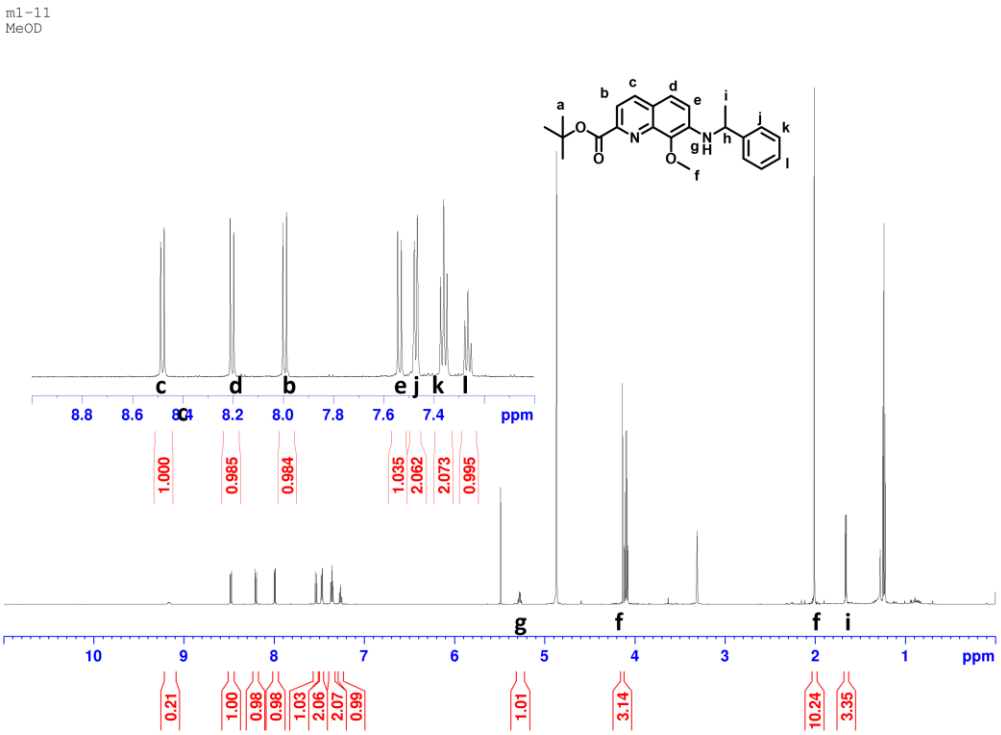

Spectrum S4-15: ^{1}H NMR spectrum of compound **M1-11**